The role of integrin alpha 7 in diet-induced obesity and signalling

James R. Taylor

Thesis submitted for the degree of Doctor of Philosophy in Biomolecular Science

University of East Anglia

School of Biological Sciences

September 2018

ABSTRACT

Integrins are heterodimeric transmembrane proteins and have been shown to play a key role in insulin signalling and glucose metabolism. Integrin α7β1 is the predominant integrin in adult skeletal muscle, a tissue responsible for approximately 80% of insulin-stimulated glucose uptake. Previous studies have demonstrated the role of integrin α7β1 in the maintenance of skeletal muscle, but no studies have investigated it with a metabolic focus. In this thesis, we used an integrin α7 whole-body deletion mouse model (α7KO) to elucidate the role of integrin α7 in metabolism.

In this study we showed that the deletion of integrin α7 resulted in leaner mice when fed either a chow or a high fat diet (HFD), as well as containing significantly less adipose tissue than controls when fed a HFD. Histological analysis showed that integrin α7KO mice suffered from significantly worse liver steatosis when fed a HFD compared to controls and had higher serum levels of indicative enzymes of liver damage. However, liver damage observed in integrin α7KO mice had no effect on bile acid production.

Integrin α7KO mice were significantly more insulin sensitive and glucose tolerant than control mice. Protein quantification of skeletal muscle showed increased levels of pAkt(Ser473) and pAkt(Thr308) in integrin α7KO mice compared to controls when fed a HFD and were exacerbated when challenged with insulin.

We demonstrated that the muscle-specific transgenic overexpression of the adult integrin α7 splice variants X2A and X2B rescued the insulin sensitive, glucose tolerant, and steatotic liver phenotype. However, splice variants X1A and X1B could not rescue the insulin sensitive or glucose tolerance phenotype, but partially rescued the steatotic liver phenotype.

In this thesis, we have demonstrated that integrin α7 plays a fundamental role in diet-induced obesity and metabolism.

TABLE OF CONTENTS

LIST OF FIGURES

LIST OF TABLES

To my parents, Nikki and Rob

ACKNOWLEDGEMENTS

Firstly, a very special thank you goes to my supervisor, Prof. Ulrike Mayer. Uli, thank you for taking a chance and offering a PhD project to an undergraduate student. Thank you for always driving me, believing in me, and putting up with me. This thesis would not have been possible without your efforts and I will be forever grateful.

I would also like to say a massive thank you to my secondary supervisors, Prof. Jeremy Turner and Dr David Vauzour. You were the optimists I needed on this journey, thank you for your encouraging words and invaluable guidance.

Thank you to Dr Ernst Pöschl for being the fountain of knowledge and enthusiasm that you are. Although not technically on my supervisory panel, you have strived to assist wherever possible. You are a fantastic teacher of both science and life.

I would like to thank Dr Devina Divekar for the support and guidance you have provided over the years. From Day 1 of my undergraduate project you have acted as a mentor and I would not be the scientist I am without you.

Thank you to the staff of the BMRC and DMU. Your daily efforts are appreciated and none of the research produced in this institute would be possible without you. I would also like to thank both the chubby and lean members of the *Mus Musculus* family. Without your sacrifice, this work would not be possible. I would like to thank my friends and colleagues in the BMRC. It has been a great pleasure working with you over the years.

I would also like to thank Hannah Felstead. Hannah, without us meeting and bonding over how tragic we were as teenagers, this adventure wouldn't have been fractionally as enjoyable as it has been. It's not us, it's everybody else who is weird. Hail yourself.

Thank you to Benjamin Gotts. Ben, you have turned our house into a very middle-class

home. Your unique sense of humour has made my time in Norwich so much better, even if we are scarily alike sometimes. ‘Do we have any ground arrowroot?’

Thank you to my friends that have stayed close even as we have wandered different paths. Jamie, Kieran, Liam and Tom, thank you for being friends that I can be comfortably ridiculous with. I can’t wait for more goony adventures.

I would like to express my heartfelt gratitude to Rachel Holmes. Rachel, words cannot explain how much you have helped me during my PhD journey. Your smile is all that I have needed to stay strong. Thank you for all your love and support.

Alex, as both my brother and best friend, you have helped me more than you could possibly know. Thank you for always being my partner in crime and sometimes not telling Mum when stick fights went wrong.

Mostly, I would like to thank my Mum and Dad. I cannot begin to express my gratitude for everything that you do for me. I am extremely lucky to have you both as role models. Everything that I have achieved is attributable to your efforts and sacrifice. Your unconditional love and guidance have made me the man that I am today. Thank you.

CHAPTER 1: INTRODUCTION

1.1 The obesity pandemic

Over the past 40 years, the world has transitioned from one where there were more than double the amount of people underweight than obese, to one in which there are more obese than underweight. If current trends are to continue, by 2025, almost 20% of the world will be classified as obese with a body mass index (BMI) of >30 kg/m^2 (NCD Risk Factor Collaboration (NCD-RisC), 2016). Matters are worse in the United Kingdom. In 2015, the UK was ranked 6th globally as having the largest percentage of obese adults (OECD, 2017). Current models predict that by 2030, 36% of men and 33% of women from the United Kingdom will be obese (World Health Organization, 2013).

The causes of obesity are multifactorial, with a combination of environmental, epigenetic and genetic factors leading to obesity. The simplest conception of obesity is when ingested energy is greater than expended energy and excess energy is stored as mostly triglyceride in adipose tissue. However, these environmental factors are avoidable with the main causes being the increased ingestion of calorie-dense food and a reduction in physical activity in daily life (Brehm and D'Alessio, 2000).

Obesity has been linked with a range of noncommunicable diseases including cardiovascular diseases, musculoskeletal disorders, cancer and type II *diabetes mellitus* (T2DM). The risk of these diseases increases with a greater BMI (World Health Organization, 2018). One of the greatest precursors of T2DM is insulin resistance (Taylor, 2012). In this study, the interplay between diet-induced obesity and insulin resistance is our focus.

1.2 Insulin

In 1921, Dr Frederick Banting began his experiments which led to the discovery of insulin. The removal of the pancreas from dogs resulted in diabetic-like symptoms. The administration of pancreas extracts to these dogs reversed the symptoms temporarily (Banting et al., 1922). A year later, the first human trial was completed on a diabetic 14-year-old boy whose symptoms were reversed by the administration of Banting's pancreas extract. The ability to restore health in such a dramatic fashion was described as "the raising of the dead". The active compound in these extracts was identified and named 'insulin' for which Banting was awarded the Nobel Prize in 1923 (Quianzon and Cheikh, 2012).

Insulin is a peptide hormone secreted by the β cells located in the islets of Langerhans found in the pancreas. It is secreted when blood glucose levels are elevated and oversees the controls of cellular glucose uptake, the regulation of carbohydrate, lipid and protein metabolism, and also affects cell division and growth.

1.2.1 Insulin structure and synthesis

Insulin is initially translated by pancreatic β cells as a single polypeptide precursor called preproinsulin. It is comprised of the signal peptide, insulin B-chain, C-peptide, and insulin A-chain. In the endoplasmic reticulum, proinsulin is formed by the enzyme signal peptidase, removing the signal peptide which causes proinsulin to adopt a 3-dimensional structure. Proinsulin is transferred to the Golgi apparatus, where the subsequent cleavage of the C-peptide forms the completed insulin dipeptide hormone. The mature insulin is accumulated in secretory granules in the cytoplasm (Liu et al., 2014) (Figure 1.1).

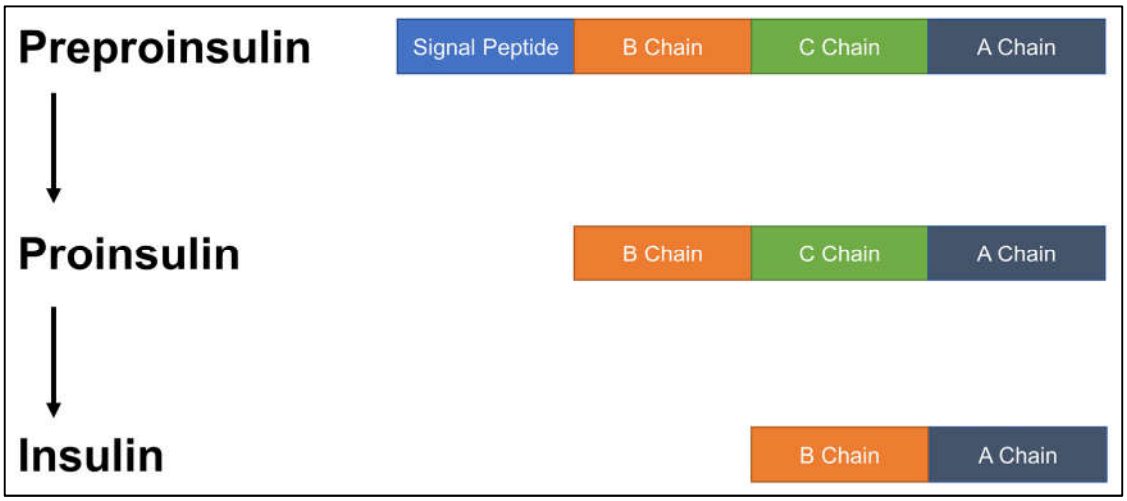

Figure 1.1: Synthesis of insulin from preproinsulin in pancreatic β cells

1.2.2 Insulin secretion

The main stimulus of insulin secretion is elevated blood glucose, which is appropriate as insulin's primary role is to regulate the concentration of blood glucose. β cells can detect changes in blood glucose concentration by clustering adjacent to vasculature. Elevated levels of blood glucose are detected by glucose diffusing into the β cells via glucose transporter-2 (GLUT2). Glucose is metabolised into pyruvate via glycolysis which is further metabolised to generate ATP. This increased ATP:ADP ratio causes ATP-dependent potassium channels to close, depolarising the cell membrane. Depolarisation causes voltage-gated calcium channels to open, allowing Ca^{2+} to stimulate the movement of secretory granules containing insulin for release into the blood (Bonfanti et al., 2015). A summary of this mechanism is depicted in Figure 1.2.

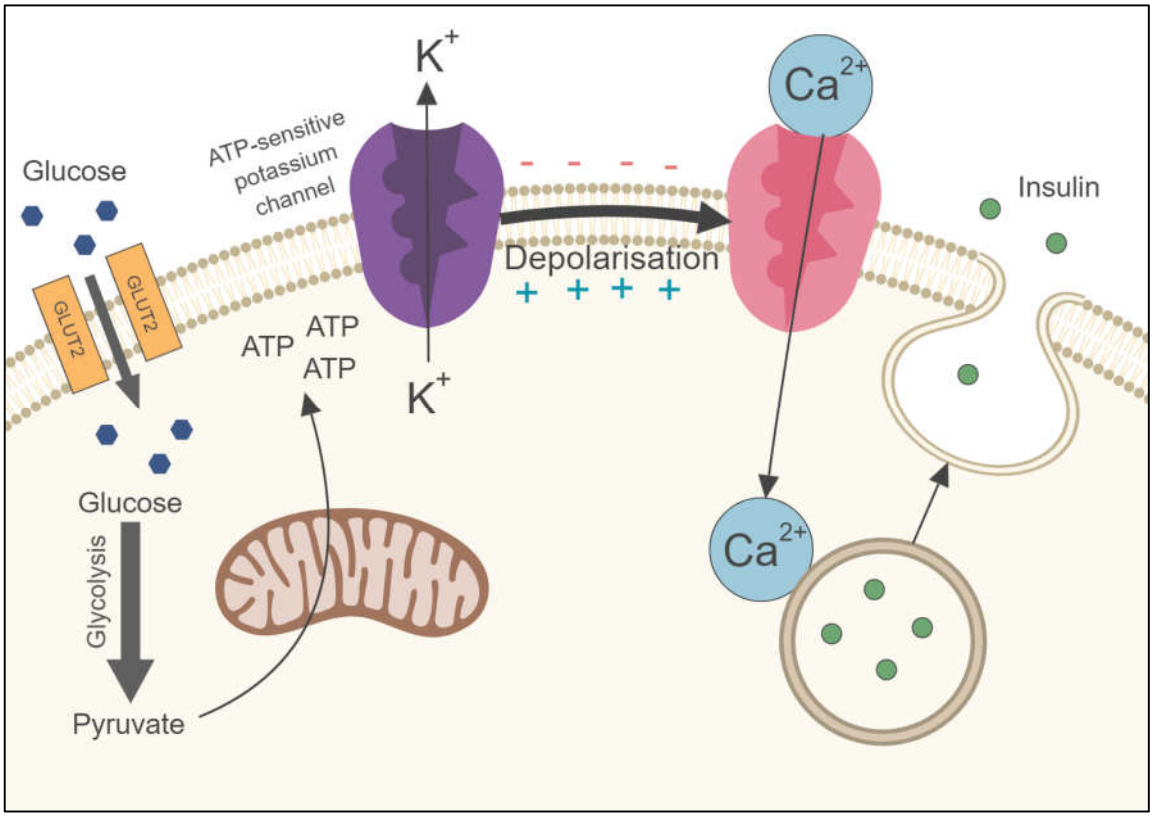

Figure 1.2: Summary of the process of insulin secretion in pancreatic β cells. Elevated blood glucose concentrations infiltrate the pancreas via GLUT2. Glucose undergoes glycolysis which results in the production of ATP. ATP-dependent K^+ channels cause depolarisation of the cell resulting in an increase in intracellular Ca^{2+}. Ca^{2+} is the primary trigger for exocytosis of the insulin-containing secretory granules. (Adapted from Bonfanti et al., 2015.)

1.2.3 Insulin signalling

1.2.3.1 Insulin receptor

Insulin mediates its actions by binding to the insulin receptor (IR) on various tissues whilst being transported via blood circulation. Mutant animal studies have demonstrated the crucial role the IR plays *in vivo.* The IR has been found to be essential for postnatal growth and metabolism, but is not required for foetal metabolism (Taylor, 1999; Sadagurski et al., 2006). Most tissue-specific knockouts of the IR led to T2DM-like conditions (Kulkarni et al., 1999). X-ray crystallography has been successfully utilised to determine the structure of the IR and also the mechanical link between insulin binding and activation (Hubbard, 1997; Scapin et al., 2018).

The IR is a heterodimeric membrane glycoprotein composed of two α-chains, two β-chains, a transmembrane helix, the juxtamembrane domain and the intracellular tyrosine kinase domain. Insulin binds to the extracellular α subunits which causes a conformational change. This change allows ATP to bind the β subunits intracellular domain, activating receptor autophosphorylation of tyrosine residues (Tavaré and Siddle, 1993; Hubbard, 1997; Scapin et al., 2018).

Insulin is not the only agonist of IR. The IR can also bind to insulin-like growth factors (IGF-1 and IGF-2). However, the affinity of IGF-1 is approximately 100-1000-fold lower than insulin (Andersen et al., 1992). But as IGF-1 circulation is approximately 100-fold higher than insulin, IGF-1 still plays a significant role in IR activation.

1.2.3.2 Insulin receptor substrates

Following activation of the IR by insulin, the auto-phosphorylated tyrosine residues act as docking sites for proteins, including the insulin receptor substrates (IRS). The IRS proteins are cytoplasmic adaptor proteins that transmit signals from the IR and IGF-1 receptor to elicit a cellular response. To date, six known IRS protein have been discovered (IRS1-6).

Both IRS-1 and IRS-2 are ubiquitously expressed and are the primary mediators of glucose metabolism and insulin-dependent mitogenesis in most cell types (White, 2002). Deletion of IRS-1 resulted in impaired growth, decreased glucose tolerance and peripheral insulin resistance. However, it has been shown that IRS-2 can compensate for a lack of IRS-1 (Araki et al., 1994). Deletion of IRS-2 also resulted in insulin resistance but also a defect in pancreatic β cells (Kubota et al., 2000). IRS-3 shares homology with IRS-1 and IRS-2, however is specific to adipocytes. In contrast to IRS-1 and IRS-2, IRS-3 deficient mice appear to have no obvious differing phenotype in terms of metabolism from control mice (Liu et al., 1999). Further studies demonstrated that IRS-3 localises to the nucleus and possesses transcription-regulating activity (Kabuta et al., 2002). IRS-4 is restricted to the thyroid, brain, kidney and pancreatic β cells. IRS-4 is able to activate downstream proteins in the insulin signalling pathway *in vitro* but *in vivo* studies have shown there is no obvious phenotype in IRS-4 deficient mice (Tsuruzoe et al., 2001; Uchida et al., 2000). IRS-5 has been shown to be restricted to kidney and liver, whilst IRS-6 is restricted to skeletal muscle. However, both have limited function in signal transduction (Cai et al., 2003).

All IRS proteins share a significant degree of homology. All contain an NH_2-terminal pleckstrin-homology (PH) domain for phospholipid binding, which lies adjacent to a phospho-tyrosine-binding (PTB) domain, followed by a COOH-terminal tail which contains a variety of tyrosine, threonine and serine phosphorylation sites. The phosphorylation status of these sites regulate the downstream signalling proteins (Sun et al., 1991; Yenush et al., 1998). It is this complex patterning of >50 serine, threonine and tyrosine residues in IRS-1 and IRS-2 which allows the intricate control of downstream effects. Most tyrosine phosphorylation sites have been shown to promote the effects of insulin stimulation. Phosphorylation of the tyrosine residues leads to the generation of binding sites for Src homology 2 (SH2) domain proteins. Activation of Phosphoinositide 3-kinase (PI3K), a critical node promoting insulin signalling, is only

possible with the phosphorylation of tyrosine-612 and tyrosine-632 in humans (Esposito et al., 2001). In contrast to tyrosine sites, serine and threonine sites have been shown to reduce the effects of insulin signalling. Tumour necrosis factor alpha (TNFα) has been shown to inhibit insulin action by activating various kinases including, Jun NH(2)-terminal kinase (JNK). JNK phosphorylates serine-307, adjacent to the PTB-domain, and has been shown to reduce tyrosine phosphorylation by disrupting the IR/IRS-1 interaction (Aguirre et al., 2000; Solinas and Karin, 2010).

1.2.3.3 Phosphoinositide 3-kinase

PI3K is one of the key targets of the IRS proteins. It is a heterodimer composed of a p110 catalytic subunit and a p85 regulatory subunit which interacts with phosphorylated tyrosine residues of the IRS proteins. When PI3K is bound to IRS, it is brought close to its substrate phosphatidylinositol-4,5-bisphosphate (PIP2), which it phosphorylates to form phosphatidylinositol-3,4,5-triphosphate (PIP3) (Lietzke et al., 2000). PIP3 is subsequently able to regulate the AGC family of serine/threonine protein kinases including phosphoinositide-dependent kinase 1 (PDK1) (Alessi et al., 1997). PDK1, along with mTORC2, is able to phosphorylate Protein Kinase B/Akt, a critical signalling node of the insulin signalling pathway (Gao et al., 2014).

Negative regulation of the insulin signalling pathway can also occur at the PI3K level. The lipid phosphatase, PTEN (phosphatase and tensin homolog deleted on chromosome 10) opposes the activity of PI3K by dephosphorylating PIP3 (Chalhoub and Baker, 2009).

1.2.3.4 Protein kinase B/Akt

Protein kinase B, or Akt as it will be referred to, is one of the key nodes of the insulin signalling pathway. As well as regulating nutrient metabolism, Akt is also heavily involved in a range of pathways which influence cell growth and apoptosis. The three isoforms of Akt (Akt1, Akt2 and Akt3) have a highly conserved structure. All contain a PH domain, a

central serine/threonine kinase domain and a carboxyl-terminal regulatory domain. Akt isoform expression is dependent on tissue. Akt1 is ubiquitously expressed and has been shown to be the key isoform involved in lipid metabolism and the stimulation of glycogen synthesis in skeletal muscle, as well as the modulator of insulin function in adipocytes (Jiang et al., 2003; Bouzakri et al., 2006). Akt2 is expressed at a higher level in insulin-responsive tissues including: adipose tissue, liver, and skeletal muscle. Akt3 has been shown to be expressed highest in the brain and other non-insulin sensitive tissues (Yu et al., 2015)

PIP3 is able to bind to the PH domain of Akt and recruit it to the plasma membrane with the assistance of phosphatidylserine (PS) where it is phosphorylated on site Threonine308 by PDK1 (Wick et al., 2000; Huang et al., 2011). Phosphorylation of Threonine308 stabilises the activation loop in an active conformation and allows mTORC2 to phosphorylate at Serine473. The phosphorylation of Threonine308 and Serine473 of Akt results in full activation of the Akt kinase (Alessi et al., 2009; Liao and Hung, 2010). Fully activated Akt is then able to link insulin signalling with downstream regulators of glucose transporters.

1.2.3.5 Glucose transporters

Glucose is transported into cells by glucose transporters (GLUTs). GLUT4 is one of 14 members of the GLUT family, a group of transmembrane hexose transporters, and is the most common GLUT in skeletal muscle and adipose tissue. GLUT4 is accompanied by GLUT1, GLUT5 and GLUT12 in skeletal muscle, and GLUT8, GLUT12, and proton-coupled myo-inositol transporter (HMIT) in adipose tissue (Huang and Czech, 2007). However, it is only GLUT4 that has the characteristic of intracellular compartmentalisation in the insulin-unstimulated state that allows insulin to sensitively regulate glucose uptake (Bryant et al., 2002). In the absence of insulin, ~95% of GLUT4 is distributed between the endosomes, the trans-Golgi network and heterogeneous tubule-vesicular structures acting as GLUT4 storage vesicles (Slot et al., 1991; Shewan

et al., 2003). These vesicles contain a multitude of proteins including: transferrin receptor, insulin-responsive aminopeptidase (IRAP), sortilin, and low-density lipoprotein receptor-related protein-1 (LRP1) (Tanner and Lienhard, 1987; Larance et al., 2005). Once formed, these vesicles remain within unstimulated cells until stimulated by insulin (Bogan and Kandror, 2010). Upon stimulation by insulin, the translocation of GLUT4 to the cell surface can increase glucose uptake by 10-40 fold, dependent on the tissue (Bryant et al., 2002). Remarkably, GLUT4-deficient mice do not develop diabetes. Although not as sensitive to insulin, GLUT4-deficient mice are still effective at clearing glucose (Katz et al., 1995). This indicates that compensation by other GLUT isoforms occurs.

As previously mentioned, Akt is the node which connects insulin and GLUT4 translocation. Studies have demonstrated that Akt is required for an insulin-mediated prefusion step of the GLUT4 vesicle to within 250 nm of the plasma membrane. The main target for phosphorylated Akt in GLUT4 translocation is Rab GTPase-activating protein AS160/TBC1D4 and it has been shown that its activation is pivotal to the translocation process. Dominant-inhibitory mutation of AS160 leads to inhibition of insulin-stimulated exocytosis of GLUT4 (Zeigerer et al., 2004; Mîinea et al., 2005). Studies have also demonstrated that soluble N-ethlymaleimide-sensitive factor attachment protein receptor (SNARE) proteins, including Synip and CDP138, are downstream substrates of Akt and further regulate GLUT4 vesicle fusion with the plasma membrane (Min et al., 1999; Yamada et al., 2005). The fusion of the GLUT4 vesicle with the plasma membrane then allows GLUT4 to interact with extracellular glucose (Gonzalez and McGraw, 2006).

1.2.3.6 Signalling through the MAP kinase pathway

Although the primary role of insulin signalling is the uptake of glucose, insulin is also involved in other signalling pathways. One such pathway is the Ras/Raf/MEK/ERK signalling cascade. Phosphorylated IRS-1 is able to serve as a docking protein for those

with SH2 domains, including GRB2/SOS (Pruett et al., 1995). Upon activation, GRB2/SOS binds to Ras, a small GTP-binding protein, which exchanges GDP for GTP and undergoes a conformational change. Active Ras then phosphorylates Raf and recruits it to the cell membrane. Raf activates MEK 1/2 which consequently phosphorylates ERK 1/2. ERK 1/2 is responsible for a variety of functions throughout the cell, but the most significant is the control of gene transcription that control cell growth and proliferation (Khoo et al., 2003). This is summarised in Figure 1.3.

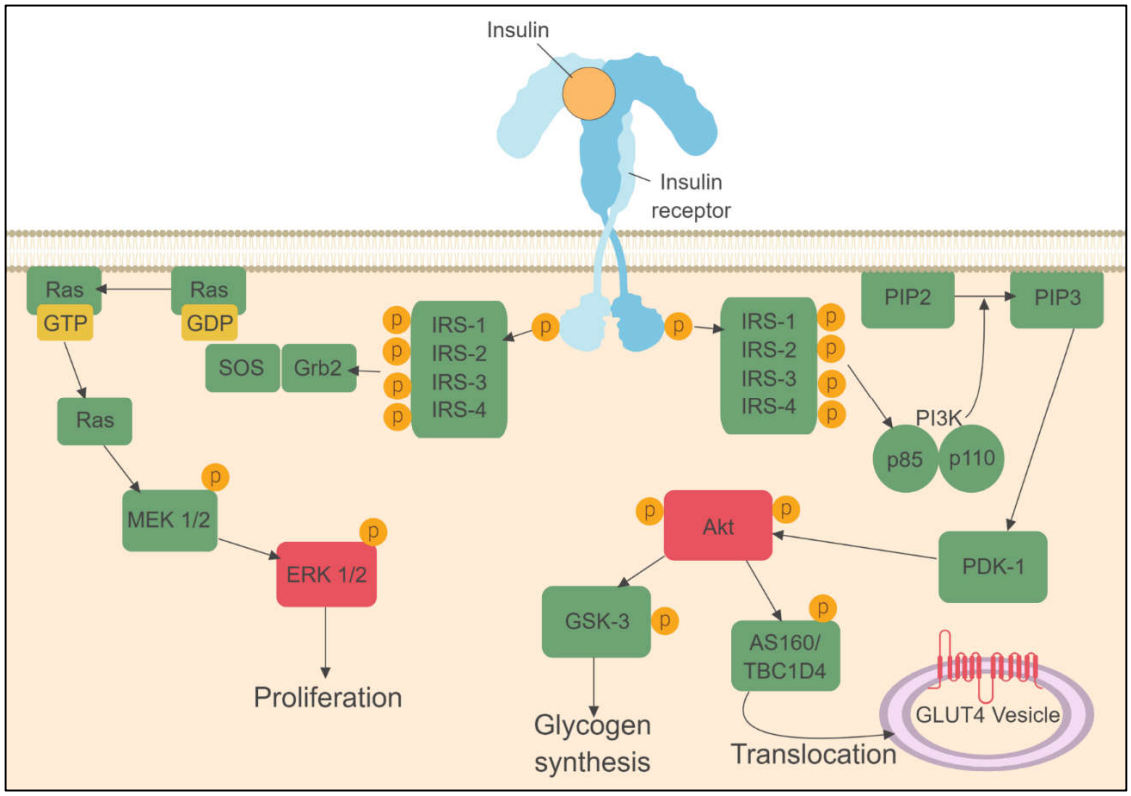

Figure 1.3: Summary of the insulin signalling pathway. Activation of the insulin receptor by insulin results in autophosphorylation of tyrosine residues in the β subunit. These residues result in the phosphorylation of the insulin-receptor substrates (IRS) and activation of phosphoinositide 3-kiase (PI3K). This results in the conversion of phosphatidylinositol-4,5-bisphosphase (PIP2) to phosphatifylinositol-3,4,5-triphosphate (PIP3) and the activation of phosphoinositide-dependent kinase 1 (PDK1). PDK1 phosphorylates Akt resulting in the translocation of GLUT4-containing vesicles (Adapted from Boucher et al. 2014).

1.2.4 Defected insulin signalling

1.2.4.1 Type I diabetes mellitus

Type I diabetes mellitus (T1DM) is an autoimmune disease typically caused by the destruction of pancreatic β cells. Lack of pancreatic β cells results in severe hyperglycaemia due to lack of insulin production (Atkinson et al., 2014). Therefore, in patients with T1DM, hyperglycaemia is not caused by insulin signalling deficiency, but rather by a lack of production of insulin. In approximately 70-90% of T1DM incidences, pancreatic β cell loss is caused by autoimmunity and is known as type Ia diabetes mellitus (T1aDM). However in other cases, there are no detectable autoantibodies and the cause of β cell loss is currently unknown, termed type Ib diabetes mellitus (Maraschin et al., 2010).

Patients with T1aDM possess autoantibodies for one or more of: insulin (IAA), glutamic acid decarboxylase (GADA), insulinoma-associated autoantigen 2 (IA-2A), and zinc transporter 8 (ZnT8A) (Bingley, 2010). Approximately 70% of patients with T1aDM have three or four of these markers, which typically appear years before symptomatic onset. Analysis of pancreata from patients with T1DM has demonstrated that approximately 70% of islets are completely absent of insulin, with a remaining 20% being inflamed (Keenan et al., 2010). Of the remaining islets, they possess a normal population of other cells (Willcox et al., 2009). Studies have demonstrated that the predominant cell types causing the inflammation of islets are CD8(+) cytotoxic T cells followed by: macrophages (CD68(+)), CD4(+) cells, B lymphocytes (CD20(+)), and plasma cells (CD138(+)).

1.2.4.2 Type II diabetes mellitus

Type II diabetes mellitus (T2DM) is a chronic metabolic disorder with both genetic and environmental factors, the largest being obesity. It is estimated that by 2045, 693 million people will suffer from T2DM (International Diabetes Federation, 2017).

T2DM is predominantly characterised by the onset of insulin resistance due to the

malfunction of various metabolic tissues. Insulin resistance typically precedes T2DM by 10 to 15 years. It is the combination of insulin resistance and pancreatic β cell impairment which results in T2DM. Proinflammatory cytokines have been associated with obesity and insulin resistance. As with T1DM, inflammation of the β cells can lead to impaired insulin production. Reduced insulin production results in hyperglycaemia, which has been associated with oxidative stress and further inflammation (Cerf, 2013). The progression of malfunction in metabolic tissues, which leads to insulin resistance, will be discussed further in following sections.

1.3 Metabolic tissues

Metabolism is a complex system overseen by multiple organs. The development of obesity and insulin resistance is also multifaceted where the synergy of these tissues is disrupted. By understanding how these organs work in the metabolomic system, the intricacies of obesity and insulin resistance can be unravelled.

1.3.1 Pancreas

The primary function of the pancreas for the regulation of energy metabolism is the release of digestive enzymes and pancreatic hormones. The majority of the pancreas is made up of acinar cells which, along with the duct cells, secrete the 'pancreatic juice' composed of amylase, pancreatic lipase, and trypsinogen (Matull et al., 2006). The hormones of the pancreas are released by endocrine cells which cluster together to form the islets of Langerhans which make up only 1-2% of the organ (Baetens et al., 1979; Chandra and Liddle, 2009). Of the population of cells in the islets of Langerhans, glucagon-producing α-cells represent 15-20%; insulin-producing β-cells represent 3-5%; pancreatic polypeptide-producing γ-cells represent 3-5%, somatostatin-producing δ-cells represent 3-10%, and ghrelin-producing ε-cells represent <1% (Katsuura et al., 2002; Brissova et al., 2005).

It is the combination of the blood glucose-increasing glucagon and the glucose-decreasing insulin which facilitates normal glucose homeostasis. The stimulation and release of insulin has been discussed previously in Section 1.2.2. The secretion of glucagon follows a similar pattern in that it is controlled by glucose levels. Hypoglycaemia directly stimulates the pancreatic α cells to release glucagon (Quesada et al., 2006). Secretion of glucagon is facilitated by sodium and calcium channels by maintaining action potentials during hypoglycaemia. Ca^{2+} influx is increased by depolarisation and promotes glucagon secretion, supported by ATP-sensitive potassium channels (Gromada et al., 1997). Glucagon is able to mediate its effects by binding to the glucagon

receptor, expressed mostly in the liver and kidney (Svoboda et al., 1994). As expected, glucagon receptor-null mice have improved glucose tolerance and lower blood glucose levels caused by increased insulin sensitivity. However, prolonged fasting resulted in severe hypoglycaemia (Conarello et al., 2007; Gelling et al., 2003).

1.3.2 Liver

In normal fed conditions, ingested carbohydrates are broken down by glucosidases in the digestive tract to generate mostly glucose. Glucose is transported into tissues to function as the primary fuel in ATP production (Nordlie et al., 1999). This is facilitated via glycolysis where tissues with mitochondria use the catabolism of glucose to pyruvate to generate GTP, NADH and $FADH_2$. These can function in electron transport chain-oxidative phosphorylation, generating ATP (Rui, 2014). The glycolysis system is summarised in Figure 1.4.

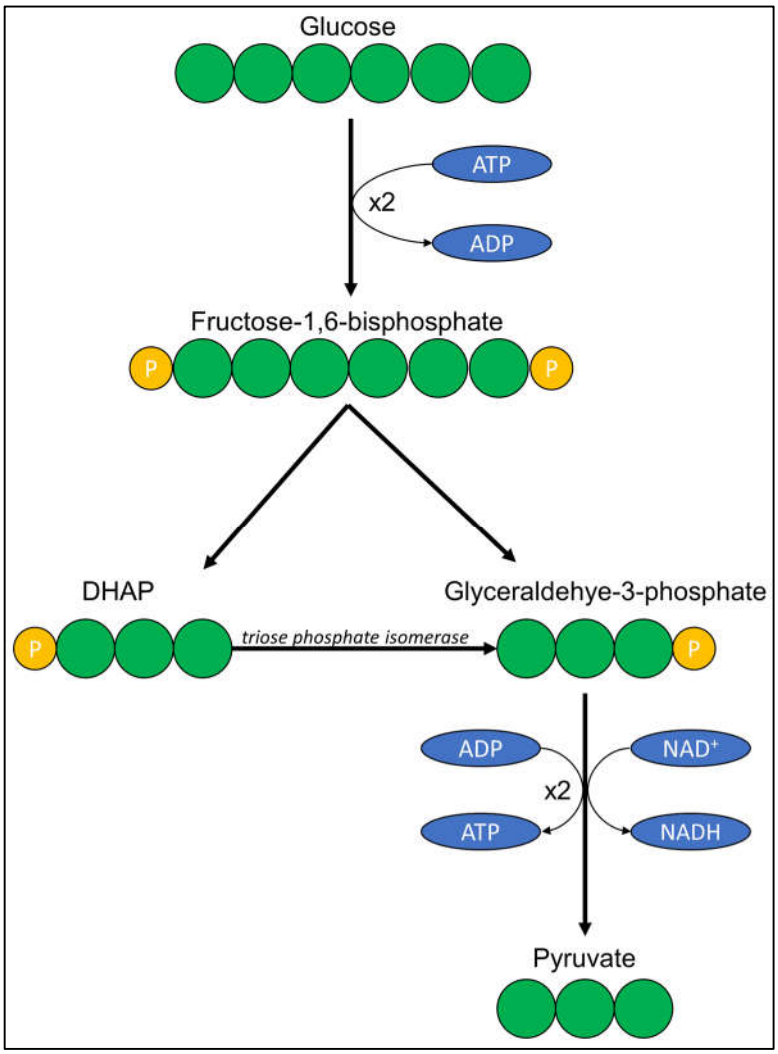

Figure 1.4: Summary of the glycolysis system. One molecule of glucose has two phosphate groups attached to it via ATP to form unstable fructose-1,6-bisphosphate. Fructose-1,6-bisphosphate is broken down to form DHAP and glyceraldegyde-3-phosphate. DHAP is easily converted to glyceraldehyde-3-phosphate by triose phosphate isomerase. From the conversion of two glyceraldehyde-3-phosphate molecules to two pyruvate moles, four ATP and two NADH molecules are generated.

The liver modulates glucose homeostasis by regulating various pathways of metabolism including glycogenesis, glycogenolysis, glycolysis, and gluconeogenesis (Rui, 2014). Energy is stored in the liver in the form of glycogen via glycogenesis in times of glucose and ATP surplus. This synthesis of glycogen from glucose takes place in the cytosol and requires an input of ATP and UTP. The key enzyme in glycogenesis is glycogen synthase, which facilitates the elongation of glycogen chains using one ATP molecule per glucose molecule incorporated into the glycogen chain (Miller and Larner, 1973). The process is promoted by insulin signalling via Akt which phosphorylates and inactivates glycogen synthase kinase-3 (GSK-3), a key inhibitor of glycogen synthase (Fang et al., 2000). The formation of glycogen is critical for maintenance of normal blood glucose concentrations in times of short-term fasting, such as overnight whilst sleeping. The liver typically contains enough glycogen storage for 12-24 hours of fasting (Hers, 1976). Under fasting conditions, glycogen is converted to glucose via glycogenolysis via glycogen phosphorylase. This enzyme is the catalyst which removes glucose residues from glycogen chains, generating glucose 1-phosphate which is further converted to glucose 6-phosphate, via phosphoglucomutase. Glucose 6-phosphate can then be utilised in glycolysis. (Rhyu et al., 1984; Agius, 2015).

As previously mentioned in Section 1.3.1, pancreatic α-cells release glucagon, a fundamental hormone in the regulation of blood glucose concentrations. The majority of glucagon receptors required to mediate the hormone's effects are located in the hepatocytes. During hypoglycaemia, glucagon is released from the pancreas into the blood stream and is able to bind to the glucagon receptor. This results in a conformational change of the glucagon receptor leading to activation of two heterotrimeric G proteins: $G_S\alpha$ and G_q (Burcelin et al., 1996). The activation of $G_S\alpha$ leads to the activation of Protein Kinase A (PKA) via cAMP. PKA has a variety of functions in the liver but it is the main method by which glucagon regulates the production of glucose as summarised in Figure 1.5. Activated PKA phosphorylates glycogen phosphorylase kinase, further activating

glycogen phosphorylase. This results in increased conversion of glycogen to glucose-1-phosphate and glucose-6-phosphate. Studies have also demonstrated that glucagon increases glucose-6-phosphatase activity via PKA-mediated transcription of peroxisome proliferator-activated receptor-γ coactivator-1 (PGC-1), further promoting the conversion of glucose-6-phosphate to glucose (Striffler et al., 1984; Yoon et al., 2001). Furthermore, PKA has been found not only to promote glycogenolysis but also to impede glycogenesis. Glycogen synthase is only active when dephosphorylated, however, PKA is able to phosphorylate the enzyme (Ramachandran et al., 1983). By promoting glycogenolysis and downregulating glycogenesis, glucagon can effectively promote glucose release.

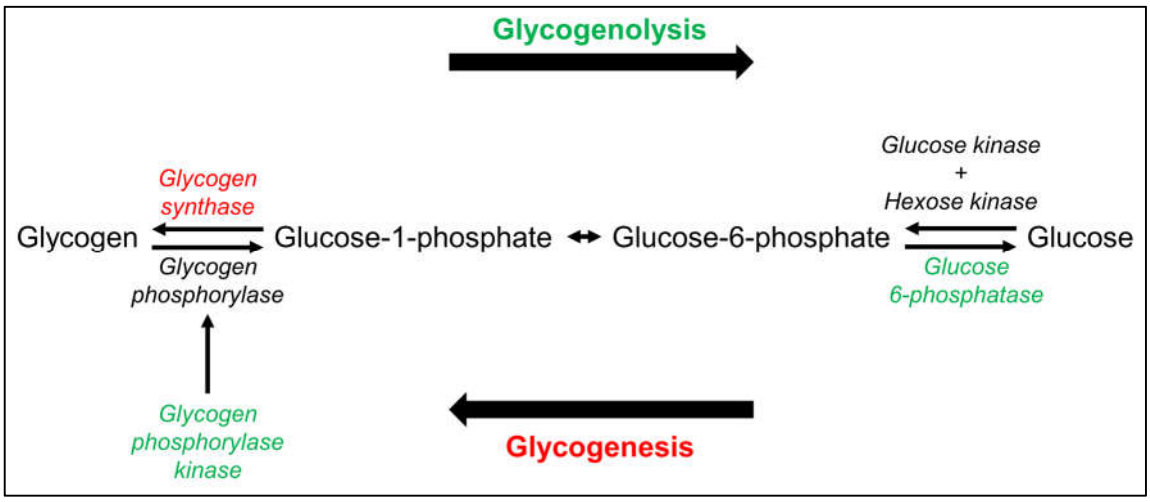

Figure 1.5: Summary of the effects of glucagon on glycogenolysis and glycogenesis in the liver. Glucagon-activated PKA activates glycogen phosphrorylase kinase, further activating glycogen phosphorylase. PKA promotes transcription of proliferator-activated receptor-γ coactivator-1 which results in glucose 6-phosphatase activity. Glycogen synthase is deactivated by glucagon-dependent PKA. Green – Positively regulated by glucagon. Red – Negatively regulated by glucagon (Modified from Jiang and Zhang, 2003).

1.3.2.1 Hepatocyte insulin resistance

Hepatocytes, like most other cells in the body, are vulnerable to becoming insulin resistant. Consequentially, there is decreased suppression of glycogenesis, resulting in increased blood glucose concentrations. Furthermore, this increased glucose in the blood is not taken up by insulin-sensitive tissues.

Mice with hepatocyte-specific deletion of the insulin receptor completely lack the ability to suppress hepatic glucose production via insulin (Michael et al., 2000). Furthermore, these mice had extremely high circulating insulin levels due to impaired insulin clearance and production and resulted in modified insulin-regulated gene transcription, with increased expression of PEPCK, the rate limiting enzyme for gluconeogenesis. Together, the liver plays a paramount role in glucose homeostasis via glucagon and insulin. Slight modifications of the intricate pathways can result in adverse glucose and insulin signalling.

1.3.3 Adipose tissue

Typically, adipose tissue is classified into two subtypes: white and brown. The most abundant form of adipose tissue in mammals is white adipose tissue (WAT) and its primary cell type is the adipocyte. White adipocytes have a single unilocular lipid droplet and few mitochondria, whereas, brown adipocytes are multilocular and abundant in mitochondria (Cedikova et al., 2016) .

The primary function of WAT is the storage and release of lipid/fatty acids in response to metabolic needs. Adipocytes are the primary cell type in adipose tissue and are commonly stored either subcutaneously or viscerally. Subcutaneous white adipose tissues (SWAT) makes up 80% of normal total body fat distribution and is typically found clustered around the abdomen and gluteofemoral regions (Lee et al., 2013b). Alternatively, adipose tissue is stored viscerally as visceral adipose tissue (VAT) which is more commonly associated with metabolic disorders (Kwon et al., 2017). However,

studies have demonstrated that SWAT has beneficial effects on metabolism. Transplantation of SWAT into VAT depots resulted in mice with a decrease in body weight, total fat mass, and glucose and insulin levels. Furthermore, these mice had markedly improved insulin sensitivity (Tran et al., 2008).

1.3.3.1 Adipose tissue and metabolism

White adipocytes mediate energy levels by storage of triglycerides (TGs) and the release of free fatty acids (FFAs). During times of hyperglycaemia, energy is stored as TGs through lipogenesis (Figure 1.6). Elevated glucose levels promote the release of insulin from pancreatic β-cells. Insulin binds to the insulin receptor and facilitates the translocation of GLUT4 and uptake of glucose through phosphorylation of Akt. Once glucose has been transported into the adipocyte, glycolysis takes place. Two of the by-products of glycolysis are acetyl-coenzyme A (acetyl-CoA) and glycerol 3-phosphate which are crucial in lipogenesis. This results in increased production of acetyl-coenzyme A carboxylase (ACC), the rate-limiting enzyme of lipogenesis (O'Callaghan et al., 2001). Although adipocytes can produce FFAs, the majority used in the generation of TGs are taken from the blood stream, which are primarily generated in the liver (Jensen-Urstad and Semenkovich, 2012). To enable hydrolysis of the circulating TGs, lipoprotein lipase (LPL) is released from tissues that oxidise or store fatty acids including muscle and adipose tissue. Strict regulation of the production of LPL occurs as it is rate limiting for plasma TG clearance (Kersten, 2014). The final step in the esterification of FFAs to form TGs uses acyl CoA:diacylglycerol acyltransferase (DGAT). DGAT catalyses the covalent addition of a fatty acyl chain to diacylglycerol. Mice lacking DGAT2, the enzyme specific to adipose tissue, had reduced TG storage in all tissues and died shortly after birth (Harris et al., 2011).

It times of energy needs, adipocytes are able to provide FFAs and glycerol via lipolysis (Figure 1.6). These freed FFAs can be used for energy via oxidation and glycerol can be used for hepatic gluconeogenesis (Kuriyama et al., 2002). Increased glucagon levels

activate PKA via cAMP. Adrenaline is released via the sympathetic nervous system during times of fasting and activates PKA via β-adrenergic receptor activation. (Leiter et al., 1984; Gelinas et al., 2008). TGs are initially converted to diglycerides (DGs) via the enzyme, adipocyte triglyceride lipase (ATGL) (Jiang et al., 2016). The second key enzyme is hormone-sensitive lipase (HSL) which is transported by phosphorylated perilipin, activated by PKA, and hydrolyses DGs to monoglycerides (MGs). MGs are further broken down by monoglyceride lipase into FFAs and glycerol, before being transported to organs which require them (Scalvini et al., 2016).

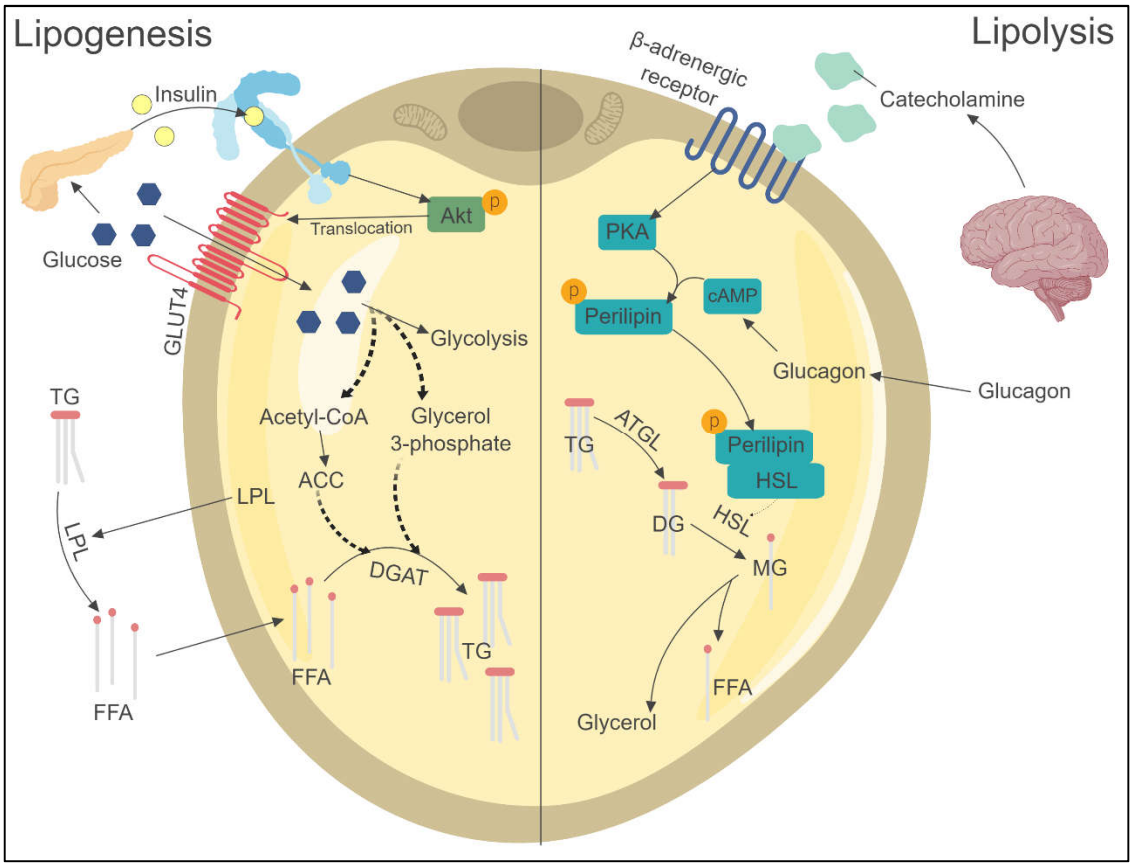

Figure 1.6: Summary of lipogenesis and lipolysis in adipocytes. Triglycerides (TGs) are stored via lipogenesis. Downstream activation of the insulin receptor causes the uptake of glucose via GLUT4. Acetyl-CoA induces the expression of Acetyl-CoA Carboxylase (ACC), a key enzyme in the conversion of free fatty acids (FFAs) to TGs. This is achieved by lipoprotein lipase (LPL) hydrolysing fatty acids from TGs before they are taken up by the adipocyte. These FFAs are converted to TGs via Acyl-CoA:diacylglycerol acyltransferase (DGAT). Lipolysis involves the liberation of FFAs from stored TGs. Downstream activation of catecholamine-activated β-adrenergic receptors phosphorylate perilipin via PKA and cAMP. Perilipin transports hormone-sensitive lipase (HSL) to hydrolyse diglycerides (DGs) to monoglycerides (MGs) before being further broken down into glycerol and FFAs (Adapted from Luo and Liu, 2016).

1.3.3.2 Brown adipose tissue function

The main difference between white and brown adipose tissue (BAT) is whilst WAT stores energy in the form of triglycerides, BAT dissipates energy by generating heat through non-shivering thermogenesis (Figure 1.7). The process is initiated by the binding of secreted adrenaline to β3-adrenergic receptors, located on mature brown adipocytes. Epinephrine is secreted by the adrenal glands during hyperglycaemia and in response to cold exposure (Johnson et al., 1977; Schwartz et al., 1983). β-adrenergic signalling activates cAMP which leads to the activation of PKA (Kim et al., 2014). As discussed in Section 1.3.3.1, PKA can lead to the breakdown of triglycerides to FFAs. Although some FFAs are released, most are shuttled to the mitochondria to act as the substrate for thermogenesis. These fatty acids undergo β-oxidation with released acetyl-CoA being oxidised in the citric acid cycle (Williamson et al., 1969). Usually, the next step would be the movement of protons through ATP synthase to generate ATP. However, non-shivering thermogenesis uses this stream of protons to sacrifice the production of ATP to produce heat via uncoupling protein 1 (UCP1). UCP1 is the key protein responsible for non-shivering thermogenesis and distinguishes WAT from BAT. UCP1 is a member of the mitochondrial carrier protein family and is located on the inner mitochondrial membrane. Its primary function is the uncoupling of proton transport from ATP production to fuel oxidation and the generation of heat (Fedorenko et al., 2012).

It was long thought that non-shivering thermogenesis was specific to BAT until UCP1 was detected in seemingly white adipocytes. However, these adipocytes were found to be of a distinct lineage of white adipocytes. Further studies also demonstrated that exposure of prolonged coldness and β-adrenergic agonist treatment resulted in them becoming more phenotypically brown (Cousin et al., 1992; Loncar, 1991). These unique adipocytes were termed ‘brite’ (brown-like-in-white) and appeared to populate WAT in sub depots (Nedergaard and Cannon, 2014). Several mouse studies have demonstrated the beneficial effects of the induction of brite adipocytes. By increasing the population of

brite adipocytes, mice showed resistance to obesity and improved insulin signalling (Kopecky et al., 1995; Cederberg et al., 2001; Seale et al., 2011). However, to date, no conclusive human studies on an effective method of inducing brite adipocytes has been completed.

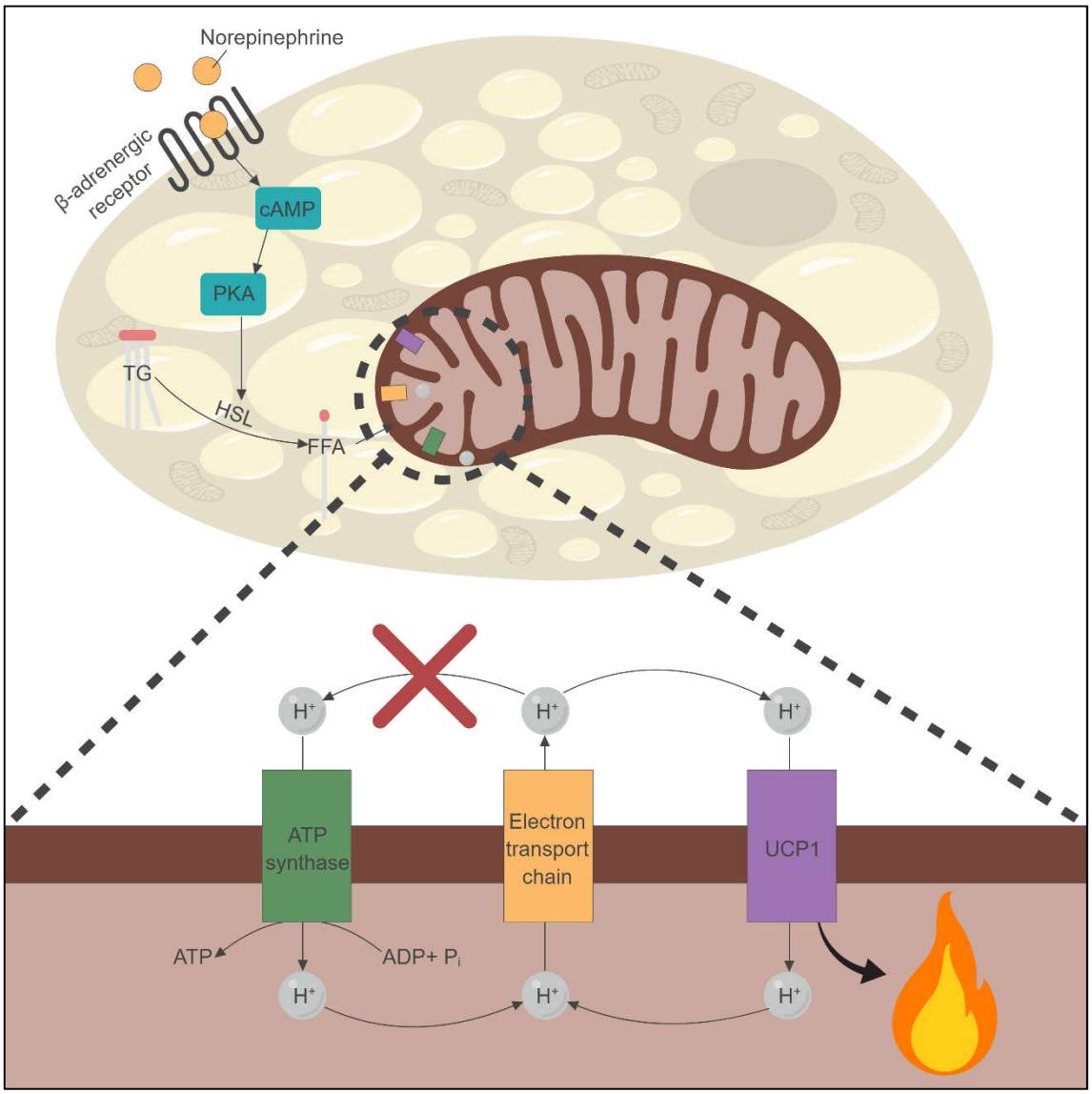

Figure 1.7: Summary of non-shivering thermogenesis pathway in brown/brite adipocytes. The mitochondria of brown and beige adipocytes are abundant in UCP1 (uncoupling protein 1). UCP1 utilises an inducible proton leak to generate heat, decoupling the flow of protons from ATP synthase.

1.3.3.3 Adipose tissue as an endocrine organ

Although adipose tissue is a crucial organ for the regulation of glucose, it has also been recognised as an important endocrine organ. Cytokines produced by adipose tissue, termed 'adipokines', are expressed by the non-adipocyte fraction of adipose tissue, namely resident immune cells. These adipokines have a spectrum of effects and can modulate the immune response, inflammation, glucose metabolism, insulin secretion, vascular growth, adipogenesis, and lipid metabolism (Fasshauer and Blüher, 2015).

One of the primary adipokines secreted by adipocytes is leptin. Leptin is secreted by adipocytes proportionally to their TG levels and has shown to be expressed higher in SWAT than VAT (Fain et al., 2004). Discovered in 1994, leptin was found to be the product of the obese (ob) gene where the primary phenotype was the suppression of satiety (Zhang et al., 1994). Studies demonstrated that those with leptin deficiency (ob/ob) and those with a mutant leptin receptor (db/db) displayed increased food consumption, decreased energy expenditure, and severe obesity.

Leptin mediates its effect on satiety by binding to the leptin receptor in the hypothalamus and influences pathways including the JAK-STAT pathway. The downstream effects of the JAK-STAT pathway include the inhibition of orexigenic neurons and regulating neuropeptides (Bjørbaek and Kahn, 2004). Furthermore, leptin has been shown to directly influence glucose homeostasis by binding to leptin receptor present on pancreatic β-cells, suppressing insulin secretion (Covey et al., 2006).

The other key adipokine secreted by adipocytes is adiponectin. Whereas leptin suppresses insulin production, adiponectin enhances insulin sensitivity (Berg et al., 2001). Adiponectin encourages adipocyte lipid storage, protecting other organs from lipid fat deposition (Fu et al., 2005). It has also been shown to suppress gluconeogenesis by the downregulation of required enzymes (Nawrocki et al., 2006).

1.3.3.4 Adipose tissue and insulin resistance

The link between obesity and insulin resistance has been countlessly reproduced, demonstrating that adipose tissue likely plays a key role in the generation of insulin resistance. The hypertrophic expansion of adipocytes is a normal function to cope with increasing levels of FFAs. By adipocytes absorbing FFAs and storing as TGs, this protects other organs from ectopic fat depositions, causing lipotoxicity. Larger adipocytes are able to deal with an immediate influx of FFAs more efficiently than smaller adipocytes (Johannsen et al., 2014). However, adipocytes have a limit on by how much they can expand. Larger adipocytes can exhibit a hypoxic response resulting in the induction of hypoxic-response genes, oxidative stress, and inflammation (Netzer et al., 2015).

The inflammatory response, caused by hypertrophic hypoxia, results in the invasion of WAT with macrophages (Dicker et al., 2013). These macrophages release a range of pro-inflammatory cytokines but also the promotion of TNFα, which results in further expression of cytokines in preadipocytes (Xu et al., 2003). *In vivo* studies have demonstrated that the neutralisation of TNFα in obese rats results in improved insulin signalling but unfortunately this has not been reproduced in humans (Hotamisligil et al., 1994; Ofei et al., 1996). Chronic inflammation caused by hypoxic adipocytes is likely one of the key nodes in the development of insulin resistance, both locally and systemically.

1.3.4 Skeletal muscle

1.3.4.1 Skeletal muscle as a metabolic tissue

In this section we will discuss the role skeletal muscle has as a metabolic tissue. The structure and function of the tissue will be further discussed in Section 1.4.

Skeletal muscle makes up 40% of total body weight and is responsible for ~80% of insulin-stimulated glucose uptake, therefore it is no surprise that the tissue has a substantial influence on metabolism. Furthermore, as the primary function of skeletal muscle is the generation of force to manipulate the skeleton, it is no surprise that reduced

physical activity is one of the key risk factors in the development of obesity.

The major limiting step for the skeletal muscle to utilise and clear glucose is the translocation of the GLUT4 receptor. Insulin resistance involves the impairment of the IRS-PI3K-Akt pathway, resulting in reduced number of GLUT4 being transported to the cell surface. A number of reasons have been proposed for the generation of insulin resistance specific to skeletal muscle. Ectopic fat deposition in skeletal muscle has been suggested to be a significant contributor to the onset of insulin resistance, as well as decreased mitochondrial oxidative capacity. It has been suggested that this is due to the accumulation of intracellular fatty acyl CoA, diacylglycerol and ceramides (Lowell and Shulman, 2005). This accumulation may result in the decreased activation of PI3K via increased IRS-1 phosphorylation of the serine sites (Morino et al., 2005).

It has also been suggested that the composition of skeletal muscle influences insulin sensitivity dependent on the ratio of type I:II fibres. Studies have demonstrated that patients with insulin resistance and higher blood pressure possess a large number of type II glycolytic fibres compared to type I fibres (Hernández et al., 2001). However, it is unclear how significant the composition of fibres is in comparison to other risk factors.

Oxidative stress has also been proposed as a potential contributor to insulin resistance in skeletal muscle. Skeletal muscle has been shown to overproduce superoxide ions and hydrogen peroxide in insulin resistant models (Blendea et al., 2005). It has been suggested that the major contributor of reactive oxygen species (ROS) is excessive glucose and free fatty acid metabolism via mitochondrial electron leak. Although not specifically tested in myocytes, elevated ROS has been shown to impair insulin-stimulated GLUT4 translocation in adipocytes, possibly via serine phosphorylation of IRS-1 (Rudich et al., 1998).

As previously mentioned when discussing adipose tissue, skeletal muscle is susceptible to the secretion of pro-inflammatory cytokines. One of the key cytokines released by

inflamed, hypoxic adipocytes is TNFα. Studies have demonstrated that chronic inflammation caused by the secretion of TNFα results in insulin resistance in skeletal muscle (de Alvaro et al., 2004). This is most probably caused by the phosphorylation of serine sites on IR or IRS-1.

Many mechanisms have been proposed as to what causes insulin resistance in skeletal muscle. Most probably, it is not due to one cause or one tissue but is in fact due to the malfunction of a variety of processes in many tissues. However, as skeletal muscle is responsible for such a large percentage of insulin-stimulated glucose, it is imperative that further studies elucidate the major mechanisms by which skeletal muscle plays a role.

1.4 Skeletal muscle

In humans, skeletal muscle is responsible for approximately 40% of the total body weight making it the largest organ in the body. Skeletal muscle, as an organ, is not restricted to mechanics via generation of force and movement of the skeleton. It is a complex tissue responsible for a range of metabolic functions and studies have demonstrated that it is responsible for approximately 80% of insulin-stimulated glucose uptake (Thiebaud et al., 1982). In this section, we will discuss development, structure, and function of skeletal muscle.

1.4.1 Development of skeletal muscle

In the developing embryo, skeletal muscle is derived from the somites. Somites originate from the paraxial mesoderm, adjacent to the notochord and neural tube, and progress along the anterior to posterior axis (Christ et al., 2007). Subsequently, they are divided into the ventral sclerotome, which form the vertebrae and ribs, and dermomyotome which gives rise to the skeletal muscle of the trunk and limbs. The first signs of the committed development of muscle tissue (myogenesis) is the activation of myogenic factor Myf5 in some cells of the dermomyotome, termed ‘myoblasts’ (Ott et al., 1991). Developmental myogenesis is split into two phases. Primary myogenesis occurs at approximately E10.5 – 12.5 in mice, where myoblasts positive for transcription factor paired box gene 3 (Pax3) proliferate and fuse to form the primary myotubes (Horst et al., 2006; Lee et al., 2013a). These primary myotubes are multi-nucleated and provide the templates for mature muscle. Secondary myogenesis occurs at E14.5 – 17.5 in mice, where Pax7+ myoblasts fuse to the primary myotubes to form secondary myotubes. These elongate and eventually separate to form multi-nuclear mature muscle fibres. Furthermore, within the mature muscle fibres reside a subset of Pax7+ progenitor cells, which form the adult muscle stem cells, termed ‘satellite cells’. It is these cells which mediate the adult muscle growth and repair (Gros et al., 2005).

1.4.2 Structure of skeletal muscle

Skeletal muscle is composed of parallel-aligned muscle cells, called myofibres, and are surrounded by connective tissue, the endomysium. Myofibres are composed of numerous myofibrils, arranged into the contractile apparatus named the sarcomere. These bundled myofibrils are surrounded by a plasma membrane called the sarcolemma, which is subsequently surrounded by a basement membrane (BM) (Frontera and Ochala, 2015).

Muscle fibres are bundled into fascicles and are surrounded by the perimysium, spanning the length of the muscle. Nutrients essential for function are provide by the large network of arteries, veins, and capillaries throughout the muscle.

Muscles are attached to the skeleton via the tendons. Tendons extend into the muscle, increasing the contact surface area, and form a collagen network with the perimysium (Passerieux et al., 2006). This strong connection permits muscles to transduce force via action potentials, allowing the skeletal muscle to perform its primary function, moving the skeleton.

1.4.3 Function of skeletal muscle

The primary function of skeletal muscle is to transduce force through tendons to the skeleton to enable mobility. The unit which enables contraction is the sarcomere, as shown in Figure 1.8.

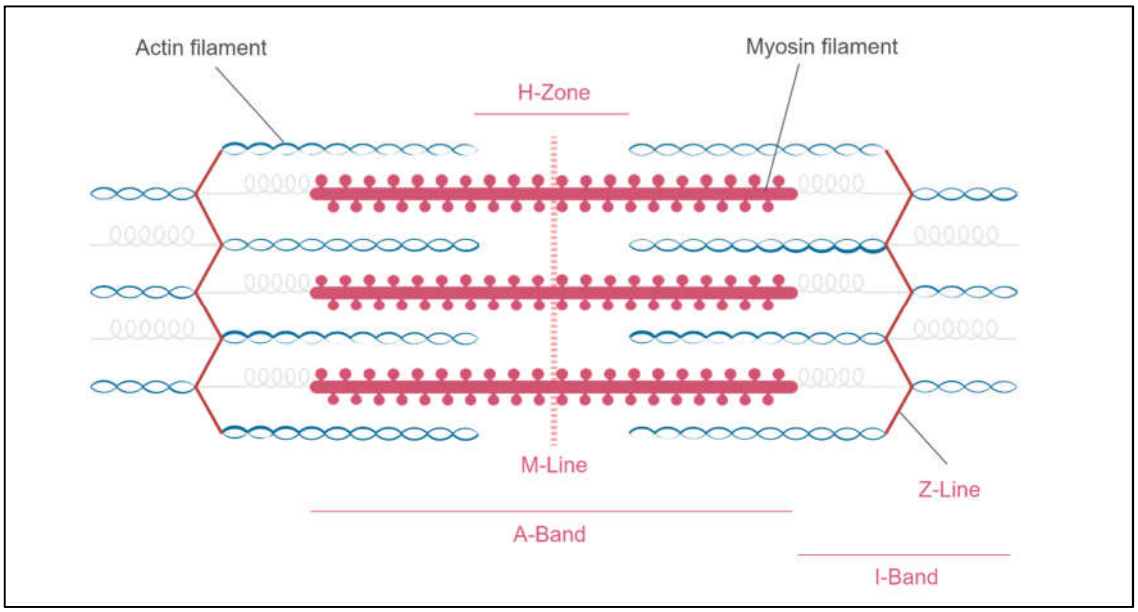

Figure 1.8: Sarcomere unit. Composed of overlapping thick/myosin and thin/actin filaments. The A-band is made up thick filaments which are overlapped on both ends by thin filaments. The H-zone consists of the part of the A-band that thin filaments do not reach. The M-line is a structural unit holding the thick filaments together and is composed of titin, myomesin, obscurin and Obsl1. The I-band is made up the thin filaments that do not extend into the A-band which also contains the darker Z-line.

The sarcomere contracts using a sliding filament mechanism, made possible using the myosin heads found in abundance in thick filaments. During contraction, tropomyosin and troponin go through a conformational change dependent on Ca^{2+}, moving them aside and exposing actin binding sites. Myosin heads bind to actin and go through a conformational change, causing the sarcomere to contract. This causes the H-zone and I-band to become shorter, however, the A-band remains the same size.

However, without strong muscle attachment to the surrounding tissues, this contraction of muscle would be worthless. One major site of force transduction is the myotendinous junction (MTJ), the site where muscle joins with the tendon. Digit-like muscle projections intersperse with the tendon to form a strong bond. This is mediated by the connection of muscle fibres to the basement membrane.

1.4.4 Basement membrane

Basement membranes are a specialised form of extracellular matrix. They were first described in 1840 by Sir William Bowman where he describes them as a highly delicate, transparent and probably elastic sheath surrounding the muscle fibres (Bowman, 1840). Electron microscopy has revealed that the basement membrane is composed of two layers: the basal lamina (Figure 1.9A), which is linked directly to the sarcolemma, and an underlying fibrillar reticular lamina. As shown in Figure 1.9B, the basement membrane is made up of protein networks comprised by laminin and collagen IV (Col IV), with linker proteins such as perlecan and nidogen.

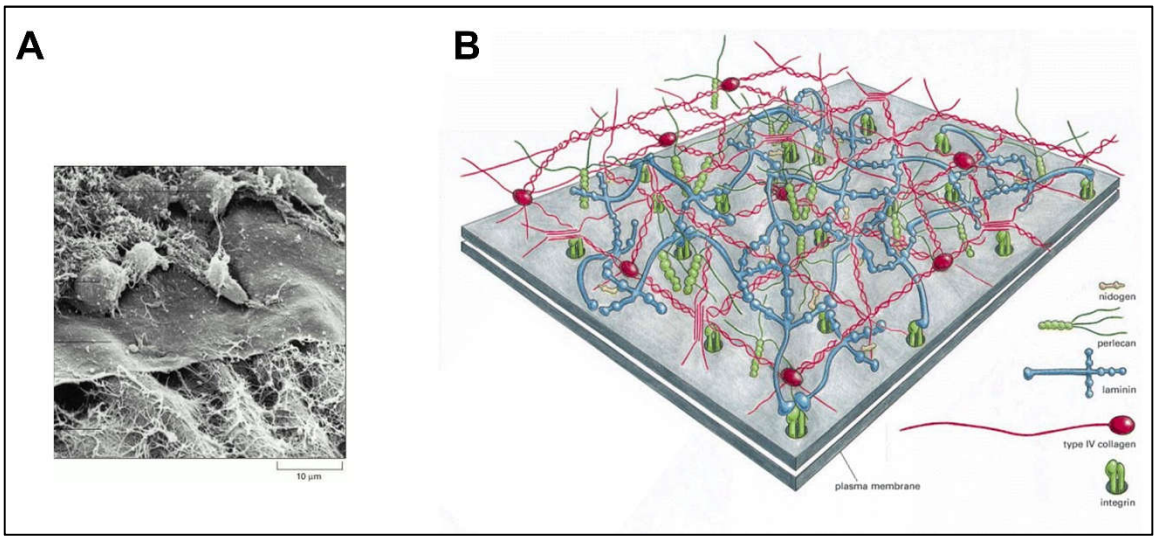

Figure 1.9: Basal lamina. (A) Scanning electron micrograph of basal lamina isolated from chick embryo. Epithelial cells have been removed to expose basal lamina. **(B)** Diagram of the basal lamina with the its individual components. (Adapted from Alberts, 2002).

One of the major constituents of the basement membrane, along with Collagen IV, are laminins comprising a family of heterotrimeric glycoproteins. They are involved in a wide variety of biological functions, including adhesion, differentiation, proliferation, migration, and survival.

Laminins are composed of an α, β, and a γ chain, in the form of a cruciform shape.

Currently, 12 distinct laminin subunits have been discovered, including 5 α, 3 β, and 3 γ chains. By combining these chains in different combinations, unique laminins can be created. The nomenclature of laminins has changed over the years. Isoforms are now named after their combination of α, β, and γ chains and designated, for example, laminin-111 for α1 β1 γ1 (Aumailley et al., 2005).

The most abundant form of laminin in the basement membrane of skeletal muscle is laminin-2 (containing laminin-211 and -221). Although not required for muscle development, laminin-211 is required for muscle integrity. Mutations in the laminin α2 chain (LAMA2) resulted in a congenital muscular dystrophy (Helbling-Leclerc et al., 1995). Patients display muscle and joint weakness, impaired motor development, and nervous system defects (Allamand and Guicheney, 2002). The functions of laminin-211 in skeletal muscle are dependent on its ability to interact with the cell surface. This is achieved through the binding of laminin-211 to the transmembrane receptors.

1.4.4.1 Transmembrane receptors

It is the transmembrane receptors which allow adult skeletal muscle and the extracellular matrix to interact. The two major transmembrane receptors in adult skeletal muscle which link laminin to the basement membrane are the dystrophin-glycoprotein complex (DGC) and integrin α7β1 (which will be reviewed in greater detail in Section 1.5).

The DGC is made up of several transmembrane and peripheral components to form a complex important in maintaining the integrity of skeletal muscle. The protein central to the DGC is dystroglycan, a large transmembrane glycoprotein, binding to laminin-211 in the BM through α-dystroglycan and to the intracellular dystrophin through β-dystroglycan (Ervasti and Campbell, 1993). The link is completed by dystrophin binding to actin, forming a strong bond between the BM and the muscle. In addition to dystroglycan and dystrophin, the DGC is composed of sarcoglycans (α, β, γ, and δ) and sarcospan. It is thought that these help to stabilise the complex, with α and β-sarcoglycan being bound

to β-dystroglycan.

Mutations in the dystrophin gene were one of the first identified causes of muscular dystrophy, and have been identified in both Duchenne muscular dystrophy and the milder Becker muscular dystrophy (Worton and Thompson, 1988). The incidence of Duchenne muscular dystrophy and Becker muscular dystrophy is 1 in 5000 live male births and 1 in 18450, respectively. Duchenne and Becker muscular dystrophies are X-linked, recessive diseases which lead to muscle weakness and degeneration. This can have major detrimental effects on breathing, the cardiac system, and general movement. Unfortunately, at this moment there is no cure for Duchenne muscular dystrophy, but through developing cardiac and respiratory treatments, more patients are surviving into their 30s.

1.5 Integrins

The integrins were named due to their ‘integral membrane nature’ and ‘probable role in the integrity of both the extracellular matrix and the cytoskeleton’ (Tamkun et al., 1986). They are heterodimeric transmembrane adhesion receptors composed of an α and a β subunit. To date, 18 α and 8 β subunits have been discovered, however some of these can be expressed in varying splice forms (Figure 1.10) (Hynes, 2002a). It is the combination of α and β subunits which form unique integrins with varying functions.

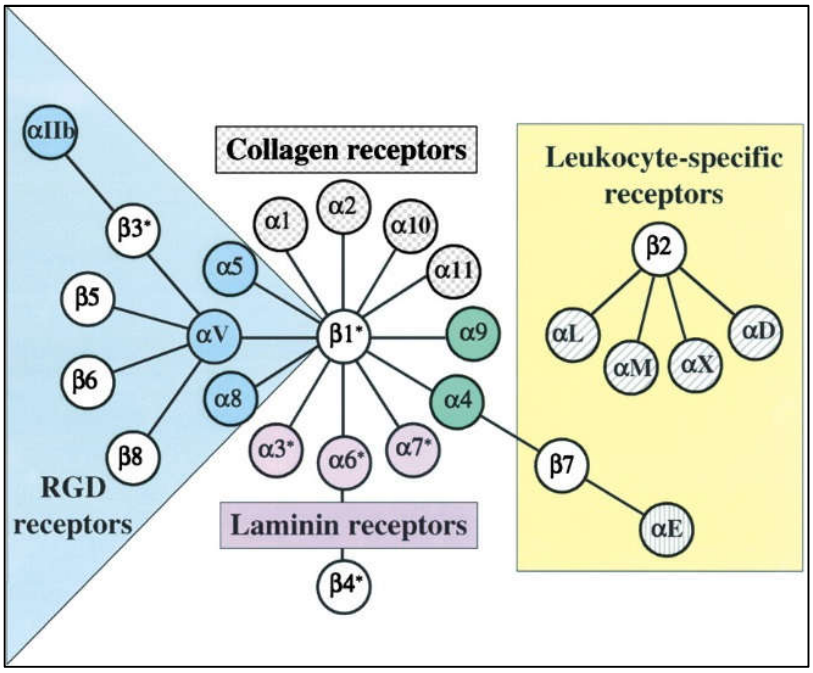

Figure 1.10: The integrin receptor family. Heterodimers composed of combinations of α and β subunits form unique integrins. Here they are classified into ligand specific families. Asterisks denotes subunits which can be expressed in different splice variants. (Taken from Hynes, 2002).

1.5.1 Structure of integrins

The integrin subunits span across the membrane. The extracellular α subunit is made up of a folded seven-bladed β-propeller, a thigh, and two calf domains (Springer, 1997). The seven-bladed β-propeller is present on all variations of the integrin α-subunit, and its upper region contains a ligand-binding domain (Xiong et al., 2002). Furthermore, eight

of the eighteen integrin α subunits possesses an I domain, which contains a metal ion-dependent adhesion site (MIDAS) (Lee et al., 1995). The extracellular β subunit has a domain similarly structured to the I domain, thus named the I-like domain. The I-like domain plays a significant role in ligand binding for the remaining α subunits which don't contain the I domain. The I-like domain is flanked by four EGF-like folds which then terminate with a β sheet domain. The structure of the integrin subunits is depicted in Figure 1.11.

The extracellular and intracellular domains are linked by a transmembrane domains formed of α-helical coiled coils (Adair and Yeager, 2002). The domain is highly conserved in all α and β subunits and is thought to play a key role in the transition from an 'inactive' to 'active' state.

Unlike the extracellular domains, no high-resolution X-ray crystallography of the intracellular domains has been completed. Instead, NMR data has been utilised. At present, there is controversy in the community as to how the intracellular α and β subunits interact with some researchers reporting a coiled coil construct, and some describing a salt bridge (Ulmer et al., 2001; Adair and Yeager, 2002). Although the intracellular domain of α subunits is diverse, the intracellular β subunit contains two well-defined motifs: the membrane proximal NpxY and membrane distal NxxY motifs. These act as sites for PTB domains and are important for signalling (Calderwood et al., 2003).

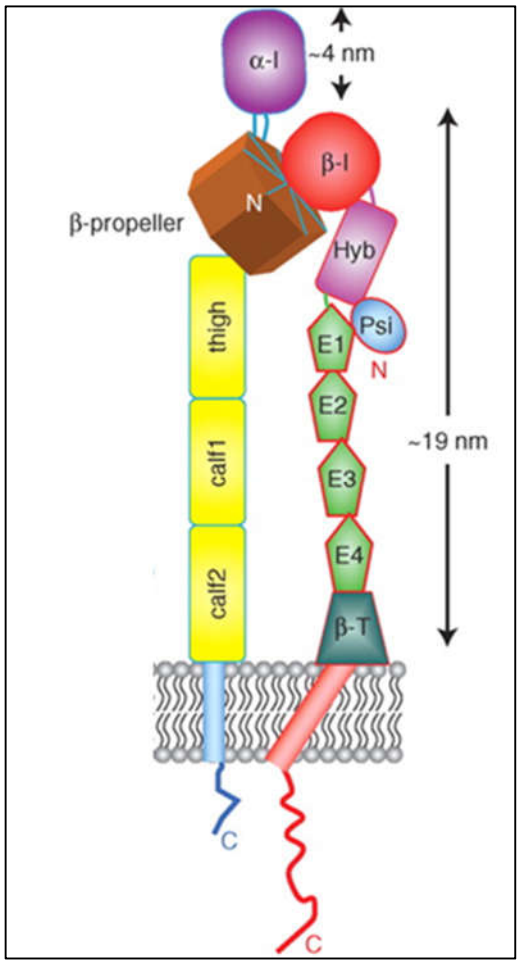

Figure 1.11: Summary of the integrin α- and β-subunit extracellular structure. (Taken from Campbell and Humphries, 2011).

1.5.2 Integrin signalling

Integrins are unique in that they can perform bidirectional signalling. Signals can be transduced from ligand to cell (outside-in) or intracellular stimuli can signal extracellularly (inside-out) as shown in Figure 1.12.

1.5.2.1 Inside-out signalling

Without intracellular stimuli, integrins exist in an inactive state with a bent conformation caused by the intracellular subunits of the integrin being bound together. Activation via intracellular stimuli results in the activation of integrins and causes them to adopt a

straightened and stabilised conformation, allowing binding to their ligand. Two models have been proposed including the 'switchblade model', where integrins are only able to bind to ligands when activated, or the 'deadbolt model' which suggests that the extension of integrins is a result of ligand binding (Xiong et al., 2003; Luo et al., 2007). When integrins are active and bound to ligands, they cluster to form focal adhesions. These focal adhesions allow integrins to convey intracellular signals to the outside.

1.5.2.2 Outside-in signalling

Outside-in signalling can affect cellular growth, differentiation, and apoptosis, as well as other cellular events. However, integrins do not contain any intrinsic kinase activity. To resolve this, integrins rely on phosphorylation events cascaded by recruitment of proteins to their intracellular domains. Two key kinases associated with the intracellular subunits of the β domain are integrin-linked kinase (ILK), and focal adhesion kinase (FAK).

ILK is a component of the ILK-PINCH-parvin (IPP) complex which binds to intracellular integrin β subunits (Legate et al., 2006). The IPP complex acts as a mediator between integrins and the actin cytoskeleton. The activation of the IPP complex is also associated with the phosphorylation of Akt, a key component of the insulin signalling pathway. However, the muscle-specific deletion of ILK results in improved insulin sensitivity in HFD-fed mice (Kang et al., 2016). It is also noteworthy that although ILK was originally dubbed a kinase, recent studies have suggested that ILK may not have intrinsic kinase abilities. Alone, ILK is not able to catalyse phosphorylation but as a component of the IPP complex, this is possible (Ghatak et al., 2013).

FAK is a non-receptor tyrosine kinase which is autophosphorylated by its interaction with intracellular β subunits. This allows FAK to activate paxillin and Grb2/SOS (Hildebrand et al., 1995). Downstream of Grb2/SOS is the MAPK/ERK pathway which leads to the transcription of many genes involved in cell survival and proliferation. FAK is also a well-known activator of PI3K and is therefore associated with the insulin signalling pathway.

The activation of FAK by the β integrin subunit causes PI3K to be recruited to the focal adhesion. This leads to downstream activation of Akt, a major contributor to the translocation of GLUT4.

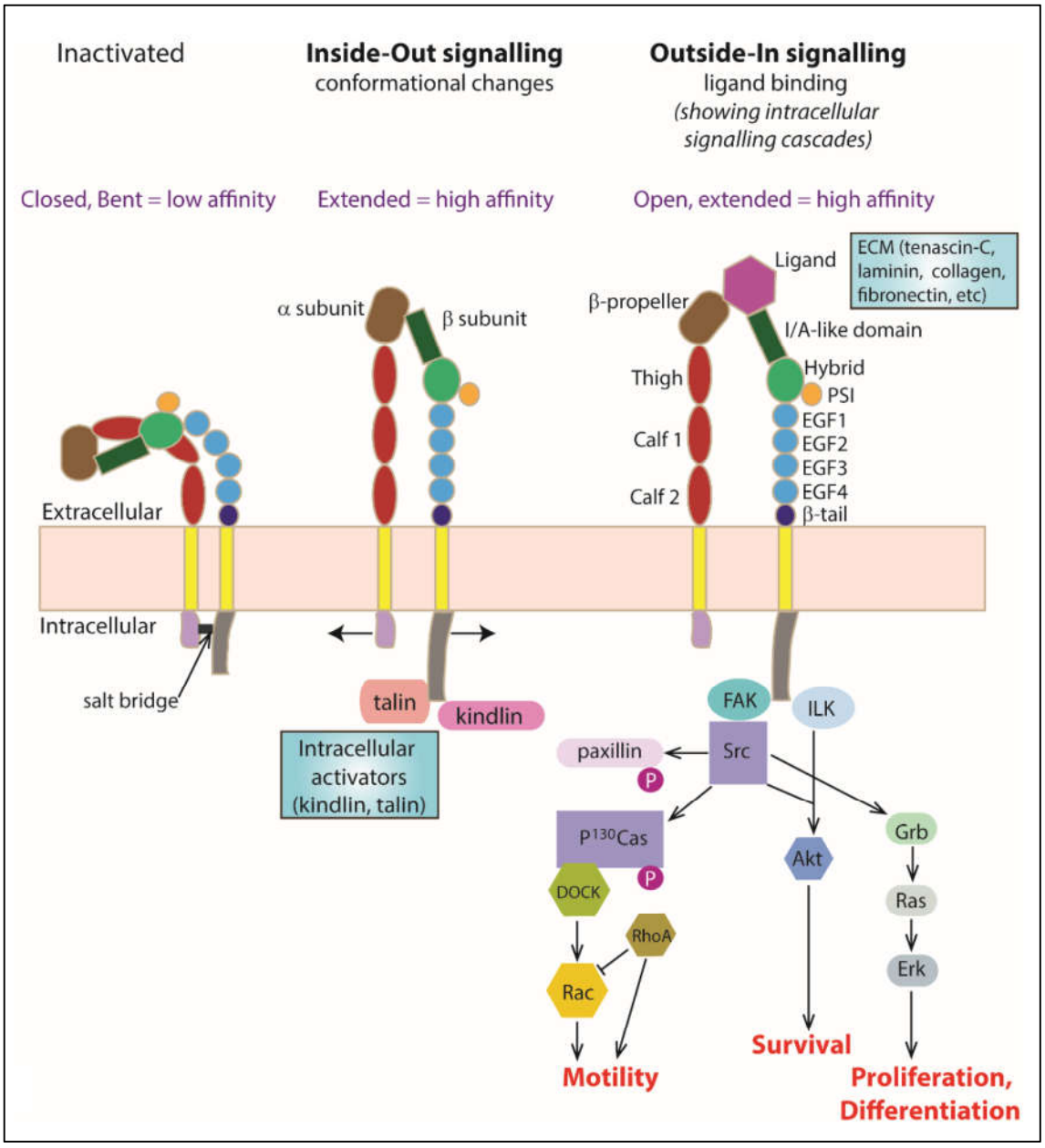

Figure 1.12: Summary of inside-out and outside-in integrin signalling. Inactivated integrins have a closed and bent conformation resulting in low ligand affinity. Inside-out signalling involves intracellular activators binding the β-subunit and causing a conformational change resulting in increased ligand affinity. Outside-in signalling involves conformational changes of the integrin structure due to binding to ligands. (Taken from Cheah and Andrews, 2018).

1.5.3 Integrin expression during skeletal muscle development

During the development and maintenance of skeletal muscle, the pattern of expression of integrins is tightly regulated (Figure 1.13). The integrins are mostly expressed at major areas of muscle function including the costameres, sarcolemma, neuromuscular junction (NMJ), and myotendinous junction (MTJ). However, the combination of α and β subunits varies throughout development.

Either in development or adult skeletal muscle, α4, α5, α6, α7, αv, and β1 subunit expression has been verified. Integrin α4, α5, α6, and αv subunits are expressed during primary myogenesis but are no longer present in adult skeletal muscle. Integrin α4β1 has been shown to mediate myoblast formation, via its ligand VCAM-1 (Rosen et al., 1992).

Integrin α7 is alternatively spliced resulting in two intracellular domains, α7A and α7B, and two extracellular domains, α7X1 and α7X2 (Song et al., 1993; Ziober et al., 1993). These intra- and extracellular splice variants form four unique integrin α7 splice variants. The only β subunit to interact with α7 is β1 which also has two variants, β1A and β1D (van der Flier et al., 1995). Studies have demonstrated that α7X1 and α7X2 are expressed in equal amount in mouse skeletal myoblast and adult cardiac muscle. However, α7X2 is the only extracellular domain expressed in adult skeletal muscle (Ziober et al., 1993). Of the intracellular domains, integrin α7B is the first to be induced in myoblasts and remains expressed throughout development into adult skeletal muscle. Integrin α7A is expressed at terminal differentiation and is weakly expressed in mature skeletal muscle (Yao et al., 1996a). Variance in the expression of integrin β1A and β1D also exists. Integrin β1A is ubiquitously expressed, whereas β1D is specific to skeletal and cardiac muscle. β1A is expressed during muscle development, but then replaced by the expression of β1D shortly after birth (van der Flier et al., 1995; Belkin et al., 1996). This strict patterning of integrins indicates that each subunit possesses distinct roles during the development and maintenance of skeletal muscle.

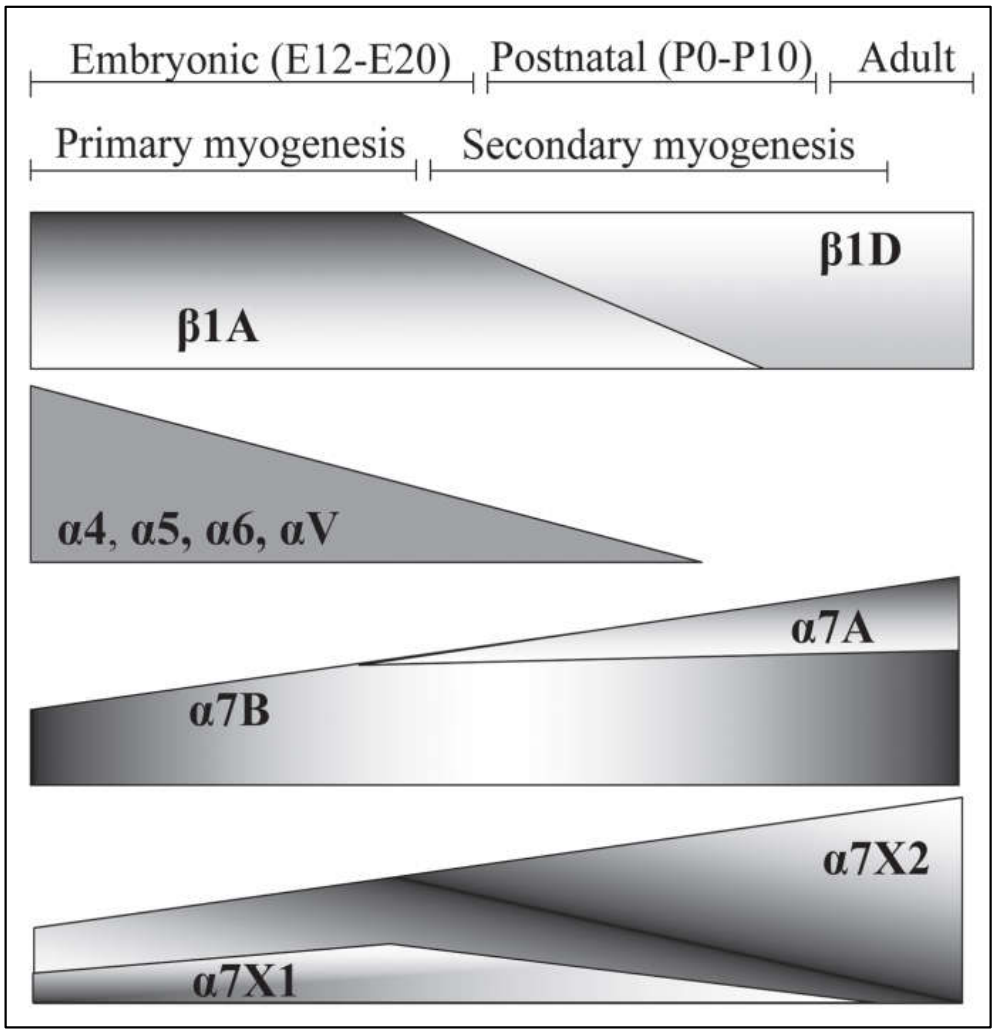

Figure 1.13: Summary of the expression of integrins during skeletal muscle development. During primary myogenesis β1A subunit is predominantly expressed but is reduced during secondary myogenesis and then completely replaced by β1D. Integrin α4, α5, α6, and αv are expressed during primary myogenesis but reduced and undetectable through secondary myogenesis. Integrin α7X1, α7X2 and α7B subunits are present during primary myogenesis. However, during secondary myogenesis, α7X1 is downregulated before being replaced by α7X2. Also, integrin α7A expression begins. (Taken from Rogers and Mayer, 2006).

1.5.4 Integrin α7β1

Integrin α7β1 is the most prominent integrin in adult skeletal muscle, however, it is also detected in cardiac and smooth muscle. The association of skeletal muscle with the basement membrane is paramount for maintaining the sarcolemma and transmitting force from the muscle to the tendon. Integrin α7β1 is part of the team which maintains that link.

The human integrin α7 gene (ITGA7) is composed of 27 exons and is situated on chromosome 12q13, in close proximity to the α5 and β7 subunit genes (Figure 1.14). The generation of different isoforms of integrin α7 is achieved through the splicing of different exons. These exons are homologous with those found in mice. The extracellular domains of integrin α7 are α7X1 and α7X2, which are composed of 1042 and 1038 aa respectively (Vignier et al., 1999). Studies have demonstrated that both integrin α7X1 and α7X2 are expressed in equal amounts in mouse skeletal myoblasts and adult cardiac muscle, however, in adult skeletal muscle it is only α7X2 which is expressed as expression of α7X1 decreases post-secondary myogenesis.

The two major intracellular domains of integrin α7 are α7A and α7B have been identified in humans and mice and are composed of 57 and 76 aa, respectively (Collo et al., 1993; Song et al., 1993). Integrin α7B is the first variant expressed during the development of skeletal muscle and remains expressed through to adulthood. The α7A variant is only induced at terminal differentiation and is then only weakly expressed in adult skeletal muscle.

To date, four different intracellular isoforms have been discovered of the β1 integrin subunit (A-D) in humans. Integrin β1A is the most widely expressed isoform, present in all cell types except red blood cells (Belkin et al., 1996). Integrin β1B has been proposed to act as a negative regulator of cell adhesion during development and β1C inhibits cell growth (Balzac et al., 1993; Meredith et al., 1995). However, neither have been found to

be expressed in mice (Baudoin et al., 1996). Integrin β1D is the most prominent variant expressed in skeletal muscle and is expressed mainly around the junctions of skeletal muscle (Bozyczko et al., 1989)

Surprisingly, no functional difference has been found between the intracellular α7A and α7B subunits (Echtermeyer et al., 1996; Yao et al., 1996b). However, the extracellular α7X2 variant favours binding to laminin-1, whereas α7X1 preferentially binds to laminin-8, although equal affinity has been observed in α7X1 and α7X2 for laminin-2 (Ziober et al., 1997; Von der Mark et al., 2002).

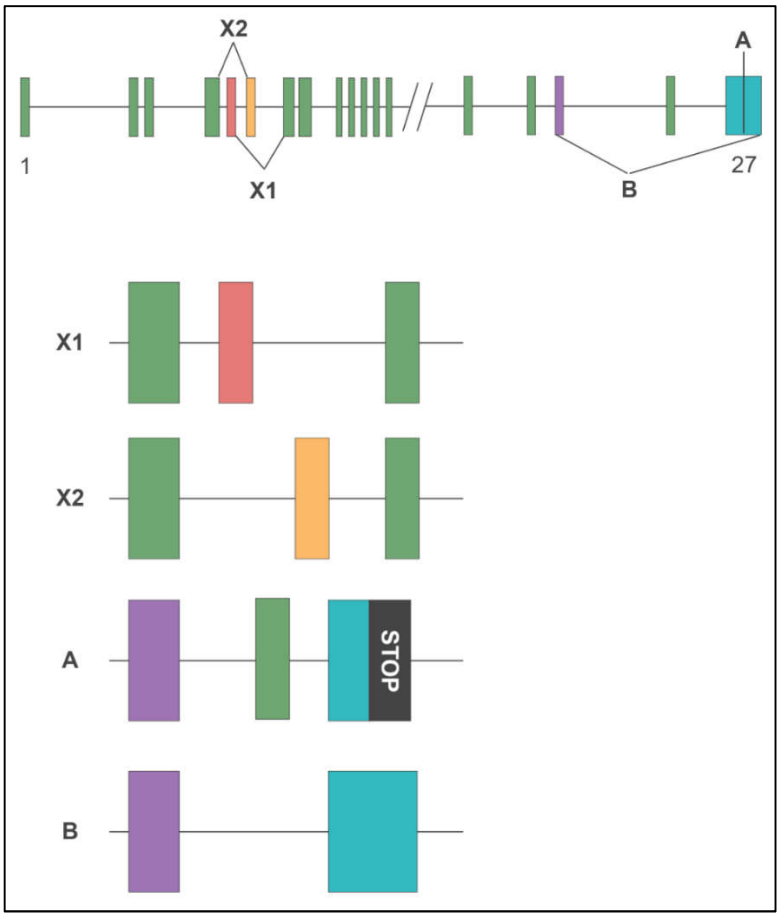

Figure 1.14: The integrin α7 gene and alternative splicing of the integrin α7 domains. Extracellular variant X1 contains exons 4, 5, and 7. X2 contains exons 4, 6, and 7. Intracellular variant A contains exons 25, 26, and 27. However, there is the formation of a stop codon after the first 19 aa of exon 27. Intracellular variant B contains exons 25, and 27 (Adapted from Vignier *et al.* 1999)

1.5.5 Role of integrins in insulin sensitivity

Diet-induced obesity has been consistently shown to be directly related to the onset of insulin resistance and glucose intolerance. Insulin signalling and glucose metabolism is a complex system with a range of organs participating in homeostasis. Increasing numbers of mouse models have been generated to further understand how this system is influenced by the integrins.

One key model in investigating this interaction was the whole-body deletion of integrin α2β1. Integrin α2β1-null mice have improved insulin signalling, when fed a high fat diet compared to control mice (Kang et al., 2011a). Feeding a high fat diet to control mice resulted in increased levels of collagen III, a fibrillar-type collagen, and collagen IV, the main component of the skeletal basement membrane. Researchers believed that the improved insulin signalling in α2β1-null mice would be due to decreased collagen III and IV, but no difference was found compared to controls. However, the authors speculated that improved insulin sensitivity was due to increased muscle vascularisation, as shown by CD31 and von Willebrand factor staining.

In contrast, the muscle-specific deletion of integrin β1 in mice resulted in a significant reduction in the insulin-stimulated glucose infusion rate (Zong et al., 2009). Yet, there was no difference in food intake, weight gain, fasting glucose, nor insulin levels compared to control mice. The study showed that there was no difference in GLUT4 protein expression, but translocation was impaired due to defected insulin signalling via a reduction in Akt phosphorylation.

Skeletal muscle is responsible for the vast majority of insulin-stimulated glucose uptake. However, no studies have investigated the role of integrin α7β1, the main integrin in adult skeletal muscle, in the context of metabolism. We hypothesised that a whole-body deletion of integrin α7 would result in a similar phenotype to that observed in the β1-deficient mice.

1.6 Aims

The role of integrin α7 has been researched extensively in terms of its role in muscle integrity and function, but no research has been completed on its role in metabolism. Studies have demonstrated that integrins can play a significant role in whole-body metabolism and insulin signalling. As skeletal muscle is responsible for approximately 80% of insulin-stimulated glucose uptake, it is imperative that we investigate the role of integrin α7 in metabolism. We used the same whole-body integrin α7 deletion mouse model that has been used in many muscular dystrophy investigations. By using an *in vivo* model, the downstream effects of the deletion of integrin α7 on tissues where it is not expressed can be investigated. In this study, we aimed to answer the following questions:

1) What effect does the deletion of integrin α7 have on insulin sensitivity and glucose tolerance?
2) If the deletion of integrin α7 affects insulin sensitivity, how does it affect the insulin signalling pathway?
3) Can the transgenic overexpression of any of the four splice variants of integrin α7β1 rescue the integrin α7-deficient metabolic phenotype?

CHAPTER 2: MATERIALS AND METHODS

2.1 Mouse lines

2.1.1 Generation of integrin α7 knockout mouse

Mice with a 129Sv background were selected for this study. Publications have demonstrated the varied susceptibility of different mouse strains to insulin-related diseases (Clee and Attie, 2007). C57BL strains have been used in a variety of metabolic-related publications, however, studies have demonstrated that C57BL mice have an innate insulin secretion defect (Kaku et al., 1988; Toye et al., 2005). In contrast, 129 strain mice maintain low insulin levels and are more glucose tolerant than other strains on both a chow and HFD (Almind and Kahn, 2004). Furthermore, obesity-related diseases including non-alcoholic fatty liver disease have been shown to be most consistently represented in 129Sv mice (Fengler et al., 2016).

Integrin α7 deficient mice were produced by previous members of the Mayer laboratory before the start of this study. All splice variants were inactivated by the replacement of the signal sequence of exon one and 107 bp of the mature protein with a neomycin cassette via homologous recombination in embryonic stem cells as previously detailed (Mayer et al., 1997). 129Sv chimeric founder mice were produced using heterozygous embryonic stem cells, before being crossed to generate mice homozygous for the mutated α7 allele (α7KO). Male mice were used throughout this study to remove the variation in metabolism between sexes. Littermates were used as controls to reduce metabolism variation due to genetic background variance.

2.1.2 Integrin α7 splice variant overexpressing transgenic mouse line

Integrin α7 splice variant overexpressing transgenic mice were generated before the start of this study by previous members of the Mayer lab. Integrin α7 subunits were generated from murine myoblast RNA by RT-PCR. The Human Skeletal α-Actin (HSA)

promotor was added 5' to the integrin α7 cDNAs (Brennan and Hardeman, 1993). Linearised DNA was injected into the pronuclei of fertilised mouse embryos before being transferred to pseudopregnant females, generating founder mice. Mice positive for the transgene were detected by PCR using a sense primer hybridising with the HSA promotor.

Mice with similar expression levels of the integrin α7 variants were selected to breed. These overexpressing mice were backcrossed for at least ten generations to the 129Sv background before crossing with heterozygous integrin α7-mutant mice to generate integrin α7-heterozygous mice overexpressing one of the four integrin α7 splice variants. These mice were further crossed with integrin α7-heterozygous mice to generate α7-knockout mice overexpressing one of the four integrin α7 splice variants ($\alpha7\text{-/-}^{TG}$).

2.2 Genotyping animals using Polymerase Chain Reaction (PCR)

To genotype mice, mouse ear biopsies were taken and lysed overnight at $55^{O}C$ in Proteinase K lysis buffer (Table 2.1). Lysate was diluted 1:10 in distilled H_2O and used in PCR. The master mix for the PCR is detailed in Table 2.2. The touchdown programme used in genotyping PCR is detailed in Table 2.3.

Table 2.1: Lysis buffer used for mouse ear/tail biopsy lysis

Reagent	Composition
Proteinase K lysis buffer	0.1M Tris-HCl, 0.2M NaCl, 0.2% (w/v) SDS, 5mM EDTA, 0.1mg/ml Proteinase K

Table 2.2: Master mix for genotyping PCR

Reagents	**Concentration**	**Volume per reaction**
Forward and Reverse primer mix	20pmol per primer	1µl
10x buffer with detergent	100mM Tris-HCl (pH 8.8 at 25^{O}C), 500mM KCl, 0.8% (v/v) Nonidet P40, 15mM $MgCl_2$	5µl
dNTPs	25µM	0.5µl
TOD (1:10 dilution)	Unknown	2µl
Sterile H_2O (Fisher)	N/A	38.5µl
DNA (1:10 dilution)	Unknown	3µl
Total volume		50µl

Table 2.3: Touchdown PCR programme

Denaturation at 95^{O}C for 5 min	
95^{O}C for 1 min	10 cycles
Annealing at 65^{O}C for 1 min (minus 1^{O}C per cycle)	
Extension at 72^{O}C for 1 min	
95^{O}C for 1 min	30 cycles
55^{O}C for 1 min	
72^{O}C for 1 min	
72^{O}C for 10 min	
4^{O}C for 15 min	

Table 2.4: Oligonucleotides used for genotyping PCR

Primer Number	Description	Sequence
1	A7 – 981.rev	CCA GAA TCG ATG GAG AAA CC
5	A7 – 3588.rev	GAT CGT CGA CTC TAG AAG ATG TTA GGC AGT GGC TGG
6	A7 – 3206.seq	CTC AGA GAT GCA TCC ACA GTG
7	A7 – 719.seq	TTC TGT GAG GGG CGC CCC CAG
12	HSA.seq	GCA CTA CCG AGG GGA ACC TG
43	A7.39.seq	GAG GGG TGC TGA GGT GAA AG
44	A7.264.rev	GCC GGT GGT AAG AAC AGT CC

2.2.1 Agarose gel electrophoresis

PCR products were mixed with 5x Orange G loading dye and loaded into 2% agarose gels, submerged in 1x TAE buffer (Table 2.5). Gels were run at a constant voltage of 150V for approximately 40 minutes. Gels were then stained with 0.5µg/ml ethidium bromide for approximately 30 minutes before visualising in a UV trans-illuminator (UVP ChemiDoc-It®2 810 Imager).

Table 2.5: Composition of reagents needed for gel electrophoresis

Reagent	Composition
50x TAE buffer	40mM Tris acetate, 2mM EDTA (pH 8.5)
5x Orange G loading dye	25ml glycerol, 5ml 10x TAE buffer, 0.25g Orange G powder, 50ml H_2O

2.3 Animal maintenance

Mice were housed and handled within Home Office guidelines. All mice were contained

in individually-ventilated cages. Routine screens for contamination were completed.

Mice were ear tagged and genotyped using ear biopsies. Unrequired mice were culled using a Schedule 1 approved method. Animals were separated by sex and housed until needed.

2.4 Animal diet and food intake

Under normal conditions, male mice were fed a chow diet (Rat and Mouse No.3 Breeding, Special Diets Services). When 3 months old, animals were selected to either continue eating a chow diet or to be switched to a high fat diet (D12451, Research Diets Inc.) (Table 2.6). High fat diet pellets were weighed before being given to mice and then weighed after a week to measure food intake.

Table 2.6: Breakdown of nutritional value of high fat diet

		gm%	**Kcal%**
Protein		24	20
Carbohydrate		41	35
Fat		24	45
	Total		100
	kcal/gm	4.73	

2.5 Metabolic tests

Intraperitoneal insulin and glucose tolerance tests were conducted initially on mice at 3 months of age. Mice were then either fed a 45% fat diet or continued with a standard breeding chow. Details can be found in section 2.4.

2.5.1 Intraperitoneal insulin tolerance test (IPITT)

Mice were moved to a clean cage with no food, access to water *ad libitum*, and fasted for 6 hours. A basal glucose reading was measured by making a small pin prick incision at the tip of the tail and reading with a glucose meter (Alphatrak 2). Mouse weights were recorded and were then intraperitoneally injected with 0.75 U/kg of human insulin (Sigma) diluted in sterile phosphate-buffered saline (PBS). Further glucose readings were measured using the same method at 15 minutes, 30 minutes, 60 minutes and 120 minutes. Mice were then given food and water *ad libitum* as before.

2.5.2 Intraperitoneal glucose tolerance test (IPGTT)

Mice were moved to a clean cage with no food, access to water *ad libitum*, and fasted for 16 hours. A basal glucose reading was measured by making a small pin prick incision at the tip of the tail and reading with a glucose meter. Mouse weights were recorded and were then intraperitoneally injected with 2 g/kg of 20% glucose solution (Sigma) in sterile PBS. Further glucose readings were measured using the same method at 15 minutes, 30 minutes, 60 minutes and 120 minutes. Mice were then given food and water *ad libitum* as before.

2.6 Dissection of mice

Mice were sacrificed, and confirmed, via a Schedule 1 approved method, according to Home office guidelines. The tibialis anterior (TA) and gastrocnemius (GC) muscles were isolated and removed. For histological analysis, muscles were pinned onto parafilm to prevent contraction before being frozen in liquid nitrogen-cooled isopentane. For protein analysis, they were snap frozen in liquid nitrogen.

Adipose tissue depots were isolated, weighed and dehydrated in increasing concentrations of ethanol. Dehydrated adipose tissue was embedded in paraffin wax for sectioning. Alternatively, adipose tissue was snap frozen for protein analysis.

2.7 Histology

2.7.1 3'aminopropyl-triethocy silane (TESPA) coating of slides

To aid tissue adhesiveness to slides, slides were coated with TESPA (Sigma) as shown in Table 2.7. Slides were dried in a 55^{O}C incubator and then stored at room temperature until required.

Table 2.7: Method of TESPA coating slides

Reagent	Incubation time
Acetone	30 secs
2% TESPA in acetone	1 min
Acetone	Quick immersion
Acetone	Quick immersion
ddH_2O	Quick immersion

2.7.2 Post fixation of liver for cryosectioning

Livers were fixed, post dissection, in 4% paraformaldehyde solution in PBS for four hours at 4^{o}C. Tissues were rinsed in PBS overnight at 4^{O}C to remove excess paraformaldehyde. Livers were then incubated in 5% sucrose in PBS solution for four hours before being replaced with 20% sucrose solution in PBS overnight. Tissue was then frozen in Optimal Cutting Temperature (OCT) compound in moulds on dry ice.

2.7.3 Paraffin embedding of adipose tissue

Adipose tissue was fixed in 4% paraformaldehyde/PBS for four hours at 4^{o}C. Tissue was rinsed in PBS overnight at 4^{O}C to remove excess paraformaldehyde. Adipose tissue was then dehydrated and embedded in paraffin wax as shown in Table 2.8. Adipose tissue was then cast, using an embedding station (Microm EC350-2), in moulds filled with paraffin wax and allowed to harden on a cool plate. Paraffin blocks were then stored at

4^{O}C before being sectioned on a microtome (Microm HM355S).

Table 2.8: Paraffin embedding protocol

Reagent	Time tissue immersed
30% ethanol	30 mins
50% ethanol	30 mins
70% ethanol	1 hour
90% ethanol	1 hour
95% ethanol	1 hour
100% ethanol	3 x 30 mins
Histo-clear (xylene substitute)	3 x 20 mins
Paraffin wax (60^{O}C)	2 x 2 hours

2.7.4 Cryosectioning

Frozen tissue was mounted onto a specimen holder using OCT. The specimen was maintained at a temperature of -24^{O}C, whilst the blade was maintained at -26^{O}C. Sections were cut 10µm thick and were collected on TESPA-coated slides. Four sections were collected on a single slide with every fifth being collected on a separate slide. The latter slide was used to gain an overall representation of the tissue.

2.7.5 Microtome sectioning

The microtome was filled with dH_2O warmed to 42^{O}C. Paraffin blocks were secured on the pre- cooled holder and were then sectioned 10µm thick. Slides were left to air dry before being stored at room temperature.

2.7.6 Hematoxylin and Eosin staining

Mayer's hematoxylin (Merck) was prepared by dilution 1:1 in dH_2O. A 0.1% (w/v) Eosin Y (Acros Organics) solution was prepared in dH_2O with a few drops of glacial acetic acid.

Solutions were filtered before use.

If using paraffin embedded sections, slides were de-waxed in histo-clear (National Diagnostics) for 5 minutes. Sections were then rehydrated through descending concentrations of ethanol solutions.

Slides were immersed in Mayer's hematoxylin for 2 minutes before being submerged in flowing tap water for 10 minutes. Slides were then immersed in eosin for 30 seconds before being dehydrated through ascending concentrations of ethanol. Slides were submerged in fresh histo-clear twice for 7 minutes before being mounted with cover slips using DPX (Fisher). Slides were left to dry at room temperature and were then stored.

2.7.7 Oil Red O staining

Oil red o stock solution was prepared by dissolving 500mg of oil red o (Sigma) in 100ml of isopropanol overnight at room temperature. To make the working solution, 30ml of the prepared oil red solution was diluted in 20ml of dH_2O and filtered with a 0.2µm filter.

Sections were fixed with 4% PFA at room temperature for 10 minutes. Slides were immersed in running tap water for 5 minutes and rinsed with 60% isopropanol. Slides were submerged in working oil red o solution for 8 minutes at $55^{O}C$. Sections were then rinsed with 60% isopropanol and counterstained with hematoxylin solution for 1 minute. Slides were immersed in running tap water for 10 minutes and mounted with cover slips using gelvatol mounting medium.

2.7.8 LipidTOX staining

LipidTOX stain working solution was prepared 1:500 in PBS and kept on ice until needed.

Every fifth section of tissue was captured on a slide to gain a better overall representation of the tissue resulting in 16 sections being captured. Sections were fixed with 4% PFA at room temperature for 10 minutes. Slides were washed 3 x 5 minutes in PBS. Sections

were incubated with LipidTOX working solution overnight at 4^{O}C overnight in the dark followed by 3 x 5 minute PBS washes and mounted with cover slips using gelvatol mounting medium.

2.7.9 Preparation of gelvatol mounting medium

A 10ml solution of 0.1M KH_2PO_4 was adjusted with a 0.1M solution of $Na_2HPO_4.H_2O$ until the pH was 7.2. Of the resulting solution, 80ml was used to dissolve 0.64g of NaCl (0.14M) and 20g of polyvinylalcohol (Gelvatol, Type II, cold water soluble, Sigma P-8136) and left to mix overnight at room temperature. To this solution, 40ml of glycerol (Sigma) was added and was left to mix for a minimum of 16 hours. The solution was centrifuged at 12000 RPM for 15 minutes. The supernatant was decanted before ensuring the pH ranged between 6-7. The anti-bleaching agent, DABCO (Sigma), was added at a concentration of 25µg/ml. Syringes were filled with the final solution and stored at -20^{O}C until required for mounting.

2.8 Microscopy

2.8.1 Imaging of muscle, liver and adipose tissue sections

A Zeiss AxioPlan 2ie microscope was used to visualise sections. Brightfield or fluorescent images were captured using a 10x or 20x PlanNeofluar objective (0.6NA) and a Zeiss AxioCam HRm or HRc camera.

Adipocyte size was calculated using the minimum Feret diameter and is the minimum distance between two parallel tangents of a shape, as shown in Figure 2.1. A standardised method of measurement has not been agreed on for measuring adipocytes. We tested different methods of measuring adipocytes including area, perimeter, minimum Feret diameter and maximum Feret diameter. By taking multiple sections of the same adipocyte and calculating the average measurement across sections it was found that minimum Feret diameter had the smallest variance and error (data not shown).

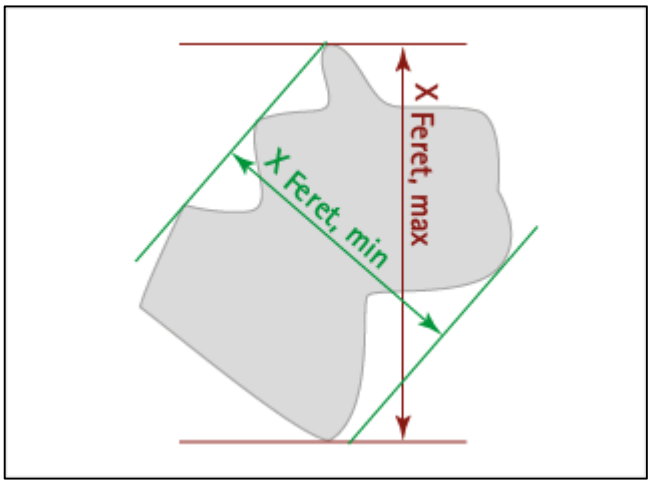

Figure 2.1: Depiction of minimum and maximum Feret diameter (Taken from Sympatec, 2008).

2.9 Blood analysis

2.9.1 Blood collection and serum isolation

Blood was isolated from cervically dislocated animals by snipping the posterior of the heart. Samples were kept at 4^{O}C overnight to allow clotting before spinning at 1,300 RCF at 4^{O}C for 15 minutes. The supernatant/serum was isolated from centrifuged samples, snap frozen in liquid nitrogen and stored at -80^{O}C until required.

2.9.2 Alanine Transaminase (ALT) and Aspartate Transaminase (AST) assay

Alanine Transaminase (ALT) and Aspartate Transaminase (AST) levels were measured in mouse serum samples using a Randox kit and analyser (Daytona) according to the manufacturer's instructions. This work was kindly completed by the Vauzour Laboratory, Norwich Research Park.

2.9.3 Bile acid analysis

Solid phase extraction was conducted on serum samples using Oasis Prime hlb (30 mg)

extraction cartridges (Waters) according to the manufacturer's instructions. Extracted bile acids were analysed via liquid chromatography-mass spectrometry. This work was kindly completed by the Vauzour Laboratory, Norwich Research Park.

2.10 Western blot analysis

2.10.1 Protein extraction from tissue

A standard RIPA lysis buffer (10mM Tris-Cl, 1mM EDTA, 0.5mM EGTA, 1% Triton X-100, 0.1% sodium deoxycholate, 0.1% sodium dodecyl sulphate (SDS), 140mM NaCl, 1x cOmplete™ ULTRA protease inhibitor cocktail (Sigma), 1x PhosSTOP phosphatase inhibitor cocktail (Sigma)) was used to lyse tissue for immunoblotting.

Gastrocnemius (GC) muscle was isolated post dissection and snap frozen in liquid nitrogen. Tissue was stored at -80^{O}C until required for protein extraction. Frozen tissues were transferred to 2ml snap-cap Eppendorf tubes with 1ml of ice-cold RIPA lysis buffer. A metal bead was added to the tube before being homogenised in a TissueLyser II (Qiagen) at 30 Hz for 8 mins at RT. Lysates were left on ice for 15 minutes before being centrifuged at 4^{O}C for 5 minutes at 14,000 RPM. The supernatant was removed before centrifugation again. The supernatant was collected and either used immediately or aliquoted and frozen on dry ice before storing at -80^{O}C.

2.10.2 Quantification of protein concentration in lysates

The bicinchoninic acid (BCA) protein assay (ThermoFisher) was used to determine protein concentration in tissue lysates. Tissue lysate samples were diluted in RIPA buffer (1:10) to give a final volume of 25µl. Protein standards were made by diluting bovine serum albumin (BSA) in RIPA lysis buffer (0-2000µg/ml). The BCA working solution was made by mixing 50 parts of solution A with 1 part solution B. To a 96 well plate, 25µl of the diluted tissue lysates and protein standards was transferred to a well. To each sample, 200µl of BCA working solution was added before being incubated at 37^{O}C for

30 minutes. The optical density of each sample was measured at 570nm using a VersaMax microplate reader (Molecular Devices). Samples were prepared in duplicate to obtain the average optical density. The standard curve was plotted of the protein standards and the gradient was used to calculate the value of the tissue lysate protein concentrations.

2.10.3 Preparation of SDS-polyacrylamide gels and samples

Glass plates were cleaned with 70% ethanol and rinsed with water before being stacked into gel chambers with 0.75mm spacers. Resolving gels (Table 2.9) were poured into the gel chambers and were levelled by pipetting a 200µl of water-saturated butanol on top. Gels were left at room temperature for 1 hour to allow to polymerise.

Once the resolving gels had polymerised, the water-saturated butanol was poured off and gels were rinsed with distilled water. Stacking gels (Table 2.9) were poured over the resolving gels and well combs were slotted in until complete polymerisation. Gels were stored in their chambers in a sealed box with a damp piece of tissue at $4^{O}C$ until required.

Table 2.9: Components of resolving SDS-polyacrylamide resolving and stacking gels

	Resolving gel					**Stacking gel**
Components	6%	8%	10%	12%	15%	5%
H_2O	2.6ml	2.3ml	1.9ml	1.6ml	1.1ml	680µl
30% acryl-bisacrylamide mix	1.0ml	1.3ml	1.7ml	2.0ml	2.5ml	170µl
1.5M Tris (pH 8.8)	1.3ml	1.3ml	1.3ml	1.3ml	1.3ml	-
1.5M Tris (pH 6.8)	-	-	-	-	-	130µl
10% SDS	50µl	50µl	50µl	50µl	50µl	10µl
10% ammonium persulphate	50µl	50µl	50µl	50µl	50µl	10µl
TEMED	4µl	3µl	2µl	2µl	2µl	1µl

Samples were prepared for loading onto SDS-polyacrylamide gels by diluting in water and 2x Laemmli sample buffer (4% SDS, 20% glycerol, 10% 2-mercaptoethanol, 0.004% bromophenol blue, 0.125M Tris-HCl) to give the required protein concentration. Samples were heated at 95^{O}C for 5 minutes, cooled and loaded onto SDS-polyacrylamide gels.

2.10.4 Immunoblotting

Samples were prepared with 30µg of muscle lysate in 1x sample buffer and denatured at 95^{O}C for 5 minutes under reducing conditions by the addition of 5% β-mercapterethanol. SDS poly-acrylamide gels were cast depending on weight of protein desired. Samples were loaded into gels and were separated at 150V. Biorad broad range molecular range marker was used as a protein standard. Proteins were transferred onto PVDF membranes in 10mM sodium borate overnight at 200mA overnight at 4^{O}C. Membranes were blocked in 5% NGS in PBS for 2 hours at RT. Appropriate primary antibody (Table 2.10) was diluted as per manufacturer's instructions in 2% NGS in PBS-T and incubated with blocked membranes overnight at 4^{O}C. Membranes were washed and incubated with the desired housekeeping antibody for 1 hour at RT. Membranes were washed and incubated with diluted secondary antibody conjugated to horseradish peroxidase (Table 2.11). Further washes were completed in PBS-T before a final in PBS. Protein bands were visualised with Pierce ECL Western Blot substrate as per manufacturer's instructions (Thermo).

Table 2.10: Primary antibodies used for Western blotting

Protein of interest	Primary antibody	Dilution	Manufacturer
Heat shock protein 70	HSC 70 Antibody (B-6): sc-7298 mouse mAb	1:10,000	Santa Cruz Biotechnology, Inc
Akt/Protein kinase B	Akt Antibody Rabbit pAb (#9272)	1:1,000	Cell Signaling Technology
Phospho-Akt (Ser473)	Phospho-Akt (Ser473) (D9E) XP® Rabbit mAb (#4060)	1:1,000	Cell Signaling Technology
Phospho-Akt (Thr308)	Phospho-Akt (Thr308) (244F9) Rabbit mAb (#4056)	1:1,000	Cell Signaling Technology
P44/42 MAPK (ERK1/2)	P44/42 MAPK (Erk1/2) (137F5) Rabbit mAb (#4695)	1:1,000	Cell Signaling Technology
Phospho-p44/42 MAPK (ERK1/2) (Thr202/Tyr204)	Phospho-p44/42 MAPK (Erk1/2) (Thr202/Tyr204) (197G2) Rabbit mAb (#4377)	1:1,000	Cell Signaling Technology

Table 2.11: Secondary antibodies used for Western blotting

Secondary Antibody	Dilution	Manufacturer
Goat Anti-Rabbit IgG (H + L)-HRP Conjugate (#1706515)	1:3,000	Bio-rad
Anti-Mouse IgG (whole molecule)-Peroxidase. Produced in Goat, IgG Fraction of Antiserum (#A5278)	1:3,000	Sigma

2.10.5 Quantification of immunoblot

ECL stained membranes were visualised using a Molecular Imager ChemiDoc XRS+ Imaging System (Bio-rad). Protein bands were quantified using densitometry using Image Lab™ software (Bio-rad). Image Lab™ indicates when exposed images are overexposed. Proteins of interest were normalised against housekeeping bands to calculate relative levels.

2.11 Metabolomics

2.11.1 Faeces collection and sample preparation

Freshly defecated faecal pellets were collected weekly and snap frozen. Pellets were diluted 1:10 in pre-reduced PBS. Pre-reduced PBS was generated by storing PBS in an anaerobic chamber overnight. Samples were vortexed for 60s to obtain a faecal slurry. Samples were centrifuged at 16000 RCF for 15 minutes at 4^{O}C. In an Eppendorf tube, 90µl of supernatant and 810µl of PBS were added before finally adding 100µl of NMR buffer (Table 2.12). Samples were vortexed briefly before being frozen at -20^{O}C until analysis.

Table 2.12: Composition of NMR buffer used in lysis of faecal pellets

Reagent	Composition
NMR buffer	0.26g NaH_2PO_4, 1.44g K_2HPO_4, 17mg TSP, 56.1mg NaN_3, 100ml D_2O

2.11.2 NMR protocol

High resolution 1H NMR spectra were recorded on a 600 MHz Bruker Avance spectrometer fitted with a 5 mm TCI cryoprobe and a 60 slot autosampler (Bruker). Samples were maintained at 300 K. Metabolites were identified using the Human Metabolome Database (www.hmdb.ca) and quantified using Chenomx® NMR Suite 7.0™. This work was kindly completed by the Vauzour Laboratory, Norwich Research Park.

CHAPTER 3: INSULIN SENSITIVITY AND TISSUE HISTOLOGY IN INTEGRIN A7 DEFICIENT MICE

3.1 Introduction

Integrin α7β1 is the most abundant integrin in adult skeletal muscle. It is located along the sarcolemma but is highly enriched around the myotendinous junction and neuromuscular junction (Bao et al., 1993). Integrin α7β1 has been shown to play a fundamental role in muscle development and function, as well as a role in differentiation and migration processes during myogenesis (Song et al., 1993). Absence of integrin α7 leads to a progressive muscular dystrophy starting shortly after birth and is located mainly in the soleus muscle and affects mainly the myotendinous junction (Mayer et al., 1997).

Previous studies have shown integrins to play a key role in insulin sensitivity. The muscle-specific deletion of β1 integrin in mice fed a chow diet resulted in decreased whole-body insulin sensitivity and glucose tolerance (Zong et al., 2009). The whole-body deletion of α2 integrin has been shown to reverse diet-induced muscle insulin resistance in high fat diet-fed mice (Kang et al., 2011b). Other studies have shown that whole-body deletion of integrin α1 resulted in hepatic insulin resistance in high fat diet-fed mice (Williams et al., 2015).

As integrin α7 is the most abundant integrin in striated muscle, we decided to investigate the role of integrin α7 in insulin sensitivity and tissue histology. We used a whole-body deletion model of integrin α7 (α7KO) as almost all integrin α7 is expressed in the muscle. Integrin α7 was deleted as previously discussed in previously published papers and all mice used in this study were descendants of those founder mice produced (Mayer et al., 1997). To delete the integrin α7 gene, 1 kb of genomic sequence was replaced, including the signal sequence of exon 1 and the first 107 bp of the mature protein, with a phosphoglycerate-kinase-neomycin (PGK-neo) cassette via homologous recombination in ES cells. Chimeric founder mice were produced using heterozygous ES cells, before being crossed to generate mice homozygous for the mutated α7 allele (α7KO).

In this chapter, we aimed to look at the whole-body effects of deleting integrin α7, including body weight and composition. We also looked at the effect deleting integrin α7 had on insulin sensitivity and glucose tolerance. Finally, we investigated the effect the deletion of integrin α7 had on the histology of key tissues involved in insulin signalling including skeletal muscle, adipose tissue and liver.

3.2 The effect of integrin α7 deficiency on body weight and food consumption

Preliminary studies showed that α7KO mice raised on the 129/Sv background, when fed a chow diet, weighed significantly less than controls. Three-month-old male α7KO mice had a mean weight of approximately 27.2g and controls had a mean weight of approximately 30.6g (Figure 3.1A). Apart from being leaner, mice appeared healthy. Preliminary studies demonstrated that chow-fed α7KO mice are more insulin sensitive than control mice (data not shown). In this study, we investigated the effect of feeding a high fat diet (HFD) to α7KO and control mice and observed to what extent this would affect body weight, insulin sensitivity and glucose tolerance.

To investigate whether feeding α7KO and control mice a HFD had a greater effect on body weight than a chow diet, mice were fed a rodent diet with 45 kcal% fat for 12 weeks. Mice were separated into cages according to genotype and were given a weighed amount of HFD food. On a weekly basis, mouse weights were recorded to measure weight change over time (Figure 3.1B).

Control mice, as expected, gained significant weight over 12 weeks of HFD feeding. Compared to Week 0 weights, control mice gained an additional 16% of body weight after the 12 weeks were completed. However, α7KO mice did not gain any significant weight over 12 weeks of HFD feeding. Compared to Week 0 weights, α7KO mice lost 2% of their body weight after the 12 weeks were completed. Control mice first began to gain significantly more weight than α7KO mice after Week 7 and then continued until Week 12 (Figure 3.1B+C). This can be seen photographically in Figure 3.1E+F.

As control mice gained more weight than α7KO mice over 12 weeks of HFD feeding, it was important to measure food intake to ensure this was not the reason for change in weight gain. On a weekly basis, the amount of food ingested by the mice was calculated by subtracting the remaining food in the cage from the initial amount given to the mice.

Average food intake was normalised against the weight of the mice (Figure 3.1D). On a weekly basis, both control and α7KO mice consumed approximately 0.6g of HFD food per gram of body weight. This indicates that greater weight gain in the control mice is not due to the consumption of more HFD food.

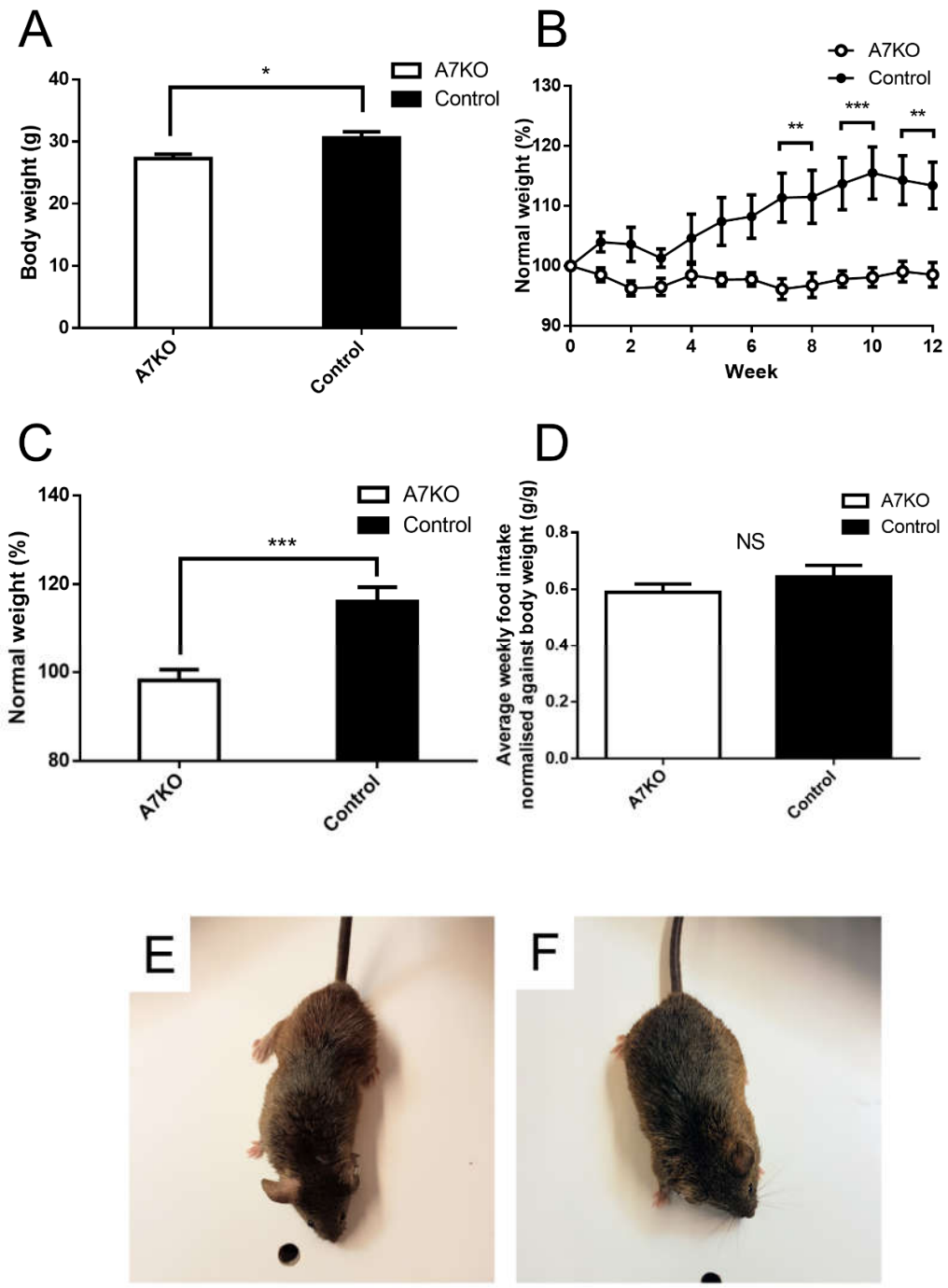

Figure 3.1: Integrin α7 deficiency results in leaner mice when fed either a chow or a HFD. **(A)** Body weight of 3-month-old α7KO and control mice when fed a chow diet. The data are mean ± SEM (n = 7). **(B)** Normalised weight of 3-month-old mice when fed a HFD for 12 weeks, compared to Week 0, chow-fed, body weight. The data are mean ± SEM (n = 7). **(C)** Normalised weight after 12 weeks of HFD feeding compared to Week 0, chow-fed, body weight. The data are shown as mean ± SEM (n = 7). **(D)** Average weekly food intake normalised against body weight (n = 3). **(E+F)** Photograph of **(E)** α7KO and **(F)** control mouse fed a HFD for 12 weeks. Statistical analysis was completed using an independent t-test. NS $p > 0.05$, *$p < 0.05$, **$p < 0.01$, ***$p < 0.001$

3.3 The effect of integrin α7 deficiency on insulin sensitivity and glucose tolerance

When fed a HFD, control mice gained significantly more weight than α7KO mice. We decided to investigate whether this had an impact on insulin sensitivity and glucose tolerance. In this experiment, mice were aged to 3 months old where initial metabolic tests were performed. The **I**ntra**p**eritoneal **I**nsulin **T**olerance **T**est (IPITT) was used to measure insulin sensitivity and the **I**ntra**p**eritoneal **G**lucose **T**olerance **T**est (IPGTT) was used to measure glucose tolerance. After initial metabolic tests, mice were fed a HFD for 12 weeks before repeating the IPITT and IPGTT. We hypothesised that α7KO mice would be more insulin sensitive and more glucose tolerant than controls.

3.3.1 Measuring insulin sensitivity in chow-fed and HFD-fed integrin α7KOs

The reduced ability of α7KO mice to gain body weight when fed a HFD indicated that these mice would also remain insulin sensitive. Insulin tolerance tests were performed at 3 months and 6 months on a chow diet and HFD, respectively. Insulin tolerance testing of 3-month-old chow-fed mice showed that both α7KOs and controls were insulin sensitive (Figure 3.2A). Statistical analysis of time points during the IPITT showed that there was no significant difference between α7KOs and controls when fed a chow diet.

Further insulin tolerance tests carried out on 6-month-old mice when fed a HFD for 12 weeks showed that control mice became less insulin sensitive. However, 6-month-old HFD-fed α7KO mice remained insulin sensitive. Statistical analysis of α7KO and controls demonstrated a significant difference at time points: 30 mins, 60 mins and 120 mins (Figure 3.2B).

Further comparison showed that when control mice were fed a HFD for 12 weeks, they were significantly less insulin sensitive than when fed a chow diet. Statistical analysis

showed they were significantly different after 60 mins of the IPITT and 120 mins (Figure 3.2C). When comparing chow-fed α7KO mice to HFD-fed, statistical analysis showed there was only a significant difference at 120 mins (Figure 3.2D).

The greatest difference in insulin sensitivity is seen between HFD-fed α7KO and control mice. However, all combinations of genotypes and diet showed that, although there is variance in the magnitude of insulin sensitivity, all are still insulin sensitive rather than insulin resistant. This is demonstrated by blood glucose levels reducing to some degree in all genotypes and diet conditions when insulin is injected into the animal.

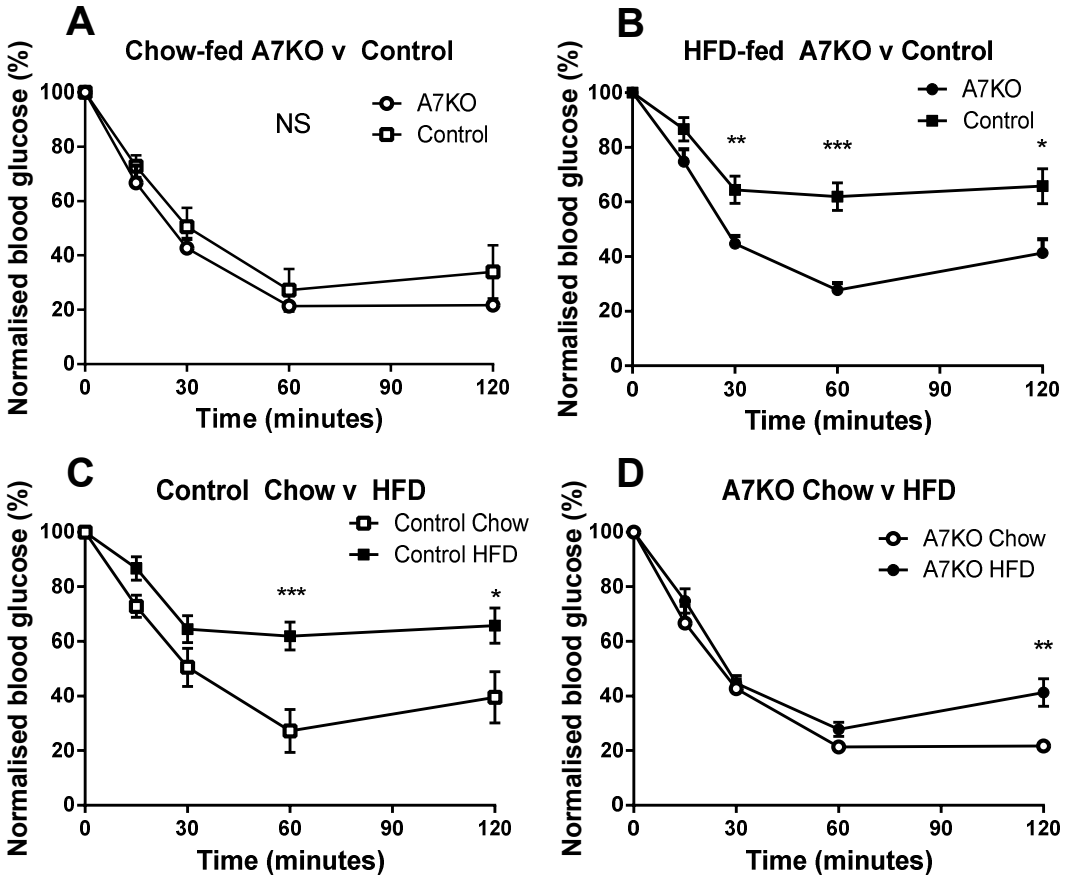

Figure 3.2: Integrin α7 deficiency causes insulin hypersensitivity on both a chow and HFD. **(A)** Following a 6-hour fast, IPITT performed using 0.75 U/kg of insulin on 3-month-old mice fed a chow diet. **(B)** Following a 6-hour fast, IPITT performed using 0.75 U/kg of insulin on 6-month-old mice fed a HFD. **(C)** Comparison of insulin sensitivity of control mice when fed a chow diet vs a HFD. **(D)** Comparison of insulin sensitivity of α7KO mice when fed a chow diet vs a HFD. The data are mean ± SEM (n = 7). Statistical analysis was completed using an independent t-test. *p < 0.05, **p < 0.01, ***p < 0.001

3.3.2 Measuring glucose tolerance in chow-fed and HFD-fed integrin α7KOs

Integrin α7KO mice were resistant to weight gain when fed a HFD as previously shown in this study. These mice were also shown to remain more insulin sensitive than controls. Therefore, we decided to investigate whether these mice also remained glucose tolerant. Glucose tolerance tests are used to measure the body's ability to clear excessive glucose. Tests were performed at 3 months and 6 months on a chow and HFD, respectively.

Glucose tolerance testing of chow-fed 3-month-old α7KO and control mice showed that both genotypes were similarly glucose tolerant. Statistical analysis showed that there was no difference between α7KO and control mice when fed a chow diet (Figure 3.3A). However, glucose tolerance testing of 6-month-old, HFD-fed α7KO and control mice revealed that although both genotypes remained glucose tolerant, α7KO mice were more glucose tolerant than controls. Statistical analysis showed that, at time points 15 and 30 minutes, blood glucose levels were significantly higher in controls than α7KO mice (Figure 3.3B).

Although there is no significant difference, further analysis demonstrated that there was a trend between the glucose tolerance in control mice that were fed a chow diet and those which were fed a HFD (15' p=0.35, 30' p=0.28) (Figure 3.3C). Additionally, there was no significant difference between chow-fed and HFD-fed α7KO mice (Figure 3.3D).

This section of the study demonstrates that there is no difference in glucose tolerance between α7KO and control mice when fed a chow diet. However, when fed a HFD for 12 weeks, α7KO mice are significantly more glucose tolerant than control mice. This is further reinforced by the trend of worsened glucose tolerance when comparing control mice on a chow and HFD. Analysis showed that α7KO mice were similarly glucose tolerant regardless of whether they were fed a chow or a HFD.

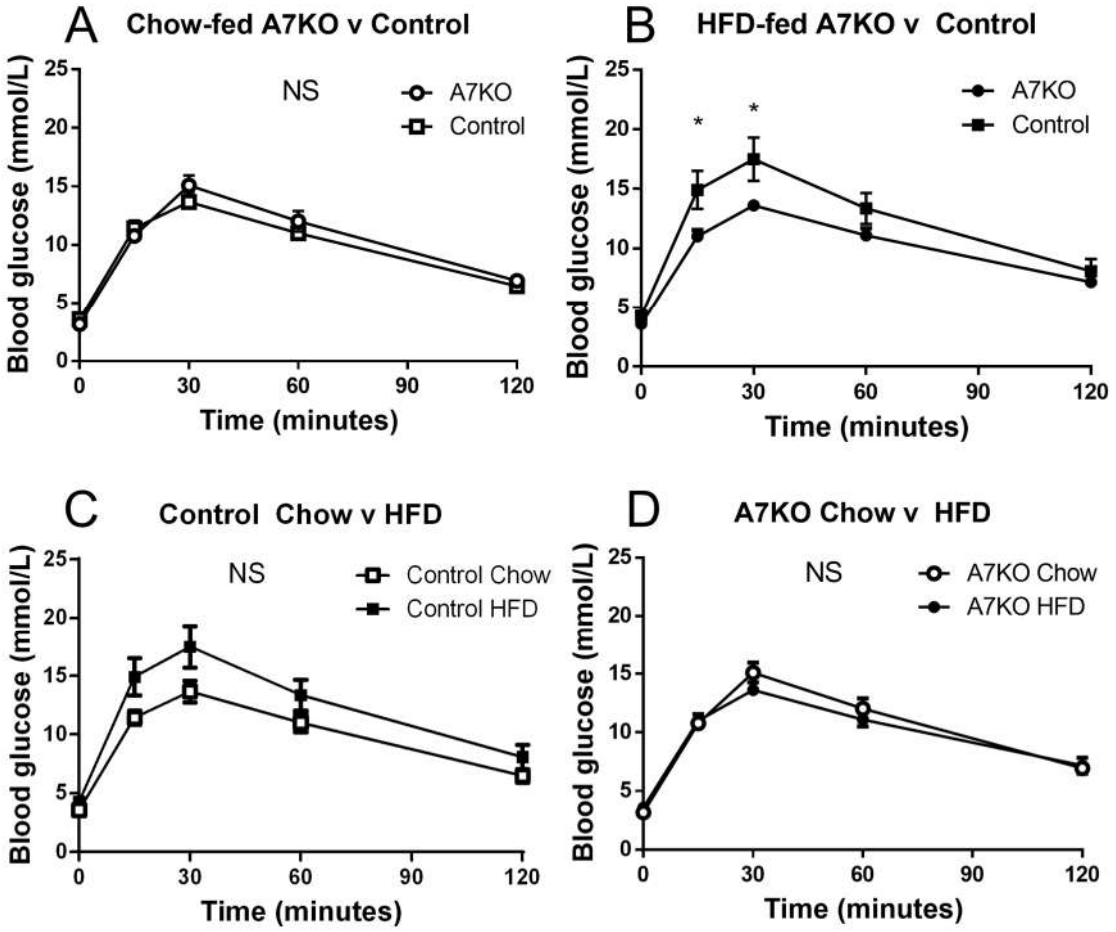

Figure 3.3: Integrin α7 deficiency increases glucose tolerance compared to control mice when fed a HFD. (A+B) Following a 16-hour fast, IPGTT performed using 2 g/kg on 3-month-old mice fed **(A)** chow diet and 6-month-old mice fed a **(B)** HFD. **(C+D)** Comparison of glucose tolerance of **(C)** control mice and **(D)** α7KO mice when fed a chow diet vs a HFD. The data are mean ± SEM (n = 7). Statistical analysis was completed using an independent t-test. NS $p > 0.05$, *$p < 0.05$

3.4 The effect of integrin α7 deficiency on adipose tissue depots

As previously discussed, when α7KO mice were fed a 45% kcal HFD, they remained approximately the same body weight as when fed a chow diet. In contrast, control mice gained significantly more body weight than α7KO mice when fed a HFD. Increased body weight due to consumption of a HFD is usually due to the accumulation of adipose tissue. However, adipose tissue function differs depending on where in the body it is located. It was important to understand whether the increased body weight observed in control mice fed a HFD was due to increased adipose tissue and, furthermore, whether the distribution of this adipose tissue differed between control and α7KO mice. To investigate this, mice were fed a HFD for 12 weeks before tissue harvest. Adipose tissue depots were isolated, weighed and normalised against the animal's total body weight.

The four depots were chosen as they represented the two main categories of adipose tissue: subcutaneous and visceral. The mammary fat pad is accepted as being structural subcutaneous adipose tissue. The mesenteric and gonadal fat pads are representative of visceral adipose tissue. The inter-scapular fat pad can be separated into white and brown adipose tissue, though both are subcutaneous fat pads.

Mammary, mesenteric and interscapular white fat pads from control mice, all weighed significantly more than α7KO (Figure 3.4A). When the combined weights of adipose tissue of control and α7KO mice were compared, it showed that control mice contained significantly more adipose tissue than α7KO mice (Figure 3.4B).

However, as the body weight of α7KO and control mice were significantly different, it was important to calculate what proportion of the mice were adipose tissue to conclude whether control mice were 'fatter'. As shown in Figure 3.4C, the visceral gonadal and subcutaneous interscapular white fat pads were shown to be significantly larger in control

mice. However, there was no significant difference between the: mammary, mesenteric or interscapular brown fat pads. Though, all white adipose tissue fat pads showed a trend of being larger in controls. Furthermore, when cumulating the total weight of the adipose tissue depots, there was significantly more in control mice (Figure 3.4D). Therefore, we can conclude that not only do control mice weigh more than α7KO mice when fed a HFD, they also possess a larger percentage of adipose tissue.

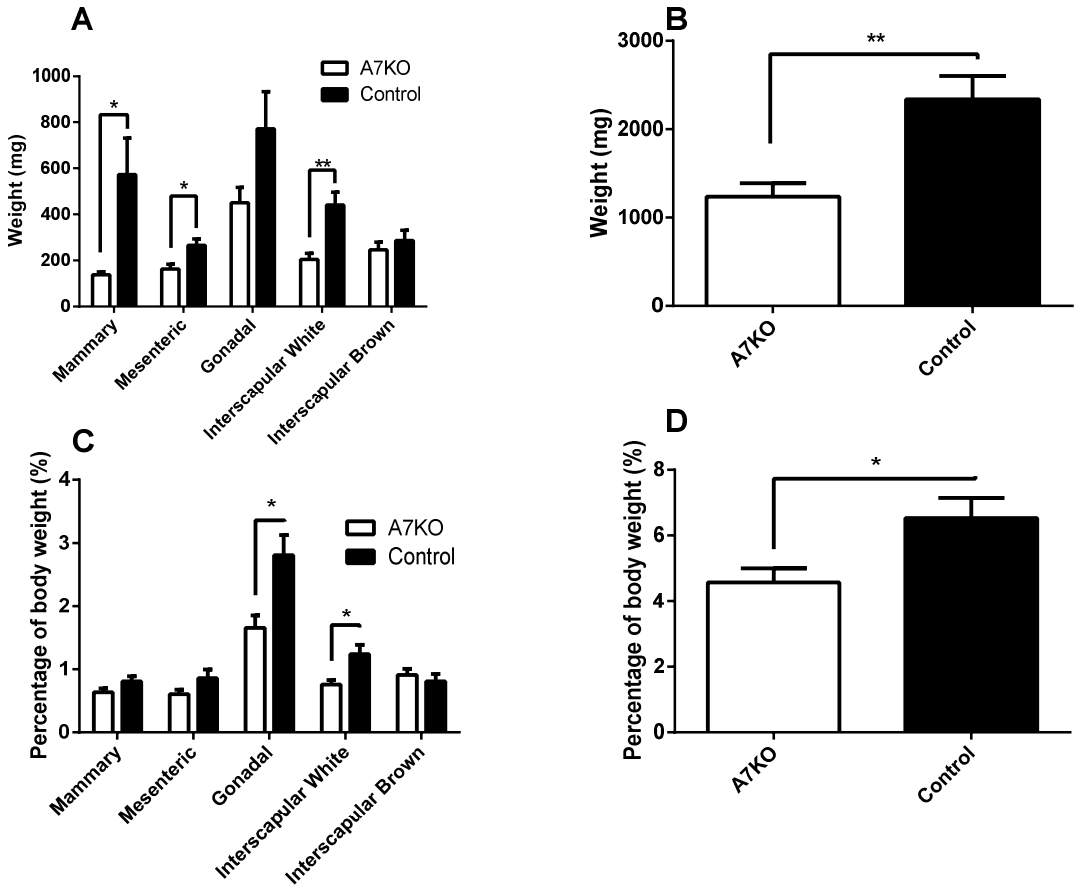

Figure 3.4: Integrin α7 deficiency causes change in distribution and abundance of adipose tissue. (A) Adipose tissue depot weights from 6-month old, HFD-fed control and α7KO mice were compared. **(B)** Total adipose tissue weight from: mammary, mesenteric, gonadal, interscapular white and interscapular brown. **(C)** Adipose tissue depot weights normalised against total body weight. **(D)** Total adipose tissue from: mammary, mesenteric, gonadal, interscapular white and interscapular brown, normalised against total body weight. The data are mean ± SEM (α7KO n=7, control n=9). Statistical analysis was completed using an independent t-test. *$p < 0.05$, **$p < 0.01$

3.5 The effect of integrin α7 deficiency on tissue histology and function

As shown previously, α7KO mice weighed significantly less than control mice on both a chow and a HFD. Further analysis showed that not only were control mice heavier than α7KO mice, control mice had a higher percentage of body fat than α7KO mice. Both genotypes were insulin sensitive when fed a chow diet. In contrast, only α7KO mice remained hypersensitive to insulin when fed a HFD. Greater glucose tolerance was measured in HFD-fed α7KO mice compared to control, but no difference was observed when fed a chow diet.

3.5.1 The role of integrin α7 in adipose tissue function

Adipose tissue plays a vital role in normal metabolism by acting as an energy buffer during fluctuating energy availability and demand. Adipocytes, the main cell type in adipose tissue, can sequester excess circulating lipid in cytoplasmic lipid droplets during times of caloric surplus. Alternatively, during times of caloric need, lipid is released from lipid droplets into circulation to be used as an energy source. To possess this function, adipose tissue has a remarkable ability to change morphologically during times of overnutrition. This is achieved either via hypertrophy of individual adipocytes or hyperplasia from progenitors. To investigate this function, adipocyte size was measured in both α7KO and control mice.

Firstly, adipose tissue was isolated from 6-month old HFD-fed mice before being fixed in 4% PFA and rinsing overnight in PBS. Tissues were dehydrated in increasing concentrations of ethanol before being embedded in paraffin wax. Sections were stained with hematoxylin and eosin to visualise the nuclei, cytoplasm and extracellular matrix. Multiple images of the adipose tissue were captured to ensure that representation of the tissue was sampled and adipocyte sizes were measured using ImageJ software by calculating the minimum Feret diameter (the smallest distance between every possible

pair of tangents). By using minimum Feret diameter, the error from irregularly shaped adipocytes is reduced. The mean minimum Feret diameter was calculated for each mouse and was then averaged to give an overall mean. Generalised Estimating Equations were used to estimate the SEM by considering the number of adipocytes from each individual biological sample.

Interestingly, there was no significant difference between mean minimum Feret diameter of the mammary and interscapular white subcutaneous, nor the mesenteric visceral, adipose tissue sites between control and α7KO mice (Figure 3.5). However, the mean minimum Feret diameter of the gonadal visceral adipose tissue depot was significantly smaller in α7KO mice compared to control.

Further to the results shown in Figure 3.4, this demonstrates that there are not only less gonadal visceral adipocytes in α7KO mice, but the adipocytes that are present are significantly smaller than controls. The deletion of integrin α7 not only alters the distribution of adipose tissue but also influences the size of adipocytes.

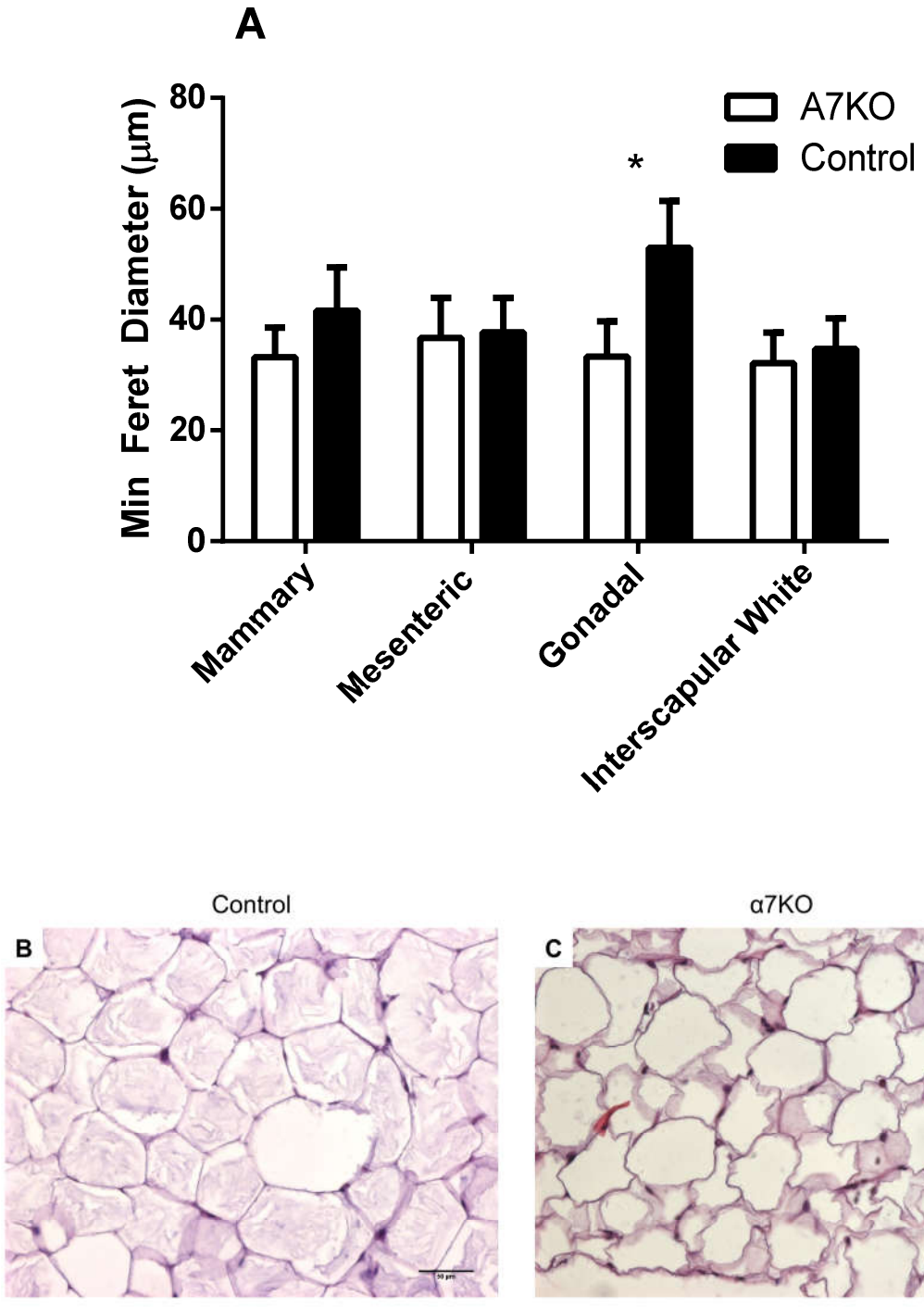

Figure 3.5: (A) Mean minimum Feret diameter of adipocytes isolated from HFD-fed α7KO and control adipose tissue. The data are mean ± SEM (n=3 mice). Statistical analysis was measured using generalised estimating equations. **(B+C)** Hematoxylin and eosin staining of paraffin-embedded **(B)** control and **(C)** α7KO gonadal adipose tissue**.** Scale bars = 50µm

3.5.2 The role of integrin α7 in skeletal muscle histology

Previous studies have demonstrated the role integrin α7 has in skeletal muscle regeneration and homeostasis. However, histological analysis has not been conducted before where the focus has been the role of integrin α7 in metabolism. Obesity and insulin resistance has been associated with chronic inflammation, therefore the dysregulation of skeletal muscle histology could be a factor in the variance of insulin sensitivity in α7KO and control mice. As integrin α7 is the most abundant integrin in skeletal muscle, the primary tissue of glucose uptake, it was necessary to investigate the histology of skeletal muscle.

The tibialis anterior (TA) muscle was isolated and pinned to parafilm before being frozen in liquid nitrogen-cooled isopentane. TA muscle was sectioned in a cryostat at 10 μm thick. Sections were stained with hematoxylin and eosin.

As previously shown by Mayer *et al.*, histological analysis of TA muscle from chow-fed, 6-month-old, α7KO mice showed evidence of a mild myopathy (Mayer et al., 1997). The combination of variable muscle fibre size and centrally located nuclei is a pattern that is typically found in muscular dystrophies (Figure 3.6). Histological staining revealed evidence of mononuclear cell infiltration and muscle fibre necrosis around the myotendinous junction in α7KO mice, whereas control mice showed no signs of degeneration or regeneration.

In 6-month-old, HFD-fed α7KO and control mice, there was very little difference when comparing to their chow-fed counterparts. There appeared to be no deposits of lipid and we observed a similar level of centrally-located nuclei in α7KO chow-fed muscle compared to α7KO HFD-fed muscle.

From the H&E-stained muscle sections we can conclude that there is no change in histology regardless of whether mice are fed a chow or HFD. However, we have

reiterated the previously recorded differences between control and α7KO mice. We observed a greater population of centrally-located nuclei in the α7KO mice compared to controls and an increase in endomysial connective tissue deposition.

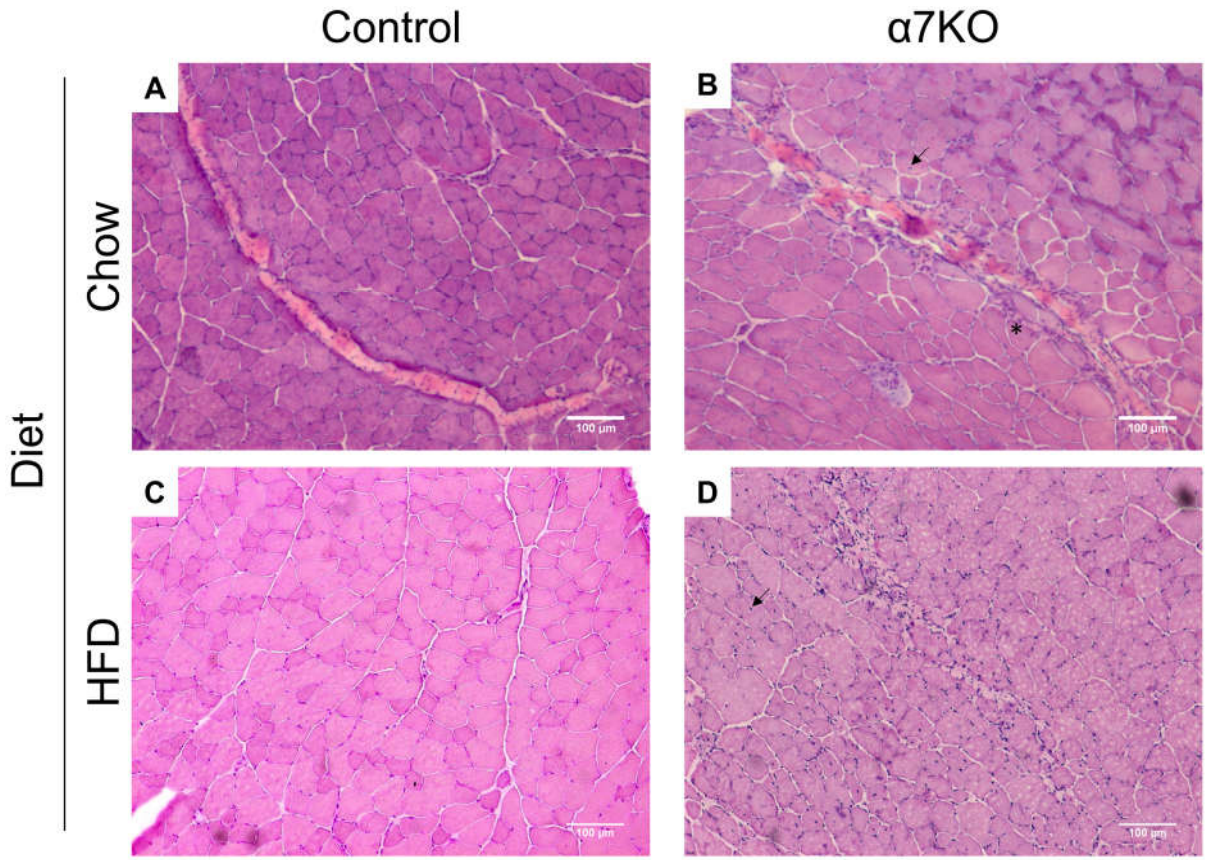

Figure 3.6: Hematoxylin and eosin staining of frozen muscle sections. **(A)** Control mice possess a regular muscle fibre pattern with peripherally located nuclei. **(B)** α7KO mice possess muscle fibres of a variable size. Many of these fibres contain centrally located nuclei with increased endomysial connective-tissue deposition (asterisk). There is also an apparent influx of mononuclear cell infiltration around the myotendinous junction (arrow). **(C)** HFD-fed control mice appear similar histologically compared to chow-fed counterparts. **(D)** HFD-fed α7KO mice appear similar histologically to chow-fed counterparts. Scale bars = 100µm

3.5.3 Ectopic fat deposition in α7KO skeletal muscle

Lipid that is stored in tissues other than adipose tissue is defined as 'ectopic fat'. Ectopic fat depositions in the skeletal muscle are associated with reduced insulin sensitivity and are typically found between muscle fibres. Small lipid droplets can also be found throughout the muscle cells (intramyocellular lipid deposition) from insulin resistant specimens. To determine the presence of lipid deposition in either chow or HFD-fed α7KO and control mice, we stained muscle sections with Oil Red O, a stain used to detect neutral triglycerides and lipids.

In neither control or α7KO 6-month old, chow-fed mice was there evidence of ectopic fat depositions in the skeletal muscle, nor was there evidence of intramyocellular lipid deposition. This was to be expected as the storage of lipid in the skeletal muscle is an abnormal observation which should not occur in control, normally-fed mice.

Both control and α7KO 6-month old, HFD-fed mice showed some degree of ectopic lipid deposition in the skeletal muscle (Figure 3.7). All depositions appeared to lie between the muscle fibres with no evidence of intramyocellular lipid deposition. Muscle fibres appeared histologically normal around lipid deposits.

ImageJ software was used to quantify the amount of lipid in skeletal muscle from the Oil Red O-stained sections. Images were 'deconvoluted' to separate the red stain from the rest of the image, the area of the red stain was quantified and the mean coverage per mm^2 of skeletal muscle was calculated. No significant difference in abundance of lipid in skeletal muscle from 6-month old, HFD-fed control and α7KO mice was measured (Figure 3.7E).

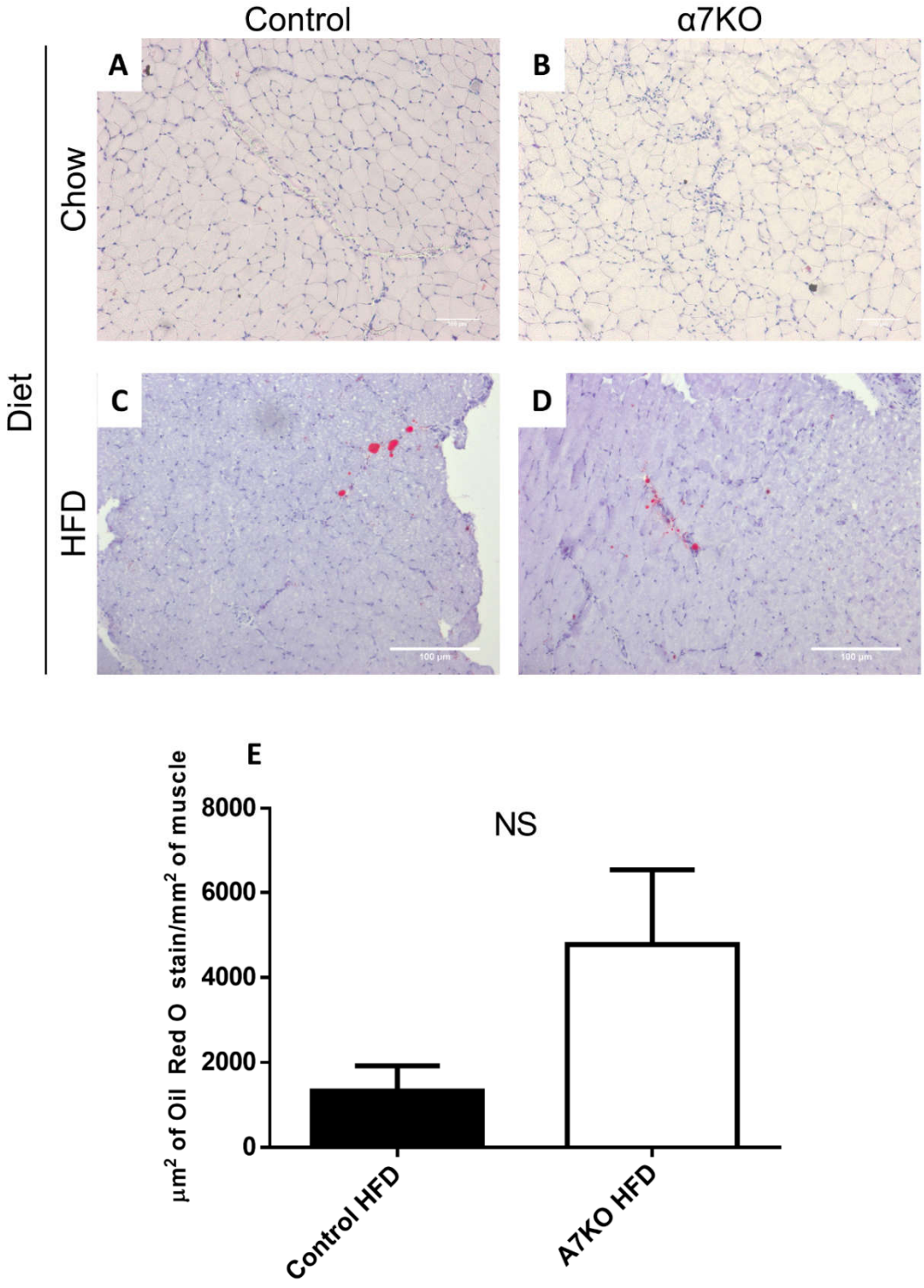

Figure 3.7: Oil Red O staining of frozen muscle sections. (A) TA sections from control chow-fed mice and **(B)** α7KO chow-fed mice. No presence of lipid detected. **(C)** TA sections from control HFD-fed mice and **(D)** α7KO HFD-fed mice show some degree of lipid deposition. **(E)** Quantification of Oil Red O staining shows no significant difference in abundance of lipid between control and α7KO muscle. The data are mean ± SEM (n=3). Statistical analysis was completed using an independent t-test. Scale bars = 100µm

3.5.4 The role of integrin α7 in liver histology

Investigating the role of α7 integrin in muscle, with a focus on metabolism, suggested that there was only a slight difference between α7KO and control mice when fed a HFD. One of the other key organs involved in insulin signalling and glucose metabolism is the liver. The liver is involved in a range of glucose metabolic processes including glycogenesis, glycogenolysis, glycolysis and gluconeogenesis (Han et al., 2016). The liver is a major site of glucose utilisation during the post-prandial period where this absorbed glucose is phosphorylated and stored as glycogen. The liver is then able to release glucose systemically when needed (Adeva-Andany et al., 2016).

Non-alcoholic fatty liver disease (NAFLD) is one of the most prevalent diseases associated with obesity and insulin resistance. Steatosis is the main phenotype of this disease but portal and lobular inflammation, apoptotic hepatocellular injury, Mallory-Denk bodies, megamitochondria and fibrosis are also key symptoms of NAFLD liver histology which can lead to non-alcoholic steatohepatitis (NASH), liver cirrhosis and finally, hepatocellular carcinoma (Kleiner and Makhlouf, 2016; Kitade et al., 2017).

3.5.5 Histology of liver

To investigate whether the deletion of integrin α7 affected the liver histology, we isolated liver from chow-fed and HFD-fed, 6-month-old mice. Livers were fixed and cryoprotected before being sectioned and stained with H&E to observe general histology.

As expected, chow-fed control and α7KO livers were very similar histologically. We saw no evidence of steatosis or inflammation when fed a chow diet. In contrast, livers isolated from HFD-fed α7KO mice showed unexpected results compared to control livers. Insulin resistance has been shown to be pivotal for the progression of NAFLD. H&E staining showed that HFD-fed control mice suffer from macrovesicular steatosis (lipid droplets large enough to distort the nucleus) (Figure 3.8C+D). Unexpectedly, insulin sensitive HFD-fed α7KO mice appeared to be suffering from macrovesicular steatosis to a higher

degree. HFD-fed α7KO mice had apparent portal and lobular inflammation whereas control mice did not (data not shown). However, neither HFD-fed α7KO or control mice livers appeared to contain Malloy-Denk bodies, megamitochondria or fibrosis from H&E analysis. This indicated that α7KO livers are at a later stage of NAFLD than controls but have not progressed into the NASH or cirrhosis stage.

These results are controversial as NAFLD is not normally associated with insulin sensitivity. The causes of insulin resistance tend to cause NAFLD so one phenotype without the other is uncharacteristic. Therefore, it was important to confirm the level of steatosis to more accurately determine the stage of NAFLD.

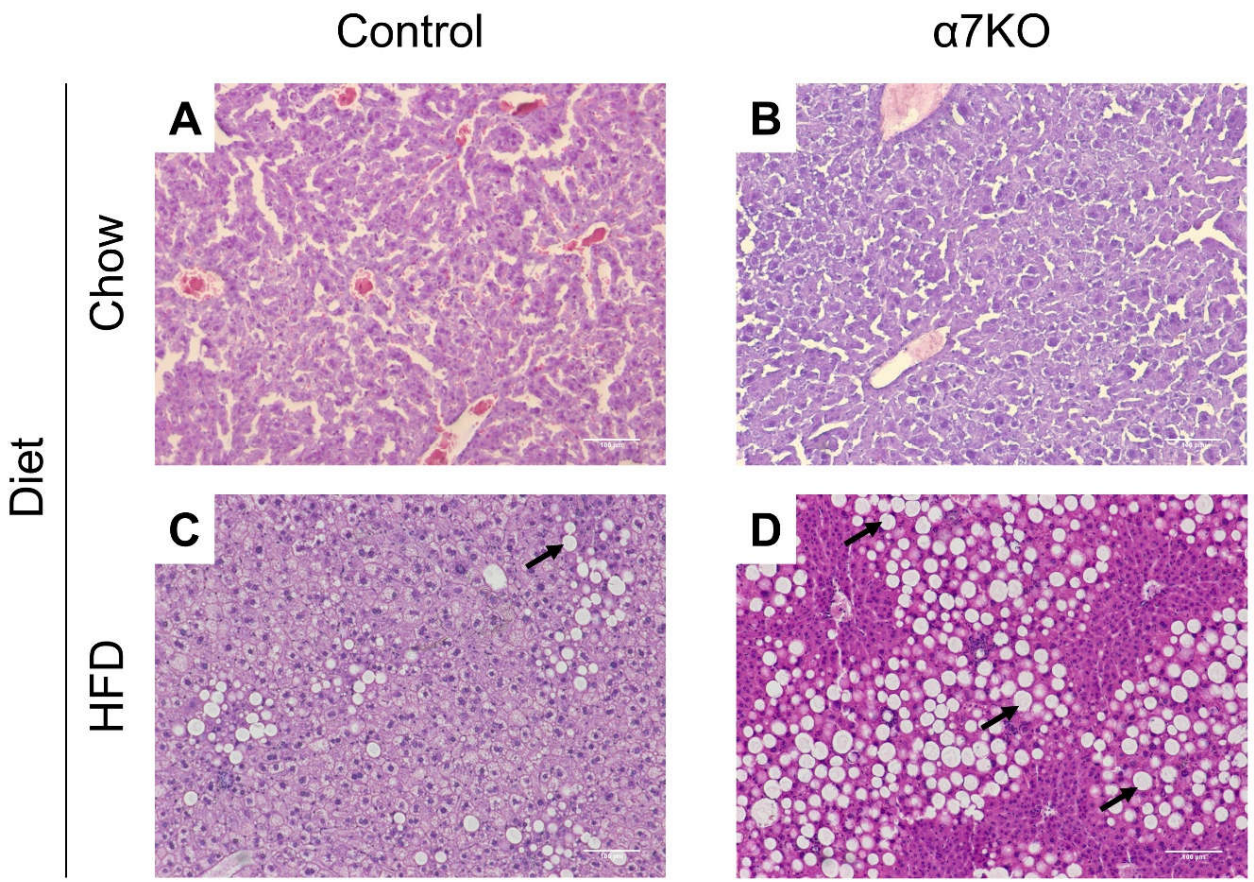

Figure 3.8: Hematoxylin and eosin staining of frozen liver sections.(A+B) Chow-fed **(A)** control and **(B)** α7KO liver show normal liver histology. **(C)** HFD-fed, control liver shows mild steatosis with evidence of ectopic lipid deposition (arrow). **(D)** HFD-fed, α7KO liver shows macrovesicular steatosis through accumulation of large ectopic lipid droplets (arrows). Scale bars = 100μm

3.5.6 Ectopic fat deposition in α7KO liver

Histological staining of liver sections from HFD-fed α7KO and control mice with H&E produced evidence of ectopic lipid droplets. This is acknowledged as a common phenotype in sufferers of insulin resistance. Surprisingly, there appeared to be more lipid deposition in HFD-fed α7KO mice compared to control. This was controversial as previous tests demonstrated α7KO HFD-fed mice were insulin sensitive and lean. Therefore, it was important to confirm that the 'holes' observed in H&E-stained liver sections were lipid droplets.

Liver sections were fixed and cryoprotected before being frozen in Optimal Cutting Temperature (OCT) Compound. Livers were cryosectioned and stained with HCS LipidTOX™ Green neutral lipid stain. HCS LipidTOX™ Green neutral lipid stain was used rather than Oil Red O, as the red stain of Oil Red O was difficult to distinguish from the natural red hue of liver. The LipidTOX™ neutral lipid stain has an extremely high affinity for neutral lipid droplets and can be observed and quantified using fluorescence microscopy. HCS LipidTOX™ Green neutral lipid-stained liver images were quantified using ImageJ software.

As was expected from previous H&E stained liver sections, there was no quantifiable amount of lipid found in chow-fed α7KO or control mice (Figure 3.9). HFD-fed, α7KO mice contained approximately 0.13μm^2 of lipid per 1μm^2 of liver. Whereas in equivalent control mice, only 0.03μm^2 of lipid was present per 1μm^2 of liver. Statistical analysis showed that there was significantly more lipid in 6-month old, HFD-fed α7KO mice compared to controls (Figure 3.9).

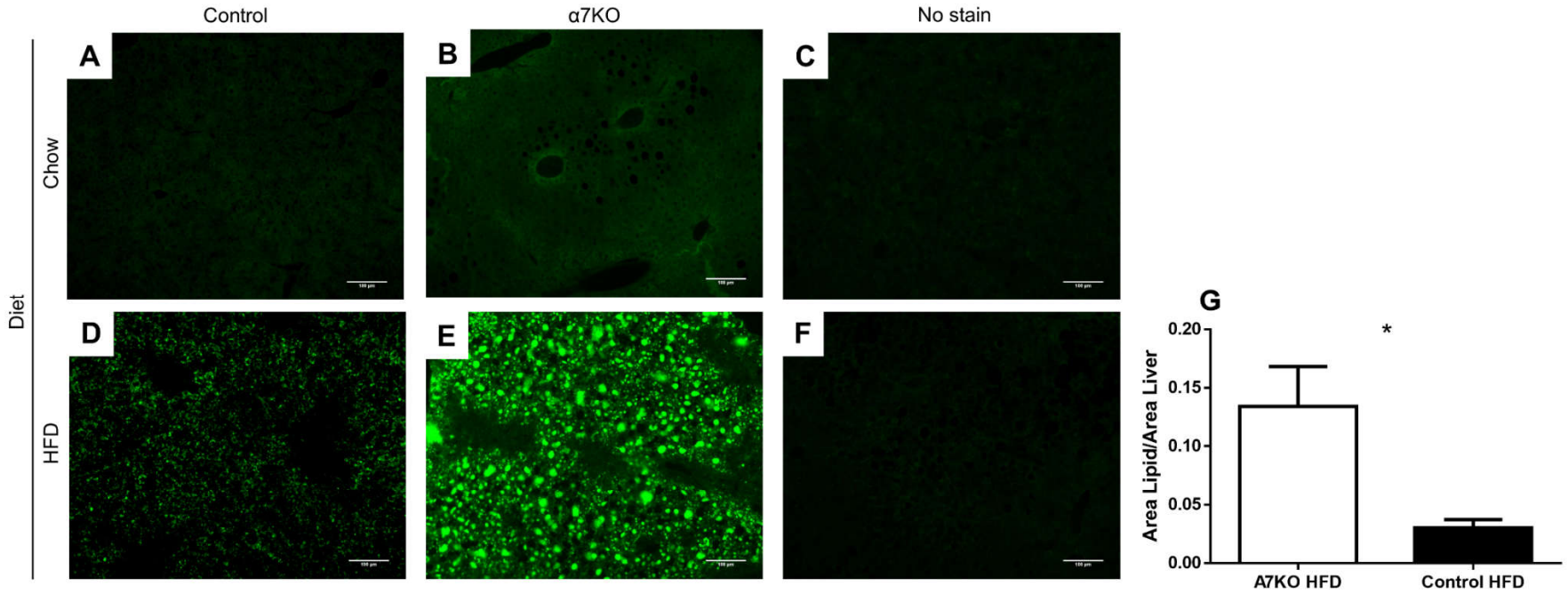

Figure 3.9: HSC LipidTOX™ Green neutral lipid stain of frozen liver sections. (A) Chow-fed control liver. No evidence of lipid deposition **(B)** α7KO chow-fed. No evidence of lipid deposition. **(C+F)** Section with no lipid stain to ensure fluorescence is specific to lipid. **(D)** HFD-fed control mice. Some lipid deposition. **(E)** HFD-fed α7KO liver. Major lipid deposition. **(G)** Comparison of mean area of lipid/area of liver between 6-month old, HFD-fed control and α7KO livers. The data are mean ± SEM (n=4 mice). Statistical analysis was completed using an independent t-test. *$p < 0.05$. Scale bars = 100μm

3.6 The role of integrin α7 in liver function

3.6.1 Liver enzymes in α7KO and control mice

We have demonstrated that livers from HFD-fed, α7KO mice contained significantly more lipid than controls. Ectopic lipid deposition in the liver is usually an indicator of liver damage, therefore, it was necessary to determine if these fatty livers were damaged and to quantify the extent to which they were damaged.

Alanine transaminase (ALT) and Aspartate transaminase (AST) are transaminase enzymes important in amino acid metabolism. ALT and AST are commonly used clinically to determine liver health. Although ALT is predominantly found in the liver, AST is also found in the heart, skeletal muscle, kidneys, brain and red blood cells. As a result of this, ALT is a better indicator of liver damage whereas AST may be increased due to other tissues (Limdi and Hyde, 2003).

Blood was isolated from HFD-fed α7KO and control mice in a fed state. Serum was isolated from these samples and snap frozen in liquid nitrogen. Serum samples were analysed using a Randox system and an ALT and AST assay kit as per manufacturer's instructions.

Analysis of ALT enzyme showed levels of 106.86 U/L in HFD-fed control mice, whereas in α7KO mice there were concentrations of 225.65 U/L. Although there was a trend of a greater concentration of ALT present in α7KO serum, it was not shown to be statistically significant (Figure 3.10A). Analysis of enzyme AST showed that there was a significantly greater concentration in HFD-fed α7KO mice compared to controls. Control animals had a mean concentration of 587.89 U/L, whilst α7KO mice had a mean concentration of 1635.29 U/L (Figure 3.10B).

This elevation of circulating liver enzymes is a key indicator of tissue damage. However, as previously mentioned, AST is not specific to the liver. Therefore, this indicates that there may be damage in multiple tissues including the liver.

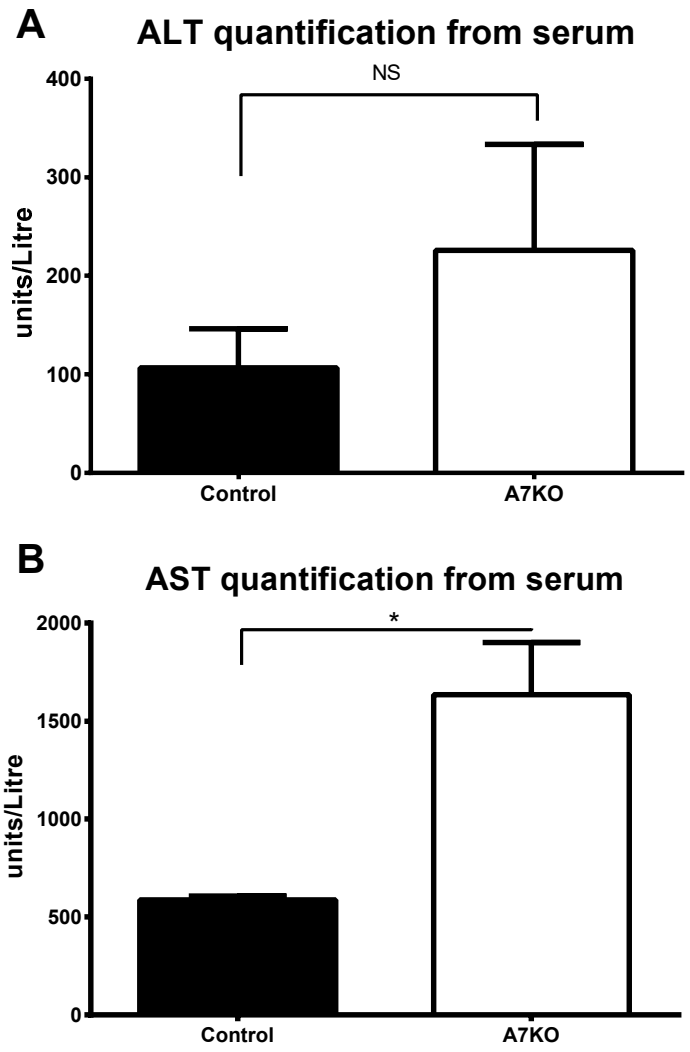

Figure 3.10: ALT and AST enzyme analysis of serum collected from HFD-fed α7KO and control mice. (A) ALT quantification of HFD-fed α7KO and control mice. **(B)** AST quantification of HFD-fed α7KO and control mice. The data are mean ± SEM (n = 3). Statistical analysis was completed using an independent t-test. NS $p > 0.05$, * $p < 0.05$

3.6.2 Bile acid production in α7KO and control mice

We have shown that livers from HFD-fed, α7KO mice contain significantly more lipid than controls and that there were greater amounts of circulating liver enzymes, indicating liver damage. Therefore, it was necessary to investigate whether α7KO liver function had been affected from this influx of lipid deposition. As α7KO animals do not gain weight when fed a HFD, we hypothesised that the production of bile acids in the liver may have been affected.

Bile acids are a group of water-soluble steroids, formed from cholesterol. They play a significant role in the absorption and digestion of fat and fat-soluble proteins. Chenodeoxycholic acid and cholic acid are referred to as the primary bile acids and are the most abundant. They are produced in the hepatocytes of the liver before being conjugated to glycine or taurine in the canaliculi of the liver. It is the glycoconjugates and tauroconjugates which increase the amphipathic nature of bile acids and are the major solute in bile. In the colon, they are deconjugated by bacterial enzymes to form secondary bile acids which are then recycled in the liver by reconjugation to either glycine or taurine, or are excreted in faeces (Stamp and Jenkins, 2008).

By quantifying the total, and the categories of bile acids, we are able to analyse if and where there is an effect caused by the deletion of integrin α7. A change in primary bile acid levels indicates a potential issue with the production in hepatocytes. Variance in the levels of glycoconjugates and tauroconjugates indicates there may be an issue with the transporters of bile acids. Finally, a change in the levels of secondary bile acids would suggest there was a change in the microbiota required to recycle bile acids.

Serum was isolated from blood samples collected from animals and was analysed via LC-MS. Analysis showed that there was no significant difference in the total amount of serum bile acids between α7KO and control animals when fed either a chow or HFD. There was also no difference in bile acid production when either genotype was fed a

chow or a HFD (Figure 3.11A).

Total bile acids were broken down into categories of: primary, secondary, glycol-conjugated and tauro-conjugated, to investigate whether the proportions of bile acids were affected. Statistical analysis showed that there was no significant difference in any of these categories when comparing genotype and diet (Figure 3.11B).

This investigation confirmed that increased lipid deposition in the liver does not affect total bile acid production regardless of genotype or diet. Neither does it affect the conversion of primary bile acid to secondary bile acid. The difference in weight gain between genotypes is not due to change in bile acid quantity affecting fat absorption.

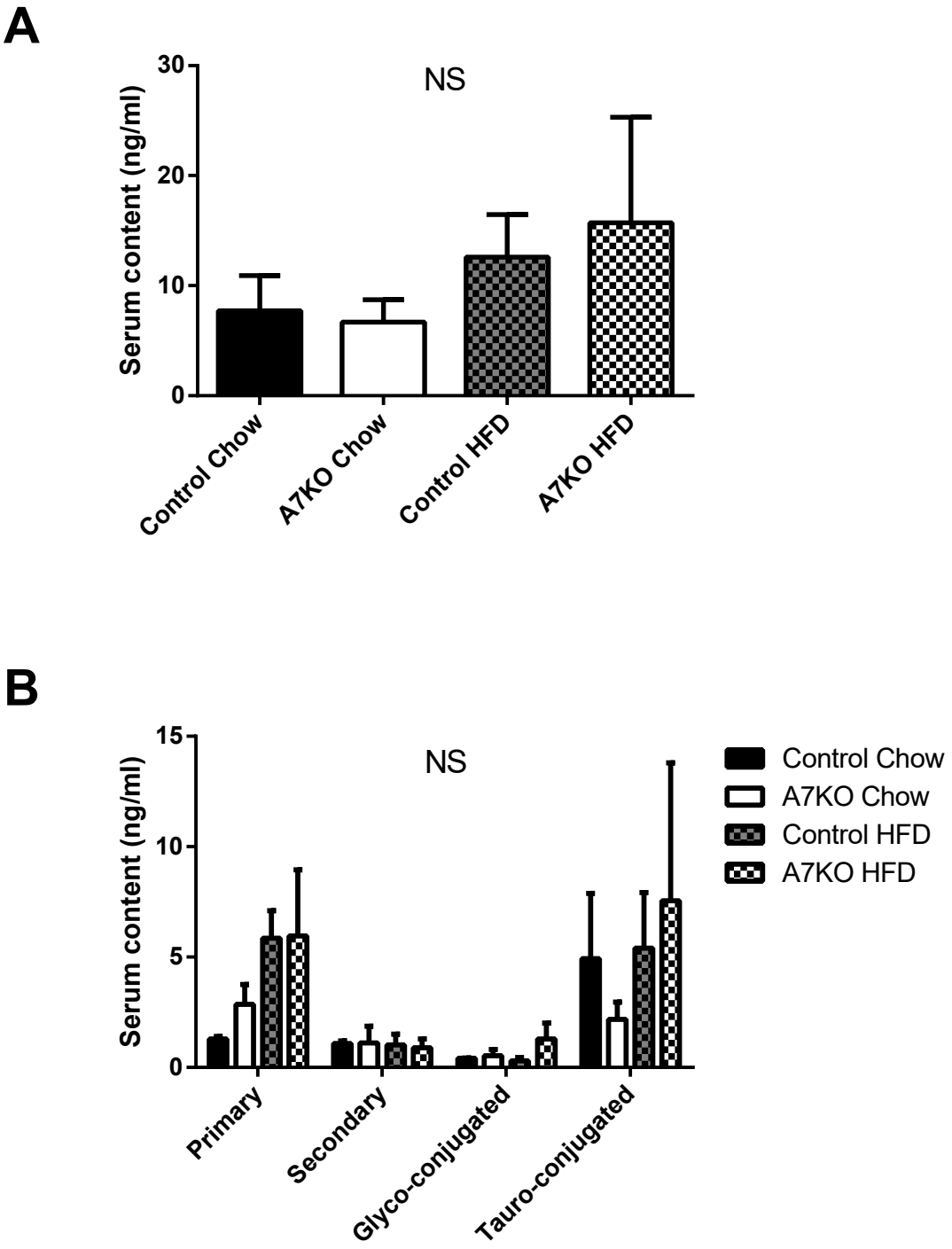

Figure 3.11: Bile acid analysis of serum collected from chow-fed and HFD-fed animals. (A) Total bile acid concentration from serum. **(B)** Breakdown of total bile acids into: primary, secondary, glycoconjugated and taurogconjugated. The data are mean ± SEM (Control Chow n = 3, α7KO Chow n = 4, Control HFD n = 6, α7KO HFD n = 5). Statistical analysis was completed using a two-way ANOVA with a Tukey post-hoc test.

3.7 Summary

In this chapter, we aimed to investigate the effect the deletion of integrin α7 had on the whole-body metabolic phenotype in mice. We successfully utilised a previously generated mouse line with a whole-body deletion of integrin α7. We ran metabolic tests on male control and α7KO at 3-months old before feeding a HFD for 12 weeks. Metabolic tests were conducted on mice post-HFD. Tissues of metabolic interest including skeletal muscle, adipose tissue and liver, were isolated and analysed.

Absence of integrin α7 has been shown to cause a novel form of muscular dystrophy *in vivo* (Mayer et al., 1997). Integrin α7 is the most abundant integrin in skeletal muscle and has been demonstrated to be involved, but not crucial, in the differentiation and migration process during muscle development. Histopathological analysis shows that deletion of integrin α7 results in impaired function of the myotendinous junction. Although many studies have been completed to investigate the role of integrin α7 in myogenesis and muscle function, no studies have sought to investigate its impact on metabolism.

The integrins, and their downstream effectors, have been shown to be implicated in the regulation of insulin action. Skeletal muscle has been recognised to be responsible for approximately 75% of all insulin-stimulated glucose uptake (Brennan et al., 2016). Therefore, we hypothesised that integrin α7 would be involved in skeletal muscle's response to insulin.

3.7.1 Body weight and composition

The deletion of integrin α7 resulted in mice that weighed significantly less than control mice when fed a chow diet. However, it was unclear whether this reduction in body weight was due to a reduction in muscle mass caused by the novel myopathy seen in the α7KO model. Surprisingly, when control and α7KO mice were fed a HFD for 12 weeks, α7KO mice remained a similar body weight to when fed a chow diet. As expected, control mice

gained significant amounts of body weight. It was important to investigate whether this lack in gain of body weight was due to reduced consumption of food compared to control mice. Mice were separated according to genotype and food was weighed alongside weekly mouse weigh-ins to calculate the average food ingested per mouse. Interestingly, there was no significant difference in the amount of food consumed between genotypes when normalised against mouse weight.

To understand whether the reason HFD-fed α7KO mice were lighter than control mice was due to less adipose tissue, we isolated adipose tissue from four different depots. We chose two subcutaneous depots (mammary and interscapular) and two visceral depots (gonadal and mesenteric). Overall, we found that there was significantly less adipose tissue in HFD-fed α7KO mice. The main difference was in the gonadal depot with there also being significantly less interscapular white adipose tissue.

We further analysed the adipose tissue depots by observing the histology of the adipocytes. Calculating the mean minimum Feret diameter demonstrated no difference in the mammary, mesenteric or interscapular white adipose tissue. However, gonadal adipocytes were shown to be significantly smaller in HFD-fed α7KO mice. Thus, the deletion of integrin α7 results in leaner mice when fed either a chow or HFD. It also causes significantly smaller adipocytes in visceral gonadal adipocytes.

3.7.2 Insulin sensitivity and glucose tolerance

IPITT and IPGTTs were performed on 3-month old chow-fed control and α7KO mice. Mice were fed a HFD for 12 weeks before undergoing further metabolic tests. There was no significant difference between control and α7KO mice in terms of insulin sensitivity when fed a chow diet. However, when fed a HFD for 12 weeks, control mice became less insulin sensitive as they gained weight and α7KO mice remained insulin sensitive when fed a HFD, as expected.

A similar trend was observed with glucose tolerance tests. Chow-fed α7KO and control mice were no different in terms of glucose tolerance when fed a chow diet. However, α7KO mice were significantly more glucose tolerant than controls when fed a HFD. Therefore, the deletion of integrin α7 results in mice remaining insulin sensitive and glucose tolerant when fed either a chow or a HFD.

3.7.3 Muscle histology

As previously mentioned, the deletion of integrin α7 results in a novel form of muscular dystrophy (Mayer et al., 1997). This was reiterated in the H&E images shown in this chapter. Though no studies have investigated integrin α7 with metabolism being the focus, intramyocellular fat deposition has been shown to be a factor of obesity and insulin resistance (Greco et al., 2002).

No evidence of intramyocellular fat deposition was seen in H&E or Oilred O-stained images of frozen chow-fed TA muscle in control or α7KO mice. There were small amounts of adipose deposition in both control and α7KO HFD-fed muscle but there was no significant difference between the mouse models. Therefore, a HFD causes some muscle fat deposition, however, there is no difference in the extent of deposition between control and α7KO mice.

3.7.4 Liver histology and function

NAFLD is a general term which ranges from the deposition of lipid in the liver, to progressive Non-alcoholic steatohepatitis (NASH), cirrhosis, and hepatocellular carcinoma (HCC) (Benedict and Zhang, 2017). NAFLD is the most common form of liver disease and typical involves steatosis and fat accumulation in the liver. Progression of NAFLD leads to NASH, which includes distortion of hepatocytes, inflammation, and fibrosis. Further progression of the disease eventually results in liver cirrhosis, and potentially HCC (Pierantonelli and Svegliati-Baroni, 2019).

The histology of the liver in chow- and HFD-fed control and α7KO mice was investigated using H&E staining. No evidence of steatosis or inflammation was observed in chow-fed mice. However, when fed a HFD, control livers began to show evidence of macrovesicular steatosis (lipids large enough to distort the nuclei of the liver). Surprisingly, the lean, α7KO, insulin-sensitive mice possessed livers which were suffering from macrovesicular steatosis more evident than seen in control mice. Furthermore, the HFD-fed α7KO livers showed evidence of portal and lobular inflammation. Further investigation of fat deposition in livers showed that HFD-fed α7KO livers possessed significantly more lipid deposition than controls. Therefore, the deletion of integrin α7 results in a later stage of NAFLD than control mice when fed a HFD.

Liver function was analysed by measuring the levels of key liver enzymes in the blood serum. There was a trend of greater alanine transaminase (ALT) levels in HFD-fed α7KO mice and significantly more aspartate transaminase (AST) levels. Unfortunately, although ALT is predominantly found in the liver, AST is found in a range of tissues (Gowda et al., 2009). Therefore, we cannot conclude that these elevated serum enzymes are solely caused by liver damage.

To further investigate the function of the liver we analysed the levels of bile acids in blood serum. The liver is responsible for the generation of bile acids which assist nutrient absorption and expulsion of toxic metabolites (Chiang, 2013). Clinical studies have demonstrated the link between NAFLD and bile acid homeostasis dysregulation. Patients with NASH have been found to have four-fold elevated serum tauroconjugates and glycoconjugates (Kalhan et al., 2011). This increase in serum bile acid levels is suggested to be due to increased cholesterol $_{7}$α-hydroxylase (CYP_7A_1) expression (Puri et al., 2017). We quantified the total amount of bile acids but also broke them down into four main categories: primary, secondary, glycoconjugates and tauroconjugates. Results showed that there was no significant difference when fed either a chow or a HFD. However, as we only measured bile acid levels in the serum, we cannot be certain that

levels are not different in the intestines of the animals, therefore affecting nutrient absorption.

3.7.5 Summary table

Table 3.1: Table summarising the results from Chapter 3, comparing control and α7KO mice. ↓ comparatively significantly lower, ↑ comparatively significantly higher

	Chow diet		High fat diet	
	Control	α7KO	Control	α7KO
Body weight	-	↓	-	↓
Insulin sensitivity	-	No difference	-	↑
Glucose tolerance	-	No difference	-	↑
Adipose tissue weight	-	↓	-	↓
Adipocyte size			-	↓ (Gonadal)
Muscle fibre histology	-	Increased central nuclei and endomysial connective tissue deposition	-	Increased central nuclei and endomysial connective tissue deposition
Muscle ectopic fat	-	No difference	-	No difference
Liver histology	-	No difference	Macrovesicular steatosis	Increased macrovesicular steatosis
Liver ectopic fat	-	-	-	↑
Serum liver enzymes	-	-	-	↑
Serum bile acids	-	-	-	No difference

CHAPTER 4: ANALYSING THE METABOLOMIC PROFILE OF INTEGRIN A7 DEFICIENT MICE

4.1 Introduction

The development of disease is often caused by interplay between genetic, epigenetic and environmental factors. This has been shown to be the case with metabolic diseases where both environmental factors (diet and exercise) and genetic factors (shown in genome wide association studies) impact the onset of disease (Imamura and Maeda, 2011). Changes in insulin sensitivity have been shown to be affected by a wide range of factors including: altered insulin signalling, accumulation of adipose tissue, oxidative stress and inflammation (Koves et al., 2008; Erion and Shulman, 2010; Lee and Lee, 2014). However, many of these changes can be influenced by the ingestion of varied diets and how the body absorbs nutrients from food. The quantification and analysis of small molecules in a biological sample have been termed the study of metabolomics. By analysing samples at a specific time and condition, it offers a snapshot of the metabolic status of the subject (Milburn and Lawton, 2013).

Integrins have been shown to play a role in the absorption of nutrients on both a whole-body and cellular level. The deletion of RGD-binding protein α8β1 from gastrointestinal smooth muscles resulted in enhanced gastric contraction, faster gastric emptying and more rapid transport of food from the small intestine. This resulted in lean mice due to malabsorption (Khalifeh-Soltani et al., 2016). Integrin α7 is ubiquitously expressed by various types of smooth muscle, including those found along the gastrointestinal tract and is crucial for the differentiation of smooth muscle (Yao et al., 1997). Therefore, it is possible that the HFD-fed, lean, insulin sensitive integrin α7KO model we have generated is influenced by altered nutrient absorption.

We sought to investigate whether the deletion of integrin α7 from chow-fed or HFD-fed control or α7KO mice resulted in a change of metabolic profile. Control and α7KO mice were housed separately as they are coprophagous animals, to prevent sharing of microbiota. Faecal samples were analysed via 1D ^{1}H Nuclear Magnetic Resonance

(NMR). Concentrations of individual metabolites were calculated from spectral peaks and were analysed using MetaboAnalyst 4.0. We used a variety of both exploratory and functional statistical analysis to explore both the individual and group effects of differences in metabolites.

4.2 Clustering of metabolites according to genotype in chow-fed mice

We used **P**artial **L**east **S**quares **D**iscriminant **A**nalysis (PLS-DA) as an exploratory method to cluster the metabolomic profiles of faeces collected from control and α7KO mice. PLS-DA links two data matrices: X (raw data) and Y (genotype category) and explores the maximal covariance of the data (Gromski et al., 2015). From this data, a predictability performance value (Q^2) can be calculated to estimate the predictive ability of a model. The closer the Q^2 value is to 1, the better the predictability (Szymańska et al., 2012). Additionally, we used clustered heatmapping to visually observe clustering of specific metabolites between genotypes.

Clustering of metabolomic profiles from control and α7KO mice fed a chow diet is shown in Figure 4.1A. Visually, there appears to be little variation in the metabolomic profile of chow-fed α7KO mice. However, there is a large variance in the profile of chow-fed control mice. This is demonstrated by the calculated Q^2 value of -1.69. This Q^2 value indicates there is poor predictability between the chow-fed control and α7KO model in terms of metabolomics.

To explore the difference in individual metabolites between chow-fed control and α7KO faecal metabolomic profiles, we performed a Student's T-Test (Figure 4.1B). Statistical analysis demonstrated that there was no significant difference between any individual metabolites measured. Full readout can be seen in Appendix Table 10.1.

A heatmap was generated, as shown in Figure 4.1C, to visually display different distribution patterns of metabolites between control and α7KO groups. However, the heatmap demonstrated the variance within genotypes previously reported in PLS-DA analysis. The varied results of these exploratory analyses make drawing conclusions about the difference between the metabolomic profiles of faeces from control and α7KO mice difficult at this time.

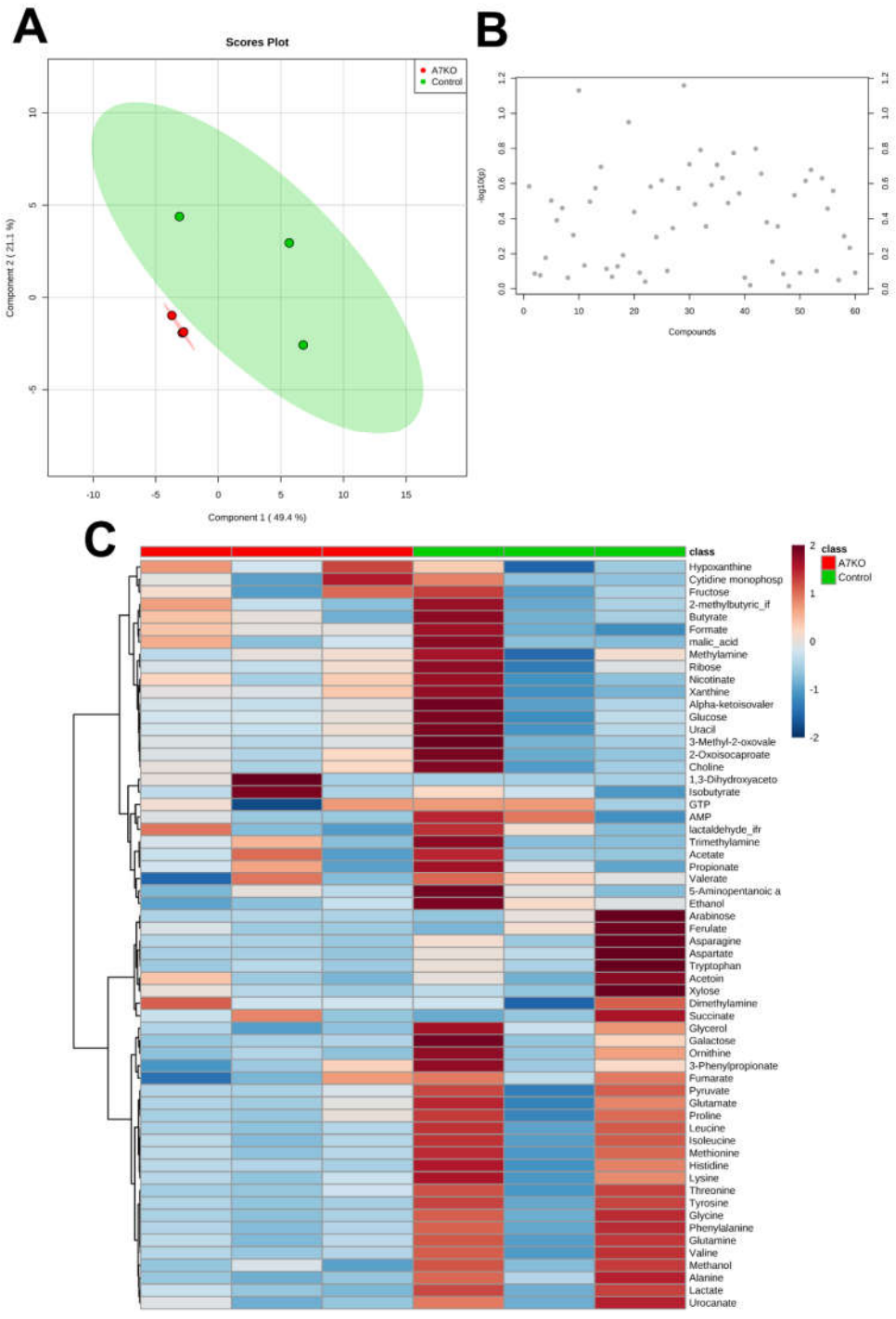

Figure 4.1: Exploratory analysis of metabolomic profiles from faeces collected from chow-fed control and α7KO mice. (A) PLS-DA analysis score plots of metabolomic profiles. Dots represent individual mouse samples. Coloured oval represents 95% confidence region of genotype. **(B)** Visual representation of Student's T-Test of individual metabolites. **(C)** Heatmap visualisation of changes in metabolite levels between control and α7KO mice.

4.3 Functional analysis of metabolites in chow-fed mice

We employed **M**etabolite **S**et **E**nrichment **A**nalysis (MSEA) to measure whether there was any difference in clusters of metabolites between control and α7KO metabolomic profiles. MSEA bypasses the need for individual metabolites to be evaluated individually for significance and to all pass a significance test. This allowed us to identify subtle but consistent changes amongst a group of related compounds which may, otherwise, go undetected.

MSEA was performed using a generalised linear model to estimate a Q-statistic for each metabolite. The Q-statistic values the correlation between the metabolite concentrations and the clinical outcome summarises the ranking of pathways changed between the metabolomic profile of faeces from chow-fed control and α7KO mice

Figure 4.2). However, as shown in Appendix Table 10.2, none of these pathways are significantly different. Therefore, with the combination of results from exploratory and functional analyses of the metabolomic profile of faeces collected from chow-fed control and α7KO mice, we can conclude that there is no significant difference caused by the deletion of integrin α7 in chow-fed mice.

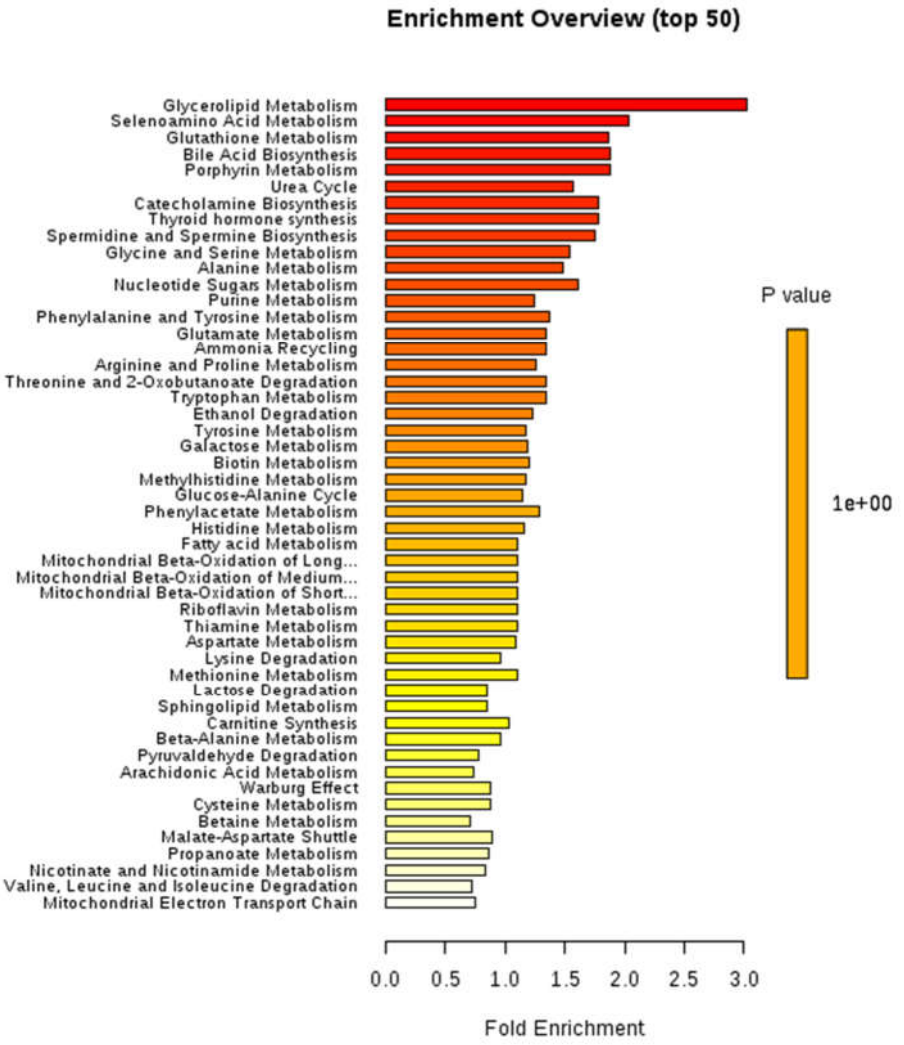

	Total Cmpd	Hits	Statistic Q	Expected Q	Raw p	FDR
Glycerolipid Metabolism	25	1	60.299	20	0.0693	0.8294
Selenoamino Acid Metabolism	28	2	40.607	20	0.0815	0.8294
Glutathione Metabolism	21	3	37.181	20	0.8784	0.8294
Bile Acid Biosynthesis	65	1	37.653	20	0.1951	0.8294
Porphyrin Metabolism	40	1	37.653	20	0.1951	0.8294

Figure 4.2: Summary plot for Metabolite Set Enrichment Analysis (MSEA) of metabolomic profile of faeces from chow-fed control and α7KO mice.

4.4 Clustering of metabolites according to genotype in HFD-fed mice

Following 12 weeks of HFD feeding, faecal samples were collected from the same mice discussed in the previous section of this chapter. Samples were extracted and measured in the same manner and were analysed using the same exploratory and functional analyses. Unfortunately, one control sample contained insufficient material to complete analysis. To compensate for this, the Missing Value Imputation function in MetaboAnalyst 4.0 was employed to replace sample values with the mean value of the remaining two to allow statistical testing.

PLS-DA was used to measure the clustering of HFD-fed samples to measure the predictability of the control and α7KO samples (Figure 4.3A). As before in chow-fed mice, there was positive clustering of the α7KO metabolomic profile but a large variation in control mice. A Q^2 value of -0.1778 was calculated, indicating that, again, HFD-fed control and α7KO models have a poor predictability in terms of metabolomics.

To explore the difference between individual metabolites we performed a Student's T-Test (Figure 4.3B). As shown in chow-fed control and α7KO mice, there was no significant difference between any individual metabolites measured. Full readout can be seen in Appendix Table 10.3.

To visually display different distribution levels in control and α7KO metabolomic profiles, a heatmap was generated (Figure 4.3C). This further demonstrated the variance in the HFD-fed metabolomic profile. There is a large variance between the two measured samples which makes the addition of a calculated mean sample nonbeneficial. This variation, again, makes concluding differences or similarities between control and HFD metabolomics profiles very difficult.

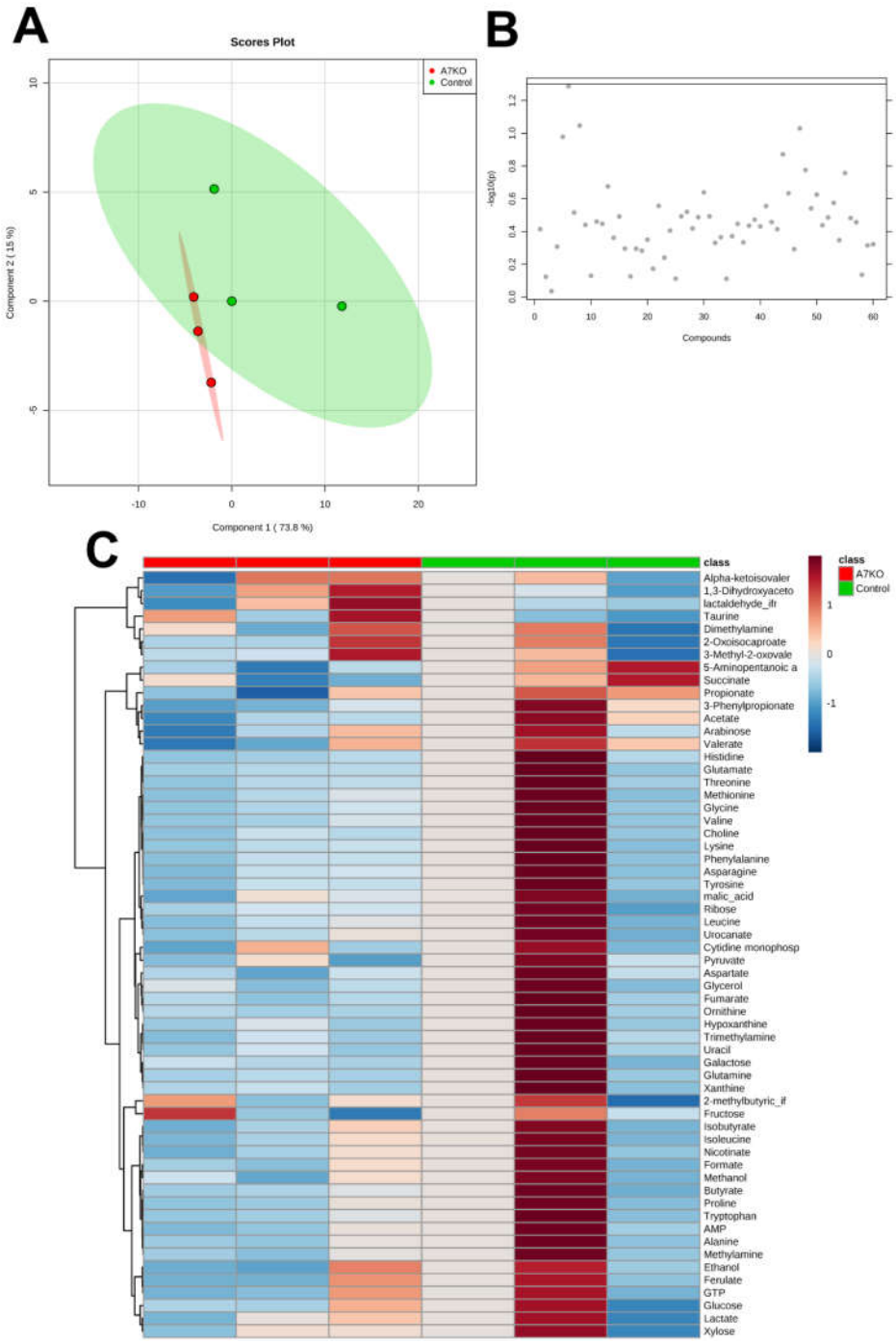

Figure 4.3: Exploratory analysis of metabolomic profiles from faeces collected from HFD-fed control and α7KO mice. (A) PLS-DA analysis score plots of metabolomic profiles. Dots represent individual mouse samples. Coloured oval represents 95% confidence region of genotype. **(B)** Visual representation of Student's T-Test of individual metabolites. **(C)** Heatmap visualisation of changes in metabolite levels between control and α7KO mice.

4.5 Functional analysis of metabolites in HFD-fed mice

As there were no single metabolites in the metabolomic profile of faeces from HFD-fed control and α7KO that were significantly different, it was important to look at the slight changes in groups of metabolites. Functional analysis was completed via MSEA in MetaboAnalyst 4.0.

A summary plot of the MSEA analysis is shown in Figure 4.4. There was very little overlap with affected pathways from chow-fed mice. Though, the butyrate metabolic pathway was shown to be significantly altered. The combination of the elevation of adenosine monophosphate, butyrate and succinate in control mice provides evidence that the butyrate metabolic pathway is significantly less active in α7KO mice. However, it is not possible to say whether this pathway is truly significantly different due to the variance and incomplete data set of HFD-fed control mice. The full readout of the MSEA can be seen in Appendix Table 10.4. With the combination of exploratory and functional analyses completed on the metabolic profiles of faeces from HFD-fed control and α7KO mice, it is not possible to draw conclusions at this time.

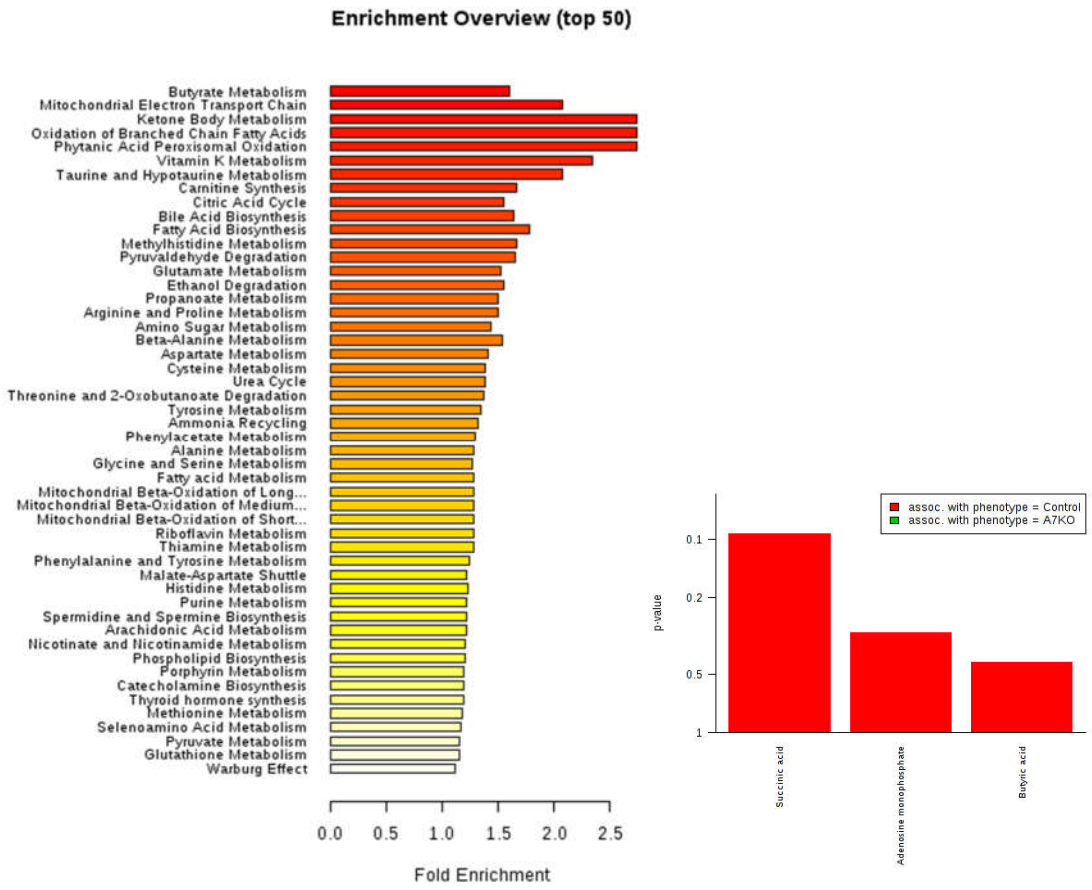

	Total Cmpd	Hits	Statistic Q	Expected Q	Raw p	FDR
Butyrate Metabolism	19	3	32.065	20	0.0280	0.5141
Mitochondrial Electron Transport Chain	19	2	41.465	20	0.0839	0.5141
Ketone Body Metabolism	13	1	54.631	20	0.0932	0.5141
Oxidation of Branched Chain Fatty Acids	26	1	54.631	20	0.0932	0.5141
Phytanic Acid Peroxisomal Oxidation	26	1	54.631	20	0.0932	0.5141

Figure 4.4: Summary plot for Metabolite Set Enrichment Analysis (MSEA) of metabolomic profile of faeces from HFD-fed control and α7KO mice

4.6 Summary

Development of metabolic diseases, including obesity and insulin resistance, are due to interplay between generic, epigenetic and environmental factors. It has been widely shown that the onset of insulin resistance is linked with obesity, however, the mechanism is still not completely understood. One such method of investigation is termed: 'metabolomics', in which small molecules that are involved in metabolic functions, deemed 'metabolites', are measured in biological samples (Goodacre et al., 2004). Metabolomics uses both qualitative and quantitative analysis where either non-target or targeted metabolite profiling is conducted. Non-targeted profiling is able to identify a large number of metabolites, whereas, targeted profiling uses existing knowledge of metabolomic pathways and can accurately quantify those selected metabolites.

In this study we isolated faecal pellets from both chow- and HFD-fed α7KO and control mice. Samples were prepared and analysed using NMR spectroscopy. Peaks were identified and quantified before being analysed by MetaboAnalyst 4.0. We used a variety of statistical tests to highlight differences between the metabolomic profile of α7KO and control mice.

4.6.1 The metabolomic profile of chow-fed integrin α7 deficient mice

Using PLS-DA, we aimed to construct a model to visually separate α7KO and control samples based on their metabolomic profile. Unfortunately, due to the variance in the metabolomic profile of control mice, the predictability value of our model (Q^2) was -1.69, indicating a very poor predictability between chow-fed control and α7KO mice. Of the samples we had, Student's T-Testing demonstrated that there was no significant difference between any of the individual metabolites measured, nor did visually representing the data in a heatmap reveal any obvious clustering.

We continued analysis of chow-fed control and α7KO metabolomic profiles by employing MSEA. The purpose of MSEA is to detect slight changes in a pattern of metabolites that may not be significantly different when compared individually. However, no pathways were found to be significantly different. The pathway which was most different according to statistical analysis was the glycerolipid metabolism pathway. In chow-fed α7KO mice we observed increased levels of glycerol excreted in the faeces. Other studies have demonstrated that increased glycerol levels are a characteristic of the onset of diabetes (Diao et al., 2014). Clearly, control chow-fed mice are not diabetic but this reduced circulation of glycerol in α7KO mice could suggest protection from the development of the disease.

4.6.2 The metabolomic profile of HFD-fed integrin α7 deficient mice

We continued our investigation by isolating faecal samples from mice fed a HFD for 12 weeks. We proceeded to use the same statistical analysis as previously used on chow-fed samples.

Unfortunately, due to a sampling error we were only able to obtain two useable samples from HFD-fed control mice. To make statistical testing possible, we utilised MetaboAnalyst 4.0's Missing Value Imputation function which creates a false sample based on the average of the two real samples. PLS-DA was used to generate a model to visually separate HFD-fed α7KO and control samples based on their metabolomic profile. However, due to the variance in the control metabolomic profile, the model had a very low predictability value. Student's T-Testing of individual metabolites showed that no individual metabolites and heatmap visualisation revealed no clustering.

We employed MSEA analysis to identify significantly different pathways between HFD-fed control and α7KO metabolomic profiles. Curiously, the butyrate metabolism pathway was found to be significantly different. Increased levels of: succinic acid, AMP and butyric

acid in controls indicated that butyrate metabolism had been altered. Studies in humans demonstrate that those suffering from type I or type II diabetes have increased levels of AMP and butyric acid (Zeng et al., 2011; Dudzinska, 2014). However, studies have also demonstrated that sufferers from type I diabetes do not possess altered succinic acid levels (Oresic et al., 2008). However, it is worth mentioning that the mechanisms of type I and type II diabetes are vastly different.

Interestingly, ingested butyrate glycerides has been shown to alter body fat deposition via regulation of gene expression (Yin et al., 2016). Increased ingestion of butyrate glycerides in broiler chickens resulted in a significant decrease in abdominal fat compared to total body weight. *THRSP, EGR-1,* and downstream genes of PPAR-α were significantly altered in chickens fed increased butyrate glycerides. *THRSP* is a transcription factor regulator of lipogenesis and adipo-genesis. *EGR-1* induces expression of IGF-2, PDGF and FGF. However as shown in our data, α7KO mice had reduced levels of butyric acid contrasting that found in the study of Yin *et al.*

Although we see a difference in one pathway in HFD-fed chow and α7KO mice it is still uncertain as to whether this result can be trusted. As previously mentioned, a false sample was generated to make statistical analysis possible. Therefore, further samples would need to be analysed to reach a conclusion.

CHAPTER 5: THE ROLE OF INTEGRIN A7 IN THE INSULIN SIGNALLING PATHWAY

5.1 Introduction

Two of the main signalling pathways activated by integrins in skeletal muscle are the mitogen-activated protein kinase (MAPK) and the Akt pathways. The MAPK pathway is made up of three families of kinases: extracellular signal-regulated kinase (ERK), Jun N-terminal kinase (JNK) and p38 (Johnson and Lapadat, 2002). Activation of ERK is initiated by extracellular stimuli that can be induced via integrins (Yee et al., 2008). There are two isoforms of ERK: ERK1 and ERK2, with differing roles. The deletion of ERK1 resulted in viable mice with no overt phenotype, whereas ERK2 deficient mice died in utero around embryonic day 6.5 (Pagès et al., 1999; Hatano et al., 2003). ERK1 and ERK2 have been shown to be involved in the synthesis of proteins in skeletal muscle but also in the regulation of insulin sensitivity (Zhang et al., 2011). The crosstalk of integrins, MAPK and insulin sensitivity is still not fully understood. Therefore, ERK has been a candidate of interest during this study.

Akt consists of three isoforms: Akt1, Akt2 and Akt3. All are ubiquitously expressed but vary in expression depending on the tissue (Yu et al., 2015). Deletion of Akt1 resulted in foetal and postnatal growth defects but possessed normal insulin sensitivity and glucose tolerance (Cho et al., 2001a). In contrast, Akt2 deficient mice were less insulin sensitive and glucose tolerant than controls (Cho et al., 2001b). Akt3-deficient mice had completely normal metabolism, with no change in insulin sensitivity or glucose tolerance, however, Akt3 levels in adipocytes were increased by insulin (Barthel et al., 1998; Easton et al., 2005). The phosphorylation of Akt on the serine 473 and threonine 308 site is involved in insulin signalling and the translocation of GLUT4. Integrin β1 has been shown to be involved in the phosphorylation of Akt1 on the serine 473 site, demonstrating the link between integrins and insulin signalling (Velling et al., 2004).

As has already been discussed in this study, the insulin sensitivity of α7KO mice is higher compared to control mice when fed either a chow or a HFD for 12 weeks. This was apparent in whole body insulin tolerance tests and glucose tolerance tests, discussed in

Chapter 3 in greater detail.

Integrins play a clear role in insulin sensitivity, however, the exact molecular mechanism that results in increased insulin sensitivity has still not been concluded. As skeletal muscle is responsible for approximately 80% of all insulin-stimulated glucose uptake, we sought to investigate what effect the deletion of integrin α7 has on the insulin signalling pathway. We achieved this by quantifying protein expression via Western blotting of various nodes of the insulin signalling pathway from α7KO and control mice fed a chow or a HFD.

5.2 ERK and Akt signalling in chow-fed integrin α7 deficient mice

As previous data in Chapter 3 has shown, α7KO mice are significantly more insulin sensitive than control mice when fed a chow diet and, to a greater extent, when fed a HFD for 12 weeks. However, we sought to investigate the mechanism of how integrin α7 deficiency results in insulin sensitivity. To understand this, we investigated the insulin signalling pathways in α7KO and control mice.

In this study, we isolated the gastrocnemius (GC) muscle from 6-month-old mice fed either a chow or a HFD. GC muscles were lysed in RIPA buffer with protease and phosphatase inhibitors. Samples were prepared under reducing conditions before being loaded and run through SDS polyacrylamide gels. Gels were transferred overnight onto membranes before being blocked. Membranes were probed with antibodies against pan-Akt, pAkt(Ser473), pAkt(Thr308), ERK1/2, pERK1/2(Thr202/Tyr204), as well as heat shock protein 70 as a loading control protein. Membranes were washed and probed with secondary antibodies before being visualised via enhanced chemiluminescence.

As shown in Figure 5.1, total levels of Akt (including Akt1, Akt2 and Akt3) were not different between chow-fed α7KO and control GC muscle lysates. There was also no significant difference between the total levels of ERK1 and ERK2 between chow-fed α7KO and control GC muscle lysates.

To quantify the activation of insulin signalling, we calculated the ratio of pAkt:Akt. As previously discussed, total activation of Akt requires phosphorylation on sites: Serine473 and Threonine308. There was no significant difference in normalised ratios of pAkt(Ser473):Akt between control and α7KO mice. Neither was there a difference in pAkt(Thr308):Akt. Phosphorylated levels of ERK were undetectable so at this moment we cannot comment on the ERK signalling pathway in chow-fed α7KO and control mice. This data replicates that of the insulin sensitivity tests discussed in Chapter 3 where there was no significant difference between chow-fed α7KO and control insulin sensitivity.

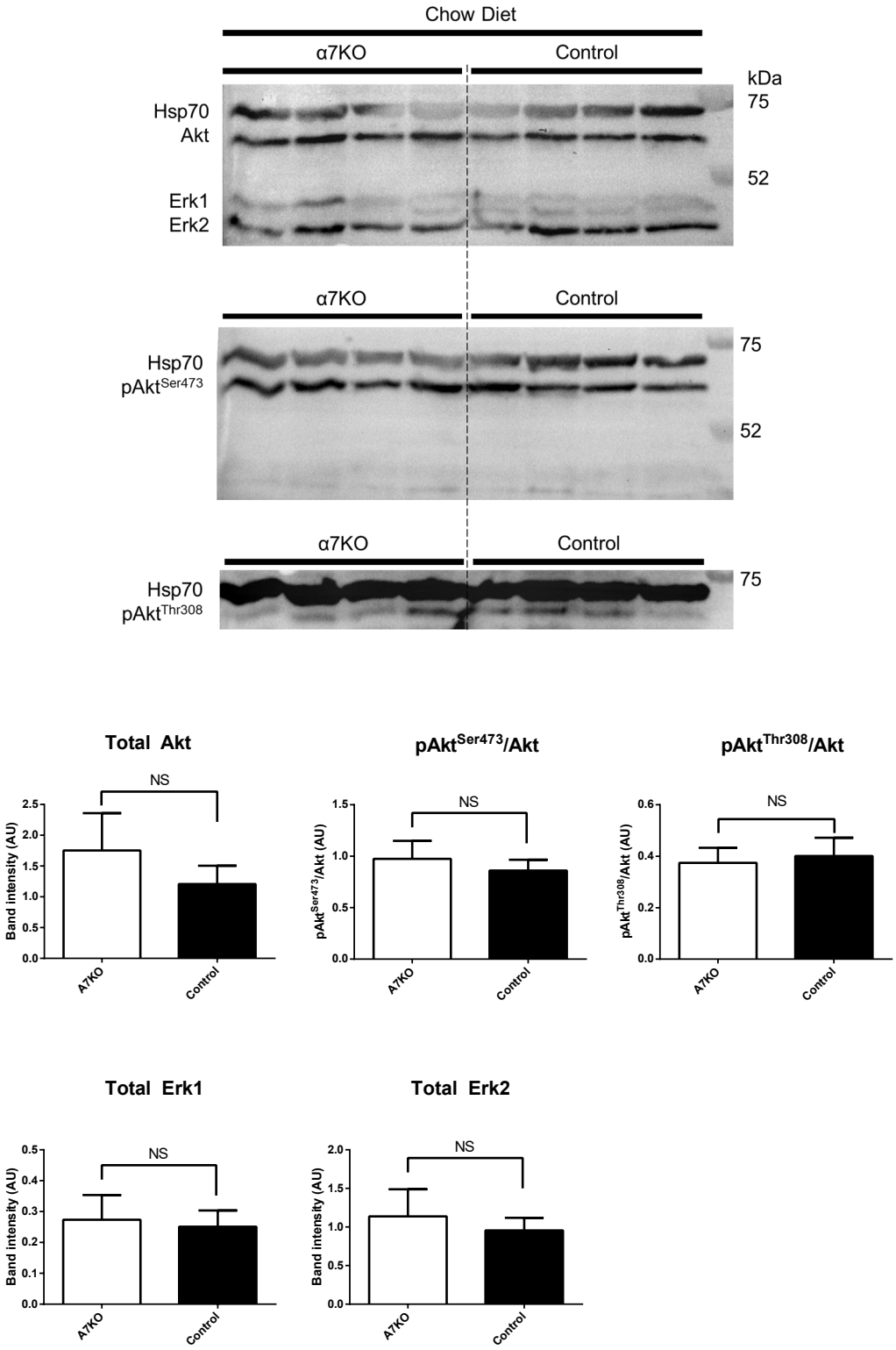

Figure 5.1: Quantification of total and phosphorylated ERK and Akt in chow-fed control and α7KO GC muscle. Immunoblot analysis of total Akt, pAkt(Ser473), pAkt(Thr308), total ERK1/2 and pERK1/2(Thr202/Tyr204) in chow-fed control and α7KO GC muscle lysates. Bar charts represent densitometry of Western blots. The data are mean ± SEM (n = 4). Statistical analysis was completed using an independent t-test.

5.3 ERK and Akt signalling in HFD-fed integrin α7 deficient mice

Chow-fed α7KO and control mice have similar insulin sensitivity which is further supported by a lack of difference between Akt and ERK signalling. However as discussed in Chapter 3, we found that when α7KO mice are fed a HFD, they remain insulin sensitive, whereas control mice become less insulin resistant. To investigate this phenotype further, we analysed protein lysates from HFD-fed α7KO and control mice.

Concurrent with results in chow-fed mice, there was no significant difference in levels of total Akt between HFD-fed α7KO or control mice (Figure 5.2). However, we observed significantly higher ratios of pAkt(Ser473):Akt and pAkt(Thr308):Akt in α7KO mice compared to controls. This data replicated that of HFD-fed mice in Chapter 3 in terms of insulin sensitivity. HFD-fed α7KO mice have a significantly higher level of basal phosphorylated Akt in GC muscle further demonstrating their insulin sensitivity. Interestingly, we observed a significantly higher level of total ERK2 in HFD-fed α7KO mice. Levels of pERK1 were undetectable, however, there was a significantly lower ratio of pERK2 :ERK2 in α7KO mice when compared to control mice.

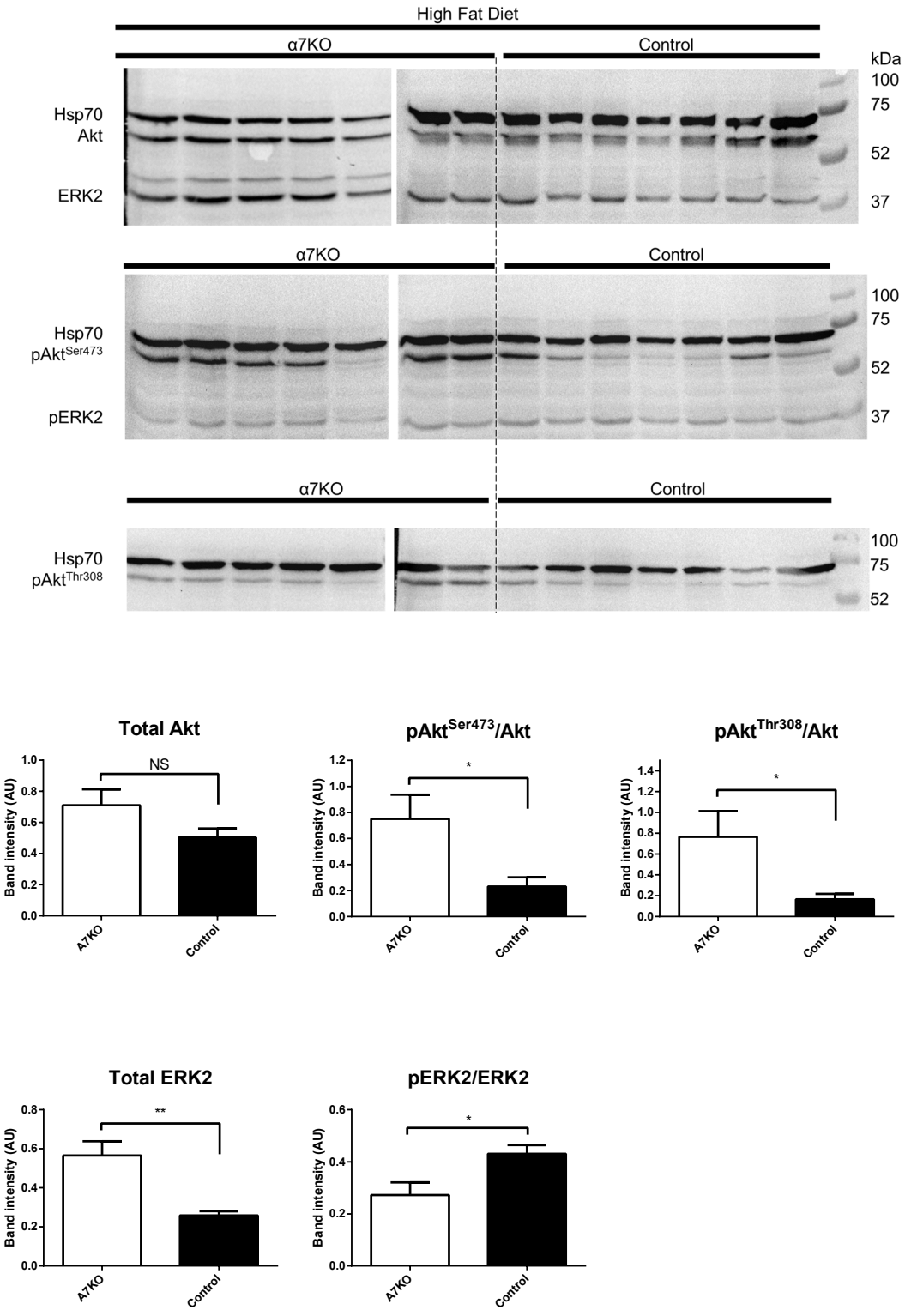

Figure 5.2: Quantification of total and phosphorylated ERK and Akt in HFD-fed control and α7KO GC muscle immunoblot. Immunoblot analysis of total Akt, pAkt(Ser473), total ERK1/2 and pERK1/2(Thr202/Tyr204) in HFD-fed control and α7KO GC muscle. Bar charts represent densitometry of Western blots. The data are mean ± SEM (n = 7). Statistical analysis was completed using an independent t-test.

5.4 ERK and Akt signalling in insulin-challenged chow-fed integrin α7 deficient mice

To further investigate the effect the deletion of integrin α7 has on insulin signalling, we sought to explore how challenging mice with insulin would affect phosphorylation levels. By challenging mice with insulin, we would be able to observe a snapshot of the insulin signalling pathway at its most active. Mice were intraperitoneally injected with 0.75 U/kg of insulin and were sacrificed 15, 30, 60 or 120 minutes later. GC muscles were isolated, lysed and immunoblotted for pAkt and Akt to determine optimal timing. We calculated the largest levels of pAkt to be at time point 60 minutes (data not shown).

Chow-fed control and α7KO mice were intraperitoneally injected with 0.75 U/kg of insulin. GC muscle was harvested after 60 minutes and snap frozen in liquid nitrogen. Protein lysates were prepared with phosphatase and protease inhibitors before being run under reducing conditions through SDS polyacrylamide gels. Gels were transferred overnight before being blocked. Membranes were probed with antibodies against insulin receptor β, p-insulin receptor β(Tyr1361), pan-Akt, pAkt(Ser473), pAkt(Thr308), ERK1/2, pERK1/2(Thr202/Tyr204) and heat shock protein 70 as a loading control protein. Membranes were washed and probed with secondary antibodies before being visualised via enhanced chemiluminescence. Protein bands were measured using densitometry and are shown in Figure 5.3.

In agreement with non-insulin challenged and chow-fed conditions, there was no significant difference in the total amount of Akt in insulin-challenged (Figure 5.3) GC muscle. Unexpectedly, there was no difference between the calculated ratio of either pAkt(Ser473):Akt or pAkt(Thr308):Akt. Curiously, we measured significantly greater levels of ERK1 in insulin-challenged, chow-fed α7KO GC muscle. However, there was no difference in between control and α7KO mice in terms of the calculated pERK1:ERK1 ratio. Similar levels of total ERK2 levels were measured between control and α7KO mice

and no difference was found in the calculated pERK2:ERK2 ratio. Furthermore, we detected no difference in the total levels of insulin receptor between control and α7KO GC muscle. Expectedly, there was no difference either in the calculated p-insulin receptor:insulin receptor level.

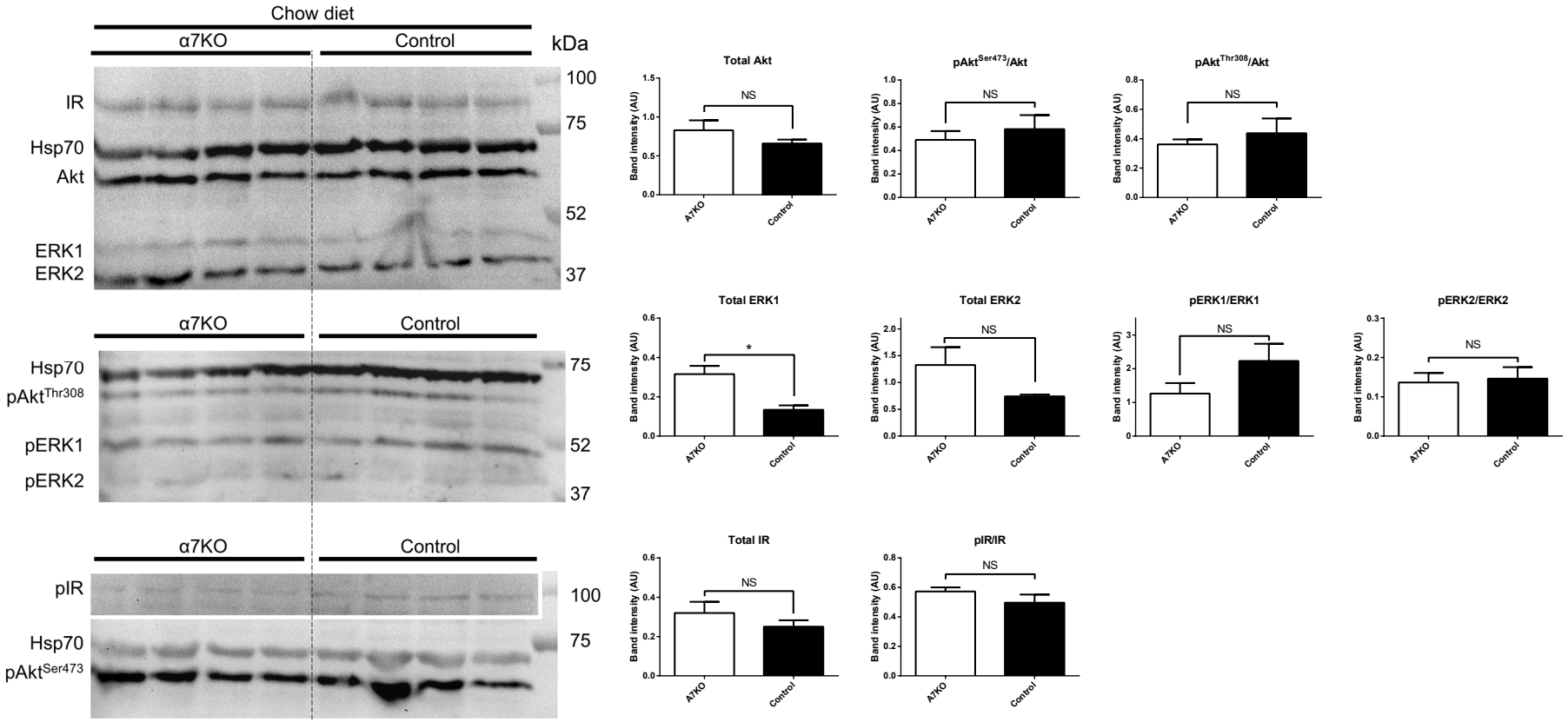

Figure 5.3: Quantification of total and phosphorylated ERK, Akt and Insulin Receptor in insulin-challenged, chow-fed control and α7KO GC muscle immunoblot. Immunoblot analysis of total Akt, pAkt(Ser473), pAkt(Thr308), total ERK1/2, pERK1/2(Thr202/Tyr204), total insulin receptor and phospho-insulin receptor in insulin-challenged chow-fed control and α7KO GC muscle. Bar charts represent densitometry of Western blots. The data are mean ± SEM (n = 4). Statistical analysis was completed using an independent t-test.

5.5 ERK and Akt in insulin-challenged HFD-fed integrin α7 deficient mice

As discussed in Chapter 3, α7KO remain significantly more insulin sensitive than control mice when fed a HFD. This is reinforced by significantly higher levels of pAkt(Ser473) and pAkt(Thr308) in α7KO GC muscle lysates compared to controls. We sought to investigate whether this observation is reflected when challenging HFD-fed control and α7KO mice with insulin.

Significantly higher levels of total Akt were measured in insulin-challenged HFD-fed α7KO GC muscles lysates compared to control (Figure 5.4). Curiously, this was not the case in non-insulin-challenged mice. Further reinforcing the insulin tolerance tests discussed in Chapter 3 and the non-insulin-challenged HFD-fed immunoblots, significantly higher levels of pAkt(Thr308):Akt were measured in α7KO mice. In contrast, no difference was measured in pAkt(Ser473):Akt levels between α7KO and control mice.

Quantification of ERK1 in a7KO and control HFD-fed insulin-challenged GC muscle showed that there was no difference in levels. In contrast to our data from HFD-fed non-insulin challenged mice, there was no difference in the calculated ratio of pERK1:ERK1. Furthermore, we found that there was no difference in levels of ERK2 or the ratio of pERK2:ERK2. Unfortunately, immunoblotting of the insulin receptor or p-insulin receptor was unsuccessful in these lysates.

To summarise, we see no change in ERK pathway in HFD-fed insulin challenged mice. Interestingly, we see no difference in the phosphorylation of Akt on the Serine473 site between α7KO and control mice but hugely more phosphorylation on the threonine308 site. This further supports our data from Chapter 3 suggesting deletion of integrin α7 results in an insulin sensitive phenotype.

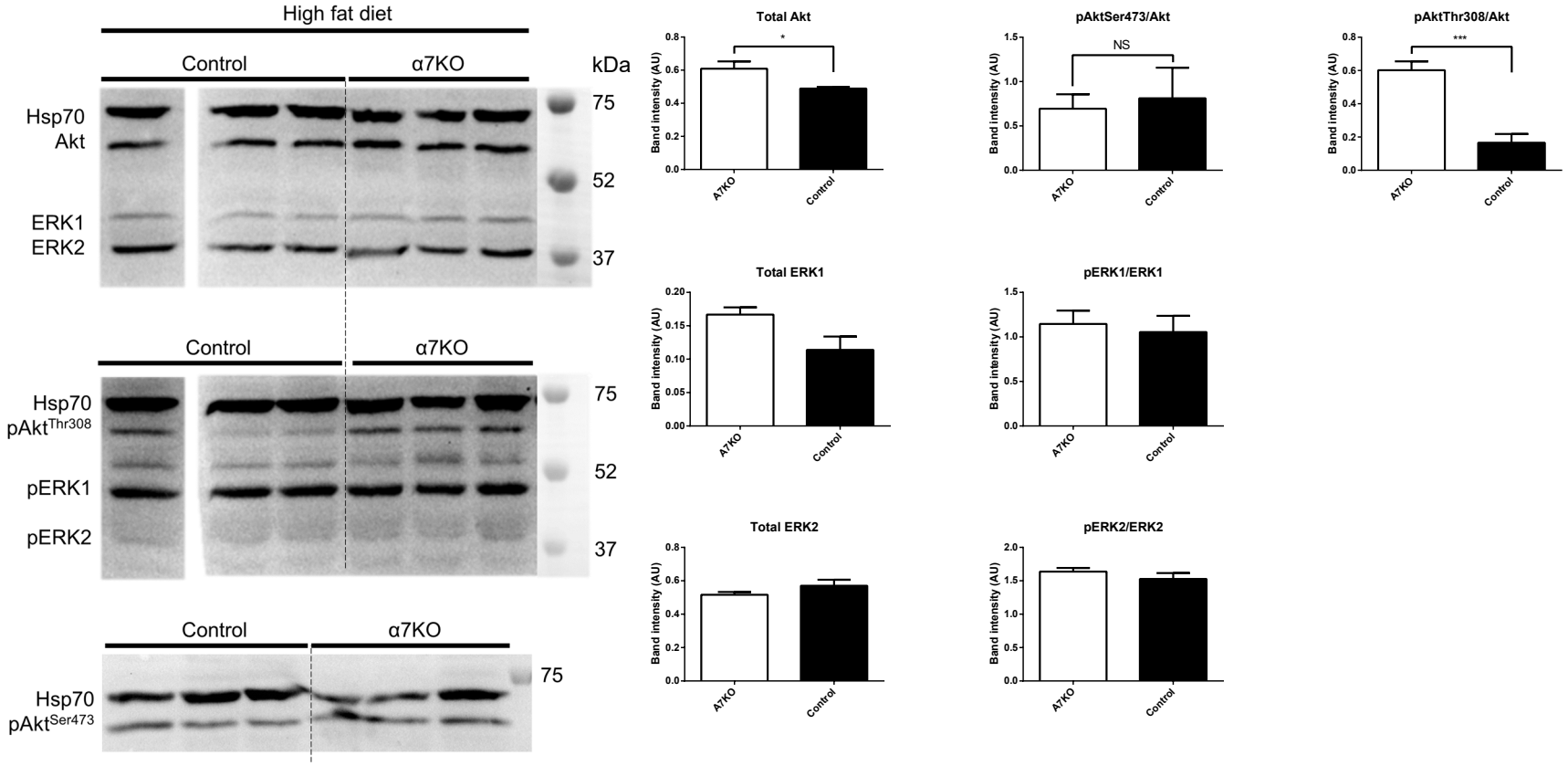

Figure 5.4: Quantification of total and phosphorylated ERK and Akt and in insulin-challenged, HFD-fed control and α7KO GC muscle immunoblot. Immunoblot analysis of total Akt, pAkt(Ser473), pAkt(Thr308), total ERK1/2 and pERK1/2(Thr202/Tyr204) in insulin-challenged HFD-fed control and α7KO GC muscle. Bar charts represent densitometry of Western blots. The data are mean ± SEM (n = 3). Statistical analysis was completed using an independent t-test.

5.6 Summary

Insulin resistance is strongly associated with metabolic syndrome, a cluster of symptoms that increases a patient's risk of developing heart disease and diabetes mellitus. These symptoms include obesity, hypertension, hyperglycemia, and dyslipidemia (Hoffman et al., 2015). The primary function of insulin signalling is the uptake of glucose and energy homeostasis predominantly in muscle, liver and adipose tissue. Imbalance of the modulation of this pathway can lead to a variety of diseases (Saltiel and Kahn, 2001). Unlocking the secrets of this pathway is essential to understanding how to treat these diseases.

Integrins are involved in a wide variety of signal transduction events modulating a variety of cellular functions including migration, proliferation and apoptosis (Cary et al., 1999). Many of these downstream effectors of integrin signalling overlap with the insulin signalling pathway, including FAK and integrin-linked kinase (ILK) (Hynes, 2002a; Moser et al., 2009). Therefore, it is no surprise that the deletion of integrin α7 may influence some of the downstream effects of the insulin signalling pathway.

In this study we analysed the protein lysates of gastrocnemius (GC) muscle from chow- and HFD-fed control and α7KO mice to investigate the effect the deletion of integrin α7 had on the insulin signalling pathway. To exacerbate this effect, we challenged the mice with 0.75 U/kg of insulin before isolating the GC muscle 60 mins later. We highlighted the Akt and ERK1/ERK2 signalling pathway as ideal candidates to investigate the insulin signalling pathway. Protein quantification was achieved by Western blotting and densitometry.

5.6.1 The effect of integrin α7 deficiency in the insulin signalling of non-insulin-challenged mice

In this section of the study, we used non-insulin challenged, chow- and HFD-fed mice to

investigate the basal insulin signalling in our models. We immunoblotted for: total Akt, pAkt(Ser473), pAkt(Thr308), ERK1, ERK2, pERK1 and pERK2.

In chow-fed mice, we discovered that there was no difference in the total levels of Akt, ERK1 or ERK2 between chow and α7KO GC muscle. Furthermore, when calculating the normalised ratios of the phosphorylated:total protein, we found that there was no significant difference in the values of pAkt(Ser473) or pAkt(Thr308). This was unsurprising as insulin tolerance tests, performed in Chapter 3, demonstrated that there was no significant difference in insulin sensitivity between the chow-fed model. Levels of phosphorylated ERK1 or ERK2 were undetectable.

In HFD-fed mice, we found, again, that there was no difference in total levels of Akt between control and α7KO GC muscle. Interestingly, when calculating the phosphorylated:total Akt ratios, we found that there was a significantly higher proportion of pAkt(Ser473) and pAkt(Thr308) in α7KO mice compared to controls. In contrast to our chow-fed data, there was significantly higher levels of total ERK2 in α7KO mice. However, this result was inversed with a significantly higher proportion of ERK2 being pERK2 in control mice. This data further suggests the glucose uptake branch of insulin signalling is more sensitive in HFD-fed α7KO mice.

5.6.2 The effect of integrin α7 deficiency in the insulin signalling of insulin-challenged mice

To investigate the insulin signalling pathway in its most active state, we injected mice intraperitoneally with 0.75 U/kg of insulin before isolating the GC muscle after 60 minutes. This would allow us to see a ‘snapshot’ of the insulin signalling pathway during active signalling.

In chow-fed mice, we observed a similar result to that of non-insulin-challenged mice with no difference in the amount of total Akt. Unsurprisingly, we also found no difference in the values of the ratio of phosphorylated:total protein of pAkt(Ser473) and

pAkt(Thr308). In contrast to our data in chow-fed mice, we detected significantly higher levels of total ERK1 in α7KO GC muscle. However, the administration of insulin should have no impact on total levels of ERK in such a small time, therefore, this result is inconclusive. In insulin-challenged mice we were able to detect phosphorylated levels of ERK1 and ERK2. However, the ratio of phosphorylated:total protein demonstrated that there was no significant difference between control and α7KO GC muscle levels. We also measured no significant difference in the total amount of insulin receptor or the ratio p-insulin receptor:total insulin receptor protein. This data supports our non-insulin-challenged data and our insulin tolerance data from Chapter 3.

In HFD-fed mice, we found that there was no significant difference in the total amount of ERK1 or ERK2 but, in contrast to non-insulin-challenged mice, a greater level of total Akt in α7KO mice. As mentioned previously, the administration of insulin should have no bearing on the total amount of Akt in such a short amount of time. Unfortunately, efforts to detect levels of insulin receptor or p-insulin receptor were unsuccessful in this study. Our data also showed that there was no difference in the proportion of pERK1 and pERK2 compared to their total protein values. In contrast to non-insulin-challenged data, we found that there was no significant difference in the ratio of pAkt(Ser473):Akt. However, we detected a greatly higher ratio of pAkt(Thr308):Akt in insulin-challenged, HFD-fed α7KO mice compared to controls. This further supports the idea of the deletion of integrin α7 markedly improving insulin sensitivity in HFD-fed mice.

CHAPTER 6: RESCUING THE INTEGRIN A7 DEFICIENCT PHENOTYPE WITH THE OVEREXPRESSION OF SPLICE VARIANTS

6.1 Introduction

Integrin α7β1 is the predominant integrin in skeletal, cardiac and smooth muscle cells. Mice deficient for integrin α7 develop a novel mild myopathy with disruption of the myotendinous junction. However, there is variation in the integrin α7 subunits with two cytoplasmic variants (α7A and α7B) and two extracellular variants (α7X1 and α7X2) (Ziober et al., 1993). The α7A cytoplasmic variant is only expressed weakly in mature skeletal muscle, whereas α7B is expressed in cardiac and skeletal muscle (Velling et al., 1996). The α7X1 and α7X2 variants are expressed at equal levels in skeletal muscle development and adult heart but only α7X2 can be found in adult skeletal muscle (Ziober et al., 1993). Through the combination of these cytoplasmic and extracellular variants, four integrin α7 splice forms are generated: α7X1A, α7X1B, α7X2A and α7X2B. This has been discussed in more detail in Section 1.5.4

Table 14: Expression of integrin α7 isoforms in adult (Von der Mark et al., 2002).

Integrin α7 isoform	Adult Expression
α7X1	Cardiac muscle
α7X2	Cardiac and skeletal muscle
α7A	Skeletal muscle
α7B	Cardiac, smooth, and skeletal muscle

Integrin α7β1 has been shown, *in vitro*, to play a crucial role in myoblast migration but also plays a pivotal role for skeletal muscle function and integrity, *in vivo,* by acting as a laminin receptor (Echtermeyer et al., 1996; Mayer et al., 1997; Von der Mark et al., 2002). However, due to the occurrence of alternative splice variants, the role of integrin α7 is probably more complicated than previously believed.

The deletion of integrin α7 in mice has led to a series of interesting phenotypes previously

discussed in this thesis. We sought to investigate whether the overexpression of any of the four integrin α7 splice variants were able to rescue the α7KO phenotype. To investigate the role of the integrin α7 splice variants in diet-induced obesity, we used α7 deficient mice crossed with transgenic mice that use the **H**uman **S**keletal Alpha **A**ctin (HSA) promoter to drive the expression of each of the four possible combinations of integrin α7 splice variants in all intra- and extracellular combinations. These mice were previously selected in our lab by ensuring that each of the four possible splice variants was expressed at similar levels in each of the founder mice.

6.2 The effect of integrin α7 splice variant overexpression on body weight

As previously discussed, α7KO mice are significantly leaner than control mice when fed a chow diet. When α7KO and control mice were fed a HFD, control mice gained weight but α7KO mice remained lean. To investigate whether the overexpression of any of the integrin α7 splice variants could rescue the α7KO phenotype, integrin α7 deficient mice overexpressing one of the four splice variants were each fed a HFD for 12 weeks and their body weights were measured over time ($\alpha7\text{-/-}^{TG}$).

When fed a chow diet, $\alpha7\text{-/-}^{X1A}$, $\alpha7\text{-/-}^{X1B}$ and $\alpha7\text{-/-}^{X2B}$ were all found to weigh significantly less than both α7KO and, to a greater extent, control mice. The reduction in body weight of the X2B splice variant overexpressing mouse was particularly surprising as X2B is the predominant splice variant of integrin α7 found in adult skeletal muscle. There was no significant difference of body weight in $\alpha7\text{-/-}^{X2A}$ mice compared to α7KO or control (Figure 6.1A).

As previously discussed, when α7KO mice were fed a HFD, they did not gain weight and remained significantly lighter than control mice. However, when integrin α7 splice variant overexpressing mice were fed a HFD, all four splice variants remarkably rescued the

α7KO trait of gaining weight. Integrin α7 splice variant: α7X1B, α7X2A and α7X2B all had a comparable ability to gain weight as that of control mice. Interestingly, integrin α7X1A mice gained significantly more normalised weight than control mice also. Together, this data shows that there is no difference between embryonic and adult integrin α7 splice variants in terms of their ability to rescue the lean α7KO phenotype.

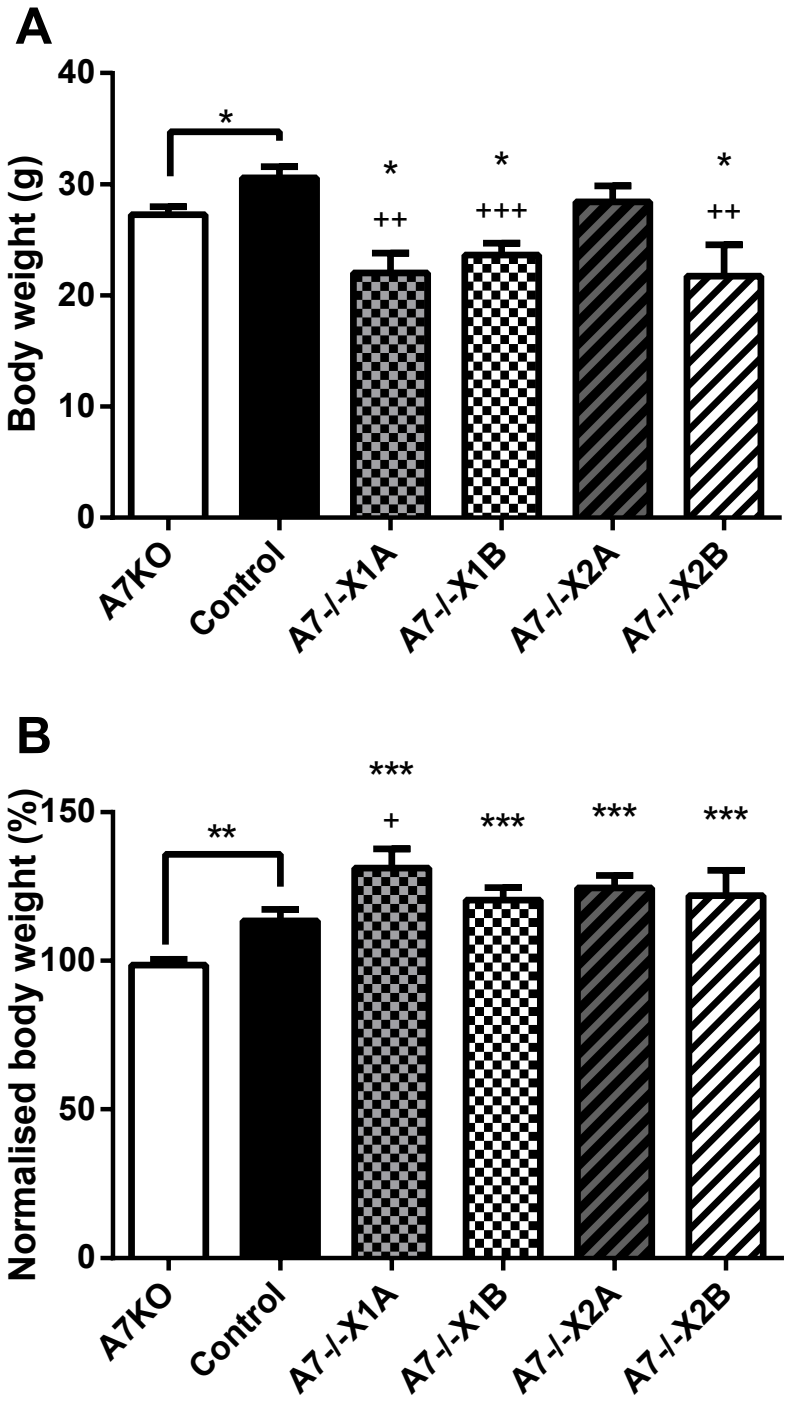

Figure 6.1: Integrin α7 splice variant overexpression affects chow-fed weight but rescues weight gain after HFD. (A) Body weight of chow-fed α7KO, control and integrin α7 deficient mice overexpressing one of the four integrin α7 splice variants. **(B)** Normalised weight over 12 weeks, when fed a HFD, compared to week 0, chow fed body weight. The data are mean ± SEM (α7KO n = 7, Control n = 7, α7-/-^{X1A} n = 4, α7-/-^{X1B} n = 5, α7-/-^{X2A} n = 6, α7-/-^{X2B} n = 3). (*) significantly different from α7KO. ($^{+}$) significantly different from control. */$^{+}$ $p < 0.05$, **/$^{++}$ $p < 0.01$, ***/$^{+++}$ $p < 0.001$. Statistical analysis was completed using a two-way ANOVA with a Tukey post-hoc test.

6.3 The effect of integrin α7 splice variant overexpression on insulin sensitivity and glucose tolerance

As previously discussed, α7KO mice are hyper insulin sensitive when fed either a chow or a HFD compared to control mice. Weight gain was rescued by overexpression of integrin α7 splice variants, therefore we sought to investigate whether the overexpression of any of the four splice variants of integrin α7 could also rescue the hyper insulin sensitive phenotype of α7KO and result in a phenotype more comparable to a control mouse. In this experiment, mice were aged to 3 months and initial metabolic tests were performed. The IPITT was used to measure insulin sensitivity and the IPGTT was used to measure glucose tolerance. Thereafter, mice were fed a HFD for 12 weeks before IPITT and IPGTT were repeated.

6.3.1 Measuring insulin sensitivity in chow and HFD-fed integrin α7 splice variant overexpressing mice

Insulin tolerance tests were performed at 3 months and 6 months old mice on a chow and HFD, respectively. When fed a chow diet, there was no significant difference in insulin sensitivity between control and α7-/-^{X1A} mice. However, α7KO mice were slightly, but significantly, less insulin sensitive than α7-/-^{X1A} (Figure 6.2A). In contrast, when fed a HFD for 12 weeks, α7-/-^{X1A} mice became significantly more insulin sensitive than control mice (Figure 6.2B). There was no difference between α7-/-^{X1A} and α7KO mice showing that overexpression of integrin α7 X1A splice variant did not rescue the insulin sensitive phenotype of α7KO mice.

There was no significant difference between control and α7-/-^{X1B} insulin sensitivity when fed a chow diet. However, α7KO mice were significantly less insulin sensitive than α7-/-^{X1B} mice (Figure 6.2C). Although, when fed a HFD, α7-/-^{X1B} become significantly more insulin sensitive than control mice but similar in insulin sensitivity to α7KO mice (Figure

6.2D). Therefore, the overexpression of α7 integrin X1B splice variant does not rescue the insulin sensitive phenotype.

When α7-/-^{X2A} mice are fed a chow diet, it is unclear whether their insulin sensitivity is more similar to α7KO or control mice. During the IPITT, α7-/-^{X2A} mice reacted at various points similarly to either α7KO or control mice (Figure 6.2E). Therefore, it is not possible to draw conclusions of the integrin α7 X2A splice variant's ability to rescue the insulin sensitive phenotype when fed a chow diet. However, when fed a HFD for 12 weeks, α7-/-^{X2A} mice were significantly less insulin sensitive than α7KO mice with no significant difference from controls (Figure 6.2F). Thus, integrin α7 X2A splice variant is able to rescue the insulin sensitive phenotype of α7KO mice, when fed a HFD, and is much more comparable to controls.

Surprisingly, when α7-/-^{X2B} mice were fed a chow diet, they were significantly less insulin sensitive than control and, , α7KO mice (Figure 6.2G). Overexpression of integrin α7 X2B splice variant is the only example of the four splice variants to significantly reduce insulin sensitivity to less than control mice. This effect was exacerbated when α7-/-^{X2B} were fed a HFD for 12 weeks. HFD-fed α7-/-^{X2B} were significantly less insulin sensitive than both α7KO and control mice. Therefore, integrin α7 X2B splice variant is able to rescue the insulin sensitive phenotype of α7KO mice on both a chow and HFD.

In contrast to our HFD-fed weight-gain experiments, only the integrin α7 splice variants: α7X2A and α7X2B predominantly found in adult skeletal muscle were able to rescue the insulin sensitive phenotype of α7KO mice. Overexpression of integrin α7 splice variants: α7X1A and α7X1B did not contribute to rescue the α7KO phenotype most probably as α7X1 is only expressed during the initial stages of myogenesis. However, it was important to explore the rescue of the α7KO phenotype further by investigating glucose tolerance.

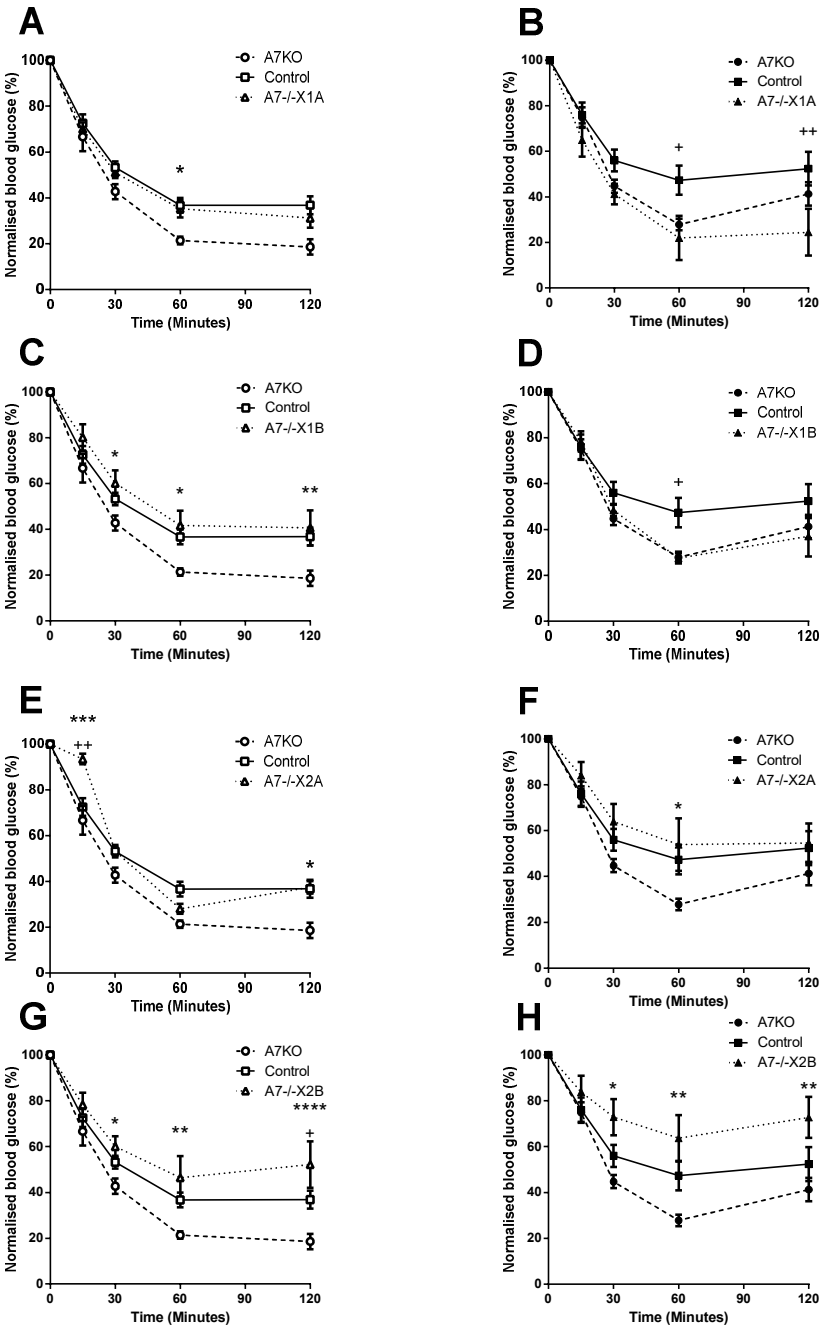

Figure 6.2: IPITT of α7KO, control and integrin α7 splice variant overexpressing mice on a chow and a HFD. (A, C, E, G) Following a 6 hour fast, IPITT was performed using 0.75 U/kg of insulin on chow fed α7KO, control and **(A)** A7-/-^{X1A}, **(C)** A7-/-^{X1B}, **(E)** A7-/-^{X2A} and **(G)** A7-/-^{X2B} mice. **(B, D, F, H)** Following a 6 hour fast, IPITT was performed using 0.75 U/kg of insulin on HFD-fed α7KO, control and **(B)** A7-/-^{X1A}, **(D)** A7-/-^{X1B}, **(F)** A7-/-^{X2A} and **(H)** A7-/-^{X2B} mice. The data are mean ± SEM (α7KO n = 7, Control n = 7, α7-/-^{X1A} n = 4, α7-/-^{X1B} n = 5, α7-/-^{X2A} n = 6, α7-/-^{X2B} n = 3). Statistical analysis was completed using an independent t-test. (*) integrin α7 splice variant overexpressing mouse significantly different from α7KO. ($^{+}$) integrin α7 splice variant overexpressing mouse significantly different from control. */$^{+}$ $p < 0.05$, **/$^{++}$ $p < 0.01$, ****/$^{++++}$ $p < 0.0001$

6.3.2 Measuring glucose tolerance in chow and HFD-fed integrin α7 splice variant overexpressing mice

Following insulin sensitivity testing via IPITT, glucose tolerance was measured using an IPGTT on a chow and HFD at 3 months and 6 months of age, respectively. It is difficult to predict if the overexpression of α7 integrin splice variants affect the glucose tolerance of mice when fed a chow diet as there was no difference in the glucose tolerance of α7KO and control mice when fed a chow diet. When α7-/-^{X1A} mice were fed a chow diet, glucose tolerance was significantly higher than both chow-fed α7KO and control mice (Figure 6.3A). However, when fed a HFD, there was no significant difference between α7-/-^{X1A} glucose tolerance and that of α7KO or control mice (Figure 6.3B).

There was no significant difference in glucose tolerance between chow-fed α7-/-^{X1B} mice and α7KO or control mice (Figure 6.3C). However, when fed a HFD, α7-/-^{X1B} were significantly more glucose tolerant than control mice and comparable with α7KO mice (Figure 6.3D).

On a chow diet, α7-/-^{X2A} mice were significantly more glucose tolerant than α7KO mice (Figure 6.3E). When fed a HFD, there is no significant difference between α7-/-^{X2A} mice and α7KO or control mice (Figure 6.3F). Glucose tolerance of α7-/-^{X2A} mice appears to fall between that of α7KO and control mice.

When α7-/-^{X2B} mice were fed a chow diet, IPGTT tests showed that they were significantly less glucose tolerant than control animals (Figure 6.3G). Data interpretation suggests that α7-/-^{X2B} mice are also less glucose tolerant than α7KO mice. Interestingly, when fed a HFD, α7-/-^{X2B} mice became significantly less glucose tolerant than α7KO mice (Figure 6.3H). Our data further indicates that these mice are also slightly less glucose tolerant than control mice.

To summarise, it is not possible to conclude whether overexpression of integrin α7 X1A and X2A splice variants rescue the α7KO phenotype as their glucose tolerance lies

between α7KO and control values. Integrin α7 X1B is not able to the rescue the α7KO phenotype. However, data suggests that as seen in insulin sensitivity tests, integrin α7 X2B splice variant overexpression is able to the rescue the glucose tolerance phenotype observed in α7KO mice.

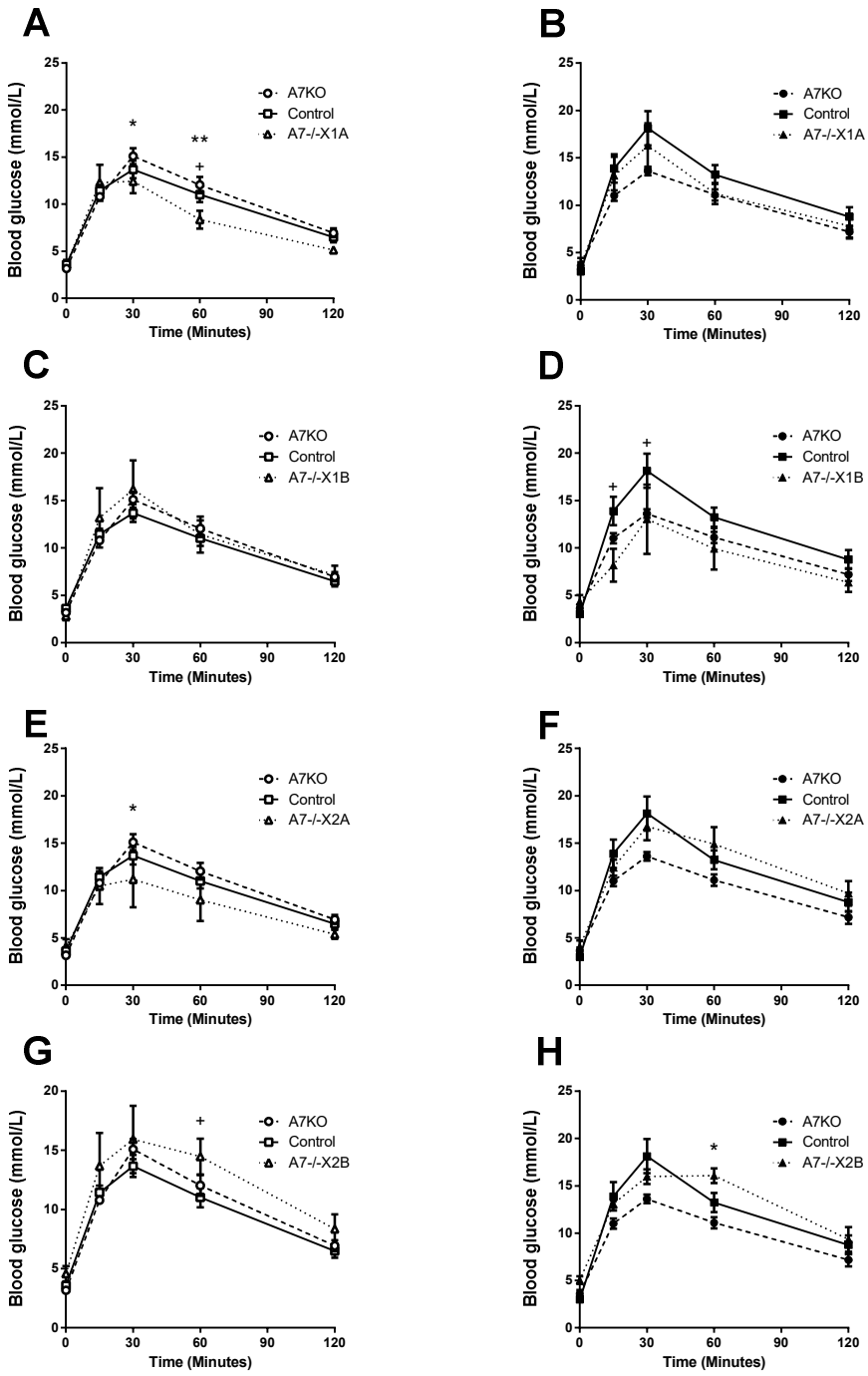

Figure 6.3: IPGTT of α7KO, control and integrin α7 splice variant overexpressing mice on a chow and a HFD. (A, C, E, G). Following a 16 hour fast, IPGTT was performed using 2 g/kg of glucose on chow fed α7KO, control and **(A)** A7-/-^{X1A}, **(C)** A7-/-^{X1B}, **(E)** A7-/-^{X2A} and **(G)** A7-/-^{X2B} mice. **(B, D, F, H)** Following a 16 hour fast, IPGTT was performed using 2 g/kg of glucose on HFD-fed α7KO, control and **(B)** A7-/-^{X1A}, **(D)** A7-/-^{X1B}, **(F)** A7-/-^{X2A} and **(H)** A7-/-^{X2B} mice. The data are mean ± SEM (α7KO n = 7, Control n = 7, α7-/-^{X1A} n = 4, α7-/-^{X1B} n = 5, α7-/-^{X2A} n = 6, α7-/-^{X2B} n = 3). Statistical analysis was completed using an independent t-test. (*) integrin α7 splice variant overexpressing mouse significantly different from α7KO. ($^{+}$) integrin α7 splice variant overexpressing mouse significantly different from control. */$^{+}$ $p < 0.05$, **/$^{++}$ $p < 0.01$

6.4 The role of integrin α7 splice variants in liver histology

As previously discussed in Chapter 3, the deletion of integrin α7 resulted in higher levels of liver steatosis compared to control mice when fed a HFD. We sought to investigate whether the overexpression of α7 integrin splice variants under the control of the muscle-specific HSA promotor would rescue the steatosis phenotype in α7KO mice.

Liver sections were fixed and cryoprotected before being frozen in OCT compound. Livers were cryosectioned and stained with HCS LipidTOX™ Green neutral lipid stain. The LipidTOX™ neutral lipid stain has an extremely high affinity for neutral lipid droplets and can be observed using fluorescence microscopy. Unfortunately, quantification of fluorescence was not possible due to time constraints.

Surprisingly, ectopic fat depositions were present in mice overexpressing integrin α7 X1A and X1B splice variants, albeit to a lesser extent that α7KO mice (Figure 6.4). However, whereas α7KO mice livers showed macrovesicular steatosis, integrin α7X1A and X1B overexpressing mice seem to be suffering from less severe early steatosis.

Interestingly, there was no evidence of lipid deposition in α7-/-^{X2A} or α7-/-^{X2B} mice (Figure 6.4) livers when fed a HFD. Livers appeared identical to those from HFD-fed control mice. This is extremely surprising as, previously discussed, the overexpression of integrin α7 splice variants in these models is done so under the control of the muscle-specific HSA promotor.

Remarkably, the muscle-specific overexpression of integrin α7 splice variants can change the histology of liver. Therefore, any change is not due to the presence of integrin α7 in liver but as a downstream effect of the reintroduction of the specific splice variants in skeletal muscle.

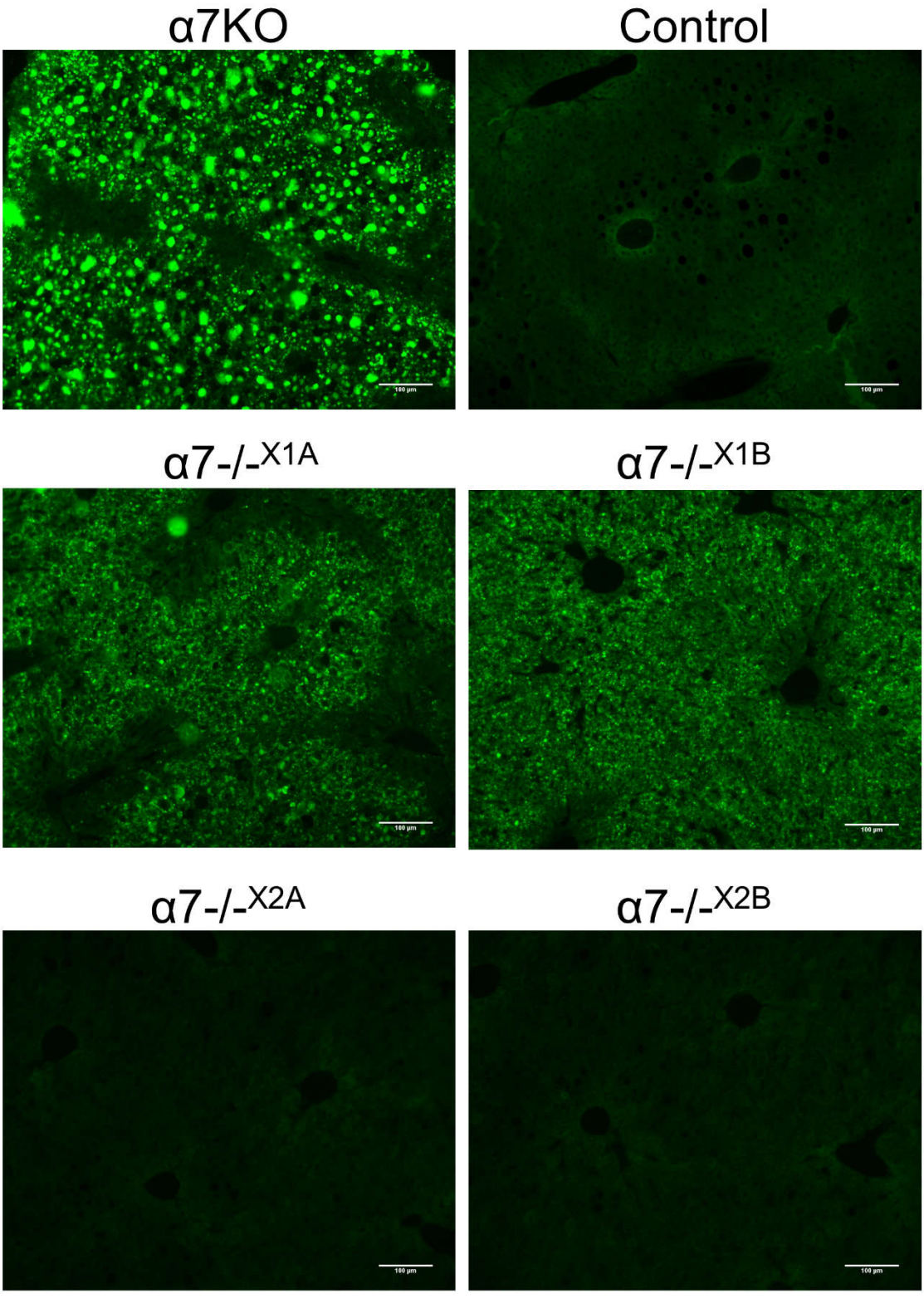

Figure 6.4: HCS LipidTOX™ Green neutral lipid stain of frozen liver sections from HFD-fed α7KO, control, α7-/-^{X1A}, α7-/-^{X1B}, α7-/-^{X2A} and α7-/-^{X2B}. Scale bars = 100μm

6.5 Summary

Integrin α7β1 is the sole β1 integrin expressed throughout muscle development and adulthood. Previously, mice deficient for integrin α7 have been shown to suffer from a novel form of muscular dystrophy (Mayer et al., 1997). Integrin α7 has also been investigated as a possible therapeutic of Duchenne muscular dystrophy, a disease caused by a lack of dystrophin. Remarkably, transgenic overexpression of the integrin α7 X2B splice variant in dystrophin deficient mice ameliorates some of the dystrophic phenotype (Burkin et al., 2001).

As previously discussed in this thesis, integrin α7 deficient mice are: lean, insulin sensitive and glucose tolerant on both a chow and HFD. At this time, no metabolically-focused studies have been conducted on integrin α7. Furthermore, no studies have investigated the roles of the four possible integrin α7 splice variants. In this chapter, we sought to investigate whether transgenic overexpression of any of the four possible integrin α7 splice variants in an α7 deficient model would be successful in rescuing the integrin α7 deficient phenotype.

6.5.1 Integrin α7 splice variants and their effect on body weight

Using integrin α7 deficient mice transgenically overexpressing each of the integrin α7 splice variants, we investigated body weight and the ability of the mice to gain weight when fed a HFD. We showed that integrin α7 deficient mice overexpressing the α7X1 splice variant are leaner than both α7KO and control mice when fed a chow diet. However, when fed a HFD, the overexpressing α7X1 mice successfully rescue the ability to gain weight by gaining significantly more than α7KO mice when normalised against starting weight. This was unexpected as the α7X1 splice variant is usually only expressed during primary myogenesis before decreasing and finally becoming absent in adult skeletal muscle. Integrin α7X2A was successfully able to rescue the lean phenotype of α7KO mice by having a comparable chow-fed body weight to that of control mice.

Overexpression of α7X2A was also successful at rescuing the ability to gain weight of α7KO mice when fed a HFD. Unexpectedly, integrin α7X2B was not able to rescue the lean phenotype of α7KO mice as data showed that mice were significantly leaner than α7KO and control mice. However, the integrin α7X2B splice variant was successful at rescuing the ability of α7KO mice to gain weight. This outcome was surprising as it is the X2B splice variant that is most predominantly found throughout myogenesis and adult skeletal muscle. Therefore, by transgenically overexpressing this splice variant, it was expected that this model would mostly resemble a wildtype model compared to the other splice variant models. Furthermore, as the expression pattern of integrin α7X2B is more similar to X2A than X1A and X1B, it was expected that the overexpression of integrin α7X2B would resemble the phenotypes of the X2A model.

6.5.2 Integrin α7 splice variants and their effect on insulin sensitivity and glucose tolerance

Following from our experiment measuring weight gain, we sought to investigate whether any of the four splice variants would be able to rescue the α7KO insulin sensitive and glucose tolerant phenotype. One limitation in this investigation was there is no significant difference in the glucose tolerance levels of chow-fed control and α7KO mice. Therefore, it is not possible to measure a rescue in these conditions.

Curiously, when either the X1A or X1B splice variants were overexpressed in chow-fed α7KO mice, they were significantly less insulin sensitive than α7KO mice. However, when fed a HFD, α7-/-^{X1A} and α7-/-^{X1B} mice had very similarly insulin sensitivity to α7KO mice and were significantly more insulin sensitive than controls. This trend continued when testing glucose tolerance. X1A or X1B overexpression resulted in significantly more glucose tolerant mice when fed a HFD compared to control mice.

It was unclear what effect the overexpression of integrin α7 X2A splice variant had on insulin sensitivity. During the chow-fed IPITT, data points were different from control and

α7KO mice at varying moments. However, when fed a HFD, mice were significantly less insulin than α7KO mice. Furthermore, we observed a trend of worsened glucose tolerance in HFD-fed mice, but statistical testing demonstrated that it was not significant.

Interestingly, in both chow- and HFD-fed conditions, integrin α7 deficient mice overexpressing the X2B splice variant were significantly less insulin sensitive than α7KO mice. This trend continued in glucose tolerance of HFD-fed mice. Integrin α7-/-^{X2B} mice were significantly less glucose tolerant than α7KO mice.

From our data, It is unclear what effect the α7X1A and X1B splice variants have on insulin sensitivity due to their conflicting results under chow- and HFD-fed conditions. However, it is clear that they cannot rescue the α7KO glucose tolerant phenotype. At this moment, we cannot conclude whether the α7X2A splice variant is able to rescue the insulin sensitive α7KO phenotype. However, evidence suggests it is possible to rescue the glucose tolerant phenotype. We can conclude that the only splice variant able to rescue the insulin sensitive and glucose tolerant α7KO phenotype in both chow- and HFD-fed conditions is the X2B splice variant. This is unsurprising as α7X2B is the predominant splice variant found in adult skeletal muscle and most closely resembles a control model.

6.5.3 Integrin α7 splice variants and their effect on liver histology

As discussed in Chapter 3, non-alcoholic fatty liver disease (NAFLD) is one of the most prevalent diseases associated with obesity and insulin resistance. Early signs of this disease include the accumulation of lipid in the liver, termed steatosis. Remarkably, integrin α7 deficient mouse livers possessed significantly higher levels of steatosis than control mice when fed a HFD. We sought to investigate whether the overexpression of any of the splice variants could rescue this phenotype.

When investigating the level of liver lipid, integrin α7 deficient mice overexpressing the X1A and X1B splice variants demonstrated similar results. Our data suggests that α7-/-

^{x1A} and α7-/-^{X1B} mouse livers are still steatotic but less so than α7KO livers. Overexpression of the X2A and X2B splice variants appeared to completely ameliorate the α7KO fatty liver phenotype with no evidence of any lipid deposition. It is important to remember that the transgenic overexpression of these four possible splice variants is controlled by the muscle-specific HSA promotor. Therefore, it is surprising that any of the four possible integrin α7 splice variants had any effect on the liver. Consequently, we can conclude that these changes in the liver are due to downstream effects of the skeletal muscle.

6.5.4 Summary table

Table 6.15: Table summarising the results from Chapter 6. ↓ - lower body weight, ↑ - higher body weight, ✓ - successfully rescues phenotype, X – unsuccessfully rescues phenotype, N/A – not applicable, ? - inconclusive

Diet	Splice variant overexpression	Body weight (in comparison to α7KO and controls)	Rescues α7KO insulin sensitive phenotype?	Rescues α7KO glucose tolerant phenotype?	Rescues α7KO liver steatosis phenotype?
Chow	X1A	α7KO - ↓ Control - ↓	✓	N/A	N/A
	X1B	α7KO - ↓ Control - ↓	✓	N/A	N/A
	X2A	No difference	?	N/A	N/A
	X2B	α7KO - ↓ Control - ↓	✓	N/A	N/A
HFD	X1A	α7KO - ↑ Control - ↑	X	X	X
	X1B	α7KO - ↑ Control – No difference	X	X	X
	X2A	α7KO - ↑ Control – No difference	✓	?	✓
	X2B	α7KO - ↑ Control – No difference	✓	✓	✓

CHAPTER 7: DISCUSSION AND CONCLUSIONS

7.1 Discussion

Significant studies in the past have demonstrated important insights into the pathological changes and abnormalities associated with integrin α7 deficiency in mice and humans (Mayer et al., 1997; Hayashi et al., 1998; Nawrotzki et al., 2003). Mounting evidence has suggested that integrins play a key role in diet-induced obesity and insulin signalling. Integrin α7 is the most predominant integrin in adult skeletal muscle, a tissue which is responsible for ~80% of insulin-stimulated glucose uptake (Thiebaud et al., 1982). Remarkably, no metabolically focused studies have been completed involving integrin α7. In this study, we aimed to investigate what effects the deletion of integrin α7 would have on diet-induced obesity and insulin signalling.

7.1.1 Integrin α7-deficient mice are lean and insulin sensitive

We sought to investigate what effect a HFD would have on the progression of diet-induced obesity and its downstream effects on α7KO mice. In this study, we used an integrin α7 whole-body deletion model (α7KO) and were fed either a standard chow diet or a HFD for 12 weeks. Control mice, as expected, gained weight when fed a HFD, but α7KO mice remained lean. These results suggested that HFD-fed α7KO mice would remain insulin sensitive.

IPITTs revealed that α7KO mice were significantly more insulin sensitive than controls when fed a HFD, but no difference in insulin sensitivity was seen when fed a chow diet. Similarly, IPGTTs showed a marked improvement in the glucose tolerance of α7KO mice compared to control mice when fed a HFD. Again, no difference was observed when fed a chow diet.

Our data seems to contradict those reported in striated muscle-specific integrin β1-deficient mice (Zong et al., 2009). Zong *et. al* generated a muscle-specific knockout of integrin β1 by crossing mice carrying a 'floxed' allele of β1 integrin with transgenic mice

carrying the Muscle Creatine Kinase (MCK) promotor driving Cre-recombinase (MCKItgβ1 KO). MCKItgβ1 KO mice were reported to have normal weight gain, fasting glucose and insulin levels compared to controls. However, euglycemic (EU) clamp tests revealed that smaller volumes of glucose were required to keep MCKItgβ1 KO mice in a euglycemic state. The glucose turnover of MCKItgβ1 KO mice was also markedly decreased during EU clamp tests. These data indicated that MCKItgβ1 KO mice were insulin resistant. Zong *et al.* reported that the whole-body insulin resistant phenotype was a direct result of impaired insulin signalling specifically in skeletal muscle and that liver and adipose tissue were fully functional. It is difficult to compare our α7KO model with the MCKItgβ1 KO model. Firstly, although the authors generated a muscle-specific knockout, the MCK promotor does not become active until birth. Therefore, the development of skeletal muscle is completely normal until birth whereas, in the α7KO model, integrin α7 will never have been expressed. Secondly, it is important to remember that although α7β1 is the predominant integrin in adult skeletal muscle, other β1 integrins are expressed at varying timepoints, albeit to a lesser degree. The tenascin-C-binding α9β1 is mildly expressed, as well as αvβ1 (deHart et al., 2008; Sinanan et al., 2008). Therefore, the effect observed in the MCKItgβ1 KO model could be a result of deficiencies of several β1-containing integrins.

Previous studies have already outlined the morphological differences in integrin α7-deficient mouse muscle but not with a metabolic focus (Mayer et al., 1997). We stained frozen TA muscle sections with H&E and Oil Red O to investigate histological differences between α7KO and control muscle. As previously shown by Mayer *et al.*, α7KO mouse muscles contained fibres with a greater variance in diameter. Many of these fibres contained centrally located nuclei, indicating past damage and regeneration. The most startling difference was the increased infiltration of mononuclear cells around the myotendinous junction demonstrating signs of necrosis. Oil Red O staining showed increased lipid deposition when fed a HFD in both α7KO and control TA muscle.

Depositions of lipid within skeletal myocytes are known as intramyocellular lipid depositions and have been strongly associated with insulin resistance (Anastasiou et al., 2009; Li et al., 2015). All evidence of lipid deposition was found outside the muscle fibres and not within in both α7KO and control mice. Furthermore, there was no significant difference in the amount of lipid-deposition in the muscle between α7KO and control TA muscle suggesting the α7KO phenotype is not caused by changes in the level of lipid deposition in the muscle.

As previously discussed, α7β1 binds to the extracellular matrix (ECM) via laminin-211 and laminin-221. Remodelling of the ECM has been linked with obesity and insulin resistance with increased inflammation and transforming growth factor-β (TGF-β) found in obese humans and has been replicated in α2β1-deficient mice (Kang et al., 2011b; Watts et al., 2013). Integrin α2β1 differs from α7β1 in that it is a collagen receptor. It preferentially binds to Type I collagen and is predominantly expressed on epithelial cells (Kirchhofer et al., 1990; Edelson et al., 2004). Whole-body deletion of integrin α2 resulted in increased insulin-stimulated glucose uptake during a hyper-insulinemic EU clamp (Kang et al., 2011b). Furthermore, HFD-fed control mice had higher expression of collagen III and IV. Increased collagen III was associated with increased transcription, whilst increased levels of collagen IV were due to reduced matrix metalloproteinase 9 (MMP9) activity. This has also been observed in obese, insulin-resistant humans (Berria et al., 2006). It was hypothesised that the accumulation of collagen III in the interstitial space would act as a physical barrier impeding insulin and glucose transport to the myocyte. Furthermore, it was suggested that the deletion of integrin α2, a positive regulator of collagen I expression, would result in less ECM accumulation in HFD-fed models as shown *in vitro* (Ivaska et al., 1999). However, collagen staining showed that there was no difference between integrin α2-deficient and control mice meaning the 'physical barrier' hypothesis is unlikely. It is also unlikely that deletion of integrin α7 rescues insulin resistance in a HFD-fed model via this mechanism. Previous studies

have investigated the structure of the basal lamina in α7KO mice and have reported no physical differences compared to control mice (Han et al., 2009).

A further hypothesis, involving remodelling of the ECM, is that an increase in muscle ECM may impair neovascular growth and vascular function. Obesity and insulin resistance has been strongly linked with endothelial dysfunction, caused by an imbalance of vasodilating and vasoconstricting factors (Harrison, 1997). Studies have also shown that insulin acts as a vasoactive hormone and its signalling action produces nitric oxide (NO) (Scherrer et al., 1994). A progressive resistance to insulin also results in less production of NO which has been associated with reduced muscle number of capillaries resulting in a smaller surface area of insulin signalling and glucose transport, exacerbating the insulin resistant phenotype (Solomon et al., 2011). This hypothesis was acknowledged by Kang *et al.* who demonstrated that their HFD-fed α2β1-deficient mouse possessed significantly higher muscle vascularisation. Previously, our lab and others have demonstrated a partial embryonic lethal phenotype in α7KO mice (Mayer et al., 1997; Flintoff-Dye et al., 2005). Approximately 68% less α7KO mice are born than expected. This was shown to be due to altered vascular smooth muscle in α7KO embryos. Curiously, the α7KO embryos which died *in utero* suffered from vascular smooth muscle hypoplasia, however, those that survived had vascular smooth muscle hyperplasia. It has been suggested that this hyperplasia may compensate for the absence of integrin α7 in these cells (Flintoff-Dye et al., 2005). Unfortunately, our study did not allow for us to investigate this particular area of interest but is a viable direction of investigation in the future.

Another key player in the maintenance of the vasculature is the pericyte. Pericytes are cells which wrap around capillaries, offering support to the microvessels (Mandarino et al., 1993). Pericytes are also involved in communication with endothelial cells via contact and paracrine signalling and defects result in compromised vascular integrity (Eilken et al., 2017). Interestingly, recent publications have reported a specialised subset of

pericytes positive for integrin α7, and were identified as myofibroblastic pericytes (Malhotra et al., 2012). These myofibroblastic pericytes have been associated with increased renal fibrosis (Chang et al., 2012). Although we did not measure the presence of fibrosis in this study, the mechanism by which myofibroblastic pericytes work could be influencing our α7KO phenotype. As we did not use a muscle-specific deletion of integrin α7, it is possible that these small subpopulations of integrin α7-expressing cells are having a larger effect on the α7KO phenotype than previously thought.

7.1.2 Integrin α7-deficiency results in increased insulin signalling

We continued our investigation as to why α7KO mice were more insulin sensitive than control mice by analysing the insulin signalling pathway via protein quantification. The gastrocnemius (GC) muscle was isolated from chow- and HFD-fed a7KO and control mice. We also challenged a sample of mice with insulin before isolation of the GC muscle to observe a 'snapshot' of the insulin signalling pathway in an activated state.

We observed significantly higher levels of pAkt on both the Serine473 and Threonine308 sites in HFD-fed α7KO non-insulin-challenged GC muscles compared to controls, whilst lower levels of pERK2 were detected in the knockout. However, no difference was seen when fed a chow diet. Similarly, we saw no differences in the amount of phosphorylated proteins in chow-fed insulin-challenged mice, but the levels of pAkt on the Threonine308 site in HFD-fed α7KO were significantly elevated when challenged with insulin.

Countless studies have demonstrated that the activation of Akt is dependent on both the Serine473 and Threonine308 phosphorylation sites. However, more recent studies have begun to dissect the complex signalling of Akt and have discovered that phosphorylation of either serine, threonine or both is required for different functions of the pathway (Kilic et al., 2017; Kitamura et al., 1998; Vincent et al., 2011; Wang et al., 2008). Beg *et al.* demonstrated this by using Akt2-mutant cells containing mutations of either the

Serine474 or Threonine309 site. They showed that phosphorylation of Threonine309 but not Serine474 is required for GLUT4-mediated glucose uptake. Furthermore, inhibition of both sites completely blocked GLUT4 translocation (Beg et al., 2017). Therefore, this indicates that increased phosphorylation on the Threonine308 site in α7KO mice results in increased GLUT4-mediated glucose uptake.

Our results conflict with those of recent studies investigating the effect integrin α7 has on skeletal muscle signalling. Boppart *et al.* investigated the effect of transgenic overexpression of integrin α7X2B, the main adult integrin α7 splice variant, in a mouse model of Duchenne muscular dystrophy (mdx/utr-/-) termed utr-/-/mdx$^{\alpha7X2B}$ mice (Boppart et al., 2011). They reported a significant increase in p70S6K(Thr389) and pAkt(Ser473). Integrin β1 has been shown to associate with ILK, which authors hypothesised causes the downstream phosphorylation of Akt on the Serine473 site. Although, they could not detect significant increases in ILK activity in utr-/-/mdx$^{\alpha7X2B}$ mice. However, controversy still surrounds ILK if it is an active kinase. Although showing homology with protein kinases, some key residues are not present for catalysis in eukaryotes (Ghatak et al., 2013; Hanks et al., 1988). ILK has been dubbed a 'pseudokinase', only able to exhibit kinase-like behaviour through the IPP complex (Ghatak et al., 2013). Furthermore, in this study, the authors did not investigate the levels of pAkt(Thr308) in utr-/-/mdx$^{\alpha7X2B}$ mice, a key element of the insulin signalling pathway. It is also difficult to compare our models as change in investigated protein levels could be caused primarily due to the lack of dystrophin and utrophin.

Another kinase associated with integrins is FAK, which has been shown to localise with integrin receptors when attached to the ECM (Hanks et al., 1992). Reduced levels of phosphorylated FAK have been observed in insulin resistance myocytes *in vitro* (Bisht et al., 2007). Furthermore, increasing FAK levels in insulin-resistant myocytes improved insulin sensitivity and glucose tolerance *in vivo* (Bisht and Dey, 2008). Recent studies, however, have indicated that FAK signalling may be downstream of Akt rather that

upstream like previously believed (Wang and Basson, 2011). Therefore, alterations in FAK level could be a biproduct of altered phosphorylation levels of Akt in insulin resistant models.

In this study we have focused on insulin-dependent signalling, but it is important to note that insulin stimulation is not the only method of glucose uptake. A second distinct pathway in skeletal muscle is the contraction-stimulated pathway reliant on activation of AMPK (Mackenzie and Elliott, 2014). Exercise, via the contraction of skeletal muscle, has been shown to increase the rate of glucose uptake via GLUT4 translocation. Muscle contractions increase the demand for energy, causing the ratio of AMP:ATP to increase, stimulating AMPK. AMPK then phosphorylates TBC1D1 allowing dissociation of Rab proteins and GLUT4 translocation to the cell surface (O'Neill, 2013). PI3K is a key node in the insulin signalling pathway and its inhibition has been demonstrated to inhibit insulin-stimulated but not contraction-stimulated glucose uptake, further distinguishing the two pathways (Yeh et al., 1995). *In vivo* studies showed that although insulin stimulation leads to phosphorylation of Akt, muscle contraction does not (Brozinick and Birnbaum, 1998). However, although insulin-dependent and -independent glucose uptake act separately, evidence suggests that contraction-induced signalling may sensitise insulin-mediated signalling. Activation of AMPK has been shown to phosphorylate IRS-1 on the Serine789 site. This resulted in a 65% increase in PI3K activity in C2C12 myotubes (Jakobsen et al., 2001). This demonstrates a possible direct link between exercise and insulin signalling. In this study, we focused primarily on insulin-dependent signalling. However, it is clear that contraction-induced glucose transport could be altered in integrin α7-deficient mice. Future studies should focus on the effects the deletion of integrin α7 has on insulin-independent signalling.

7.1.3 Integrin α7-deficiency alters adipose tissue location and structure

As previously mentioned, when α7KO mice were fed a HFD, they remained lean whilst control mice gained weight. To ensure this was not due to differences in satiety, we confirmed that mice were ingesting the same weight of diet normalised to their body weight.

To further understand the body composition of the α7KO mice, we compared the weight of a selection of adipose tissue depots to the overall body weight. We found that α7KO mice had significantly less adipose tissue in relation to their overall body weight. Further dissection of results demonstrated that α7KO mice contained less visceral gonadal adipose tissue and subcutaneous interscapular white adipose tissue. Furthermore, gonadal adipocytes were significantly smaller than controls.

The normal response of adipose tissue to nutrient surplus is through adipocyte hypertrophy and hyperplasia via ECM remodelling and increased vascularisation (Catalán et al., 2012). The link between the excessive accumulation of adipose tissue and metabolic diseases has been excessively documented. However, the mechanism by which this occurs in still unclear. The importance of ECM remodelling is signified by the accumulation of collagen VI in the adipose tissue of obese humans (Pasarica et al., 2009). Excessive build-up of fibrotic collagen deposition acts as a physical barrier in adipocytes and prevent the expansion of the cells required to accommodate nutrient surplus (Sun et al., 2014). This restriction of expansion results in the secretion of proinflammatory cytokines, leading to fibrosis, and the necessity to store lipid in other tissues (Keophiphath et al., 2009). This was confirmed by the deletion of collagen VI in *ob/ob* mice which resulted in unrestricted expansion of adipocytes and improved whole-body energy homeostasis (Khan et al., 2009). There is no evidence that integrin α7 is present in adipose tissue, so it is unlikely that changes in the adipose tissue structure

are directly influenced by its deletion. It is more likely that these changes occur due to an indirect effect of skeletal muscle.

In this study, we have primarily focused on white adipose (WAT) and brown adipose tissue. The primary function of WAT is the storage of excess energy as triglyceride whilst BAT specialises in heat production via non-shivering thermogenesis (Coelho et al., 2013). However, a third type of adipocyte, termed ‘brite’, appears morphologically as WAT until stimulated via cold exposure or the ingestion of a HFD. (García-Ruiz et al., 2015; Giralt and Villarroya, 2013). Following stimulation, brite adipocytes adopt a morphology more similar to BAT and begin to generate heat via UCP1 This transformation is termed ‘browning’. During oiur study, we generated preliminary data suggesting browning in WAT in α7KO but not control mice. When fed a HFD, in multiple instances we found subcutaneous evidence of brite adipocytes in histological analysis of subcutaneous adipose tissue. However, these observations were not consistent enough to be reported in this study. Studies have demonstrated the link between increased ‘browning’ of adipocytes and improved glucose and lipid homeostasis (Cousin et al., 1992; Kajimura et al., 2015). By increasing the population of energy-dissipating adipocytes, excess energy is used in heat generation rather than being stored in WAT or ectopically. Recent studies have demonstrated the distinct lineage of white and brown adipocytes. Interestingly, brown adipocytes are now believed to be closer in relation to myocytes than white adipocytes due to their common precursors expressing Pax3, Pax7 and Myf5, whilst white adipocytes are negative for all of these markers (Seale et al., 2008). The lineage of brite adipocytes has proved to be even more complicated. Depending on the adipose tissue they are located in, brite adipocytes have been shown to be positive or negative for Pax3 and Myf5, indicating further separation of lineages (Xue et al., 2007). Unfortunately, our study could not investigate the effect of the deletion of integrin α7 on the generation of brite adipocytes. However, preliminary data suggests there could be increased populations of brite adipocytes. Previous studies have

confirmed the link between increased brite adipocyte populations and improved glucose metabolism. Therefore, this could be a possible mechanism as to why integrin α7-deficient mice remain more insulin sensitive than controls.

As previously mentioned, adipose tissue releases various cytokines, termed 'adipokines', to communicate with other organs. Many of the released adipokines are pro- or anti-inflammatory and their dysregulation has been associated with insulin resistance. The pivotal adipokines associated with the onset of insulin resistance are leptin and adiponectin. The pro-inflammatory adipokine, leptin, is produced by adipocytes proportionally to their triglyceride content to regulate satiety. However, obesity has been linked to leptin resistance (Münzberg et al., 2004). This resistance to leptin results in increased inflammation from excessive production and increase food ingestion (Myers et al., 2010). Although we did not measure leptin levels of α7KO mice, we propose that our data showing that α7KO mice consume no more food than controls as evidence of no difference in leptin signalling.

7.1.4 Altered liver morphology in integrin α7-deficient mice

In this study, we discovered that the livers from HFD-fed insulin-sensitive mice contained significantly more steatosis than control mice. This was confirmed via histological staining and fluorescent lipid staining. However, evidence suggests that non-alcoholic fatty liver disease (NAFLD) is the hepatic branch of metabolic syndrome and studies suggest it is very rare to see NAFLD without insulin resistance (Kitade et al., 2017; Manco, 2011).

As discussed with other tissues, the ECM of the liver expands with the ingestion of a HFD. Studies have demonstrated increased expression of α-smooth muscle actin (αSMA) in hepatic stellate cells and collagen in the sinusoidal space of mice fed a HFD (Dixon et al., 2013). Human studies have also reported increased expression of collagen IV, laminin and αSMA in obese patients (Jaskiewicz et al., 2008). However, it is still not

completely understood how ECM remodelling in the liver contributes to insulin resistance. It has been suggested that, as the liver can clear 40% of insulin via a first pass of the receptor-mediated process, patients with liver damage will continue to circulate elevated insulin levels, leading to insulin resistance (Field, 1973)

We further confirmed the damage of livers from HFD-fed α7KO mice by measuring alanine transaminase (ALT) and aspartate transaminase (AST) in blood serum. We measured more ALT and AST in α7KO mice, indicating steatosis. However, although confirmed to be excellent markers of hepatic injury, it is important to note that these enzymes are also found in other tissues, albeit to a lesser extent. Although ALT is mostly specific to the liver, AST is also found in skeletal muscle, kidneys, brain, pancreas, lungs, leucocytes, and red blood cells (Pratt and Kaplan, 2000). Therefore, although there is evidence supporting liver damage, the release of 'liver' enzymes into the blood may also be due to other tissue damage, including skeletal muscle.

We sought to investigate whether the liver damage seen in HFD-fed α7KO mice also affected the production of bile acids. Bile acids are a group of water-soluble steroids which aid the absorption of fat-and fat-soluble proteins synthesised in the hepatocytes of the liver. Increased levels of bile acids have been shown to protect from obesity and insulin resistance. Therefore, we sought to investigate whether bile acid levels were altered in α7KO mice. However, our data suggests there is no difference between serum bile acid levels in α7KO compared to controls. Nevertheless, in our study we only analysed bile acid levels in the serum. To truly understand whether bile acid levels are altered, levels from multiple locations including the liver and the gut will need to be analysed.

Six integrins have been detected in the liver: α1, α2, α3, α4, α5 and α6; all of which associate with the β1 subunit, however only α1β1 and α5β1 are expressed in hepatocytes (Volpes et al., 1991). Few studies have investigated the effect of the deletion

of integrins on liver histology. Williams *et al.* demonstrated that deletion of collagen-binding integrin α1 resulted in severe hepatic insulin resistance in HFD-fed mice. However, lipid deposition was no different from chow-fed levels in α1-null mice. It has been suggested that this phenotype is possibly due to enhanced α5β1 signalling to compensate for the lack of integrin α1. The fibronectin receptor, integrin α5β1, has been shown to be involved in embryonic myogenesis and is expressed at the adult MTJ until postnatal day 10. However, in the absence of integrin α7 the expression of α5β1 is continually expressed at the MTJ and regenerated muscle fibres. The persistence of α5β1 results in the deposition of fibronectin in the basement membrane of integrin α7-deficient adult muscle fibres. It is thought that this α5β1-fibronectin link is weaker than the α7β1-laminin link and results in the myopathy observed in integrin α7-deficient mice (Nawrotzki et al., 2003). It is unclear how the expression of integrin α7 results in the reduction of integrin α5. It is also unknown whether this effect is confined to the skeletal muscle. Although speculative, if not specific to skeletal muscle, the deletion of integrin α7 could result in maintained or increased expression of integrin α5 in the liver, leading to a similar effect observed in integrin α1-deficient mice.

7.1.5 Deletion of integrin α7 does not alter the metabolomic profile

Integrin α7 is vital to the differentiation of smooth muscle cells along the gastrointestinal tract. These smooth muscle cells maintain organ dimensions and can generate contractions to move along bolus. In our study, we aimed to detect whether a deletion of integrin α7 would alter the metabolomic profile of mice fed both a chow or a HFD. We analysed faecal pellets from α7KO and control animals and measured their metabolomic profile via NMR. Results from chow-fed control and α7KO mice indicated that there was no difference of the metabolomic profile between mice. However, at this moment, no conclusions can be drawn from HFD-fed mice. Due to a laboratory error, the metabolomic profile could only be measured from two HFD-fed control mice. The

software we used, MetaboAnalyst 4.0, possesses an algorithm to generate a 'false sample' from other data to make statistical analysis possible. However, due to the huge variance, no reliable outcome could be concluded.

Recently, there has been increased interest in identifying biomarkers in the metabolomic profiles of sufferers of insulin resistance and obesity. By identifying key biomarkers, this would make early treatment easier. To date, four categories of metabolism have been identified as potential candidates of biomarkers: amino acid, lipid, carbohydrate, and nucleotide metabolism (Park et al., 2015). Countless studies have provided evidence of unique metabolites which can act as early markers of metabolomic disorder. It is important that further analysis be completed on integrin α7 deficient mice to determine whether they possess any of these.

7.1.6 Integrin α7 splice variants rescue the integrin α7-deficient phenotype

Throughout this study, we have reported numerous phenotypes in the α7KO mouse model. As mentioned, four possible splice variants of integrin α7 are expressed at varying times throughout development. Previous studies have demonstrated that overexpression of the adult forms of integrin α7 reduced the development of myopathy in mice deficient for dystrophin and utrophin (Burkin et al., 2001). We sought to investigate whether transgenic overexpression of any of the four possible splice variants in the α7-deficient model could rescue the phenotypes discovered during our study.

The expression of transgenic integrin α7 splice variants was promoted by the HSA promotor. HSA promoter activity begins on embryonic day 9.5 and is specific to skeletal muscle (Leu et al., 2003). Therefore, all expression of the transgene was specific to skeletal muscle. Random insertion of the transgenic gene into the genome resulted in varying degrees of protein expression but past protein expression experiments have selected founder mice that have similar expression of the four splice variants.

During our study, we discovered that when fed a chow diet, curiously, α7KO mice overexpressing: X1A, X1B or X2B were significantly leaner than both α7KO and control mice. However, overexpression of any of the four splice variants rescued the ability to gain weight when fed a HFD. Further studies confirmed that only the X2A and X2B adult variants of integrin α7 were able to rescue the insulin sensitive phenotype on a HFD. Furthermore, only the X2B splice variant was found to rescue glucose tolerance with X2A data being inconclusive. Previous studies have demonstrated it is integrin α7X2 and β1D which provide the strong connection between the muscle and tendon in adult skeletal muscle. Integrin α7X1 is more transiently expressed during early stages of regeneration. Integrin α7A and α7B are both expressed in adult skeletal muscle, although α7B is more predominant (Ziober et al., 1993). Consequently, we can assume that each of the splice variants has specific functions in skeletal muscle function. Therefore, it is not surprising that the predominant adult splice variant of integrin α7 is the variant that was able to rescue the weight gain phenotype, insulin sensitivity and glucose tolerance.

We reported that the deletion of integrin α7 resulted in the onset of liver steatosis when fed a HFD. Surprising data in our study demonstrated that the transgenic expression of adult integrin α7 splice variants X2A and X2B could rescue the fatty liver phenotype in HFD-fed α7KO mice, but not the overexpression of X1A or X1B. Integrin α7-null mice overexpressing transgenic α7X2A or α7X2B showed no signs of lipid deposition when fed a HFD and were comparable to controls. Curiously, α7KO mice overexpressing α7X1A and α7X1B showed a partially rescued phenotype. As transgenic expression was linked to the HSA promotor, we can be sure that this rescue is not due to integrin α7 being expressed in liver. We postulate that the novel muscular dystrophy induced by the deletion of integrin α7 may be having downstream effects on the liver. The increase of pro-inflammatory cytokines has been linked with muscular dystrophies. Increased TNFα, an important regulatory of chronic inflammation, has been measured in the regenerating fibres from sufferers of Duchenne Muscular Dystrophy (DMD) (Saito et al., 2000).

Increased levels of interleukin-6 have also been observed the serum of patients of DMD, a cytokine with both pro- and anti-inflammatory properties (Rufo et al., 2011). Elevated systemic pro-inflammatory cytokines have been associated with the onset of NAFLD (Kumar et al., 2012). We can presume that the reduced development of muscular dystrophy by the overexpression of integrin α7X2B could also be observed in those overexpressing α7X2A. The amelioration of the dystrophic phenotype may also result in the reduction of pro-inflammatory cytokines released by the muscle, thus preventing downstream inflammatory effects on the liver.

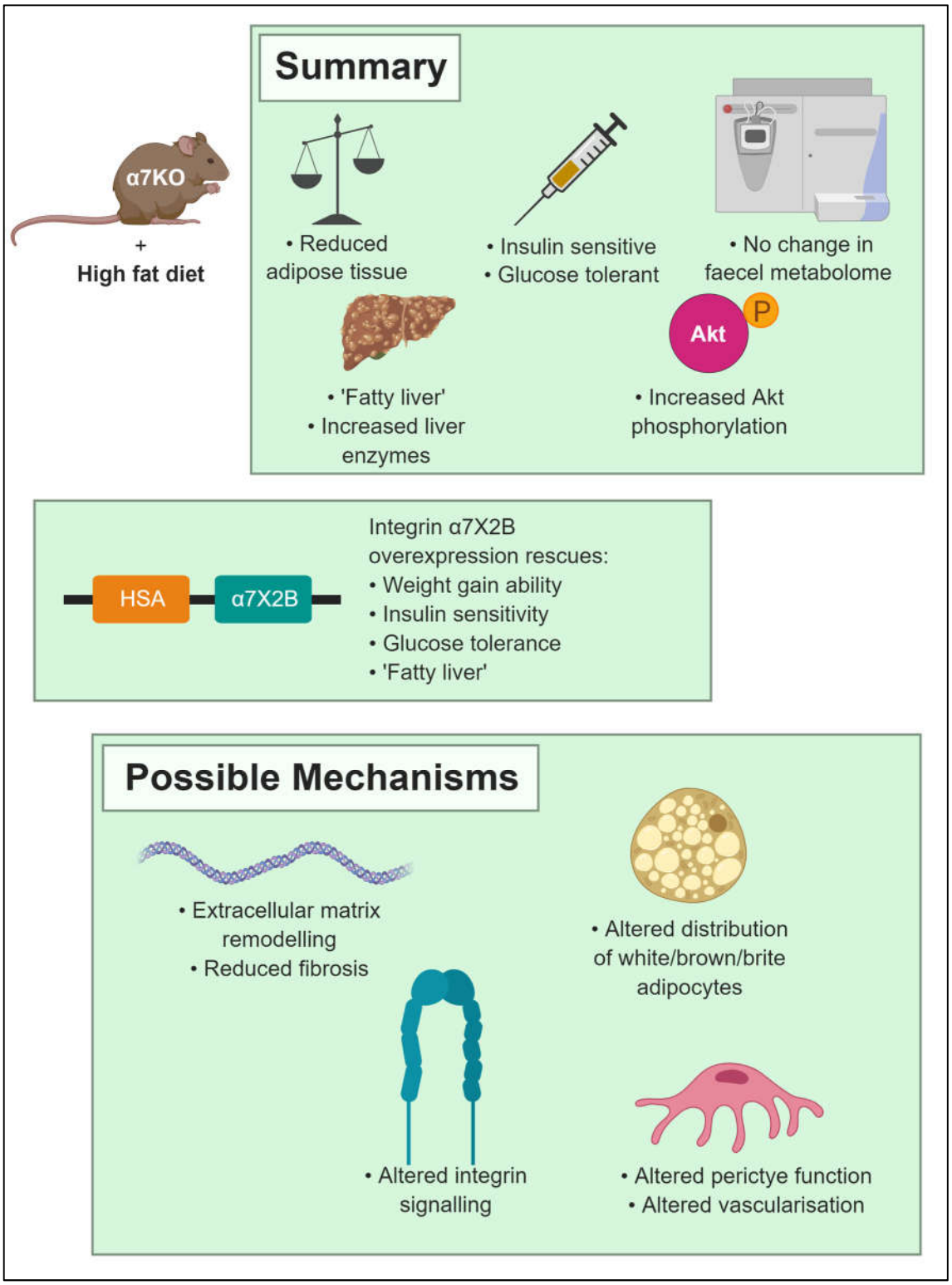

Figure 7.1: Summary diagram depicting the key findings from this study and possible mechanisms of action.

7.2 Future Studies

During this study, we have identified the main metabolic differences between control and α7KO mice. However, it is unclear whether there is a difference in glucose uptake between the models. *In vitro* assays can be performed on myocytes to determine whether glucose translocation is affected. The gold standard for measuring glucose uptake is using radio-labelled 2-deoxy-D-glucose (^{3}H-2DG) (Yamamoto et al., 2015). Unlike glucose, the 2-deoxyglucose 6-phosphase (DG6P) formed from ^{3}H-2DG cannot be rapidly metabolised leading to an accumulation of DG6P, therefore isotope efflux is decreased. Myocytes are incubated with ^{3}H-2DG before uptake is measured using a liquid scintillation counter. By comparing uptake of glucose in myocytes, this would highlight whether α7KO mice are leaner and more insulin sensitive due to altered glucose uptake.

It could be possible that α7KO mice are leaner due to differences in exercise patterns. To investigate this further, future studies should include the use of “metabolic cages”. Although we measured food intake throughout this study, “metabolic cages” are able to measure food and water intake in real time, energy expenditure via O_2 consumption and CO_2 production, and movement. This would highlight whether any changes in leanness and insulin sensitivity are due to differences in activity.

We observed differences in liver histology between control and α7KO mice. However, further investigations into how the liver is altered should be explored. The deposition of ECM proteins is one of the main responses to NAFLD, but it was unclear to see exactly how the liver histology differed between control and α7KO mice from H&E staining alone. Immunohistochemistry staining for fibronectin should be conducted to observe the differences in the ECM of the livers. Staining for α-smooth muscle actin should also be performed to quantify liver fibrosis.

Inflammation has also shown to be a key participant in the progression of insulin

resistance. To more accurately measure inflammation in tissues including liver and muscle, a CD68 stain should be used to measure monocyte infiltration. Pro-inflammatory serum cytokines should also be measured to estimate the degree of inflammation. Production of TNF-α and IL-1β have been shown to be linked to the progression of insulin resistance (Memon et al., 2013).

7.3 Concluding remarks

In this thesis, we have demonstrated the pivotal effect integrin α7 has on metabolism. Our novel data shows that the deletion of integrin α7 results in lean and insulin sensitive mice. Furthermore, phenotypes of the deletion of integrin α7 are not constricted to the skeletal muscle but are also shown in adipose tissue and liver. We have demonstrated that the transgenic overexpression of the integrin α7 splice variants can rescue some of the phenotypes observed in integrin α7-deficient mice. Our study, along with others', has demonstrated the critical role integrins play in metabolism and insulin signalling. Our data will assist in the understanding of the alterations in metabolism associated with integrin α7-deficiency.

ACRONYMS AND ABBREVIATIONS

α7KO – Integrin α7-deficient mouse

ACC – Acetyl-coenzyme A carboxylase

Acetyl-CoA – Acetyl-coenzyme A

ADP – Adenosine diphosphate

ATP – Adenosine triphosphate

BAT – Brown adipose tissue

BM – Basement membrane

BMI – Body mass index

cAMP – Cyclic adenosine monophosphate

DG – Diglyceride

DGAT - Diacylglycerol acyltransferase

DGC – Dystrophin-glycoprotein complex

ECM – Extracellular matrix

ERK – Extracellular signal-regulated kinase

EU – Euglycemic

FAK – Focal adhesion kinase

FFA – Free fatty acid

GC – Gastrocnemius

GLUT – Glucose transporter

GSK-3 – Glycogen synthase kinase-3

HFD – High fat diet

HMIT – Proton-couple myoinositol transporter

HSL – Hormone-sensitive lipase

IGF – Insulin-like growth factor

ILK – Integrin-linked kinase

IPGTT – Intraperitoneal glucose tolerance test

IPITT – Intraperitoneal insulin tolerance test

IPP – ILK-PINCH-Parvin

IR – Insulin receptor

IRS – Insulin receptor substrate

JNK – Jun NH(2)-terminal kinase

LPL – Lipoprotein lipase

MAPK – Mitogen-activated protein kinase

MG – Monoglyceride

Myf5 – Myogenic factor 5

NAFLD – Non-alcoholic fatty liver disease

NASH - Non-alcoholic steatohepatitis

Pax – Paired box gene

PGC-1 - Peroxisome proliferator-activated receptor-γ coactivator-1

PH – Pleckstrin-homology

PI3K – Phosphoinositide 3-kinase

PIP2 - Phosphatidylinositol-4,5-bisphosphate

PIP3 - Phosphatidylinositol-3,4,5-triphosphate

PKA – Protein kinase A

PTB – Phospho-tyrosine binding

PTEN – Phosphatase and tensin homolog detected on chromosome 10

ROS – Reactive oxygen species

SH2 – Src homology 2

SWAT – Subcutaneous white adipose tissue

T2DM – Type II diabetes mellitus

TA – Tibialis anterior

TG – Triglyceride

TNFα – Tumour necrosis factor alpha

UCP1 – Uncoupling protein 1

VAT – Visceral adipose tissue

WAT – White adipose tissue

BIBLIOGRAPHY

Adair, B.D., and Yeager, M. (2002). Three-dimensional model of the human platelet integrin alpha IIbbeta 3 based on electron cryomicroscopy and x-ray crystallography. Proc. Natl. Acad. Sci. U.S.A. *99*, 14059–14064.

Adeva-Andany, M.M., Pérez-Felpete, N., Fernández-Fernández, C., Donapetry-García, C., and Pazos-García, C. (2016). Liver glucose metabolism in humans. Biosci Rep *36*.

Agius, L. (2015). Role of glycogen phosphorylase in liver glycogen metabolism. Mol. Aspects Med. *46*, 34–45.

Aguirre, V., Uchida, T., Yenush, L., Davis, R., and White, M.F. (2000). The c-Jun NH(2)-terminal kinase promotes insulin resistance during association with insulin receptor substrate-1 and phosphorylation of Ser(307). J. Biol. Chem. *275*, 9047–9054.

Alberts, B., Johnson, A., Lewis, J., Raff, M., Roberts, K., and Walter, P. (2002). The Extracellular Matrix of Animals. Molecular Biology of the Cell. 4th Edition.

Alessi, D.R., James, S.R., Downes, C.P., Holmes, A.B., Gaffney, P.R., Reese, C.B., and Cohen, P. (1997). Characterization of a 3-phosphoinositide-dependent protein kinase which phosphorylates and activates protein kinase Balpha. Curr. Biol. *7*, 261–269.

Alessi, D.R., Pearce, L.R., and García-Martínez, J.M. (2009). New insights into mTOR signaling: mTORC2 and beyond. Sci Signal *2*, pe27.

Allamand, V., and Guicheney, P. (2002). Merosin-deficient congenital muscular dystrophy, autosomal recessive (MDC1A, MIM#156225, LAMA2 gene coding for alpha2 chain of laminin). Eur. J. Hum. Genet. *10*, 91–94.

Almind, K., and Kahn, C.R. (2004). Genetic determinants of energy expenditure and insulin resistance in diet-induced obesity in mice. Diabetes *53*, 3274–3285.

de Alvaro, C., Teruel, T., Hernandez, R., and Lorenzo, M. (2004). Tumor necrosis factor alpha produces insulin resistance in skeletal muscle by activation of inhibitor kappaB kinase in a p38 MAPK-dependent manner. J. Biol. Chem. *279*, 17070–17078.

Anastasiou, C.A., Kavouras, S.A., Lentzas, Y., Gova, A., Sidossis, L.S., and Melidonis, A. (2009). Diabetes mellitus is associated with increased intramyocellular triglyceride, but not diglyceride, content in obese humans. Metab. Clin. Exp. *58*, 1636–1642.

Andersen, A.S., Kjeldsen, T., Wiberg, F.C., Vissing, H., Schäffer, L., Rasmussen, J.S., Meyts, P.D., and Møller, N.P. (1992). Identification of determinants that confer ligand specificity on the insulin receptor. J. Biol. Chem. *267*, 13681–13686.

Araki, E., Lipes, M.A., Patti, M.E., Brüning, J.C., Haag, B., Johnson, R.S., and Kahn, C.R. (1994). Alternative pathway of insulin signalling in mice with targeted disruption of the IRS-1 gene. Nature *372*, 186–190.

Atkinson, M.A., Eisenbarth, G.S., and Michels, A.W. (2014). Type 1 diabetes. Lancet *383*, 69–82.

Aumailley, M., Bruckner-Tuderman, L., Carter, W.G., Deutzmann, R., Edgar, D., Ekblom, P., Engel, J., Engvall, E., Hohenester, E., Jones, J.C.R., et al. (2005). A

simplified laminin nomenclature. Matrix Biol. *24*, 326–332.

Baetens, D., Malaisse-Lagae, F., Perrelet, A., and Orci, L. (1979). Endocrine pancreas: three-dimensional reconstruction shows two types of islets of langerhans. Science *206*, 1323–1325.

Balzac, F., Belkin, A.M., Koteliansky, V.E., Balabanov, Y.V., Altruda, F., Silengo, L., and Tarone, G. (1993). Expression and functional analysis of a cytoplasmic domain variant of the beta 1 integrin subunit. J. Cell Biol. *121*, 171–178.

Banting, F.G., Best, C.H., Collip, J.B., Campbell, W.R., and Fletcher, A.A. (1922). Pancreatic Extracts in the Treatment of Diabetes Mellitus. Can Med Assoc J *12*, 141–146.

Bao, Z.Z., Lakonishok, M., Kaufman, S., and Horwitz, A.F. (1993). Alpha 7 beta 1 integrin is a component of the myotendinous junction on skeletal muscle. Journal of Cell Science *106*, 579–589.

Barthel, A., Nakatani, K., Dandekar, A.A., and Roth, R.A. (1998). Protein kinase C modulates the insulin-stimulated increase in Akt1 and Akt3 activity in 3T3-L1 adipocytes. Biochem. Biophys. Res. Commun. *243*, 509–513.

Baudoin, C., Van der Flier, A., Borradori, L., and Sonnenberg, A. (1996). Genomic organization of the mouse beta 1 gene: conservation of the beta 1D but not of the beta 1B and beta 1C integrin splice variants. Cell Adhes. Commun. *4*, 1–11.

Beg, M., Abdullah, N., Thowfeik, F.S., Altorki, N.K., and McGraw, T.E. (2017). Distinct Akt phosphorylation states are required for insulin regulated Glut4 and Glut1-mediated glucose uptake. ELife *6*.

Belkin, A.M., Zhidkova, N.I., Balzac, F., Altruda, F., Tomatis, D., Maier, A., Tarone, G., Koteliansky, V.E., and Burridge, K. (1996). Beta 1D integrin displaces the beta 1A isoform in striated muscles: localization at junctional structures and signaling potential in nonmuscle cells. J. Cell Biol. *132*, 211–226.

Benedict, M., and Zhang, X. (2017). Non-alcoholic fatty liver disease: An expanded review. World J Hepatol *9*, 715–732.

Berg, A.H., Combs, T.P., Du, X., Brownlee, M., and Scherer, P.E. (2001). The adipocyte-secreted protein Acrp30 enhances hepatic insulin action. Nat. Med. *7*, 947–953.

Berria, R., Wang, L., Richardson, D.K., Finlayson, J., Belfort, R., Pratipanawatr, T., De Filippis, E.A., Kashyap, S., and Mandarino, L.J. (2006). Increased collagen content in insulin-resistant skeletal muscle. Am. J. Physiol. Endocrinol. Metab. *290*, E560-565.

Bingley, P.J. (2010). Clinical Applications of Diabetes Antibody Testing. J Clin Endocrinol Metab *95*, 25–33.

Bisht, B., and Dey, C.S. (2008). Focal Adhesion Kinase contributes to insulin-induced actin reorganization into a mesh harboring Glucose transporter-4 in insulin resistant skeletal muscle cells. BMC Cell Biology *9*, 48.

Bisht, B., Goel, H.L., and Dey, C.S. (2007). Focal adhesion kinase regulates insulin

resistance in skeletal muscle. Diabetologia *50*, 1058–1069.

Bjørbaek, C., and Kahn, B.B. (2004). Leptin signaling in the central nervous system and the periphery. Recent Prog. Horm. Res. *59*, 305–331.

Blendea, M.C., Jacobs, D., Stump, C.S., McFarlane, S.I., Ogrin, C., Bahtyiar, G., Stas, S., Kumar, P., Sha, Q., Ferrario, C.M., et al. (2005). Abrogation of oxidative stress improves insulin sensitivity in the Ren-2 rat model of tissue angiotensin II overexpression. Am. J. Physiol. Endocrinol. Metab. *288*, E353-359.

Bogan, J.S., and Kandror, K.V. (2010). Biogenesis and regulation of insulin-responsive vesicles containing GLUT4. Current Opinion in Cell Biology *22*, 506–512.

Bonfanti, D.H., Alcazar, L.P., Arakaki, P.A., Martins, L.T., Agustini, B.C., de Moraes Rego, F.G., and Frigeri, H.R. (2015). ATP-dependent potassium channels and type 2 diabetes mellitus. Clinical Biochemistry *48*, 476–482.

Boppart, M.D., Burkin, D.J., and Kaufman, S.J. (2011). Activation of AKT signaling promotes cell growth and survival in α7β1 integrin-mediated alleviation of muscular dystrophy. Biochim Biophys Acta *1812*, 439–446.

Boucher, J., Kleinridders, A., and Kahn, C.R. (2014). Insulin Receptor Signaling in Normal and Insulin-Resistant States. Cold Spring Harb Perspect Biol *6*.

Bouzakri, K., Zachrisson, A., Al-Khalili, L., Zhang, B.B., Koistinen, H.A., Krook, A., and Zierath, J.R. (2006). siRNA-based gene silencing reveals specialized roles of IRS-1/Akt2 and IRS-2/Akt1 in glucose and lipid metabolism in human skeletal muscle. Cell Metab. *4*, 89–96.

Bowman, W. (1840). XXI. On the minute structure and movements voluntary muscle. Phil. Trans. R. Soc. Lond. *130*, 457–501.

Bozyczko, D., Decker, C., Muschler, J., and Horwitz, A.F. (1989). Integrin on developing and adult skeletal muscle. Exp. Cell Res. *183*, 72–91.

Brehm, B.J., and D'Alessio, D.A. (2000). Environmental Factors Influencing Obesity. In Endotext, L.J. De Groot, G. Chrousos, K. Dungan, K.R. Feingold, A. Grossman, J.M. Hershman, C. Koch, M. Korbonits, R. McLachlan, M. New, et al., eds. (South Dartmouth (MA): MDText.com, Inc.), p.

Brennan, K.J., and Hardeman, E.C. (1993). Quantitative analysis of the human alpha-skeletal actin gene in transgenic mice. J. Biol. Chem. *268*, 719–725.

Brennan, E., McClelland, A., Hagiwara, S., Godson, C., and Kantharidis, P. (2016). Chapter 31 - miRNAs in the Pathophysiology of Diabetes and Their Value as Biomarkers. In Epigenetic Biomarkers and Diagnostics, J.L. García-Giménez, ed. (Boston: Academic Press), pp. 643–661.

Brissova, M., Fowler, M.J., Nicholson, W.E., Chu, A., Hirshberg, B., Harlan, D.M., and Powers, A.C. (2005). Assessment of human pancreatic islet architecture and composition by laser scanning confocal microscopy. J. Histochem. Cytochem. *53*, 1087–1097.

Brozinick, J.T., and Birnbaum, M.J. (1998). Insulin, but Not Contraction, Activates Akt/PKB in Isolated Rat Skeletal Muscle. J. Biol. Chem. *273*, 14679–14682.

Bryant, N.J., Govers, R., and James, D.E. (2002). Regulated transport of the glucose transporter GLUT4. Nat. Rev. Mol. Cell Biol. *3*, 267–277.

Burcelin, R., Katz, E.B., and Charron, M.J. (1996). Molecular and cellular aspects of the glucagon receptor: role in diabetes and metabolism. Diabetes Metab. *22*, 373–396.

Burkin, D.J., Wallace, G.Q., Nicol, K.J., Kaufman, D.J., and Kaufman, S.J. (2001). Enhanced Expression of the α7β1 Integrin Reduces Muscular Dystrophy and Restores Viability in Dystrophic Mice. J Cell Biol *152*, 1207–1218.

Cai, D., Dhe-Paganon, S., Melendez, P.A., Lee, J., and Shoelson, S.E. (2003). Two New Substrates in Insulin Signaling, IRS5/DOK4 and IRS6/DOK5. J. Biol. Chem. *278*, 25323–25330.

Calderwood, D.A., Fujioka, Y., de Pereda, J.M., García-Alvarez, B., Nakamoto, T., Margolis, B., McGlade, C.J., Liddington, R.C., and Ginsberg, M.H. (2003). Integrin beta cytoplasmic domain interactions with phosphotyrosine-binding domains: a structural prototype for diversity in integrin signaling. Proc. Natl. Acad. Sci. U.S.A. *100*, 2272–2277.

Campbell, I.D., and Humphries, M.J. (2011). Integrin Structure, Activation, and Interactions. Cold Spring Harb Perspect Biol *3*, a004994.

Cary, L.A., Han, D.C., and Guan, J.L. (1999). Integrin-mediated signal transduction pathways. Histol. Histopathol. *14*, 1001–1009.

Catalán, V., Gómez-Ambrosi, J., Rodríguez, A., and Frühbeck, G. (2012). Role of extracellular matrix remodelling in adipose tissue pathophysiology. Relevance in the development of obesity. Histology and Histopathology *27*, 1515–1528.

Cederberg, A., Grønning, L.M., Ahrén, B., Taskén, K., Carlsson, P., and Enerbäck, S. (2001). FOXC2 is a winged helix gene that counteracts obesity, hypertriglyceridemia, and diet-induced insulin resistance. Cell *106*, 563–573.

Cedikova, M., Kripnerová, M., Dvorakova, J., Pitule, P., Grundmanova, M., Babuska, V., Mullerova, D., and Kuncova, J. (2016). Mitochondria in White, Brown, and Beige Adipocytes. Stem Cells Int *2016*.

Cerf, M.E. (2013). Beta Cell Dysfunction and Insulin Resistance. Front Endocrinol (Lausanne) *4*.

Chalhoub, N., and Baker, S.J. (2009). PTEN and the PI3-Kinase Pathway in Cancer. Annu Rev Pathol *4*, 127–150.

Chandra, R., and Liddle, R.A. (2009). Neural and hormonal regulation of pancreatic secretion. Curr. Opin. Gastroenterol. *25*, 441–446.

Chang, F.-C., Chou, Y.-H., Chen, Y.-T., and Lin, S.-L. (2012). Novel insights into pericyte-myofibroblast transition and therapeutic targets in renal fibrosis. J. Formos. Med.

Assoc. *111*, 589–598.

Cheah, M., and Andrews, M.R. (2018). Integrin Activation: Implications for Axon Regeneration. Cells *7*, 20.

Chiang, J.Y.L. (2013). Bile Acid Metabolism and Signaling. Compr Physiol *3*, 1191–1212.

Cho, H., Thorvaldsen, J.L., Chu, Q., Feng, F., and Birnbaum, M.J. (2001a). Akt1/PKBalpha is required for normal growth but dispensable for maintenance of glucose homeostasis in mice. J. Biol. Chem. *276*, 38349–38352.

Cho, H., Mu, J., Kim, J.K., Thorvaldsen, J.L., Chu, Q., Crenshaw, E.B., Kaestner, K.H., Bartolomei, M.S., Shulman, G.I., and Birnbaum, M.J. (2001b). Insulin resistance and a diabetes mellitus-like syndrome in mice lacking the protein kinase Akt2 (PKB beta). Science *292*, 1728–1731.

Christ, B., Huang, R., and Scaal, M. (2007). Amniote somite derivatives. Developmental Dynamics *236*, 2382–2396.

Clee, S.M., and Attie, A.D. (2007). The Genetic Landscape of Type 2 Diabetes in Mice. Endocr Rev *28*, 48–83.

Coelho, M., Oliveira, T., and Fernandes, R. (2013). Biochemistry of adipose tissue: an endocrine organ. Arch Med Sci *9*, 191–200.

Collo, G., Starr, L., and Quaranta, V. (1993). A new isoform of the laminin receptor integrin alpha 7 beta 1 is developmentally regulated in skeletal muscle. J. Biol. Chem. *268*, 19019–19024.

Conarello, S.L., Jiang, G., Mu, J., Li, Z., Woods, J., Zycband, E., Ronan, J., Liu, F., Roy, R.S., Zhu, L., et al. (2007). Glucagon receptor knockout mice are resistant to diet-induced obesity and streptozotocin-mediated beta cell loss and hyperglycaemia. Diabetologia *50*, 142–150.

Cousin, B., Cinti, S., Morroni, M., Raimbault, S., Ricquier, D., Pénicaud, L., and Casteilla, L. (1992). Occurrence of brown adipocytes in rat white adipose tissue: molecular and morphological characterization. J. Cell. Sci. *103 (Pt 4)*, 931–942.

Covey, S.D., Wideman, R.D., McDonald, C., Unniappan, S., Huynh, F., Asadi, A., Speck, M., Webber, T., Chua, S.C., and Kieffer, T.J. (2006). The pancreatic β cell is a key site for mediating the effects of leptin on glucose homeostasis. Cell Metabolism *4*, 291–302.

deHart, G.W., Jin, T., McCloskey, D.E., Pegg, A.E., and Sheppard, D. (2008). The α9β1 integrin enhances cell migration by polyamine-mediated modulation of an inward-rectifier potassium channel. Proc Natl Acad Sci U S A *105*, 7188–7193.

Diao, C., Zhao, L., Guan, M., Zheng, Y., Chen, M., Yang, Y., Lin, L., Chen, W., and Gao, H. (2014). Systemic and characteristic metabolites in the serum of streptozotocin-induced diabetic rats at different stages as revealed by a (1)H-NMR based metabonomic approach. Mol Biosyst *10*, 686–693.

Dicker, D., Salook, M.A., Marcoviciu, D., Djaldetti, M., and Bessler, H. (2013). Role of peripheral blood mononuclear cells in the predisposition of obese individuals to inflammation and infection. Obes Facts *6*, 146–151.

Dixon, L.J., Flask, C.A., Papouchado, B.G., Feldstein, A.E., and Nagy, L.E. (2013). Caspase-1 as a Central Regulator of High Fat Diet-Induced Non-Alcoholic Steatohepatitis. PLOS ONE *8*, e56100.

Dudzinska, W. (2014). Purine nucleotides and their metabolites in patients with type 1 and 2 diabetes mellitus. Journal of Biomedical Science and Engineering *07*, 38.

Easton, R.M., Cho, H., Roovers, K., Shineman, D.W., Mizrahi, M., Forman, M.S., Lee, V.M.-Y., Szabolcs, M., Jong, R. de, Oltersdorf, T., et al. (2005). Role for Akt3/Protein Kinase Bγ in Attainment of Normal Brain Size. Molecular and Cellular Biology *25*, 1869–1878.

Echtermeyer, F., Schöber, S., Pöschl, E., Mark, H. von der, and Mark, K. von der (1996). Specific Induction of Cell Motility on Laminin by 7 Integrin. J. Biol. Chem. *271*, 2071–2075.

Edelson, B.T., Li, Z., Pappan, L.K., and Zutter, M.M. (2004). Mast cell-mediated inflammatory responses require the alpha 2 beta 1 integrin. Blood *103*, 2214–2220.

Eilken, H.M., Diéguez-Hurtado, R., Schmidt, I., Nakayama, M., Jeong, H.-W., Arf, H., Adams, S., Ferrara, N., and Adams, R.H. (2017). Pericytes regulate VEGF-induced endothelial sprouting through VEGFR1. Nature Communications *8*, 1574.

Erion, D.M., and Shulman, G.I. (2010). Diacylglycerol-mediated insulin resistance.

Ervasti, J.M., and Campbell, K.P. (1993). A role for the dystrophin-glycoprotein complex as a transmembrane linker between laminin and actin. The Journal of Cell Biology *122*, 809–823.

Esposito, D.L., Li, Y., Cama, A., and Quon, M.J. (2001). Tyr612 and Tyr632 in Human Insulin Receptor Substrate-1 Are Important for Full Activation of Insulin-Stimulated Phosphatidylinositol 3-Kinase Activity and Translocation of GLUT4 in Adipose Cells. Endocrinology *142*, 2833–2840.

Fain, J.N., Madan, A.K., Hiler, M.L., Cheema, P., and Bahouth, S.W. (2004). Comparison of the release of adipokines by adipose tissue, adipose tissue matrix, and adipocytes from visceral and subcutaneous abdominal adipose tissues of obese humans. Endocrinology *145*, 2273–2282.

Fang, X., Yu, S.X., Lu, Y., Bast, R.C., Woodgett, J.R., and Mills, G.B. (2000). Phosphorylation and inactivation of glycogen synthase kinase 3 by protein kinase A. PNAS *97*, 11960–11965.

Fasshauer, M., and Blüher, M. (2015). Adipokines in health and disease. Trends in Pharmacological Sciences *36*, 461–470.

Fedorenko, A., Lishko, P.V., and Kirichok, Y. (2012). Mechanism of fatty-acid-dependent UCP1 uncoupling in brown fat mitochondria. Cell *151*, 400–413.

Fengler, V.H.I., Macheiner, T., Kessler, S.M., Czepukojc, B., Gemperlein, K., Müller, R., Kiemer, A.K., Magnes, C., Haybaeck, J., Lackner, C., et al. (2016). Susceptibility of Different Mouse Wild Type Strains to Develop Diet-Induced NAFLD/AFLD-Associated Liver Disease. PLoS One *11*.

Field, J.B. (1973). Extraction of Insulin by Liver. Annu. Rev. Med. *24*, 309–314.

van der Flier, A., Kuikman, I., Baudoin, C., van der Neut, R., and Sonnenberg, A. (1995). A novel beta 1 integrin isoform produced by alternative splicing: unique expression in cardiac and skeletal muscle. FEBS Lett. *369*, 340–344.

Flintoff-Dye, N.L., Welser, J., Rooney, J., Scowen, P., Tamowski, S., Hatton, W., and Burkin, D.J. (2005). Role for the α7β1 integrin in vascular development and integrity. Developmental Dynamics *234*, 11–21.

Frontera, W.R., and Ochala, J. (2015). Skeletal Muscle: A Brief Review of Structure and Function. Calcif Tissue Int *96*, 183–195.

Fu, Y., Luo, N., Klein, R.L., and Garvey, W.T. (2005). Adiponectin promotes adipocyte differentiation, insulin sensitivity, and lipid accumulation. J. Lipid Res. *46*, 1369–1379.

Gao, Y., Moten, A., and Lin, H.-K. (2014). Akt: a new activation mechanism. Cell Res *24*, 785–786.

García-Ruiz, E., Reynés, B., Díaz-Rúa, R., Ceresi, E., Oliver, P., and Palou, A. (2015). The intake of high-fat diets induces the acquisition of brown adipocyte gene expression features in white adipose tissue. Int J Obes (Lond) *39*, 1619–1629.

Gelinas, J.N., Tenorio, G., Lemon, N., Abel, T., and Nguyen, P.V. (2008). β-Adrenergic receptor activation during distinct patterns of stimulation critically modulates the PKA-dependence of LTP in the mouse hippocampus. Learn. Mem. *15*, 281–289.

Gelling, R.W., Du, X.Q., Dichmann, D.S., Romer, J., Huang, H., Cui, L., Obici, S., Tang, B., Holst, J.J., Fledelius, C., et al. (2003). Lower blood glucose, hyperglucagonemia, and pancreatic alpha cell hyperplasia in glucagon receptor knockout mice. Proc. Natl. Acad. Sci. U.S.A. *100*, 1438–1443.

Ghatak, S., Morgner, J., and Wickström, S.A. (2013). ILK: a pseudokinase with a unique function in the integrin–actin linkage. Biochemical Society Transactions *41*, 995–1001.

Giralt, M., and Villarroya, F. (2013). White, Brown, Beige/Brite: Different Adipose Cells for Different Functions? Endocrinology *154*, 2992–3000.

Gonzalez, E., and McGraw, T.E. (2006). Insulin signaling diverges into Akt-dependent and -independent signals to regulate the recruitment/docking and the fusion of GLUT4 vesicles to the plasma membrane. Mol. Biol. Cell *17*, 4484–4493.

Goodacre, R., Vaidyanathan, S., Dunn, W.B., Harrigan, G.G., and Kell, D.B. (2004). Metabolomics by numbers: acquiring and understanding global metabolite data. Trends in Biotechnology *22*, 245–252.

Gowda, S., Desai, P.B., Hull, V.V., Math, A.A.K., Vernekar, S.N., and Kulkarni, S.S.

(2009). A review on laboratory liver function tests. Pan Afr Med J *3*.

Greco, A.V., Mingrone, G., Giancaterini, A., Manco, M., Morroni, M., Cinti, S., Granzotto, M., Vettor, R., Camastra, S., and Ferrannini, E. (2002). Insulin resistance in morbid obesity: reversal with intramyocellular fat depletion. Diabetes *51*, 144–151.

Gromada, J., Bokvist, K., Ding, W.-G., Barg, S., Buschard, K., Renström, E., and Rorsman, P. (1997). Adrenaline Stimulates Glucagon Secretion in Pancreatic A-Cells by Increasing the Ca2+ Current and the Number of Granules Close to the L-Type Ca2+ Channels. J Gen Physiol *110*, 217–228.

Gromski, P.S., Muhamadali, H., Ellis, D.I., Xu, Y., Correa, E., Turner, M.L., and Goodacre, R. (2015). A tutorial review: Metabolomics and partial least squares-discriminant analysis – a marriage of convenience or a shotgun wedding. Analytica Chimica Acta *879*, 10–23.

Gros, J., Manceau, M., Thomé, V., and Marcelle, C. (2005). A common somitic origin for embryonic muscle progenitors and satellite cells. Nature *435*, 954–958.

Han, H.-S., Kang, G., Kim, J.S., Choi, B.H., and Koo, S.-H. (2016). Regulation of glucose metabolism from a liver-centric perspective. Experimental & Molecular Medicine *48*, e218.

Han, R., Kanagawa, M., Yoshida-Moriguchi, T., Rader, E.P., Ng, R.A., Michele, D.E., Muirhead, D.E., Kunz, S., Moore, S.A., Iannaccone, S.T., et al. (2009). Basal lamina strengthens cell membrane integrity via the laminin G domain-binding motif of α-dystroglycan. PNAS *106*, 12573–12579.

Hanks, S.K., Quinn, A.M., and Hunter, T. (1988). The protein kinase family: conserved features and deduced phylogeny of the catalytic domains. Science *241*, 42–52.

Hanks, S.K., Calalb, M.B., Harper, M.C., and Patel, S.K. (1992). Focal adhesion protein-tyrosine kinase phosphorylated in response to cell attachment to fibronectin. PNAS *89*, 8487–8491.

Harris, C.A., Haas, J.T., Streeper, R.S., Stone, S.J., Kumari, M., Yang, K., Han, X., Brownell, N., Gross, R.W., Zechner, R., et al. (2011). DGAT enzymes are required for triacylglycerol synthesis and lipid droplets in adipocytes. J. Lipid Res. *52*, 657–667.

Harrison, D.G. (1997). Cellular and molecular mechanisms of endothelial cell dysfunction. J. Clin. Invest. *100*, 2153–2157.

Hatano, N., Mori, Y., Oh-hora, M., Kosugi, A., Fujikawa, T., Nakai, N., Niwa, H., Miyazaki, J., Hamaoka, T., and Ogata, M. (2003). Essential role for ERK2 mitogen-activated protein kinase in placental development. Genes To Cells: Devoted To Molecular & Cellular Mechanisms *8*, 847–856.

Hayashi, Y.K., Chou, F.L., Engvall, E., Ogawa, M., Matsuda, C., Hirabayashi, S., Yokochi, K., Ziober, B.L., Kramer, R.H., Kaufman, S.J., et al. (1998). Mutations in the integrin alpha7 gene cause congenital myopathy. Nat. Genet. *19*, 94–97.

Helbling-Leclerc, A., Zhang, X., Topaloglu, H., Cruaud, C., Tesson, F., Weissenbach, J.,

Tomé, F.M., Schwartz, K., Fardeau, M., and Tryggvason, K. (1995). Mutations in the laminin alpha 2-chain gene (LAMA2) cause merosin-deficient congenital muscular dystrophy. Nat. Genet. *11*, 216–218.

Hernández, N., Torres, S.H., Vera, O., De Sanctis, J.B., and Flores, E. (2001). Muscle fiber composition and capillarization in relation to metabolic alterations in hypertensive men. J Med *32*, 67–82.

Hers, H.G. (1976). The control of glycogen metabolism in the liver. Annu. Rev. Biochem. *45*, 167–189.

Hildebrand, J.D., Schaller, M.D., and Parsons, J.T. (1995). Paxillin, a tyrosine phosphorylated focal adhesion-associated protein binds to the carboxyl terminal domain of focal adhesion kinase. Mol. Biol. Cell *6*, 637–647.

Hoffman, E.L., VonWald, T., and Hansen, K. (2015). The metabolic syndrome. S D Med *Spec No*, 24–28.

Horst, D., Ustanina, S., Sergi, C., Mikuz, G., Juergens, H., Braun, T., and Vorobyov, E. (2006). Comparative expression analysis of Pax3 and Pax7 during mouse myogenesis. Int. J. Dev. Biol. *50*, 47–54.

Hotamisligil, G.S., Budavari, A., Murray, D., and Spiegelman, B.M. (1994). Reduced tyrosine kinase activity of the insulin receptor in obesity- diabetes. Central role of tumor necrosis factor-α. Journal of Clinical Investigation *94*, 1543–1549.

Huang, S., and Czech, M.P. (2007). The GLUT4 Glucose Transporter. Cell Metabolism *5*, 237–252.

Huang, B.X., Akbar, M., Kevala, K., and Kim, H.-Y. (2011). Phosphatidylserine is a critical modulator for Akt activation. J Cell Biol *192*, 979–992.

Hubbard, S.R. (1997). Crystal structure of the activated insulin receptor tyrosine kinase in complex with peptide substrate and ATP analog. EMBO J. *16*, 5572–5581.

Hynes, R.O. (2002a). Integrins: Bidirectional, Allosteric Signaling Machines. Cell *110*, 673–687.

Hynes, R.O. (2002b). Integrins: Bidirectional, Allosteric Signaling Machines. Cell *110*, 673–687.

Imamura, M., and Maeda, S. (2011). Genetics of type 2 diabetes: the GWAS era and future perspectives [Review]. Endocrine Journal *58*, 723–739.

International Diabetes Federation (2017). IDF Diabetes Atlas, 8th edn.

Ivaska, J., Reunanen, H., Westermarck, J., Koivisto, L., Kähäri, V.-M., and Heino, J. (1999). Integrin α2β1 Mediates Isoform-Specific Activation of p38 and Upregulation of Collagen Gene Transcription by a Mechanism Involving the α2 Cytoplasmic Tail. J Cell Biol *147*, 401–416.

Jakobsen, S.N., Hardie, D.G., Morrice, N., and Tornqvist, H.E. (2001). 5′-AMP-activated

Protein Kinase Phosphorylates IRS-1 on Ser-789 in Mouse C2C12 Myotubes in Response to 5-Aminoimidazole-4-carboxamide Riboside. J. Biol. Chem. *276*, 46912–46916.

Jaskiewicz, K., Rzepko, R., and Sledzinski, Z. (2008). Fibrogenesis in Fatty Liver Associated with Obesity and Diabetes Mellitus Type 2. Dig Dis Sci *53*, 785–788.

Jensen-Urstad, A.P.L., and Semenkovich, C.F. (2012). Fatty acid synthase and liver triglyceride metabolism: housekeeper or messenger? Biochim Biophys Acta *1821*, 747–753.

Jiang, G., and Zhang, B.B. (2003). Glucagon and regulation of glucose metabolism. American Journal of Physiology-Endocrinology and Metabolism *284*, E671–E678.

Jiang, Y.-P., Li, L., Liu, Z.-Y., You, L.-L., Wu, Y., Xu, B., Ge, L.-Q., Song, Q.-S., and Wu, J.-C. (2016). Adipose triglyceride lipase (Atgl) mediates the antibiotic jinggangmycin-stimulated reproduction in the brown planthopper, *Nilaparvata lugens* Stål. Scientific Reports *6*, 18984.

Jiang, Z.Y., Zhou, Q.L., Coleman, K.A., Chouinard, M., Boese, Q., and Czech, M.P. (2003). Insulin signaling through Akt/protein kinase B analyzed by small interfering RNA-mediated gene silencing. Proc Natl Acad Sci U S A *100*, 7569–7574.

Johannsen, D.L., Tchoukalova, Y., Tam, C.S., Covington, J.D., Xie, W., Schwarz, J.-M., Bajpeyi, S., and Ravussin, E. (2014). Effect of 8 weeks of overfeeding on ectopic fat deposition and insulin sensitivity: testing the "adipose tissue expandability" hypothesis. Diabetes Care *37*, 2789–2797.

Johnson, G.L., and Lapadat, R. (2002). Mitogen-Activated Protein Kinase Pathways Mediated by ERK, JNK, and p38 Protein Kinases. Science *298*, 1911–1912.

Johnson, D.G., Hayward, J.S., Jacobs, T.P., Collis, M.L., Eckerson, J.D., and Williams, R.H. (1977). Plasma norepinephrine responses of man in cold water. J Appl Physiol Respir Environ Exerc Physiol *43*, 216–220.

Kabuta, T., Hakuno, F., Asano, T., and Takahashi, S.-I. (2002). Insulin Receptor Substrate-3 Functions as Transcriptional Activator in the Nucleus. J. Biol. Chem. *277*, 6846–6851.

Kajimura, S., Spiegelman, B.M., and Seale, P. (2015). Brown and beige fat: Physiological roles beyond heat-generation. Cell Metab *22*, 546–559.

Kaku, K., Fiedorek, F.T., Province, M., and Permutt, M.A. (1988). Genetic analysis of glucose tolerance in inbred mouse strains. Evidence for polygenic control. Diabetes *37*, 707–713.

Kalhan, S.C., Guo, L., Edmison, J., Dasarathy, S., McCullough, A.J., Hanson, R.W., and Milburn, M. (2011). Plasma Metabolomic Profile in Non-Alcoholic Fatty Liver Disease. Metabolism *60*, 404–413.

Kang, L., Ayala, J.E., Lee-Young, R.S., Zhang, Z., James, F.D., Neufer, P.D., Pozzi, A., Zutter, M.M., and Wasserman, D.H. (2011a). Diet-induced muscle insulin resistance is associated with extracellular matrix remodeling and interaction with integrin alpha2beta1

in mice. Diabetes *60*, 416–426.

Kang, L., Ayala, J.E., Lee-Young, R.S., Zhang, Z., James, F.D., Neufer, P.D., Pozzi, A., Zutter, M.M., and Wasserman, D.H. (2011b). Diet-induced muscle insulin resistance is associated with extracellular matrix remodeling and interaction with integrin alpha2beta1 in mice. Diabetes *60*, 416–426.

Kang, L., Mokshagundam, S., Reuter, B., Lark, D.S., Sneddon, C.C., Hennayake, C., Williams, A.S., Bracy, D.P., James, F.D., Pozzi, A., et al. (2016). Integrin-Linked Kinase in Muscle Is Necessary for the Development of Insulin Resistance in Diet-Induced Obese Mice. Diabetes *65*, 1590–1600.

Katsuura, G., Asakawa, A., and Inui, A. (2002). Roles of pancreatic polypeptide in regulation of food intake. Peptides *23*, 323–329.

Katz, E.B., Stenbit, A.E., Hatton, K., DePinho, R., and Charron, M.J. (1995). Cardiac and adipose tissue abnormalities but not diabetes in mice deficient in GLUT4. Nature *377*, 151–155.

Keenan, H.A., Sun, J.K., Levine, J., Doria, A., Aiello, L.P., Eisenbarth, G., Bonner-Weir, S., and King, G.L. (2010). Residual insulin production and pancreatic ß-cell turnover after 50 years of diabetes: Joslin Medalist Study. Diabetes *59*, 2846–2853.

Keophiphath, M., Achard, V., Henegar, C., Rouault, C., Clément, K., and Lacasa, D. (2009). Macrophage-Secreted Factors Promote a Profibrotic Phenotype in Human Preadipocytes. Mol Endocrinol *23*, 11–24.

Kersten, S. (2014). Physiological regulation of lipoprotein lipase. Biochim. Biophys. Acta *1841*, 919–933.

Khalifeh-Soltani, A., Ha, A., Podolsky, M.J., McCarthy, D.A., McKleroy, W., Azary, S., Sakuma, S., Tharp, K.M., Wu, N., Yokosaki, Y., et al. (2016). α8β1 integrin regulates nutrient absorption through an Mfge8-PTEN dependent mechanism. ELife *5*.

Khan, T., Muise, E.S., Iyengar, P., Wang, Z.V., Chandalia, M., Abate, N., Zhang, B.B., Bonaldo, P., Chua, S., and Scherer, P.E. (2009). Metabolic Dysregulation and Adipose Tissue Fibrosis: Role of Collagen VI. Molecular and Cellular Biology *29*, 1575–1591.

Khoo, S., Griffen, S.C., Xia, Y., Baer, R.J., German, M.S., and Cobb, M.H. (2003). Regulation of Insulin Gene Transcription by ERK1 and ERK2 in Pancreatic β Cells. J. Biol. Chem. *278*, 32969–32977.

Kilic, U., Caglayan, A.B., Beker, M.C., Gunal, M.Y., Caglayan, B., Yalcin, E., Kelestemur, T., Gundogdu, R.Z., Yulug, B., Yılmaz, B., et al. (2017). Particular phosphorylation of PI3K/Akt on Thr308 via PDK-1 and PTEN mediates melatonin's neuroprotective activity after focal cerebral ischemia in mice. Redox Biol *12*, 657–665.

Kim, T.-J., Sun, J., Lu, S., Zhang, J., and Wang, Y. (2014). The regulation of β-adrenergic receptor-mediated PKA activation by substrate stiffness via microtubule dynamics in human MSCs. Biomaterials *35*, 8348–8356.

Kirchhofer, D., Languino, L.R., Ruoslahti, E., and Pierschbacher, M.D. (1990). Alpha 2

beta 1 integrins from different cell types show different binding specificities. J. Biol. Chem. *265*, 615–618.

Kitade, H., Chen, G., Ni, Y., and Ota, T. (2017). Nonalcoholic Fatty Liver Disease and Insulin Resistance: New Insights and Potential New Treatments. Nutrients *9*.

Kitamura, T., Ogawa, W., Sakaue, H., Hino, Y., Kuroda, S., Takata, M., Matsumoto, M., Maeda, T., Konishi, H., Kikkawa, U., et al. (1998). Requirement for Activation of the Serine-Threonine Kinase Akt (Protein Kinase B) in Insulin Stimulation of Protein Synthesis but Not of Glucose Transport. Molecular and Cellular Biology *18*, 3708–3717.

Kleiner, D.E., and Makhlouf, H.R. (2016). Histology of NAFLD and NASH in Adults and Children. Clin Liver Dis *20*, 293–312.

Kopecky, J., Clarke, G., Enerbäck, S., Spiegelman, B., and Kozak, L.P. (1995). Expression of the mitochondrial uncoupling protein gene from the aP2 gene promoter prevents genetic obesity. J. Clin. Invest. *96*, 2914–2923.

Koves, T.R., Ussher, J.R., Noland, R.C., Slentz, D., Mosedale, M., Ilkayeva, O., Bain, J., Stevens, R., Dyck, J.R.B., Newgard, C.B., et al. (2008). Mitochondrial Overload and Incomplete Fatty Acid Oxidation Contribute to Skeletal Muscle Insulin Resistance. Cell Metabolism *7*, 45–56.

Kubota, N., Tobe, K., Terauchi, Y., Eto, K., Yamauchi, T., Suzuki, R., Tsubamoto, Y., Komeda, K., Nakano, R., Miki, H., et al. (2000). Disruption of insulin receptor substrate 2 causes type 2 diabetes because of liver insulin resistance and lack of compensatory beta-cell hyperplasia. Diabetes *49*, 1880–1889.

Kulkarni, R.N., Brüning, J.C., Winnay, J.N., Postic, C., Magnuson, M.A., and Kahn, C.R. (1999). Tissue-specific knockout of the insulin receptor in pancreatic beta cells creates an insulin secretory defect similar to that in type 2 diabetes. Cell *96*, 329–339.

Kumar, R., Prakash, S., Chhabra, S., Singla, V., Madan, K., Gupta, S.D., Panda, S.K., Khanal, S., and Acharya, S.K. (2012). Association of pro-inflammatory cytokines, adipokines & oxidative stress with insulin resistance & non-alcoholic fatty liver disease. Indian J Med Res *136*, 229–236.

Kuriyama, H., Shimomura, I., Kishida, K., Kondo, H., Furuyama, N., Nishizawa, H., Maeda, N., Matsuda, M., Nagaretani, H., Kihara, S., et al. (2002). Coordinated Regulation of Fat-Specific and Liver-Specific Glycerol Channels, Aquaporin Adipose and Aquaporin 9. Diabetes *51*, 2915–2921.

Kwon, H., Kim, D., and Kim, J.S. (2017). Body Fat Distribution and the Risk of Incident Metabolic Syndrome: A Longitudinal Cohort Study. Scientific Reports *7*, 10955.

Larance, M., Ramm, G., Stöckli, J., van Dam, E.M., Winata, S., Wasinger, V., Simpson, F., Graham, M., Junutula, J.R., Guilhaus, M., et al. (2005). Characterization of the Role of the Rab GTPase-activating Protein AS160 in Insulin-regulated GLUT4 Trafficking. Journal of Biological Chemistry *280*, 37803–37813.

Lee, B.-C., and Lee, J. (2014). Cellular and molecular players in adipose tissue inflammation in the development of obesity-induced insulin resistance. Biochimica et

Biophysica Acta (BBA) - Molecular Basis of Disease *1842*, 446–462.

Lee, A.S.J., Harris, J., Bate, M., Vijayraghavan, K., Fisher, L., Tajbakhsh, S., and Duxson, M. (2013a). Initiation of primary myogenesis in amniote limb muscles. Developmental Dynamics *242*, 1043–1055.

Lee, J.O., Rieu, P., Arnaout, M.A., and Liddington, R. (1995). Crystal structure of the A domain from the alpha subunit of integrin CR3 (CD11b/CD18). Cell *80*, 631–638.

Lee, M.-J., Wu, Y., and Fried, S.K. (2013b). Adipose Tissue Heterogeneity: Implication of depot differences in adipose tissue for Obesity Complications. Mol Aspects Med *34*, 1–11.

Legate, K.R., Montañez, E., Kudlacek, O., and Fässler, R. (2006). ILK, PINCH and parvin: the tIPP of integrin signalling. Nat. Rev. Mol. Cell Biol. *7*, 20–31.

Leiter, L.A., Grose, M., Yale, J.F., and Marliss, E.B. (1984). Catecholamine responses to hypocaloric diets and fasting in obese human subjects. Am. J. Physiol. *247*, E190-197.

Leu, M., Bellmunt, E., Schwander, M., Fariñas, I., Brenner, H.R., and Müller, U. (2003). Erbb2 regulates neuromuscular synapse formation and is essential for muscle spindle development. Development *130*, 2291–2301.

Li, Y., Xu, S., Zhang, X., Yi, Z., and Cichello, S. (2015). Skeletal intramyocellular lipid metabolism and insulin resistance. Biophys Rep *1*, 90–98.

Liao, Y., and Hung, M.-C. (2010). Physiological regulation of Akt activity and stability. Am J Transl Res *2*, 19–42.

Lietzke, S.E., Bose, S., Cronin, T., Klarlund, J., Chawla, A., Czech, M.P., and Lambright, D.G. (2000). Structural basis of 3-phosphoinositide recognition by pleckstrin homology domains. Mol. Cell *6*, 385–394.

Limdi, J.K., and Hyde, G.M. (2003). Evaluation of abnormal liver function tests. Postgraduate Medical Journal *79*, 307–312.

Liu, M., Wright, J., Guo, H., Xiong, Y., and Arvan, P. (2014). Chapter Two - Proinsulin Entry and Transit Through the Endoplasmic Reticulum in Pancreatic Beta Cells. In Vitamins & Hormones, G. Litwack, ed. (Academic Press), pp. 35–62.

Liu, S.C., Wang, Q., Lienhard, G.E., and Keller, S.R. (1999). Insulin receptor substrate 3 is not essential for growth or glucose homeostasis. J. Biol. Chem. *274*, 18093–18099.

Loncar, D. (1991). Convertible adipose tissue in mice. Cell Tissue Res. *266*, 149–161.

Lowell, B.B., and Shulman, G.I. (2005). Mitochondrial dysfunction and type 2 diabetes. Science *307*, 384–387.

Luo, L., and Liu, M. (2016). Adipose tissue in control of metabolism. J. Endocrinol. *231*, R77–R99.

Luo, B.-H., Carman, C.V., and Springer, T.A. (2007). Structural basis of integrin

regulation and signaling. Annu. Rev. Immunol. *25*, 619–647.

Mackenzie, R.W., and Elliott, B.T. (2014). Akt/PKB activation and insulin signaling: a novel insulin signaling pathway in the treatment of type 2 diabetes. Diabetes Metab Syndr Obes *7*, 55–64.

Malhotra, D., Fletcher, A.L., Astarita, J., Lukacs-Kornek, V., Tayalia, P., Gonzalez, S.F., Elpek, K.G., Chang, S.K., Knoblich, K., Hemler, M.E., et al. (2012). Transcriptional profiling of stroma from inflamed and resting lymph nodes defines immunological hallmarks. Nature Immunology *13*, 499–510.

Manco, M. (2011). Metabolic syndrome in childhood from impaired carbohydrate metabolism to nonalcoholic fatty liver disease. J Am Coll Nutr *30*, 295–303.

Mandarino, L.J., Sundarraj, N., Finlayson, J., and Hassell, H.R. (1993). Regulation of fibronectin and laminin synthesis by retinal capillary endothelial cells and pericytes in vitro. Exp. Eye Res. *57*, 609–621.

Maraschin, J. de F., Murussi, N., Witter, V., and Silveiro, S.P. (2010). Diabetes mellitus classification. Arquivos Brasileiros de Cardiologia *95*, 40–46.

Matull, W.R., Pereira, S.P., and O'Donohue, J.W. (2006). Biochemical markers of acute pancreatitis. Journal of Clinical Pathology *59*, 340–344.

Mayer, U., Saher, G., Fässler, R., Bornemann, A., Echtermeyer, F., Mark, H. von der, Miosge, N., Pösch, E., and Mark, K. von der (1997). Absence of integrin α7 causes a novel form of muscular dystrophy. Nature Genetics *17*, 318–323.

Memon, A.A., Sundquist, J., Wang, X., Palmér, K., Sundquist, K., and Bennet, L. (2013). The association between cytokines and insulin sensitivity in Iraqi immigrants and native Swedes. BMJ Open *3*, e003473.

Meredith, J., Takada, Y., Fornaro, M., Languino, L.R., and Schwartz, M.A. (1995). Inhibition of cell cycle progression by the alternatively spliced integrin beta 1C. Science *269*, 1570–1572.

Michael, M.D., Kulkarni, R.N., Postic, C., Previs, S.F., Shulman, G.I., Magnuson, M.A., and Kahn, C.R. (2000). Loss of Insulin Signaling in Hepatocytes Leads to Severe Insulin Resistance and Progressive Hepatic Dysfunction. Molecular Cell *6*, 87–97.

Mîinea, C.P., Sano, H., Kane, S., Sano, E., Fukuda, M., Peränen, J., Lane, W.S., and Lienhard, G.E. (2005). AS160, the Akt substrate regulating GLUT4 translocation, has a functional Rab GTPase-activating protein domain. Biochem J *391*, 87–93.

Milburn, M.V., and Lawton, K.A. (2013). Application of Metabolomics to Diagnosis of Insulin Resistance. Annual Review of Medicine *64*, 291–305.

Miller, T.B., and Larner, J. (1973). Mechanism of Control of Hepatic Glycogenesis by Insulin. J. Biol. Chem. *248*, 3483–3488.

Min, J., Okada, S., Kanzaki, M., Elmendorf, J.S., Coker, K.J., Ceresa, B.P., Syu, L.-J., Noda, Y., Saltiel, A.R., and Pessin, J.E. (1999). Synip: A Novel Insulin-Regulated

Syntaxin 4–Binding Protein Mediating GLUT4 Translocation in Adipocytes. Molecular Cell *3*, 751–760.

Morino, K., Petersen, K.F., Dufour, S., Befroy, D., Frattini, J., Shatzkes, N., Neschen, S., White, M.F., Bilz, S., Sono, S., et al. (2005). Reduced mitochondrial density and increased IRS-1 serine phosphorylation in muscle of insulin-resistant offspring of type 2 diabetic parents. J Clin Invest *115*, 3587–3593.

Moser, M., Legate, K.R., Zent, R., and Fässler, R. (2009). The Tail of Integrins, Talin, and Kindlins. Science *324*, 895–899.

Münzberg, H., Flier, J.S., and Bjørbaek, C. (2004). Region-specific leptin resistance within the hypothalamus of diet-induced obese mice. Endocrinology *145*, 4880–4889.

Myers, M.G., Leibel, R.L., Seeley, R.J., and Schwartz, M.W. (2010). Obesity and Leptin Resistance: Distinguishing Cause from Effect. Trends Endocrinol Metab *21*, 643–651.

Nawrocki, A.R., Rajala, M.W., Tomas, E., Pajvani, U.B., Saha, A.K., Trumbauer, M.E., Pang, Z., Chen, A.S., Ruderman, N.B., Chen, H., et al. (2006). Mice Lacking Adiponectin Show Decreased Hepatic Insulin Sensitivity and Reduced Responsiveness to Peroxisome Proliferator-activated Receptor γ Agonists. J. Biol. Chem. *281*, 2654–2660.

Nawrotzki, R., Willem, M., Miosge, N., Brinkmeier, H., and Mayer, U. (2003). Defective integrin switch and matrix composition at alpha 7-deficient myotendinous junctions precede the onset of muscular dystrophy in mice. Hum. Mol. Genet. *12*, 483–495.

NCD Risk Factor Collaboration (NCD-RisC) (2016). Trends in adult body-mass index in 200 countries from 1975 to 2014: a pooled analysis of 1698 population-based measurement studies with 19·2 million participants. Lancet *387*, 1377–1396.

Nedergaard, J., and Cannon, B. (2014). The browning of white adipose tissue: some burning issues. Cell Metab. *20*, 396–407.

Netzer, N., Gatterer, H., Faulhaber, M., Burtscher, M., Pramsohler, S., and Pesta, D. (2015). Hypoxia, Oxidative Stress and Fat. Biomolecules *5*, 1143–1150.

Nordlie, R.C., Foster, J.D., and Lange, A.J. (1999). Regulation of glucose production by the liver. Annu. Rev. Nutr. *19*, 379–406.

O'Callaghan, B.L., Koo, S.-H., Wu, Y., Freake, H.C., and Towle, H.C. (2001). Glucose Regulation of the Acetyl-CoA Carboxylase Promoter PI in Rat Hepatocytes. J. Biol. Chem. *276*, 16033–16039.

OECD (2017). OECD Health Statistics.

Ofei, F., Hurel, S., Newkirk, J., Sopwith, M., and Taylor, R. (1996). Effects of an engineered human anti-TNF-α antibody (CDP571) on insulin sensitivity and glycemic control in patients with NIDDM. Diabetes *45*, 881–885.

O'Neill, H.M. (2013). AMPK and Exercise: Glucose Uptake and Insulin Sensitivity. Diabetes Metab J *37*, 1–21.

Oresic, M., Simell, S., Sysi-Aho, M., Näntö-Salonen, K., Seppänen-Laakso, T., Parikka, V., Katajamaa, M., Hekkala, A., Mattila, I., Keskinen, P., et al. (2008). Dysregulation of lipid and amino acid metabolism precedes islet autoimmunity in children who later progress to type 1 diabetes. J. Exp. Med. *205*, 2975–2984.

Ott, M.O., Bober, E., Lyons, G., Arnold, H., and Buckingham, M. (1991). Early expression of the myogenic regulatory gene, myf-5, in precursor cells of skeletal muscle in the mouse embryo. Development *111*, 1097–1107.

Pagès, G., Guérin, S., Grall, D., Bonino, F., Smith, A., Anjuere, F., Auberger, P., and Pouysségur, J. (1999). Defective thymocyte maturation in p44 MAP kinase (Erk 1) knockout mice. Science *286*, 1374–1377.

Park, S., Sadanala, K.C., and Kim, and E.-K. (2015). A Metabolomic Approach to Understanding the Metabolic Link between Obesity and Diabetes. Molecules and Cells *38*, 587–596.

Pasarica, M., Gowronska-Kozak, B., Burk, D., Remedios, I., Hymel, D., Gimble, J., Ravussin, E., Bray, G.A., and Smith, S.R. (2009). Adipose Tissue Collagen VI in Obesity. J Clin Endocrinol Metab *94*, 5155–5162.

Passerieux, E., Rossignol, R., Chopard, A., Carnino, A., Marini, J.F., Letellier, T., and Delage, J.P. (2006). Structural organization of the perimysium in bovine skeletal muscle: Junctional plates and associated intracellular subdomains. J. Struct. Biol. *154*, 206–216.

Pierantonelli, I., and Svegliati-Baroni, G. (2019). Nonalcoholic Fatty Liver Disease: Basic Pathogenetic Mechanisms in the Progression From NAFLD to NASH. Transplantation *103*, e1–e13.

Pratt, D.S., and Kaplan, M.M. (2000). Evaluation of abnormal liver-enzyme results in asymptomatic patients. N. Engl. J. Med. *342*, 1266–1271.

Pruett, W., Yuan, Y., Rose, E., Batzer, A.G., Harada, N., and Skolnik, E.Y. (1995). Association between GRB2/Sos and insulin receptor substrate 1 is not sufficient for activation of extracellular signal-regulated kinases by interleukin-4: implications for Ras activation by insulin. Mol. Cell. Biol. *15*, 1778–1785.

Puri, P., Daita, K., Joyce, A., Mirshahi, F., Santhekadur, P.K., Cazanave, S., Luketic, V.A., Siddiqui, M.S., Boyett, S., Min, H.-K., et al. (2017). The presence and severity of nonalcoholic steatohepatitis is associated with specific changes in circulating bile acids. Hepatology.

Quesada, I., Todorova, M.G., and Soria, B. (2006). Different metabolic responses in alpha-, beta-, and delta-cells of the islet of Langerhans monitored by redox confocal microscopy. Biophys. J. *90*, 2641–2650.

Quianzon, C.C., and Cheikh, I. (2012). History of insulin. J Community Hosp Intern Med Perspect *2*.

Ramachandran, C., Angelos, K.L., and Walsh, D.A. (1983). Hormonal regulation of the phosphorylation of glycogen synthase in perfused rat heart. Effects of insulin, catecholamines, and glucagon. J. Biol. Chem. *258*, 13377–13383.

Rhyu, G.I., Ray, W.J., and Markley, J.L. (1984). Enzyme-bound intermediates in the conversion of glucose 1-phosphate to glucose 6-phosphate by phosphoglucomutase. Phosphorus NMR studies. Biochemistry *23*, 252–260.

Rogers, L., and Mayer, U. (2005). Insights into Integrin Function in Skeletal Muscle. In Integrins and Development, (Landes Biosciences), pp. 138–151.

Rogers, L.K., and Mayer, U. (2006). Insights into integrin function in skeletal muscle. In Integrins and Development, E. Danen, ed. (Landes Bioscience), pp. 138–151.

Rosen, G.D., Sanes, J.R., LaChance, R., Cunningham, J.M., Roman, J., and Dean, D.C. (1992). Roles for the integrin VLA-4 and its counter receptor VCAM-1 in myogenesis. Cell *69*, 1107–1119.

Rudich, A., Tirosh, A., Potashnik, R., Hemi, R., Kanety, H., and Bashan, N. (1998). Prolonged oxidative stress impairs insulin-induced GLUT4 translocation in 3T3-L1 adipocytes. Diabetes *47*, 1562–1569.

Rufo, A., Fattore, A.D., Capulli, M., Carvello, F., Pasquale, L.D., Ferrari, S., Pierroz, D., Morandi, L., Simone, M.D., Rucci, N., et al. (2011). Mechanisms inducing low bone density in duchenne muscular dystrophy in mice and humans. Journal of Bone and Mineral Research *26*, 1891–1903.

Rui, L. (2014). Energy Metabolism in the Liver. Compr Physiol *4*, 177–197.

Sadagurski, M., Yakar, S., Weingarten, G., Holzenberger, M., Rhodes, C.J., Breitkreutz, D., LeRoith, D., and Wertheimer, E. (2006). Insulin-Like Growth Factor 1 Receptor Signaling Regulates Skin Development and Inhibits Skin Keratinocyte Differentiation. Mol Cell Biol *26*, 2675–2687.

Saito, K., Kobayashi, D., Komatsu, M., Yajima, T., Yagihashi, A., Ishikawa, Y., Minami, R., and Watanabe, N. (2000). A Sensitive Assay of Tumor Necrosis Factor α in Sera from Duchenne Muscular Dystrophy Patients. Clinical Chemistry *46*, 1703–1704.

Saltiel, A.R., and Kahn, C.R. (2001). Insulin signalling and the regulation of glucose and lipid metabolism.

Scalvini, L., Piomelli, D., and Mor, M. (2016). Monoglyceride lipase: structure and inhibitors. Chem Phys Lipids *197*, 13–24.

Scapin, G., Dandey, V.P., Zhang, Z., Prosise, W., Hruza, A., Kelly, T., Mayhood, T., Strickland, C., Potter, C.S., and Carragher, B. (2018). Structure of the insulin receptor–insulin complex by single-particle cryo-EM analysis. Nature *556*, 122–125.

Scherrer, U., Randin, D., Vollenweider, P., Vollenweider, L., and Nicod, P. (1994). Nitric oxide release accounts for insulin's vascular effects in humans. J. Clin. Invest. *94*, 2511–2515.

Schwartz, J.H., Young, J.B., and Landsberg, L. (1983). Effect of dietary fat on sympathetic nervous system activity in the rat. J Clin Invest *72*, 361–370.

Seale, P., Bjork, B., Yang, W., Kajimura, S., Chin, S., Kuang, S., Scimè, A.,

Devarakonda, S., Conroe, H.M., Erdjument-Bromage, H., et al. (2008). PRDM16 controls a brown fat/skeletal muscle switch. Nature *454*, 961–967.

Seale, P., Conroe, H.M., Estall, J., Kajimura, S., Frontini, A., Ishibashi, J., Cohen, P., Cinti, S., and Spiegelman, B.M. (2011). Prdm16 determines the thermogenic program of subcutaneous white adipose tissue in mice. J. Clin. Invest. *121*, 96–105.

Shewan, A.M., van Dam, E.M., Martin, S., Luen, T.B., Hong, W., Bryant, N.J., and James, D.E. (2003). GLUT4 Recycles via a trans-Golgi Network (TGN) Subdomain Enriched in Syntaxins 6 and 16 But Not TGN38: Involvement of an Acidic Targeting Motif. Mol Biol Cell *14*, 973–986.

Sinanan, A.C.M., Machell, J.R.A., Wynne-Hughes, G.T., Hunt, N.P., and Lewis, M.P. (2008). αvβ3 and αvβ5 integrins and their role in muscle precursor cell adhesion. Biology of the Cell *100*, 465–477.

Slot, J.W., Geuze, H.J., Gigengack, S., Lienhard, G.E., and James, D.E. (1991). Immuno-localization of the insulin regulatable glucose transporter in brown adipose tissue of the rat. J. Cell Biol. *113*, 123–135.

Solinas, G., and Karin, M. (2010). JNK1 and IKKbeta: molecular links between obesity and metabolic dysfunction. FASEB J. *24*, 2596–2611.

Solomon, T.P.J., Haus, J.M., Li, Y., and Kirwan, J.P. (2011). Progressive Hyperglycemia across the Glucose Tolerance Continuum in Older Obese Adults Is Related to Skeletal Muscle Capillarization and Nitric Oxide Bioavailability. J Clin Endocrinol Metab *96*, 1377–1384.

Song, W.K., Wang, W., Sato, H., Bielser, D.A., and Kaufman, S.J. (1993). Expression of alpha 7 integrin cytoplasmic domains during skeletal muscle development: alternate forms, conformational change, and homologies with serine/threonine kinases and tyrosine phosphatases. Journal of Cell Science *106*, 1139–1152.

Springer, T.A. (1997). Folding of the N-terminal, ligand-binding region of integrin alpha-subunits into a beta-propeller domain. Proc. Natl. Acad. Sci. U.S.A. *94*, 65–72.

Stamp, D., and Jenkins, G. (2008). Chapter 1 :An Overview of Bile-Acid Synthesis, Chemistry and Function. In Bile Acids: Toxicology and Bioactivity, pp. 1–13.

Striffler, J.S., Garfield, S.A., Cardell, E.L., and Cardell, R.R. (1984). Effects of glucagon on hepatic microsomal glucose-6-phosphatase in vivo. Diabete Metab *10*, 91–97.

Sun, K., Park, J., Gupta, O.T., Holland, W.L., Auerbach, P., Zhang, N., Marangoni, R.G., Nicoloro, S.M., Czech, M.P., Varga, J., et al. (2014). Endotrophin triggers adipose tissue fibrosis and metabolic dysfunction. Nat Commun *5*, 3485.

Sun, X.J., Rothenberg, P., Kahn, C.R., Backer, J.M., Araki, E., Wilden, P.A., Cahill, D.A., Goldstein, B.J., and White, M.F. (1991). Structure of the insulin receptor substrate IRS-1 defines a unique signal transduction protein. Nature *352*, 73–77.

Svoboda, M., Tastenoy, M., Vertongen, P., and Robberecht, P. (1994). Relative quantitative analysis of glucagon receptor mRNA in rat tissues. Mol. Cell. Endocrinol.

105, 131–137.

Sympatec (2008). Particle Shape.

Szymańska, E., Saccenti, E., Smilde, A.K., and Westerhuis, J.A. (2012). Double-check: validation of diagnostic statistics for PLS-DA models in metabolomics studies. Metabolomics *8*, 3–16.

Tamkun, J.W., DeSimone, D.W., Fonda, D., Patel, R.S., Buck, C., Horwitz, A.F., and Hynes, R.O. (1986). Structure of integrin, a glycoprotein involved in the transmembrane linkage between fibronectin and actin. Cell *46*, 271–282.

Tanner, L.I., and Lienhard, G.E. (1987). Insulin elicits a redistribution of transferrin receptors in 3T3-L1 adipocytes through an increase in the rate constant for receptor externalization. J. Biol. Chem. *262*, 8975–8980.

Tavaré, J.M., and Siddle, K. (1993). Mutational analysis of insulin receptor function: Consensus and controversy. Biochimica et Biophysica Acta (BBA) - Molecular Cell Research *1178*, 21–39.

Taylor, R. (2012). Insulin Resistance and Type 2 Diabetes. Diabetes *61*, 778–779.

Taylor, S.I. (1999). Deconstructing Type 2 Diabetes. Cell *97*, 9–12.

Thiebaud, D., Jacot, E., Defronzo, R.A., Maeder, E., Jequier, E., and Felber, J.-P. (1982). The Effect of Graded Doses of Insulin on Total Glucose Uptake, Glucose Oxidation, and Glucose Storage in Man. Diabetes *31*, 957–963.

Toye, A.A., Lippiat, J.D., Proks, P., Shimomura, K., Bentley, L., Hugill, A., Mijat, V., Goldsworthy, M., Moir, L., Haynes, A., et al. (2005). A genetic and physiological study of impaired glucose homeostasis control in C57BL/6J mice. Diabetologia *48*, 675–686.

Tran, T.T., Yamamoto, Y., Gesta, S., and Kahn, C.R. (2008). Beneficial effects of subcutaneous fat transplantation on metabolism. Cell Metab. *7*, 410–420.

Tsuruzoe, K., Emkey, R., Kriauciunas, K.M., Ueki, K., and Kahn, C.R. (2001). Insulin Receptor Substrate 3 (IRS-3) and IRS-4 Impair IRS-1- and IRS-2-Mediated Signaling. Mol Cell Biol *21*, 26–38.

Uchida, T., Myers, M.G., and White, M.F. (2000). IRS-4 Mediates Protein Kinase B Signaling during Insulin Stimulation without Promoting Antiapoptosis. Mol. Cell. Biol. *20*, 126–138.

Ulmer, T.S., Yaspan, B., Ginsberg, M.H., and Campbell, I.D. (2001). NMR Analysis of Structure and Dynamics of the Cytosolic Tails of Integrin αIIbβ3 in Aqueous Solution. Biochemistry *40*, 7498–7508.

Velling, T., Collo, G., Sorokin, L., Durbeej, M., Zhang, H., and Gullberg, D. (1996). Distinct α7Aβ1 and α7Bβ1 integrin expression patterns during mouse development: α7A is restricted to skeletal muscle but α7B is expressed in striated muscle, vasculature, and nervous system. Developmental Dynamics *207*, 355–371.

Velling, T., Nilsson, S., Stefansson, A., and Johansson, S. (2004). beta1-Integrins induce phosphorylation of Akt on serine 473 independently of focal adhesion kinase and Src family kinases. EMBO Rep. *5*, 901–905.

Vignier, N., Moghadaszadeh, B., Gary, F., Beckmann, J., Mayer, U., and Guicheney, P. (1999). Structure, Genetic Localization, and Identification of the Cardiac and Skeletal Muscle Transcripts of the Human Integrin α7 Gene (ITGA7). Biochemical and Biophysical Research Communications *260*, 357–364.

Vincent, E.E., Elder, D.J.E., Thomas, E.C., Phillips, L., Morgan, C., Pawade, J., Sohail, M., May, M.T., Hetzel, M.R., and Tavaré, J.M. (2011). Akt phosphorylation on Thr308 but not on Ser473 correlates with Akt protein kinase activity in human non-small cell lung cancer. Br J Cancer *104*, 1755–1761.

Volpes, R., Van Den Oord, J.J., and Desmet, V.J. (1991). Distribution of the VLA family of integrins in normal and pathological human liver tissue. Gastroenterology *101*, 200–206.

Von der Mark, H., Williams, I., Wendler, O., Sorokin, L., Mark, K. von der, and Pöschl, E. (2002). Alternative Splice Variants of α7β1Integrin Selectively Recognize Different Laminin Isoforms. J. Biol. Chem. *277*, 6012–6016.

Wang, S., and Basson, M.D. (2011). Akt directly regulates focal adhesion kinase through association and serine phosphorylation: implication for pressure-induced colon cancer metastasis. Am. J. Physiol., Cell Physiol. *300*, C657-670.

Wang, H.-V., Chang, L.-W., Brixius, K., Wickström, S.A., Montanez, E., Thievessen, I., Schwander, M., Müller, U., Bloch, W., Mayer, U., et al. (2008). Integrin-linked kinase stabilizes myotendinous junctions and protects muscle from stress-induced damage. J Cell Biol *180*, 1037–1049.

Watts, R., McAinch, A.J., Dixon, J.B., O'Brien, P.E., and Cameron-Smith, D. (2013). Increased Smad signaling and reduced MRF expression in skeletal muscle from obese subjects. Obesity *21*, 525–528.

White, M.F. (2002). IRS proteins and the common path to diabetes. Am. J. Physiol. Endocrinol. Metab. *283*, E413-422.

Wick, M.J., Dong, L.Q., Riojas, R.A., Ramos, F.J., and Liu, F. (2000). Mechanism of Phosphorylation of Protein Kinase B/Akt by a Constitutively Active 3-Phosphoinositide-dependent Protein Kinase-1. J. Biol. Chem. *275*, 40400–40406.

Willcox, A., Richardson, S.J., Bone, A.J., Foulis, A.K., and Morgan, N.G. (2009). Analysis of islet inflammation in human type 1 diabetes. Clin. Exp. Immunol. *155*, 173–181.

Williams, A.S., Kang, L., Zheng, J., Grueter, C., Bracy, D.P., James, F.D., Pozzi, A., and Wasserman, D.H. (2015). Integrin α1-null Mice Exhibit Improved Fatty Liver When Fed a High Fat Diet Despite Severe Hepatic Insulin Resistance. J. Biol. Chem. *290*, 6546–6557.

Williamson, J.R., Scholz, R., and Browning, E.T. (1969). Control Mechanisms of

Gluconeogenesis and Ketogenesis II. INTERACTIONS BETWEEN FATTY ACID OXIDATION AND THE CITRIC ACID CYCLE IN PERFUSED RAT LIVER. J. Biol. Chem. *244*, 4617–4627.

World Health Organization (2013). WHO Global Health Observatory Data Repository [online database].

World Health Organization (2018). World Health Organisation: Obesity and Overweight Fact Sheet.

Worton, R.G., and Thompson, M.W. (1988). Genetics of Duchenne Muscular Dystrophy. Annual Review of Genetics *22*, 601–629.

Xiong, J.-P., Stehle, T., Zhang, R., Joachimiak, A., Frech, M., Goodman, S.L., and Arnaout, M.A. (2002). Crystal structure of the extracellular segment of integrin alpha Vbeta3 in complex with an Arg-Gly-Asp ligand. Science *296*, 151–155.

Xiong, J.-P., Stehle, T., Goodman, S.L., and Arnaout, M.A. (2003). New insights into the structural basis of integrin activation. Blood *102*, 1155–1159.

Xu, H., Barnes, G.T., Yang, Q., Tan, G., Yang, D., Chou, C.J., Sole, J., Nichols, A., Ross, J.S., Tartaglia, L.A., et al. (2003). Chronic inflammation in fat plays a crucial role in the development of obesity-related insulin resistance. J Clin Invest *112*, 1821–1830.

Xue, B., Rim, J.-S., Hogan, J.C., Coulter, A.A., Koza, R.A., and Kozak, L.P. (2007). Genetic variability affects the development of brown adipocytes in white fat but not in interscapular brown fat. J. Lipid Res. *48*, 41–51.

Yamada, E., Okada, S., Saito, T., Ohshima, K., Sato, M., Tsuchiya, T., Uehara, Y., Shimizu, H., and Mori, M. (2005). Akt2 phosphorylates Synip to regulate docking and fusion of GLUT4-containing vesicles. J Cell Biol *168*, 921–928.

Yamamoto, N., Ueda-Wakagi, M., Sato, T., Kawasaki, K., Sawada, K., Kawabata, K., Akagawa, M., and Ashida, H. (2015). Measurement of Glucose Uptake in Cultured Cells. Current Protocols in Pharmacology *71*, 12.14.1-12.14.26.

Yao, C.C., Ziober, B.L., Sutherland, A.E., Mendrick, D.L., and Kramer, R.H. (1996a). Laminins promote the locomotion of skeletal myoblasts via the alpha 7 integrin receptor. J. Cell. Sci. *109 (Pt 13)*, 3139–3150.

Yao, C.-C., Ziober, B.L., Squillace, R.M., and Kramer, R.H. (1996b). α7 Integrin Mediates Cell Adhesion and Migration on Specific Laminin Isoforms. J. Biol. Chem. *271*, 25598–25603.

Yao, C.C., Breuss, J., Pytela, R., and Kramer, R.H. (1997). Functional expression of the alpha 7 integrin receptor in differentiated smooth muscle cells. J. Cell. Sci. *110 (Pt 13)*, 1477–1487.

Yee, K.L., Weaver, V.M., and Hammer, D.A. (2008). Integrin-mediated signalling through the MAP-kinase pathway. IET Syst Biol *2*, 8–15.

Yeh, J.-I., Gulve, E.A., Rameh, L., and Birnbaum, M.J. (1995). The Effects of

Wortmannin on Rat Skeletal Muscle DISSOCIATION OF SIGNALING PATHWAYS FOR INSULIN- AND CONTRACTION-ACTIVATED HEXOSE TRANSPORT. J. Biol. Chem. *270*, 2107–2111.

Yenush, L., Zanella, C., Uchida, T., Bernal, D., and White, M.F. (1998). The Pleckstrin Homology and Phosphotyrosine Binding Domains of Insulin Receptor Substrate 1 Mediate Inhibition of Apoptosis by Insulin. Mol. Cell. Biol. *18*, 6784–6794.

Yin, F., Yu, H., Lepp, D., Shi, X., Yang, X., Hu, J., Leeson, S., Yang, C., Nie, S., Hou, Y., et al. (2016). Transcriptome Analysis Reveals Regulation of Gene Expression for Lipid Catabolism in Young Broilers by Butyrate Glycerides. PLOS ONE *11*, e0160751.

Yoon, J.C., Puigserver, P., Chen, G., Donovan, J., Wu, Z., Rhee, J., Adelmant, G., Stafford, J., Kahn, C.R., Granner, D.K., et al. (2001). Control of hepatic gluconeogenesis through the transcriptional coactivator PGC-1. Nature *413*, 131–138.

Yu, H., Littlewood, T., and Bennett, M. (2015). Akt isoforms in vascular disease. Vascul Pharmacol *71*, 57–64.

Zeigerer, A., McBrayer, M.K., and McGraw, T.E. (2004). Insulin stimulation of GLUT4 exocytosis, but not its inhibition of endocytosis, is dependent on RabGAP AS160. Mol. Biol. Cell *15*, 4406–4415.

Zeng, M., Liang, Y., Li, H., Wang, B., and Chen, X. (2011). A metabolic profiling strategy for biomarker screening by GC-MS combined with multivariate resolution method and Monte Carlo PLS-DA. Anal. Methods *3*, 438–445.

Zhang, W., Thompson, B.J., Hietakangas, V., and Cohen, S.M. (2011). MAPK/ERK Signaling Regulates Insulin Sensitivity to Control Glucose Metabolism in Drosophila. PLoS Genet *7*.

Zhang, Y., Proenca, R., Maffei, M., Barone, M., Leopold, L., and Friedman, J.M. (1994). Positional cloning of the mouse obese gene and its human homologue. Nature *372*, 425–432.

Ziober, B.L., Vu, M.P., Waleh, N., Crawford, J., Lin, C.S., and Kramer, R.H. (1993). Alternative extracellular and cytoplasmic domains of the integrin alpha 7 subunit are differentially expressed during development. J. Biol. Chem. *268*, 26773–26783.

Ziober, B.L., Chen, Y., and Kramer, R.H. (1997). The laminin-binding activity of the alpha 7 integrin receptor is defined by developmentally regulated splicing in the extracellular domain. Mol Biol Cell *8*, 1723–1734.

Zong, H., Bastie, C.C., Xu, J., Fassler, R., Campbell, K.P., Kurland, I.J., and Pessin, J.E. (2009). Insulin Resistance in Striated Muscle-specific Integrin Receptor β1-deficient Mice. J. Biol. Chem. *284*, 4679–4688.

APPENDICES

Table 10.1: Student's T-Test results from metabolomic profile analysis of faeces collected from chow-fed control and α7KO mice

	t.stat	p.value	-LOG10(p)	FDR
Glycerol	-2.4648	0.069332	1.1591	0.72228
Alanine	-2.4037	0.074058	1.1304	0.72228
Ethanol	-2.0292	0.11232	0.94954	0.72228
Ornithine	-1.7281	0.15903	0.79851	0.72228
Hypoxanthine	1.7132	0.16183	0.79094	0.72228
Methanol	-1.6801	0.16823	0.77411	0.72228
Glycine	-1.5542	0.1951	0.70975	0.72228
Lactate	-1.5484	0.19646	0.70674	0.72228
Aspartate	-1.5261	0.20169	0.69531	0.72228
Tyrosine	-1.4922	0.20992	0.67795	0.72228
Phenylalanine	-1.4497	0.22073	0.65614	0.72228
Leucine	-1.4026	0.23339	0.63191	0.72228
Urocanate	-1.4	0.2341	0.6306	0.72228
Galactose	-1.3763	0.24074	0.61845	0.72228
Tryptophan	-1.3699	0.24259	0.61513	0.72228
Isoleucine	-1.3236	0.25621	0.59141	0.72228
1,3-Dihydroxyacetone	1.3093	0.26057	0.58407	0.72228
Fumarate	-1.3055	0.26175	0.58212	0.72228
Glutamine	-1.2899	0.26662	0.57411	0.72228
Asparagine	-1.2896	0.26671	0.57396	0.72228
Valine	-1.259	0.27651	0.55829	0.72228
Methionine	-1.231	0.28577	0.54399	0.72228
Threonine	-1.2102	0.29282	0.5334	0.72228
3-Phenylpropionate	-1.1501	0.3142	0.5028	0.72228
Arabinose	-1.1373	0.3189	0.49634	0.72228
Lysine	-1.1227	0.32441	0.4889	0.72228
Histidine	-1.1092	0.32955	0.48207	0.72228
AMP	-1.066	0.34649	0.46031	0.72228
Valerate	-1.0595	0.3491	0.45705	0.72228
Ferulate	-1.0213	0.36484	0.43789	0.72969
5-Aminopentanoic acid	-0.92625	0.40674	0.39068	0.77387
Proline	-0.90242	0.41786	0.37897	0.77387
Pyruvate	-0.85561	0.44044	0.35611	0.77387
Isobutyrate	0.85476	0.44086	0.3557	0.77387
Glutamate	-0.83353	0.45142	0.34542	0.77387
Acetoin	-0.75153	0.49413	0.30616	0.80078
Xylose	-0.73896	0.50095	0.30021	0.80078
GTP	-0.72761	0.50716	0.29486	0.80078
lactaldehyde_ifr	-0.59394	0.58451	0.23321	0.89925
Dimethylamine	0.5	0.64333	0.19157	0.92706
3-Methyl-2-oxovalerate	-0.46499	0.66612	0.17645	0.92706

Propionate	-0.41417	0.7	0.1549	0.92706
Alpha-ketoisovaleric acid	-0.361	0.73636	0.13291	0.92706
Cytidine monophosphate	0.34874	0.74487	0.12792	0.92706
Butyrate	-0.31415	0.76911	0.11401	0.92706
Glucose	-0.28488	0.78988	0.10244	0.92706
Uracil	-0.28333	0.79098	0.10183	0.92706
Formate	0.25889	0.8085	0.092322	0.92706
malic_acid	-0.25623	0.81041	0.091293	0.92706
Trimethylamine	-0.25482	0.81142	0.090752	0.92706
2-Oxoisocaproate	-0.24373	0.81943	0.086489	0.92706
Ribose	-0.2397	0.82234	0.084946	0.92706
2-methylbutyric_ifr	-0.21997	0.83666	0.077449	0.92706
Choline	-0.19528	0.85469	0.068192	0.92706
Methylamine	-0.1822	0.86429	0.06334	0.92706
Acetate	-0.18088	0.86526	0.062854	0.92706
Xanthine	0.14479	0.89188	0.049693	0.93882
Fructose	0.11933	0.91077	0.040592	0.94217
Nicotinate	0.062017	0.95352	0.020668	0.96528
Succinate	-0.046315	0.96528	0.015347	0.96528

Table 10.2: Results from Metabolite Set Enrichment Analysis of metabolomic profiles of faeces collected from chow-fed control and α7KO mice

	Total Cmpd	Hits	Statistic Q	Expected Q	Raw p	FDR
Glycerolipid Metabolism	25	1	60.299	20	0.069332	0.82948
Selenoamino Acid Metabolism	28	2	40.607	20	0.081585	0.82948
Glutathione Metabolism	21	3	37.181	20	0.18784	0.82948
Bile Acid Biosynthesis	65	1	37.653	20	0.1951	0.82948
Porphyrin Metabolism	40	1	37.653	20	0.1951	0.82948
Urea Cycle	29	8	31.285	20	0.20005	0.82948
Catecholamine Biosynthesis	20	1	35.761	20	0.20992	0.82948
Thyroid hormone synthesis	13	1	35.761	20	0.20992	0.82948
Spermidine and Spermine Biosynthesis	18	2	35.11	20	0.20998	0.82948
Glycine and Serine Metabolism	59	8	30.77	20	0.22849	0.82948
Alanine Metabolism	17	5	29.827	20	0.22873	0.82948
Nucleotide Sugars Metabolism	20	1	32.138	20	0.24074	0.82948
Purine Metabolism	74	9	25.018	20	0.24076	0.82948
Phenylalanine and Tyrosine Metabolism	28	5	27.401	20	0.2516	0.82948
Glutamate Metabolism	49	8	26.92	20	0.26173	0.82948
Ammonia Recycling	32	9	26.888	20	0.2698	0.82948
Arginine and Proline Metabolism	53	8	25.121	20	0.28899	0.82948
Threonine and 2-Oxobutanoate Degradation	20	1	26.802	20	0.29282	0.82948
Tryptophan Metabolism	60	4	26.868	20	0.29305	0.82948
Ethanol Degradation	19	3	24.553	20	0.30024	0.82948
Tyrosine Metabolism	72	5	23.612	20	0.31591	0.82948
Galactose Metabolism	38	4	23.695	20	0.31838	0.82948
Biotin Metabolism	8	1	23.96	20	0.32441	0.82948

Methylhistidine Metabolism	4	1	23.522	20	0.32955	0.82948
Glucose-Alanine Cycle	13	4	22.837	20	0.33365	0.82948
Phenylacetate Metabolism	9	2	25.75	20	0.33773	0.82948
Histidine Metabolism	43	4	23.333	20	0.33814	0.82948
Fatty acid Metabolism	43	1	22.124	20	0.34649	0.82948
Mitochondrial Beta-Oxidation of Long Chain Saturated Fatty Acids	28	1	22.124	20	0.34649	0.82948
Mitochondrial Beta-Oxidation of Medium Chain Saturated Fatty Acids	27	1	22.124	20	0.34649	0.82948
Mitochondrial Beta-Oxidation of Short Chain Saturated Fatty Acids	27	1	22.124	20	0.34649	0.82948
Riboflavin Metabolism	20	1	22.124	20	0.34649	0.82948
Thiamine Metabolism	9	1	22.124	20	0.34649	0.82948
Aspartate Metabolism	35	8	21.855	20	0.36855	0.84208
Lysine Degradation	30	2	19.379	20	0.3824	0.84208
Methionine Metabolism	43	4	22.049	20	0.38373	0.84208
Lactose Degradation	9	2	17.063	20	0.41967	0.84865
Sphingolipid Metabolism	40	2	17.063	20	0.41967	0.84865
Carnitine Synthesis	22	3	20.555	20	0.42557	0.84865
Beta-Alanine Metabolism	34	4	19.271	20	0.43321	0.84865
Pyruvaldehyde Degradation	10	1	15.47	20	0.44044	0.84865
Arachidonic Acid Metabolism	69	1	14.799	20	0.45142	0.84911
Warburg Effect	58	8	17.591	20	0.4939	0.88415
Cysteine Metabolism	26	3	17.464	20	0.50433	0.88415
Betaine Metabolism	21	2	14.209	20	0.5106	0.88415
Malate-Aspartate Shuttle	10	3	17.737	20	0.51482	0.88415
Propanoate Metabolism	42	4	17.354	20	0.53454	0.88431
Nicotinate and Nicotinamide Metabolism	37	4	16.599	20	0.5373	0.88431
Valine, Leucine and Isoleucine Degradation	60	8	14.551	20	0.55979	0.89959

Mitochondrial Electron Transport Chain	19	2	14.966	20	0.58638	0.89959
Citric Acid Cycle	32	4	14.273	20	0.63258	0.89959
Gluconeogenesis	35	5	13.647	20	0.63596	0.89959
Pantothenate and CoA Biosynthesis	21	2	12.537	20	0.64105	0.89959
Pentose Phosphate Pathway	29	2	11.77	20	0.65431	0.89959
Glycolysis	25	2	8.7294	20	0.65472	0.89959
Transfer of Acetyl Groups into Mitochondria	22	2	8.7294	20	0.65472	0.89959
Pyruvate Metabolism	48	6	15.945	20	0.65675	0.89959
Amino Sugar Metabolism	33	5	12.162	20	0.67263	0.89959
Pyrimidine Metabolism	59	3	11.431	20	0.68567	0.89959
Vitamin K Metabolism	14	1	4.112	20	0.7	0.89959
Folate Metabolism	29	2	8.2235	20	0.73486	0.89959
Cardiolipin Biosynthesis	11	1	2.9508	20	0.74487	0.89959
Phosphatidylinositol Phosphate Metabolism	17	1	2.9508	20	0.74487	0.89959
Plasmalogen Synthesis	26	1	2.9508	20	0.74487	0.89959
Butyrate Metabolism	19	3	8.1951	20	0.77293	0.89959
Fructose and Mannose Degradation	32	2	6.0215	20	0.78238	0.89959
Lactose Synthesis	20	1	1.9885	20	0.78988	0.89959
Pterine Biosynthesis	29	2	6.6682	20	0.801	0.89959
Androgen and Estrogen Metabolism	33	1	1.648	20	0.8085	0.89959
Androstenedione Metabolism	24	1	1.648	20	0.8085	0.89959
Steroid Biosynthesis	48	1	1.648	20	0.8085	0.89959
Phospholipid Biosynthesis	29	1	0.94439	20	0.85469	0.93778
Starch and Sucrose Metabolism	31	1	0.35471	20	0.91077	0.9557
Fatty Acid Biosynthesis	35	2	1.6095	20	0.91662	0.9557
Phosphatidylcholine Biosynthesis	14	2	1.9476	20	0.91941	0.9557

Phosphatidylethanolamine Biosynthesis	12	2	1.9476	20	0.91941	0.9557
Ketone Body Metabolism	13	1	0.053598	20	0.96528	0.96528
Oxidation of Branched Chain Fatty Acids	26	1	0.053598	20	0.96528	0.96528
Phytanic Acid Peroxisomal Oxidation	26	1	0.053598	20	0.96528	0.96528

Table 10.3 Student's T-Test results from metabolomic profile analysis of faeces collected from HFD-fed control and α7KO mice

	t.stat	p.value	-LOG10(p)	FDR
5-Aminopentanoic acid	-2.7474	0.051514	1.2881	0.61268
Acetate	-2.2299	0.089621	1.0476	0.61268
Succinate	-2.1947	0.093206	1.0306	0.61268
3-Phenylpropionate	-2.0889	0.10496	0.97899	0.61268
Propionate	-1.8737	0.13425	0.87208	0.61268
Taurine	1.6833	0.1676	0.77572	0.61268
Valerate	-1.6481	0.17468	0.75776	0.61268
Aspartate	-1.4877	0.21104	0.67564	0.61268
Histidine	-1.4161	0.2297	0.63884	0.61268
Pyruvate	-1.4055	0.23259	0.63342	0.61268
Trimethylamine	-1.3903	0.23681	0.6256	0.61268
Uracil	-1.2927	0.26573	0.57556	0.61268
Fumarate	-1.2565	0.27732	0.55703	0.61268
Ornithine	-1.2534	0.27832	0.55546	0.61268
Threonine	-1.2265	0.28727	0.5417	0.61268
Glutamine	-1.1844	0.30181	0.52026	0.61268
AMP	-1.1764	0.30467	0.51616	0.61268
Glutamate	-1.1311	0.32123	0.49319	0.61268
Hypoxanthine	-1.1308	0.32133	0.49305	0.61268
Choline	-1.1283	0.32228	0.49176	0.61268
Glycine	-1.1207	0.32517	0.48789	0.61268
Tyrosine	-1.1165	0.32676	0.48578	0.61268
Valine	-1.1101	0.32918	0.48257	0.61268
Methylamine	-1.0909	0.33663	0.47285	0.61268
Arabinose	-1.0673	0.34597	0.46096	0.61268
Phenylalanine	-1.0606	0.34868	0.45758	0.61268
Xanthine	-1.0593	0.34918	0.45695	0.61268
Asparagine	-1.0409	0.35669	0.44771	0.61268
Lysine	-1.0395	0.35727	0.44701	0.61268
Alanine	-1.0268	0.36255	0.44063	0.61268
Tryptophan	-1.0226	0.36432	0.43852	0.61268
Methionine	-1.0167	0.36679	0.43558	0.61268
Nicotinate	-1.0089	0.37012	0.43166	0.61268
Glycerol	-0.98327	0.38114	0.41891	0.61268
1,3-Dihydroxyacetone	0.97543	0.38458	0.41501	0.61268
Proline	-0.9738	0.3853	0.41421	0.61268
Galactose	-0.95673	0.39288	0.40574	0.61268
Leucine	-0.88706	0.42516	0.37144	0.61268
Isoleucine	-0.87436	0.43128	0.36524	0.61268
Butyrate	-0.86832	0.43421	0.3623	0.61268
Formate	-0.84425	0.44607	0.3506	0.61268

Urocanate	-0.83724	0.44957	0.34721	0.61268
Methanol	-0.81054	0.4631	0.33433	0.61268
Isobutyrate	-0.80381	0.46656	0.33109	0.61268
malic_acid	-0.78602	0.47581	0.32257	0.61268
lactaldehyde_ifr	0.77007	0.48421	0.31496	0.61268
3-Methyl-2-oxovalerate	0.75509	0.49222	0.30784	0.61268
Cytidine monophosphate	-0.72909	0.50634	0.29556	0.61268
Ethanol	-0.72844	0.5067	0.29525	0.61268
Ribose	-0.72142	0.51057	0.29195	0.61268
Ferulate	-0.70159	0.52161	0.28266	0.61365
GTP	-0.60946	0.57514	0.24023	0.66362
Fructose	-0.45689	0.67146	0.17298	0.76014
Xylose	-0.36784	0.73163	0.13571	0.78678
Alpha-ketoisovaleric acid	0.35355	0.74152	0.12988	0.78678
Dimethylamine	0.34394	0.74821	0.12597	0.78678
2-Oxoisocaproate	0.33806	0.75231	0.1236	0.78678
Glucose	-0.3103	0.77183	0.11248	0.78678
Lactate	-0.3077	0.77367	0.11145	0.78678
2-methylbutyric_ifr	0.10555	0.92102	0.035731	0.92102

Table 10.4: Results from Metabolite Set Enrichment Analysis of metabolomic profiles of faeces collected from HFD-fed control and α7KO mice

	Total Cmpd	Hits	Statistic Q	Expected Q	Raw p	FDR
Butyrate Metabolism	19	3	32.065	20	0.028035	0.51411
Mitochondrial Electron Transport Chain	19	2	41.465	20	0.083931	0.51411
Ketone Body Metabolism	13	1	54.631	20	0.093206	0.51411
Oxidation of Branched Chain Fatty Acids	26	1	54.631	20	0.093206	0.51411
Phytanic Acid Peroxisomal Oxidation	26	1	54.631	20	0.093206	0.51411
Vitamin K Metabolism	14	1	46.744	20	0.13425	0.51411
Taurine and Hypotaurine Metabolism	12	1	41.465	20	0.1676	0.51411
Carnitine Synthesis	22	3	33.265	20	0.1828	0.51411
Citric Acid Cycle	32	4	31.121	20	0.19067	0.51411
Bile Acid Biosynthesis	65	2	32.68	20	0.19474	0.51411
Fatty Acid Biosynthesis	35	2	35.64	20	0.19585	0.51411
Methylhistidine Metabolism	4	1	33.391	20	0.2297	0.51411
Pyruvaldehyde Degradation	10	1	33.059	20	0.23259	0.51411
Glutamate Metabolism	49	8	30.496	20	0.23382	0.51411
Ethanol Degradation	19	3	30.945	20	0.23709	0.51411
Propanoate Metabolism	42	4	30.059	20	0.24213	0.51411
Arginine and Proline Metabolism	53	8	29.969	20	0.2438	0.51411
Amino Sugar Metabolism	33	5	28.727	20	0.24649	0.51411
Beta-Alanine Metabolism	34	4	30.679	20	0.25126	0.51411
Aspartate Metabolism	35	8	28.132	20	0.27128	0.51411
Cysteine Metabolism	26	3	27.666	20	0.27754	0.51411
Urea Cycle	29	8	27.743	20	0.2787	0.51411
Threonine and 2-Oxobutanoate Degradation	20	1	27.329	20	0.28727	0.51411

Tyrosine Metabolism	72	5	26.969	20	0.28916	0.51411
Ammonia Recycling	32	9	26.455	20	0.293	0.51411
Phenylacetate Metabolism	9	2	25.835	20	0.30152	0.51411
Alanine Metabolism	17	5	25.55	20	0.30268	0.51411
Glycine and Serine Metabolism	59	8	25.477	20	0.30457	0.51411
Fatty acid Metabolism	43	1	25.704	20	0.30467	0.51411
Mitochondrial Beta-Oxidation of Long Chain Saturated Fatty Acids	28	1	25.704	20	0.30467	0.51411
Mitochondrial Beta-Oxidation of Medium Chain Saturated Fatty Acids	27	1	25.704	20	0.30467	0.51411
Mitochondrial Beta-Oxidation of Short Chain Saturated Fatty Acids	27	1	25.704	20	0.30467	0.51411
Riboflavin Metabolism	20	1	25.704	20	0.30467	0.51411
Thiamine Metabolism	9	1	25.704	20	0.30467	0.51411
Phenylalanine and Tyrosine Metabolism	28	5	24.789	20	0.31386	0.51411
Malate-Aspartate Shuttle	10	3	24.412	20	0.31584	0.51411
Histidine Metabolism	43	4	24.56	20	0.31637	0.51411
Purine Metabolism	74	9	24.261	20	0.31789	0.51411
Spermidine and Spermine Biosynthesis	18	2	24.368	20	0.3189	0.51411
Arachidonic Acid Metabolism	69	1	24.234	20	0.32123	0.51411
Nicotinate and Nicotinamide Metabolism	37	4	24.047	20	0.32216	0.51411
Phospholipid Biosynthesis	29	1	24.143	20	0.32228	0.51411
Porphyrin Metabolism	40	1	23.894	20	0.32517	0.51411
Catecholamine Biosynthesis	20	1	23.759	20	0.32676	0.51411
Thyroid hormone synthesis	13	1	23.759	20	0.32676	0.51411
Methionine Metabolism	43	4	23.569	20	0.32849	0.51411
Selenoamino Acid Metabolism	28	2	23.282	20	0.33227	0.51411
Pyruvate Metabolism	48	6	22.984	20	0.33279	0.51411
Glutathione Metabolism	21	3	22.996	20	0.33547	0.51411

Warburg Effect	58	8	22.419	20	0.33871	0.51411
Lysine Degradation	30	2	22.752	20	0.33871	0.51411
Pyrimidine Metabolism	59	3	22.387	20	0.34176	0.51411
Betaine Metabolism	21	2	22.339	20	0.34364	0.51411
Biotin Metabolism	8	1	21.269	20	0.35727	0.51411
Tryptophan Metabolism	60	4	20.235	20	0.37073	0.51411
Glucose-Alanine Cycle	13	4	20.126	20	0.37422	0.51411
Folate Metabolism	29	2	19.679	20	0.37844	0.51411
Glycerolipid Metabolism	25	1	19.466	20	0.38114	0.51411
Nucleotide Sugars Metabolism	20	1	18.622	20	0.39288	0.51411
Pentose Phosphate Pathway	29	2	18.608	20	0.39389	0.51411
Pantothenate and CoA Biosynthesis	21	2	18.717	20	0.39649	0.51411
Phosphatidylcholine Biosynthesis	14	2	17.937	20	0.40486	0.51411
Phosphatidylethanolamine Biosynthesis	12	2	17.937	20	0.40486	0.51411
Glycolysis	25	2	17.705	20	0.43135	0.52372
Transfer of Acetyl Groups into Mitochondria	22	2	17.705	20	0.43135	0.52372
Androgen and Estrogen Metabolism	33	1	15.124	20	0.44607	0.52372
Androstenedione Metabolism	24	1	15.124	20	0.44607	0.52372
Steroid Biosynthesis	48	1	15.124	20	0.44607	0.52372
Valine, Leucine and Isoleucine Degradation	60	8	19.148	20	0.45171	0.52372
Cardiolipin Biosynthesis	11	1	11.73	20	0.50634	0.55871
Phosphatidylinositol Phosphate Metabolism	17	1	11.73	20	0.50634	0.55871
Plasmalogen Synthesis	26	1	11.73	20	0.50634	0.55871
Pterine Biosynthesis	29	2	11.81	20	0.50982	0.55871
Gluconeogenesis	35	5	11.92	20	0.54153	0.58345
Lactose Degradation	9	2	10.486	20	0.55428	0.58345

Sphingolipid Metabolism	40	2	10.486	20	0.55428	0.58345
Galactose Metabolism	38	4	11.349	20	0.63243	0.65707
Starch and Sucrose Metabolism	31	1	4.9599	20	0.67146	0.68868
Lactose Synthesis	20	1	2.3505	20	0.77183	0.7816
Fructose and Mannose Degradation	32	2	6.7285	20	0.80509	0.80509